UNIVERSITÀ DEGLI STUDI DI PADOVA

Dipartimento di Ingegneria Industriale DII

Corso di Laurea Magistrale in Ingegneria Elettrica

TESI DI LAUREA

Development of a discrete-time analytical model for Thyristor Controlled Reactors and application to the ITER fusion experimental reactor

Relatore: Prof. Paolo Bettini
Correlatori: Dott. Ing. Elena Gaio, Dott. Ing. Claudio Finotti

Laureando: Stefano Da Lio,   1033812

CONTENTS

Sommario

In questo lavoro di tesi si è sviluppato, utilizzando un approccio analitico, un modello lineare tempo discreto a coefficienti costanti del Sistema di Compensazione della Potenza reattiva (Static Var Compensation System, SVC) dell'impianto di alimentazione del reattore sperimentale a fusione ITER; tale modello è stato poi validato sia nel dominio del tempo, confrontando i risultati trovati con gli andamenti istantanei di tensione e corrente prodotti dal software di simulazione PSIM, sia nel dominio della frequenza, prendendo le simulazioni di quest'ultimo come riferimento. Il presente lavoro è finalizzato a studiare il sottosistema costituito da reattori controllati a tiristori (Thyristor Controlled Reactor, TCR) di ITER attraverso un modello analitico basato su un approccio tempo discreto. Dopo una breve introduzione volta a spiegare il contesto di ricerca nel quale si situa il progetto ITER, con particolare riferimento al suo sistema di alimentazione, si sono presentati i concetti teorici necessari allo sviluppo di modelli analitici tempo-discreti con cui analizzare circuiti di potenza controllati a tiristori. Il punto di partenza è stato lo sviluppo di un modello monofase equivalente del Sistema di compensazione della Potenza reattiva, già presente in letteratura [1], dopodichè procedendo per gradi, si è via via aumentato il livello di dettaglio, estendendo il precedente modello al caso trifase con TCR connesso a stella. Si è poi studiato il caso del TCR connesso a triangolo, adottato nel Sistema SVC di ITER, con angolo di conduzione $\sigma \in (0, 60°)$. Infine si è considerato anche il caso $\sigma \in (60, 120°)$, complicando ulteriormente la trattazione per l'aggiunta di una variabile di stato nel modello. La validazione in frequenza invece è stata effettuata solo nella prima modalità operativa, trasformando il modello tempo-discreto in uno corrispondente valido nel continuo. Infine quest'ultimo è stato anche confrontato (nel tempo e in frequenza) con un altro modello tempo continuo presente in letteratura [2], che era stato sviluppato direttamente con un approccio tempo-continuo, non rispettando quindi fisicamente l'operativita "discreta" di questo tipo di circuiti. In questo senso tale confronto ha permesso anche la validazione di quest'ultimo.

Abstract

In this work a Linear Time Invariant (LTI) discrete-time model of the Static Var Compensation System of the ITER power supply system has been developed, using an analytical approach, and validated by comparison with PSIM program, which reproduces instantaneous voltage and current profiles. This thesis aims to study the Thyristor Controlled Reactor (TCR) subsystem of ITER experimental reactor through analytical model based on discrete-time approach. After a brief introduction to the fusion research framework and to the ITER experiment with its power supply systems, basics concepts of discrete-time analytical models of thyristor-based static switching circuits are presented. The starting point of this study has been the development of an equivalent single phase SVC model already presented in literature [1], then the details of the model have been increased in different steps, firstly extended the previus one for three-phase operation. Then the development of a TCR model in delta-configuration, which is adopted in the ITER SVC, is described. The application to the ITER case is presented considering different operation modes, according to the conduction angle $\sigma \in (0, 60°)$ and $\sigma \in (60, 120°)$. Finally, the LTI discrete-time model related to the first case has been expressed in a continuous-time frame to allow comparison with another one developed in [2]. The comparison is carried out in time and frequency domain.

Introduction

ITER experiment [3] will be built at Cadarache (France) and its main goal will be to prove the viability of fusion as an energy source. In a fusion reactor, the plasma (an ionized gas of Deuterium and Tritium) has to be heated up to temperatures of millions of Celsius degrees in order to sustain the fusion reaction. No materials are able to withstand these temperatures; therefore the plasma is kept away from the walls of the reactor vacuum vessel by means of appropriate magnetic fields, produced by the currents flowing in the superconducting coils, which interact with the charged particles of the plasma.

The ac/dc conversion system necessary to supply the superconducting coils of the magnet system and the auxiliary heating systems may consume a total active and reactive power respectively up to 500 MW and 950 Mvar, but, the reactive power demand has to be limited to around 200 MVar [4], [5]. Indeed, several methods have been considered to improve the power factor, based both on Q reduction and compensation techniques. Concerning the last one, the current reference design is based on Static Var Compensation System with nominal power of 750 Mvar based on Thyristor Controlled Reactor (TCR) + Tuned Filter (as fixed capacitor).

In the past years many studies have been carried out on the ITER power supply system and its impact on the electrical network, considering the huge power demand and the expected power transients during the plasma pulses. One concern in particular is related to the interactions phenomena among the ac/dc conversion, Q compensation, filtering systems and the related controllers, which may cause unpredicted instability conditions.

The stability and performance of the whole ITER power supply can be investigated using different techniques: numerical simulations, able to reproduce instantaneous current and voltage waveforms, or studies by analytical models. As for the former, being the whole system very complex, these simulations require very long calculation time and often they do not provide any sensitivity data concerning the stability of the whole power system. Analytical models, even if less accurate, allow a faster approach than those based on the electrical transient simulation programs and are able to provide sensitivity data concerning the dynamic stability of the whole power system, allowing an easier identification of unstable conditions and optimization of the control of ITER power supply system.

Analytical models can be developed via continuous-time or discrete-time approach. In both cases the problem of the non-linear behavior of the circuit with switching components (like thyristors) can be solved by linearizing the model around the operating point; often a direct-quadrature frame is used, because the variables with sinusoidal evolution are transformed in constant ones in d-q frame, making easier the small signal analysis.

The development of a continuous-time analytical model of ITER Power Supply System is described in [2]: suitable transfer functions were worked out to reproduce the dynamic behavior of the ac/dc thyristor converter units and of the SVC, then a state space model of the whole system was built to allow the stability study by the eigenvalue analysis.

The models described in [2] have been worked out starting from similar ones presented in literature. As for TCR model, however, to reproduce its operation, novel provisions have been introduced to solve some limits of the available models. To further validate this continuous-time TCR model, it was decided to workout another one, based on a discrete-time approach and to compare the performance. The development of a discrete-time TCR model and the comparison with the continuous-one are the object of this thesis.

The TCR is an electrical network with switching devices with a periodic behavior, where a periodic sequence of Linear Time Invariant (LTI) systems depending on the configuration of the switches may be identified, allowing the development of a whole LTI discrete-time state space model at the small signals by the Poincarè map theory. These concepts already developed in [1] and [6] are reviewed in Appendix I, rearranging the notation as it is used here, as they represent the basis for this work.

The starting point of this study has been the development of an equivalent single phase SVC model already presented in literature [1], then the details of the model have been increased in different steps, obtaining a LTI discrete-time model valid for the SVC configuration of ITER case. In the end, it has been compared with the continuous model, presented in [2], in term of accuracy, in time and frequency domain. To perform the comparison the discrete time model has been converted to an equivalent continuous-time one.

This thesis is organized as follows.

In the Chapter 1 a brief introduction to the fusion research framework and to the ITER experiment with its power supply systems is given. In Chapter 2 basics concepts of discrete-

time analytical models of thyristor-based static switching circuits are presented and the circuit used for the development of the model of the TCR subsystem is described. In Chapter 3 LTI models are synthesized for a Static Var Compensator in single-phase and three phase operation with a TCR in star-configuration. In Chapter 4 the development of a TCR model in delta-configuration, which is adopted in the ITER SVC is described. The application to the ITER case is presented, considering different operation modes, according to the conduction angle $\sigma \in (0, 60°)$ and $\sigma \in (60, 120°)$.

Finally, the discrete-state space model related to the first one is expressed in a continuous-time frame to allow comparison with the other one developed in [2]. The comparison is carried out in time and frequency domain.

1 ITER experiment

1.1 *Introduction to ITER fusion experimental reactor*

Nowadays the need of energy is mainly satisfied for 80% by fossil fuels (oil, coal, natural gas, see) and it is expect to grow in the next years [7]. Moreover, this use of energy has relevant impact on the environment due to the emissions of greenhouse gas and other air pollutants. Therefore new safe and sustainable energy source are being researched. The nuclear fusion technology is one of them also because it is safer than the fission one: in case of loss of the control in a fusion reactor the plasma gets cold very fast and the reaction stop, while the runaway in a fission reactor can be very dangerous. Moreover, at the same output power condition, in a fusion reactor the production of radioactive wastes are less and their radioactive decay time is lower.

The most viable fusion reaction for a future fusion power plant considers as reacting elements Deuterium and Tritium, which are isotopes of Hydrogen [8], [9]:

$$D + T \rightarrow {}^4He \ (3.5 \ \text{MeV}) + \ \text{n} \ (14.1 \ \text{MeV})$$

(1.1)
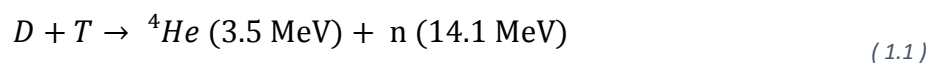
If Deuterium and Tritium are heated at very high temperatures, in the order of 200×10^6 K, the kinetic energy of the nuclei overcomes the Coulomb repulsion, then the nuclei likely collide and react, producing a nucleus of Helium, a neutron and energy.

A significant amount of energy to reach temperatures of millions of Celsius degrees is necessary, but the main problem is how to confine and insulate the plasma in order to maintain it. No materials are able to withstand these temperatures; therefore the plasma is kept away from the walls of the reactor vacuum vessel by means of appropriate magnetic fields which interact with the charged particles of the plasma: this approach is called "magnetic confinement fusion".

The long-term objective of the magnetic confinement fusion R&D is a prototype reactor for power station, which will allow an energy production without emission of greenhouse gas and other air pollutants, safe and long-term availability of the fuels.

The strategy to achieve this long term objective includes the development of an international experimental reactor ITER [3], which aims to demonstrate the scientific and technological feasibility of fusion energy and it is being built at Cadarache, in France.

The ITER fusion reactor is designed to produce 500 MW of thermal power, with a ratio Q between output fusion power and input power to the tokamak higher than 10. Hereby the machine is expected to demonstrate the principle of getting more energy out of the fusion process than is used to sustain it, a target not yet achieved in the present experiments. Nevertheless, ITER will be still an experimental device, unable to inject electricity into the grid. The main parameters of the ITER experimental reactor are listed in Table 1-1.

Table 1-1 Main parameters of the ITER experimental reactor

Parameter	Value
Total fusion power	500 MW
Q = fusion power/auxiliary heating power	≥10 (inductive)
Average neutron wall loading	0.57 MW/m^2
Plasma inductive burn time	≥400 s
Plasma major radius	6.2 m
Plasma minor radius	2.0 m
Plasma current	15 MA
Toroidal field 6.2 m radius	5.3 T
Plasma volume	837 m^3
Plasma surface	678 m^2
Installed auxiliary heating/current drive output power	73 MW

ITER will also develop and test technologies and processes needed for future fusion plants: superconducting magnets, components able to withstand high neutron fluxes and remote manipulation. In the following paragraph the magnet system used to confine the plasma and the relevant power supply system are described

1.1.1   The ITER magnet system

The magnetic confinement of ITER is based on tokamak configuration [10], which consist of a toroidal machine where the plasma acts as the secondary winding of a transformer while the primary winding is made of the poloidal field coils: a change of current in the primary winding induces a current in the plasma (inductive phenomena) (Figure 1-1). The central solenoid provides the inductive flux to ramp up plasma current and contribute to plasma shaping. The

equilibrium field coils provide the position control of plasma column (i.e. the fields to confine the plasma pressure) and the plasma vertical stability. There are also additional coils which allow the correction of error field due to position errors as well as from busbars and feeders. Finally, a high toroidal field of 5.3T is imposed by toroidal field coils to confine the plasma. The main electrical data of the coils of ITER magnet system are given in Table 1-2 and they are visible in Figure 1-2.

The plasma current generates a further magnetic field which contributes to confine the plasma and it also provides some heating because of electrical resistance of the plasma. Nevertheless the heating due to the Joule losses on the resistance of the plasma is not sufficient to achieve a plasma temperature of millions of Celsius degrees and a transformer cannot generate current continuously, therefore additional systems are necessary to further rise the temperature and sustain the current of plasma.
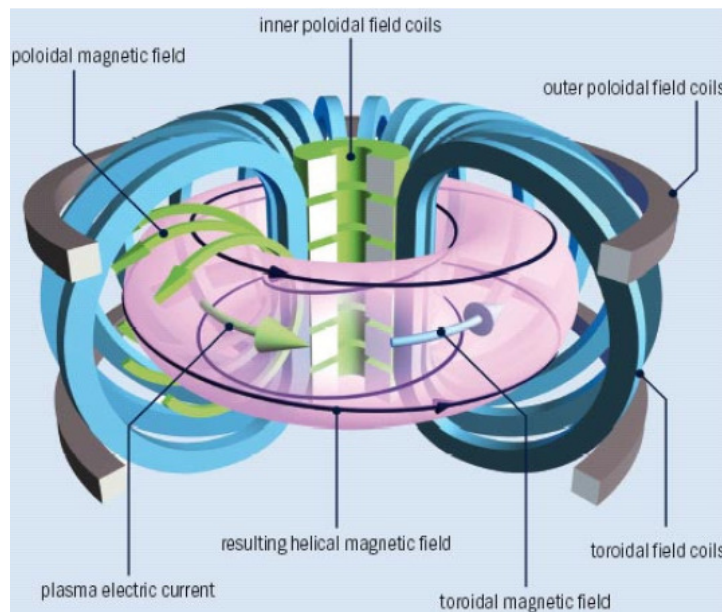
Figure 1-1 Schematic view of the main field coils and of plasma current in a tokamak

Table 1-2 Main electrical data of the coils of ITER magnet system

	Poloidal Field	Central Solenoid	Toroidal Field	Correction Coils
Number of coils	6	6	18	18
Stored magnetic energy [GJ]	4	7	41	-
Maximum operating current [kA]	45	45	68	10
Nominal peak field [T]	6	13.0	11.8	5
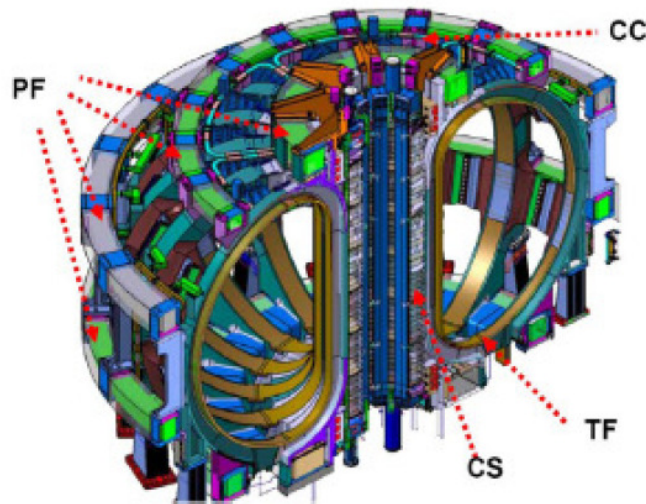
Figure 1-2 Schematic view of the main field coils of ITER magnet system

1.2 The ITER Power Supply System

The ITER experiment is supplied by the High Voltage grid at 400 kV with a short circuit power of about 12 GVA: the ac/dc conversion system necessary to supply the superconducting coils of the magnet system and the auxiliary heating systems can consume a reactive power up to 950 Mvar. This large demand of reactive power cannot be feed only by HV grid because it has to be limited to around 200 MVar [4], [5]. The ac/dc conversion systems are equally distributed among three independent 66 kV and 22 kV distribution systems, called Pulse Power Electrical Network (PPEN) (see Figure 1-3), supplied by three identical winding step-down transformers. The largest power supplies (mainly the superconducting coil ac/dc converters with nominal power >20 MVA and the power supplies of the heating systems) are connected to 66 kV busbars; for each one the total installed power of the ac/dc converters and of the reactive power compensation system (TCR + Tuned Filters) are about 500 MVA and 250 Mvar respectively.

Figure 1-3 Schematic representation of the ITER Pulsed Power Electrical Network

Figure 1-4 shows the active and reactive pulse power demand of the ac/dc converters P_{grid} and Q_{load} respectively, the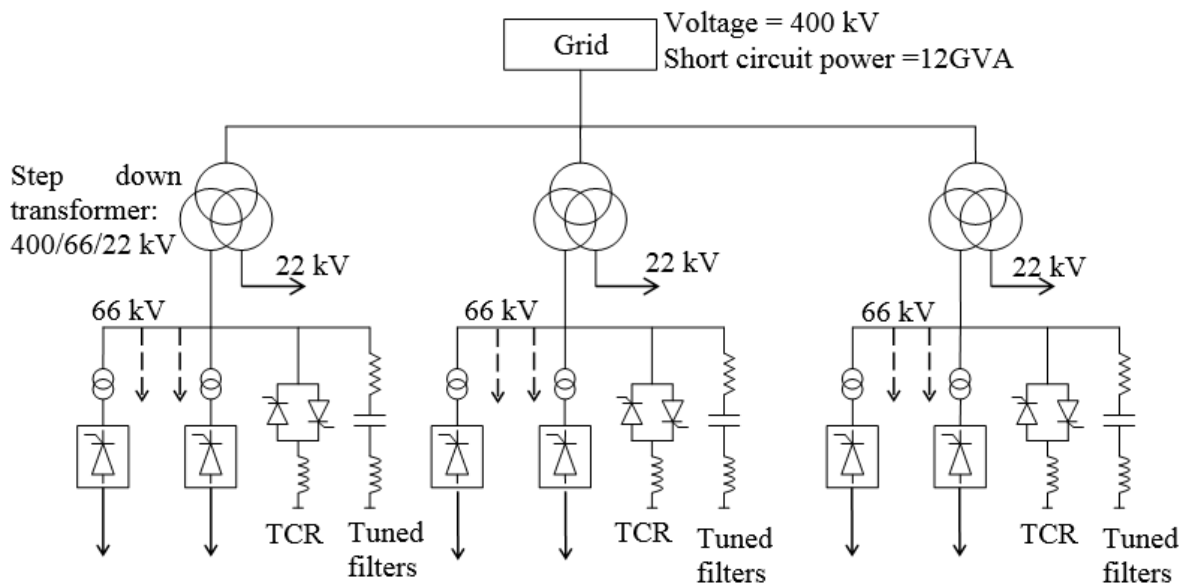 reactive power consume from the grid at 400 kV busbar Q_{grid} and the contribution Q_{SVC} provide from Static Var Compensation system. The following phases may be identified during the experimental shot:

- Pre-magnetisation: the ac/dc converters charge the magnet system;
- Plasma Initiation: the ac/dc converters of the some poloidal coils apply the maximum output voltage to rise the plasma current;
- Plasma sustainment: in this phases the plasma current is kept constant and the voltage required to the ac/dc converter is low, but the current are near to the nominal values, consequently the ac/dc converters consume very high reactive power;
- De-magnetisation: the plasma current is taken to zero.

It can be seen that with the Reactive Power Compensation system (rated at 750 Mvar), the reactive power supplied from grid is limited around 200 Mvar. As it has been just shown, there is a huge power demand that could have a significant impact on the electrical network. Moreover the operation of a single component (for example ac/dc converter, TCR, etc ...) may be stable if considered alone, while in the whole system the interactions phenomena among the different components and the related controllers may cause unpredicted instability conditions. In this way it's important to be able to predict and prevent possible unstable

13

conditions throughout analytical models. In the next two paragraphs brief descriptions of the base unit of the main ac/dc converters and of the reactive power compensation system are given.
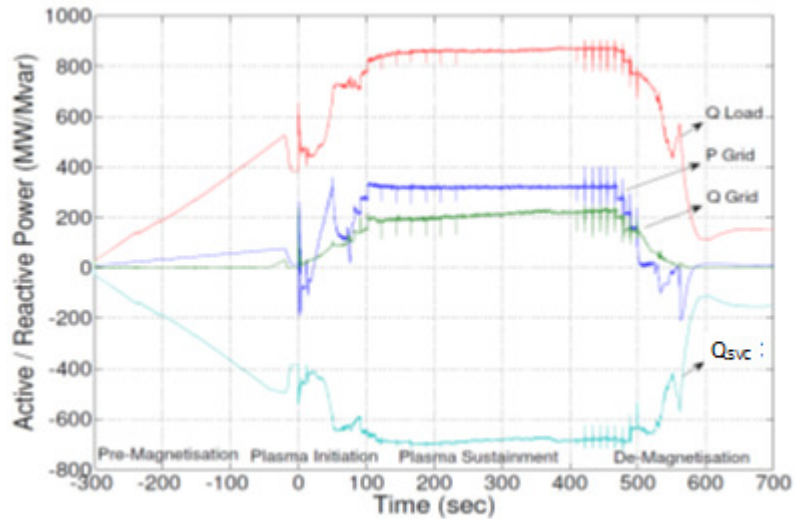
Figure 1-4 Active (P$_{grid}$) and reactive (Q$_{load}$) power demand during an experimental shot. Note that the reactive power supplied by compensation system is Q$_{SVC}$ = Q$_{load}$ − Q$_{grid}$

1.3   The ac/dc converter base unit

The superconducting coils are supplied by ac/dc converters based on thyristor technology. For each type of coil different requirements of currents, voltages and dynamic response are specified (Table 1-3); nevertheless, a modular approach has been chosen for the design and a base unit has been defined. Their requirements are satisfied by using appropriate series/parallel connections of the base units. The ac/dc converter base unit is shown in Figure 1-5.

It consists of two subunits connected in parallel in twelve pulses configuration, each one composed of two back to back thyristor bridges. During the ITER operation the ac/dc converter are voltage and current controlled. The voltage control allows supplying to the coil the right voltage required from the ITER operating scenarios, while the current control is necessary to control the current sharing between the subunits in parallel.
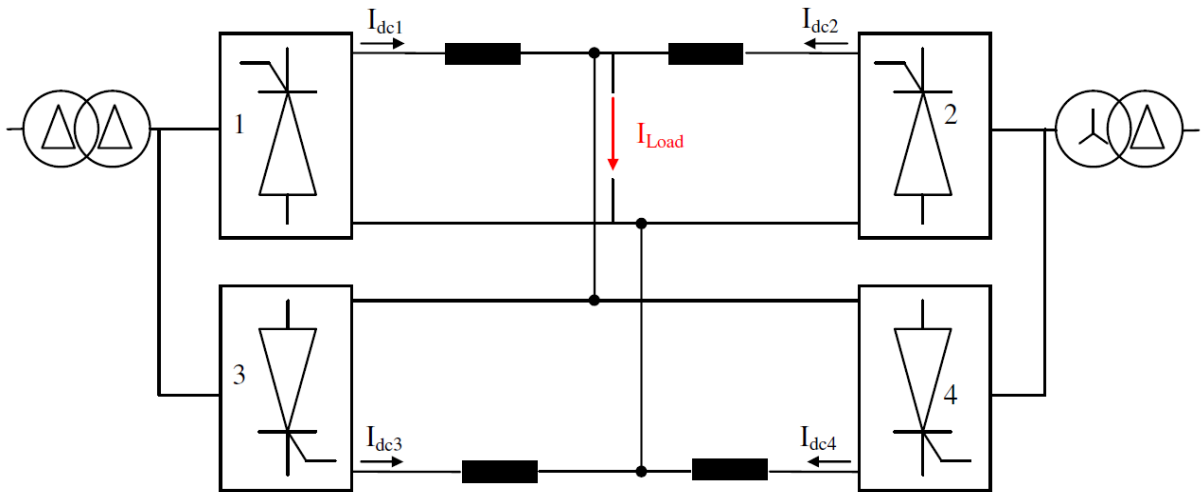
Figure 1-5 ac/dc converter base unit supplying the coils of the ITER main magnet systems

Table 1-3. Main parameters of the ac/dc converter base unit of some superconducting coils

Converter type	Poloidal Field (PF)	Central Solenoid (CS)	Toroidal Field (TF)	Correction Coils Upper/Lower (CCU/CCL)	Correction Coils Side (CCS)
DC side data					
Rated DC current (A) Ir	55000	45000	68000	10000	10000
DC no load voltage (V)	1366	1366	351	90.5	455
Transformer data					
Rated power S_N [MVA]	39(×2)	32(×2)	13(×2)	0.5(×2)	2.4(×2)
Primary rms voltage U_{1N} [kV]	66	66	66	22	22
Secondary rms voltage U_{2N} [V]	1012	1012	260	67	337
Winding resistance r_W (‰)	2.3	2.3	2.3	2.3	2.3
No load current (%)	0.3	0.3	0.3	0.3	0.3
Iron losses (%)	0.053	0.053	0.053	0.053	0.053
Short-circuit reactance x_{SC} (%)	17.5	17.5	35	17.5	17.5

1.4   The Static Var Compensation system

Thyristor Controlled Reactor (TCR) in combination with tuned filters provide reactive-capacitance power and the compensation of the converter. The whole system is called Reactive Power Compensation and Harmonic Filtering (RPC&HF) system (see Figure 1-6). The TCR system is controlled to minimize the reactive power demand from the grid; it operates in

feed-forward mode, i.e. the reference signal to control the firing angle α_L of the TCR system is calculated using the measurement of the reactive power of the ac/dc conversion system corrected on the basis of the measurement of the busbar voltage. The phase inductance (delta-connection) of the TCR is 112.17 mH, and the main parameters of the tuned filters (star connection) are listed in the Table 1-4.

Table 1-4 Main parameters of the tuned filters

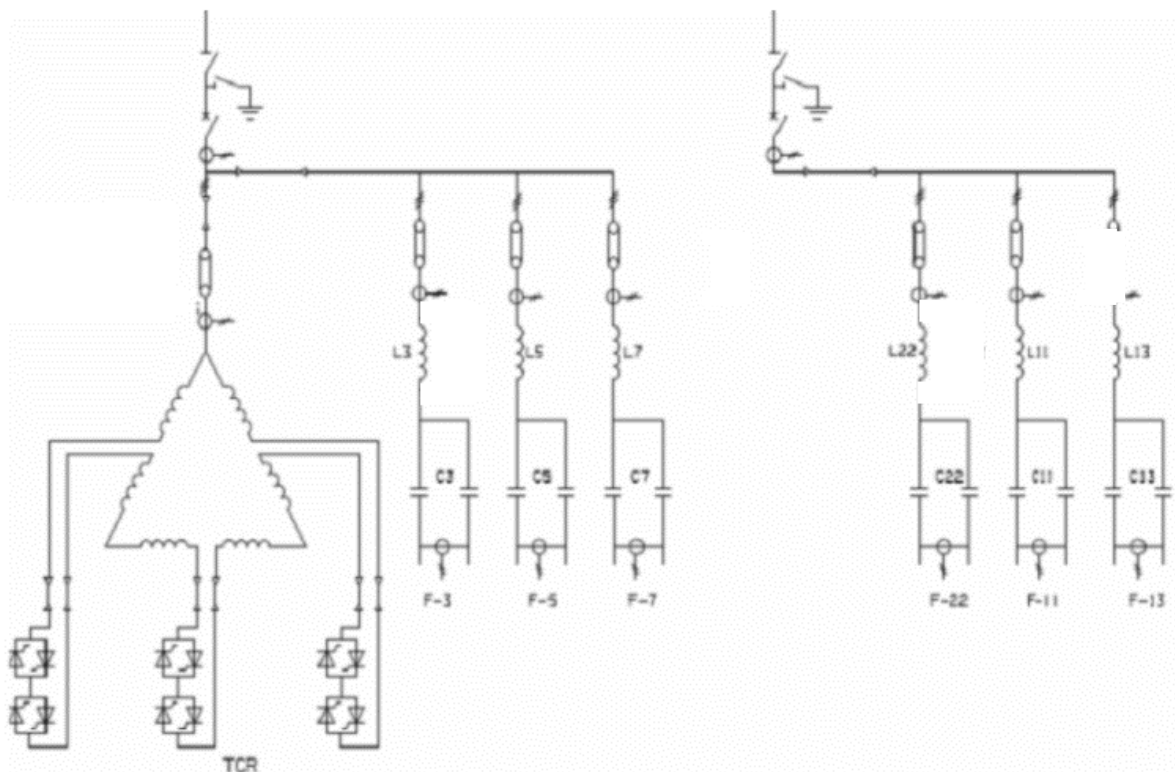| Filter order	Resonant frequency	Capacity	Inductance	Quality factor	Resistance	Q at 50 Hz, 66kV	P at 50Hz, 66kV
h	[Hz]	[μF]	[mH]		[Ω]	[Mvar]	[kW]
3	149	9.71	118.2	50	2.2066	15	114
5	247	41.92	9.9	25	0.6136	60	504
7	346	35.78	4.9	17	0.7703	50	442
11	539	43.63	2	13	0.536	60	446
13	637	36.74	1.7	10	0.6732	51	396
23	1129	11.05	1.8	8	1.5178	15	80
TOTAL						251	1982

Figure 1-6 Diagram of the ITER RPC&HF System on one 66kV busbar.

2 Discrete-time approach and system modeling

This chapter explains the modeling approach used for the development of the discrete-time state space model (whose theoretical concepts for the analysis are deeply described in Appendix I) for a thyristor-based static switching circuit. This approach is then used in the next Chapters to develop a linear, time-invariant (LTI) discrete state space model of the ITER Static Var Compensator previous described. So, in order to be able to apply such described approach, it has been simplified as in Figure 2-3.

2.1 Discrete-time approach

A circuit with switching components as thyristors is non-linear and its dynamic behavior may be described by a function f of the inputs and of the state variables, which generally, at steady state, are periodic, with period T. For this reason the system dynamics can be studied by sampling the system with a sampling time T_s. This concept is formalized as the Poincaré mapping H which maps the system states forward in time from t_0 to $t_0 + kT_s$ for $k = 0,1,\dots$ that indicates the sequence of the sampling time. Figure 2-1 describes a system dynamic with half-wave symmetry over a period T of a thyristor-based static switching circuit. Inside each sampling instant $T_s = T/2$ there are an interval (ON) in which a thyristor is conducting (between firing instant Φ and time τ when the thyristor current goes through zero) and two interval (OFF) in which a thyristor is in its non-conducting mode. These intervals are delimitated by the sampling time t_0 and $t_0 + T_s$. The Poincaré map H takes into account the dependence of the switching times on the system states (that determinates the non-linearity of the circuit) and can be computed by integrating over a sampling period T_s the appropriate state equations as determined by the switching times. In this sense, Poincarè map "maps" the system dynamics with sample period T_s: for the cycle depicted in Figure 2-1 it can be written as $H[x(t_0)] = x(t_0 + T_s)$ where x represents the system states. Consequently this allows passing from the non-linear model as depicted in Figure 2-2(a) to the non-linear sampled-data model in Figure 2-2(b). The nonlinear model, expressed in continuous time frame, relates the inputs to the outputs, where the inputs are the source voltages u and the firing instant Φ of thyristors, and the outputs v are function of the state variables, while the second one relates them sampling with period T_s , as shown in (2.1).

$$v(t) = f\big(x(t), u(t), \Phi(t)\big)$$

<div align="right">(2.1)</div>

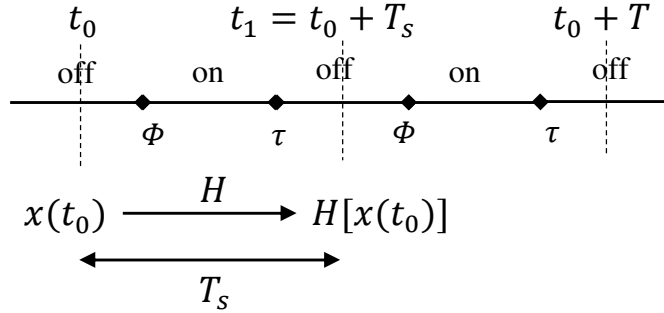$$v(kT_s) = H\big(x(kT_s), u(kT_s), \Phi(kT_s)\big) \ with \ k = 0,1, \dots$$

Figure 2-1 System dynamics of a thyristor-based static switching circuit over one sample period

It is highlighted that in a thyristor-based static switching circuit using Poicarè map to pass from the continuous-time domain to the discrete one, the outputs v of the model are same state variables x that represents the system state. The small signal stability of the model can be computed by linearizing (2.1), finding a linear discrete state space model (depicted in Figure 2-2(c)) which relates the perturbed outputs $\tilde{v}$ to a small variation on input variables ($\tilde{u}$ or $\widetilde{\Phi}$) in the form:

$$\tilde{x}((k+1)T_s) = \widehat{\Psi} \cdot \tilde{x}(kT_s) + \hat{\Gamma}(k) \cdot \begin{pmatrix} \widetilde{\Phi}(kT_s) \\ \tilde{u}(kT_s) \end{pmatrix}$$
$$\tilde{v} = \widehat{\Sigma}(k) \cdot \tilde{x}(kT_s))$$

<div align="right">(2.2)</div>

where, for the reason previous said, $\widehat{\Sigma}(k)$ is the identity matrix. However (2.2) is time-varying: to write the model in a more useful time invariant form often a direct-quadrature frame is used, because the variables with sinusoidal evolution are transformed in constant ones in d-q frame, making easier the small signal analysis. Finally, LTI discrete-time model (shown in Figure 2-2(d)) has the form:

$$\tilde{x}((k+1)T_s) = \Psi \cdot \tilde{x}(kT_s) + \Gamma \cdot \begin{pmatrix} \widetilde{\Phi}(kT_s) \\ \tilde{u}(kT_s) \end{pmatrix}$$
$$\tilde{v} = \Sigma \cdot \tilde{x}(kT_s), \quad with \ \Sigma = I$$

<div align="right">(2.3)</div>

which is consistent with the canonical form for the LTI discrete-state space model demonstrated in Section I.16 of Appendix I and where Ψ, Γ and Σ are consequently time invariant matrices.

input   system   output

(a) Non-linear model

$u(t)$

$\Phi(t)$

$f\big(x(t), u(t), \Phi(t)\big)$

$v(t)$

(b) Non-linear sampled-data model

$u(kT_s)$

$\Phi(kT_s)$

$H\big(x(kT_s), u(kT_s), \Phi(kT_s)\big)$

$v\,(kT_s)$

(c) Linear time-varying sampled-data model

$\tilde{u}(kT_s)$

$\widetilde{\Phi}(kT_s)$

$\hat{\Gamma}(k)$ $+$ z^{-1} $\hat{\Sigma}(k)$ $\tilde{v}\,(kT_s)$

$\widehat{\Psi}$

(d) LTI discrete-time state space model

$\tilde{u}(kT_s)$

$\widetilde{\Phi}(kT_s)$

Γ $+$ z^{-1} Σ $\tilde{v}\,(kT_s)$
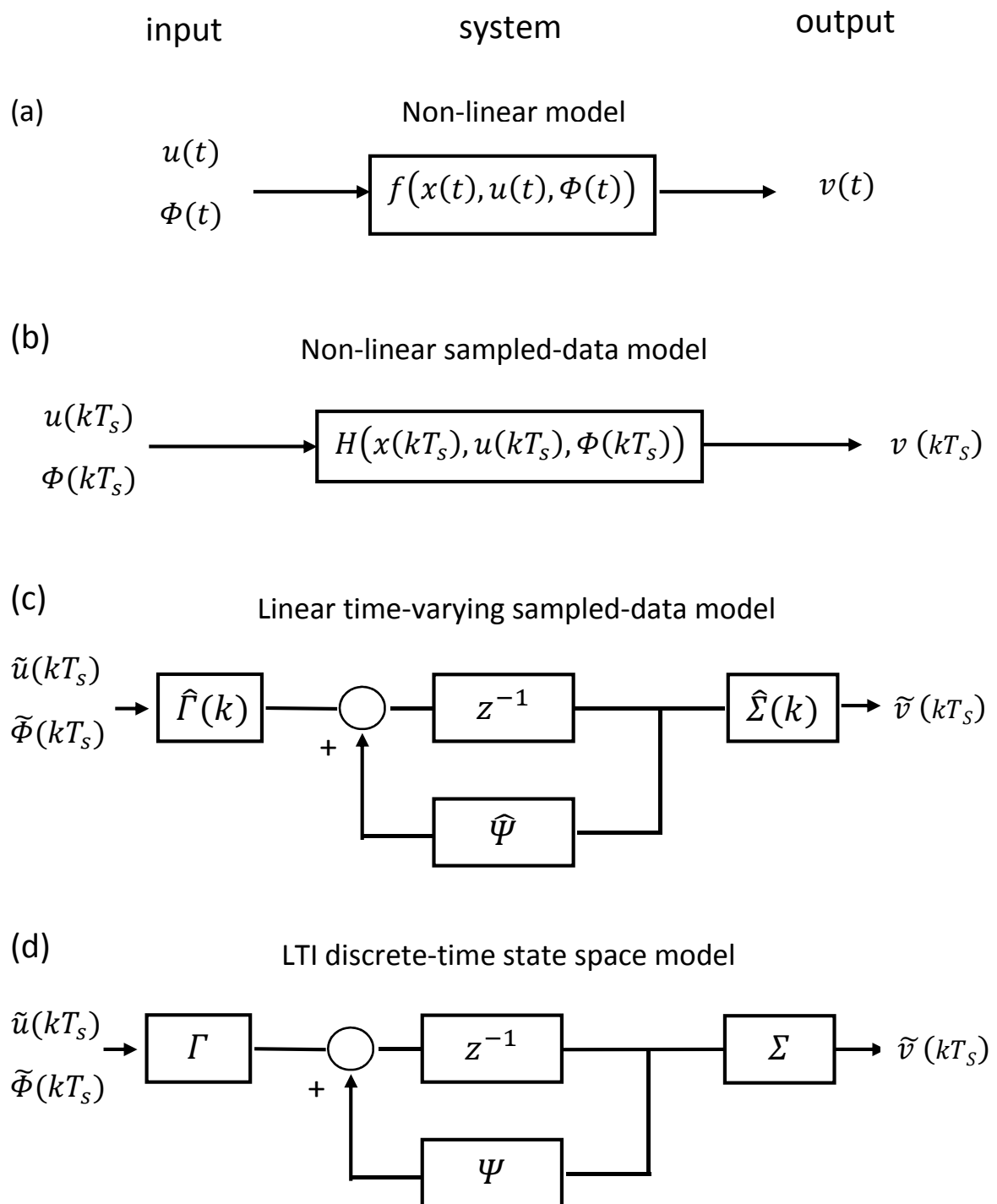
Ψ

Figure 2-2 (a) Nonlinear model of the static switching circuit (b) Non-linear sampled-data model (c) linear time-varying sampled-data model relating perturbed quantities (d) LTI discrete-time state space model relating perturbed quantities

It is highlighted that the main difficulty to create a non-linear model in the discrete form is the change in circuit topology with the thyristor transitions. Indeed, it has been overcome identifying inside a sampling time some intervals where the topology of the circuit remains constant and defining projection and injection matrices (see Appendix I.1) that relate together state variables before and after a thyristor switching. In this way it's possible to relate state variables through a sampling period, building a non-linear Poincarè Map. Finally, to carry out small signal analysis, it is necessary to linearize the previous model, which is intrinsically non-linear, because of the uncontrolled nature of thyristor turn-off, due to its dependence on the circuit evolution. However it's possible to demonstrate (see Appendix I.2.2) that this dependence doesn't directly affect the state variables evaluated at the sampling instants. This allows neglecting it, finding a linear discrete time model in the form (2.2).

2.2   System modeling

As it has already been presented in Chapter 1.4, ITER Static Var Compensation System is composed by the Tuned Filters and TCR subsystem and it is one of the main components of the ITER power supply system. For this reason, it has been studied here through the analytical approach described in the previous chapter that respect the discrete time operation of such switching circuit. Some simplifications have been assumed. The Tuned filter subsystem (depicted in Figure 1-6) is considered with an equivalent capacitance C_r at grid frequency f. It has been calculated from the total reactive power given by all Tuned filter subsystem and the RMS supply voltage, according to the formula $C_r = Q/(\omega U_s{}^2)$. This simplification allows to represet ITER Pulsed Power Electrical Network previous presented as in Figure 2-3. It is considered an equivalent supply power busbar characterized by global average parameters of the three ones to take into account the voltage drop in each of them. Moreover, resistance line is not considered and the ac/dc conversion system is neglected, obtaining an equivalent SVC system that has been studied in this thesis by the discrete-time analytical approach. Hence a simple Static Var Compensation system (Figure 2-3) is obtained in order to analyze deeply the TCR subsystem in different operating modes, defined by fixed TCR conduction angle, so that the control system of the TCR is not included in the model.

Following there are the parameters used in the analysis:

- $U_s = 66$ kV (RMS phase-to-phase voltage)

- $L_s = 8.278$ mH

- $C_r = 183\ \mu F$

- $L_r = 112.17$ mH (delta-connected TCR)
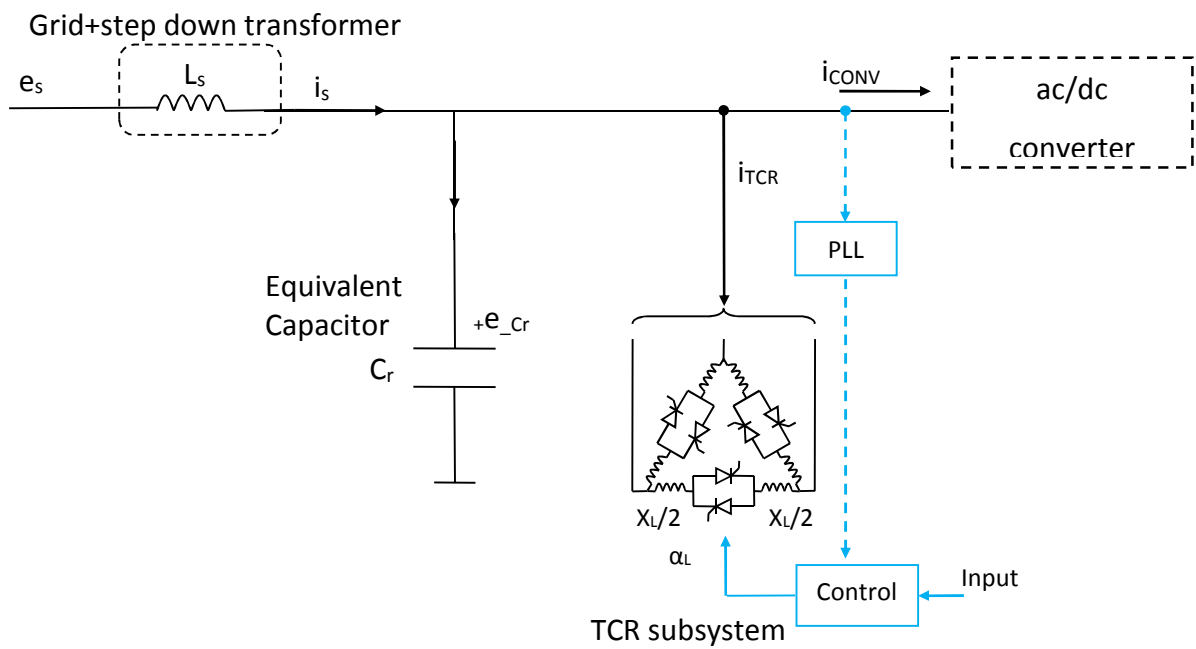
- $f = 50\ Hz$ (grid frequency)

Figure 2-3 Simplified SVC system composed by TCR subsystem and an equivalent capacitor. Note that the connection of the control system of TCR is in dashed line because it is not considered in this study.

3 Discrete-time model of a TCR in SVC application

The goal of this thesis is to develop a linear, time-invariant (LTI) discrete state space model of the simplified SVC system of ITER shown in the Figure 2-3. It is highlighted that the TCR is three-phase in delta configuration, while in literature the analysis of the TCR are limited to the single-phase or three-phase in star configuration. Therefore a step-by-step approach has been chosen: in this chapter the models of the single phase and three phase star configuration of the TCR have been investigated, while in the next chapter the model of the simplified SVC system has been developed for the delta-configuration and in particular applied to the ITER case.

In this chapter the conduction angle of the TCR is assumed to be less than 60°, so there is always a time interval with all the thyristors off.

All the models derive from a linearization around an operating point, therefore a nominal steady-state solution is required a priori, and, in this case, it is given by a numerical simulation (i.e. PSIM).

3.1 *System modelling of the single-phase SVC*

Considering the single-phase SVC depicted in Figure 3-1(a), when either thyristor conducts the circuit has state vector:

$$x = (i_s \quad v_c \quad i_r)^t \qquad (3.1)$$

where i_s is the line current in the inductor L_s, v_c is the voltage in the capacitor and i_r is the current in the inductor of the TCR, the system dynamics is described by:

$$\dot{x} = Ax + Bu_s \qquad (3.2)$$

where:

$$A = \begin{bmatrix} 0 & -L_s^{-1} & 0 \\ C_r^{-1} & 0 & -C_r^{-1} \\ 0 & -L_r^{-1} & 0 \end{bmatrix} \qquad B = \begin{bmatrix} -L_s^{-1} \\ 0 \\ 0 \end{bmatrix} \text{The}$$

$$i_r = cx = (0 \quad 0 \quad 1)x = 0 \qquad (3.3)$$

22

The injection and projection matrices (for more details see Section I.1 in the Appendix I) associated with either thyristor are

$$Q = \begin{bmatrix} 1 & 0 \\ 0 & 1 \\ 0 & 0 \end{bmatrix} \qquad P = Q' \qquad\qquad (3.4)$$

Thus, in nonconduction mode ($i_r = 0$) the system state vector consists of the source current i_s and the capacitor voltage v_r

$$y = Px = \begin{bmatrix} i_s \\ v_r \end{bmatrix} \qquad\qquad (3.5)$$

with system dynamics described by

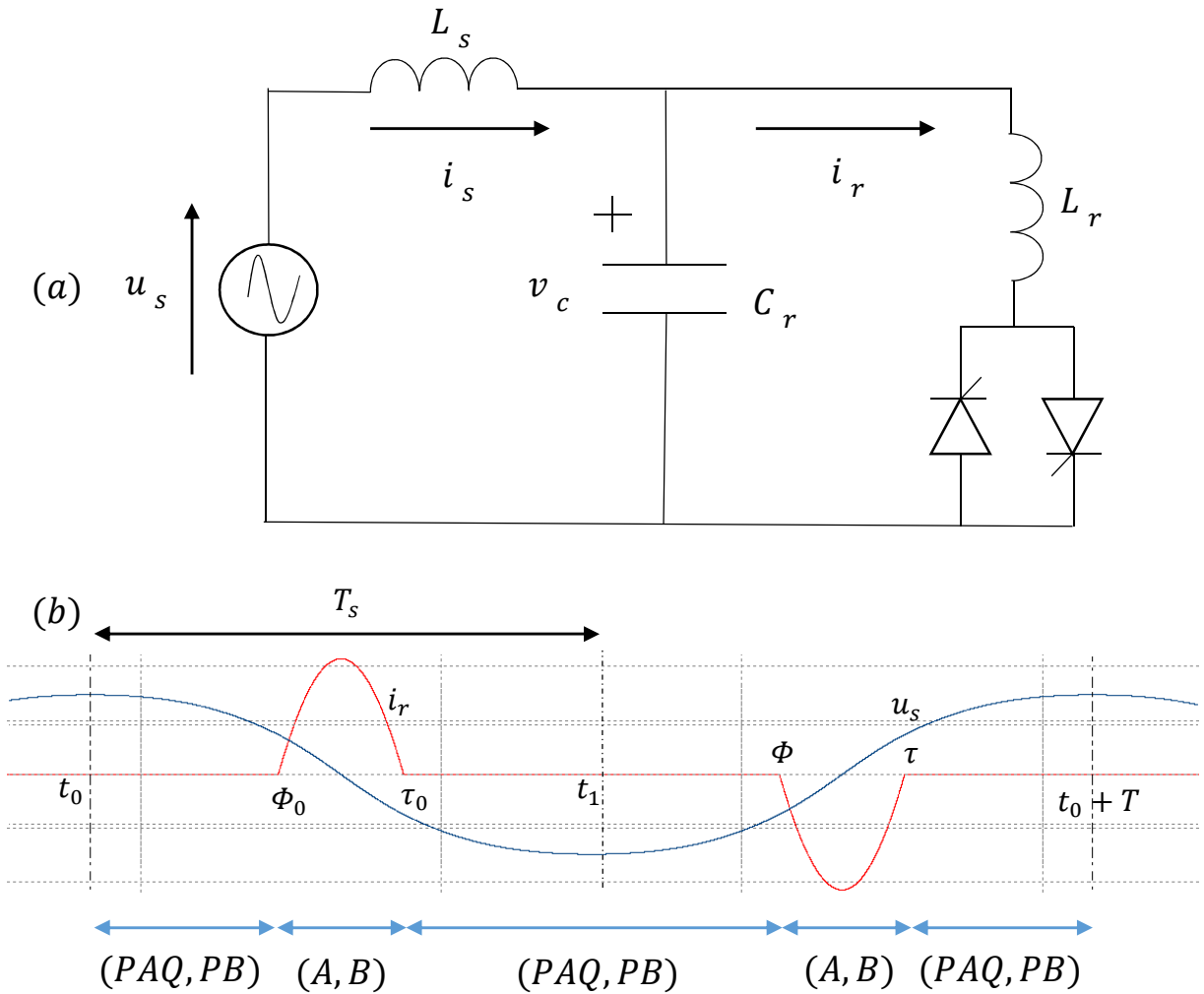$$\dot{y} = PAQy + PBu_s \qquad\qquad (3.6)$$

Figure 3-1 Single-phase SVC system (a) circuit diagram (b) system dynamics over one period

Figure 3-1(b) describe the system dynamics as the circuit state evolves over a period. A conduction mode described by (3.2) begins at instant Φ and ends when the thyristor current goes through zero at instant $\tau = \Phi + \sigma_t$, where σ_t is the conduction angle associated with the conduction mode (expressed in time unit, taking into account the equivalence between electrical degree and time given by $\vartheta = \omega t$, with ω equal to the angular frequency of the period). The non-conduction mode described by (3.6) follows the conduction mode and continues until the next firing pulse is applied and an analogous on-off cycle begins.

3.1.1 Single phase non-linear model

If it is defined $W_a(t) = (cos\omega t \quad sen\omega t)$, the source voltage $u_s(t)$ (sinusoidal with period T) may be written:

$$u_s(t) = W_a(t) \cdot u_{dq}, \quad u_{dq} = \begin{pmatrix} u_d \\ u_q \end{pmatrix}$$

(3.7)

where u_d and u_q are the direct and quadrature voltages respectively for a given reference frame. In Figure 3-1(b) $u_s(t)$ is shown. The representation of the state at thyristor turn-on and turn-off are

$$x(\Phi^+) = Qy(\Phi^-) \quad \text{and} \quad y(\tau^+) = Px(\tau^-)$$

(3.8)

respectively. As discussed in Section I.1, injection matrix Q allows changing state vector at a thyristor turn-on (including also the thyristor current), while projection matrix P modifies the state vector x of the conducting mode into a new one y in which thyristor current is not considered (because after the switching-off, thyristor current is zero). On the assumption that u_{dq} is constant over the first cycle $T_s = \dfrac{T}{2} = \dfrac{\pi}{\omega}$, the Poincarè map projects the system state through a sample period T_s

$$H: \quad y(kT_s) \to y((k+1)T_s)$$

(3.9)

It is obtained by considering separately each phase of operation inside a sampling period T_s, starting from t_0 (where the system is at steady state operation with state vector y_0) choosen as the positive maximum of $u_s(t)$ (see Figure 3-1(b)): firstly, equation (3.6) is integrating, finding state vector $y(\Phi)$ at turn-on instant. Then the integration of equation (3.2) allows to find state

vector $x(\tau)$ at turn-off instant, starting from $x(\Phi)$, computed as in (3.8). Finally the mode of operation of first phase is repeted to find the state vector after a sampling period $y(T_s)$ from the previous calculation of $y(\tau)$, as in (3.8).

The sequence of the formulas used has been summarized as follows:

$$y(\Phi) = e^{PAQ\,\Phi}y_0 + \int_0^\Phi e^{PAQ\,(\Phi-\xi)}PB\,W_a(\omega\xi)d\xi u_{dq}$$

$$x(\Phi) = Qy(\Phi)$$

$$x(\tau) = e^{A(\tau-\Phi)}x(\Phi) + \int_\Phi^\tau e^{A(\tau-\xi)}B\,W_a(\omega\xi)d\xi u_{dq} \qquad (3.10)$$

$$y(\tau) = Px(\tau)$$

$$y(T_s) = e^{PAQ\,(T_s-\tau)}y(\tau) + \int_\tau^{T_s} e^{PAQ\,(T_s-\xi)}PB\,W_a(\omega\xi)d\xi u_{dq}$$

Relations in (3.10) are written for a generic instant of thyristor turn-on Φ and turn-off τ. From the fist one of (3.10) it's possible to substitute each relation inside the next one, obtaining the non- linear Poincarè Map over a general sample period, which relates $y(T_s)$ to y_0 as follows:

$$y(T_s) = e^{PAQ\,(T_s-\tau)}Pe^{A(\tau-\Phi)}Qe^{PAQ\,\Phi} \cdot y_0 + h(\Phi, u_{dq}) \qquad (3.11)$$

where

$$h(\Phi, u_{dq}) = e^{PAQ\,(T_s-\tau)}P$$

$$\cdot \left\{ e^{A(\tau-\Phi)}Q \int_0^\Phi e^{PAQ\,(\Phi-\xi)}PB\,W_a(\xi)d\xi u_{dq} \right.$$

$$\left. + \int_\Phi^\tau e^{A(\tau-\xi)}B\,W_a(\xi)d\xi u_{dq} \right\} + \int_\tau^{T_s} e^{PAQ\,(T_s-\xi)}PB\,W_a(\xi)d\xi u_{dq}. \qquad (3.12)$$

Continuing with the above integration over some cycles, it's highlighted that $W_a(t + kT_s) = (-1)^k \cdot W_a(t)$. So, the non-linear model of the system at steady state can be succinctly expressed

$$y((k+1)T_s) = H\left(y(kT_s), \Phi(kT_s), u_{dq}(kT_s)\right)$$

$$= e^{PAQ\,(T_s-\tau)}Pe^{A(\tau-\Phi)}Qe^{PAQ\,\Phi} \cdot y(kT_s) + (-1)^k$$

$$\cdot h\left(\Phi(kT_s), u_{dq}(kT_s)\right) \qquad (3.13)$$

3.1.2 Single-phase linear model

In order to investigate small signal stability of the system, it is necessary to linearize (3.13) to a first order approximation, under the assumption that the inputs u_{dq} and Φ are constant over the sampling period T_s. Indeed, considering a perturbation from the nominal steady-state solution given in (3.11), the perturbed inputs and outputs (denoted with tilde) at the generical cycle can be related by a linear model expressed according (3.13):

$$\tilde{y}((k+1)T_s) = \Psi \cdot \tilde{y}(kT_s) + (-1)^k \cdot \left\{ \Gamma_\Phi \tilde{\Phi}(kT_s) + \Gamma_u \, \breve{u}_{dq}(kT_s) \right\} \qquad (3.14)$$

Matrix Ψ represents the Jacobian $\dfrac{\partial H}{\partial y_0}$ of the Poincarè map (3.11) rewritten considering the steady-state conduction angle $\sigma_t = \tau - \Phi$, hence:

$$\Psi = \frac{\partial H}{\partial y_0} = e^{PAQ\,(T_s-\sigma_t)/2} P e^{A\sigma_t} Q e^{PAQ(T_s-\sigma_t)/2} \qquad (3.15)$$

Now differentiating (3.12) with respect to the firing instant (as it is reported in Section I.2.1), always considering the steady-state conduction angle σ_t.

$$\Gamma_\Phi = \frac{\partial H}{\partial \Phi}\bigg|_{\Phi_0} = \frac{\partial h(\Phi, u_{dq})}{\partial \Phi}\bigg|_{\Phi_0} = e^{PAQ\frac{T_s-\sigma_t}{2}} P e^{A\sigma_t}\{Q\dot{y}(\Phi_0) - Ax(\Phi_0) - Bu_s(\Phi_0)\}$$

$$= e^{PAQ\frac{T_s-\sigma_t}{2}} P e^{A\sigma_t}\{QP - I\}\dot{x}(\Phi_0) = -e^{PAQ\frac{T_s-\sigma_t}{2}} P e^{A\sigma_t} c^t c \dot{x}(\Phi_0) \qquad (3.16)$$

where $\{QP - I\} = c^t c$ from the properties of projection and injection matrices. Note that $c\dot{x}(\Phi)$ is the gradient of the thyristor current at turn-on. Finally,

$$\Gamma_{u\_d} = \frac{\partial H}{\partial u_{dq}} = \frac{\partial h(\Phi_0, u_{dq})}{\partial u_{dq}} = h(\Phi_0, u_{dq}), \, with \, u_{dq} = \begin{pmatrix} 1 \\ 0 \end{pmatrix} \qquad (3.17)$$

26

$$\Gamma_{u\_q} = \frac{\partial H}{\partial u_{dq}} = \frac{\partial h(\Phi_0, u_{dq})}{\partial u_{dq}} = h(\Phi_0, u_{dq}), with\ u_{dq} = \begin{pmatrix} 0 \\ 1 \end{pmatrix}$$

3.1.3 Single-phase case study

The equivalent single phase system of the one reported in Chapter 2.2 has been considered:

$$L_s = 8.278\ mH\ , \qquad C_r = 183\ \mu F, \qquad L_{r\_star} = \frac{L_r}{3} = 37.3913\ mH \qquad (3.18)$$

The dq frame has been synchronized in order to obtain the peak voltage in the d axis, and it yields:

$$U_d = \sqrt{\frac{2}{3}} U_s = \sqrt{\frac{2}{3}} 66000 = 53{,}889\ kV$$

$$U_q = 0$$

Table 3-1 depicts the parameters of the discrete state space model of (3.14) obtained for steady-state operating points corresponding to a conduction angle of the TCR $\sigma_d = 15°, 30°, 45°$ and their associated characteristic multipliers. Note that the damping (characterized by the magnitude of the characteristic multiplier) increases significantly as the steady-state conduction angle is increased.

Table 3-1 Single-phase SVC linear model parameters and associated characteristic multipliers

σ	Ψ		Γ_Φ	$\Gamma_u = (\Gamma_{u\_d}\quad \Gamma_{u\_q})$	
15°	$\begin{pmatrix} -0.2421 & -0.1396 \\ 6.3137 & 0.2905 \end{pmatrix}$		$\begin{pmatrix} 1.1370e+05 \\ -5.7794e+05 \end{pmatrix}$	$\begin{pmatrix} 0.1638 & 0.05749 \\ -0.8326 & 0.3865 \end{pmatrix}$	
30°	$\begin{pmatrix} -0.1991 & -0.1295 \\ 5.8601 & -0.3669 \end{pmatrix}$		$\begin{pmatrix} 4.4129e+05 \\ -2.1567e+06 \end{pmatrix}$	$\begin{pmatrix} 0.1500 & 0.07486 \\ -0.7334 & 0.2296 \end{pmatrix}$	
45°	$\begin{pmatrix} -0.1879 & -0.1166 \\ 5.2742 & -0.4823 \end{pmatrix}$		$\begin{pmatrix} 9.2298e+05 \\ -4.0978e+06 \end{pmatrix}$	$\begin{pmatrix} 0.1301 & 0.09072 \\ -0.5777 & -0.006907 \end{pmatrix}$	

σ	Characteristic multiplier
15°	$-0.266 \pm 0.938i$
30°	$-0.283 \pm 0.867i$
45°	$-0.335 \pm 0.770i$

Figure 3-2 depicts the locus of characteristic multipliers of Ψ with respect to the conduction angle $\sigma \epsilon (0, 60°)$: all of them are inside the unit circle so, from the theory of discrete state space systems (reported in Section II) the system is asymptotically stable.
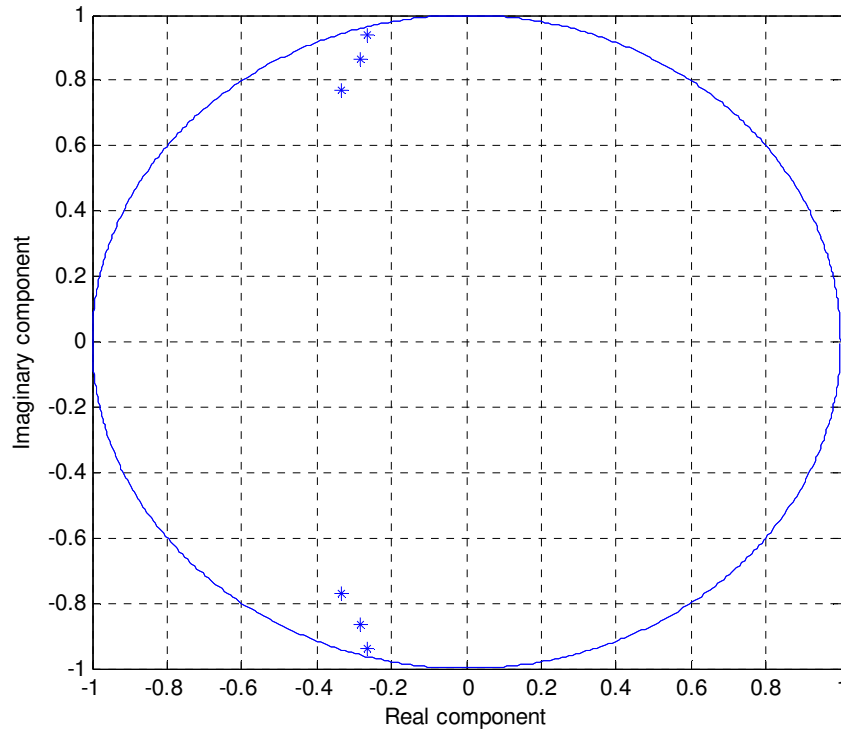

Figure 3-2 Locus of the characteristic multipliers of the Jacobian Ψ with different conduction angles

Figure 3-3, Figure 3-4 and Figure 3-5 show the sampled perturbed capacitor voltage $\tilde{V}_c$ and line current $\tilde{I}_s$, after that a +0.1° step change (sincronized with the maximum of voltage source being a sampling instant) has been applied to the firing angle at $t = 1,605s$, when the system is in steady-state operation for the three different conduction angle of the TCR, $\sigma_d = 15°, 30°, 45°$ respectively. It may be noted a good agreement between the waveforms at the sampled instants obtained by the linear discrete state space model (blue line) and PSIM (green line) for $\sigma_d = 30°$ and $\sigma_d = 45°$, while it is not so good for $\sigma_d = 15°$ because probably the conduction angle is too little, even if it is compatible with numerical errors.
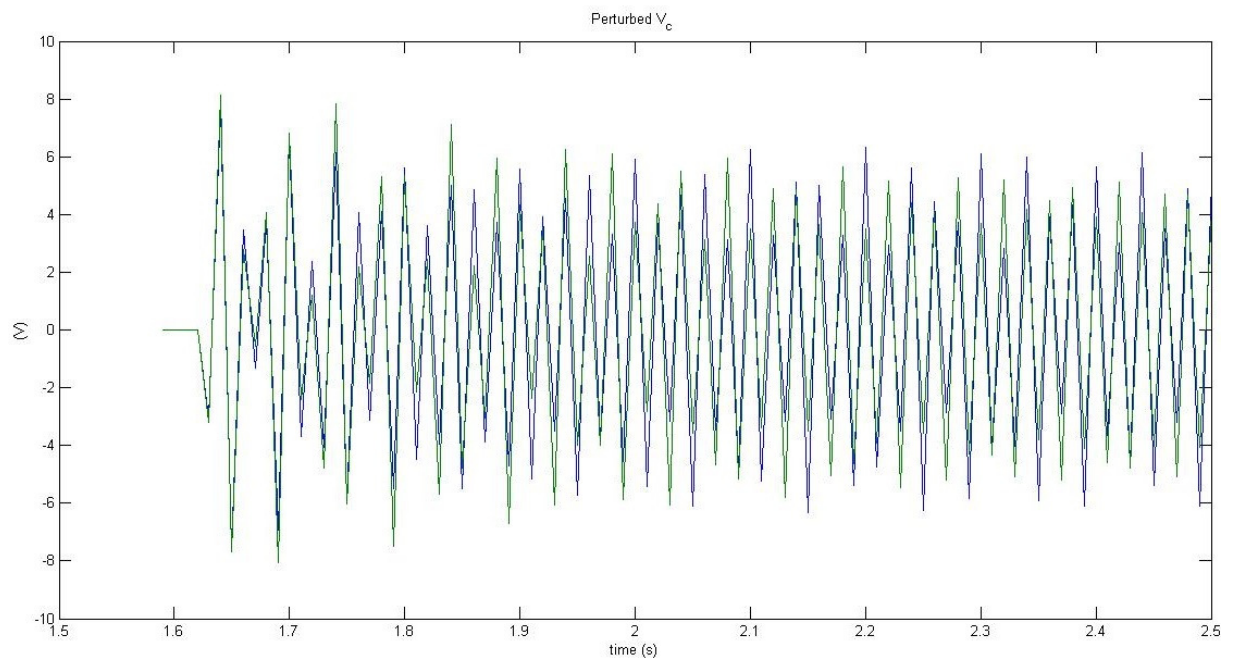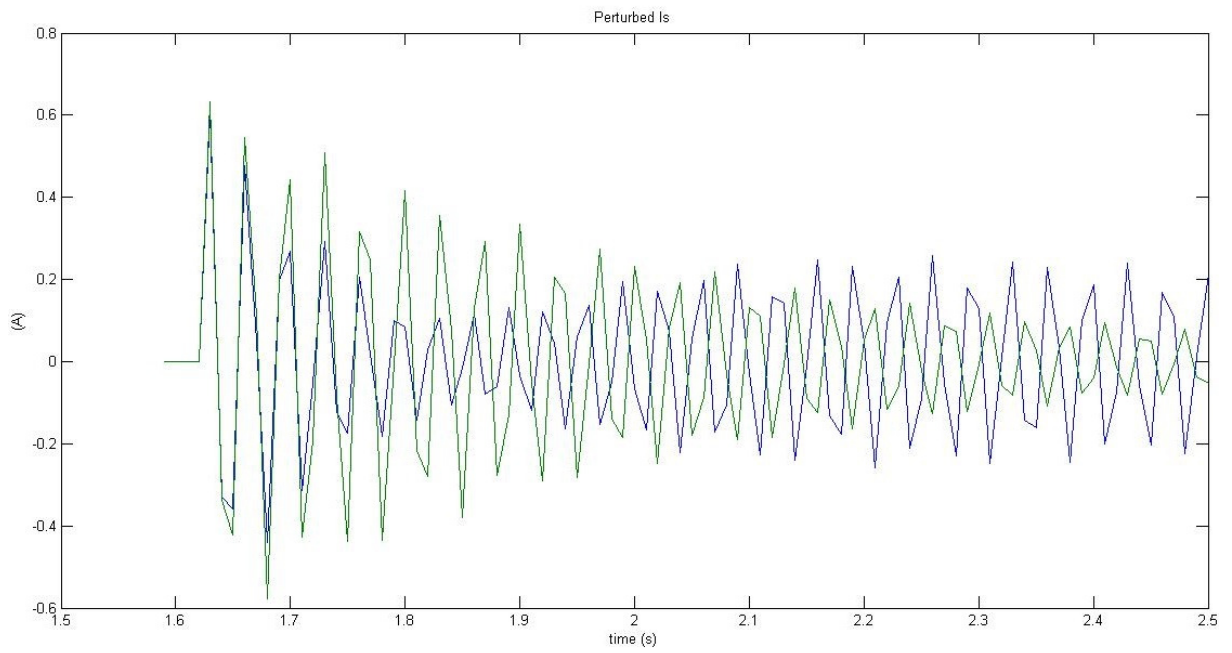
Figure 3-3. Perturbed line current Is and capacitor voltage Vc to a +0.1° step change in the firing angle for σ = 15°. Green line for PSIM model and blue line for linear one.

Figure 3-4 Perturbed line current Is and capacitor voltage Vc to a +0.1° step change in the firing angle for σ = 30°. Green line for PSIM model and blue line for linear one.

Figure 3-5 Perturbed line current Is and capacitor voltage Vc to a +0.1° step change in the firing angle for σ = 45°. Green line for PSIM model and blue line for linear one.

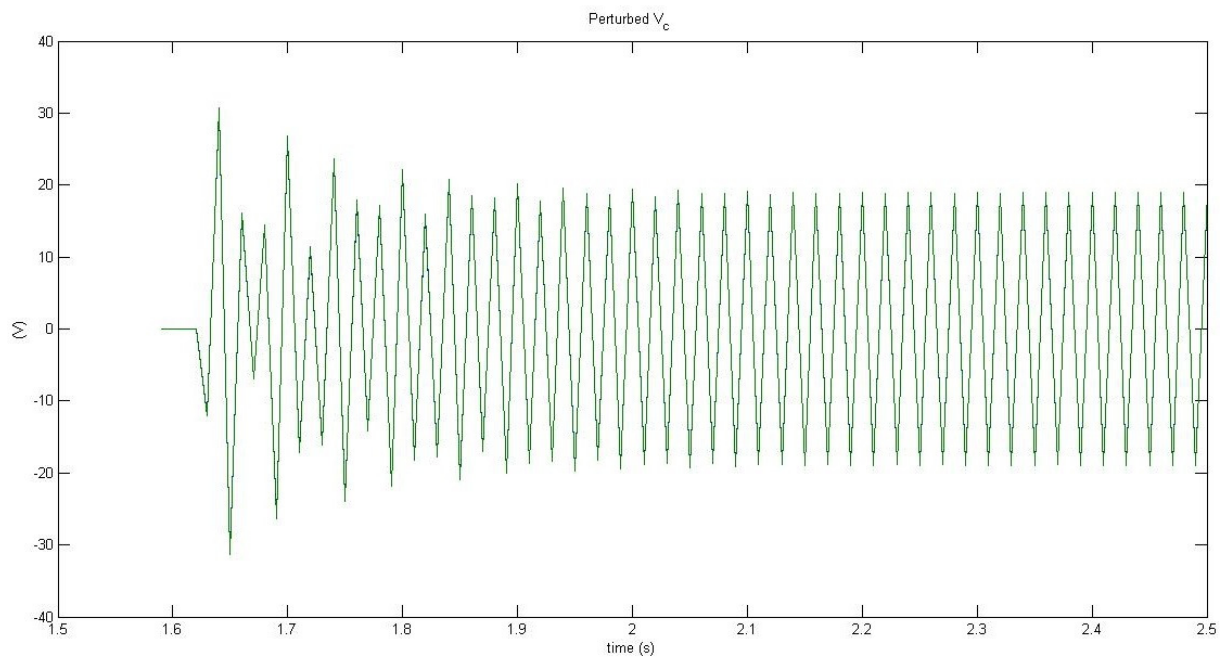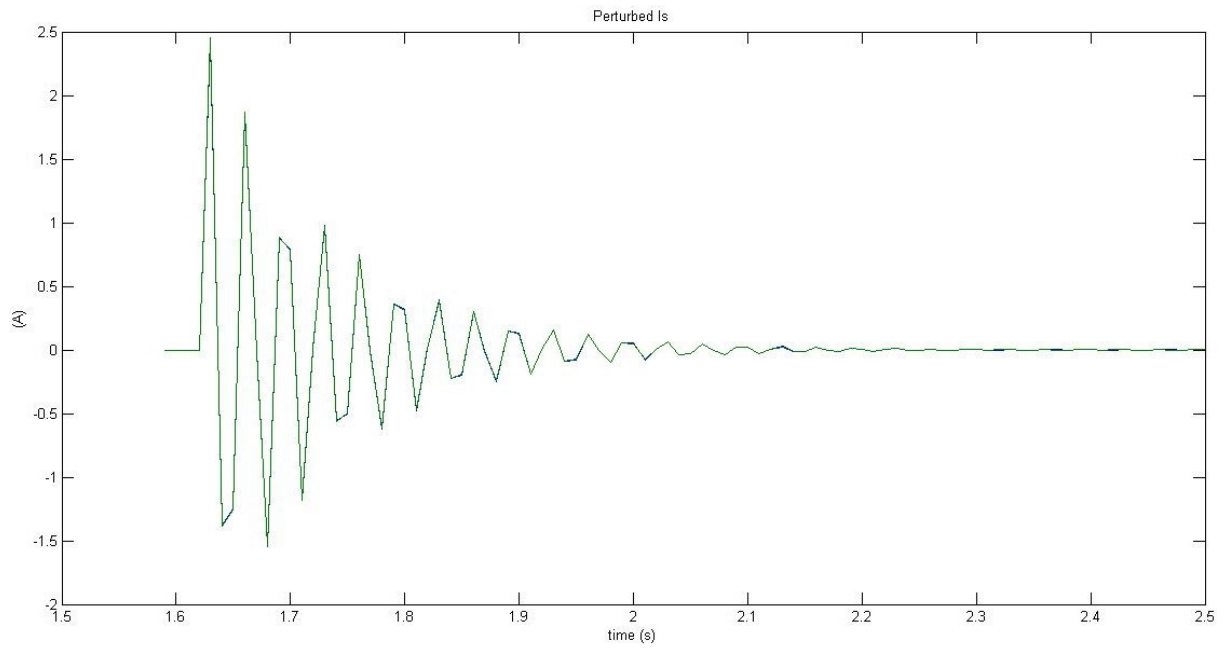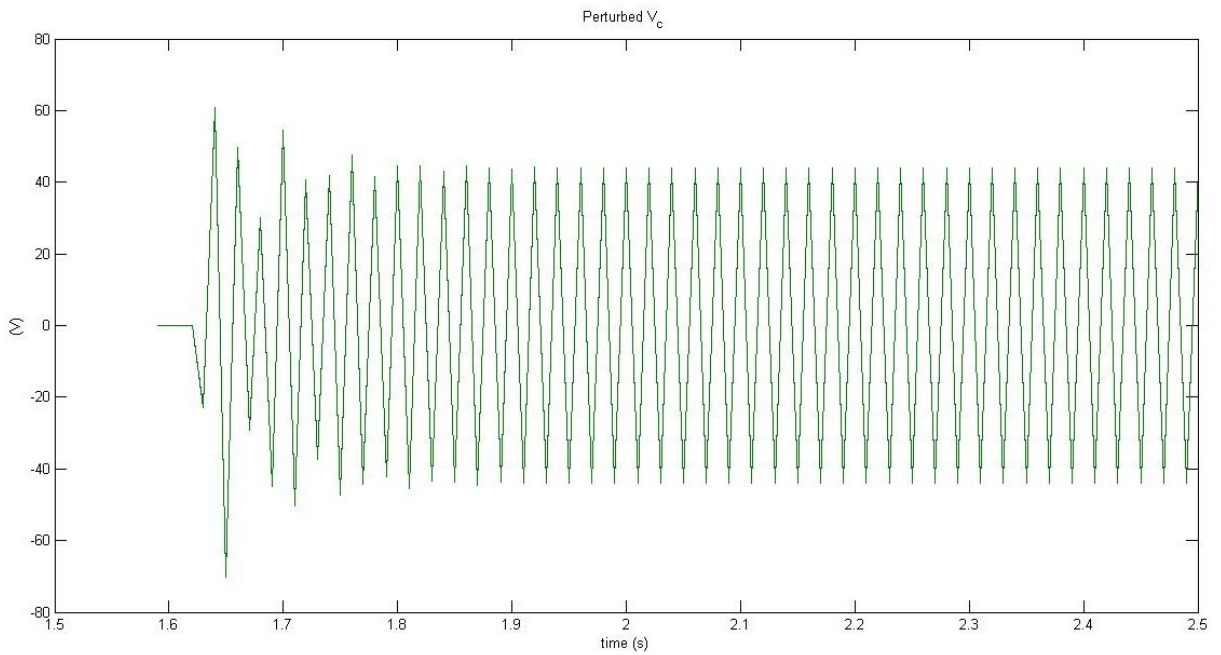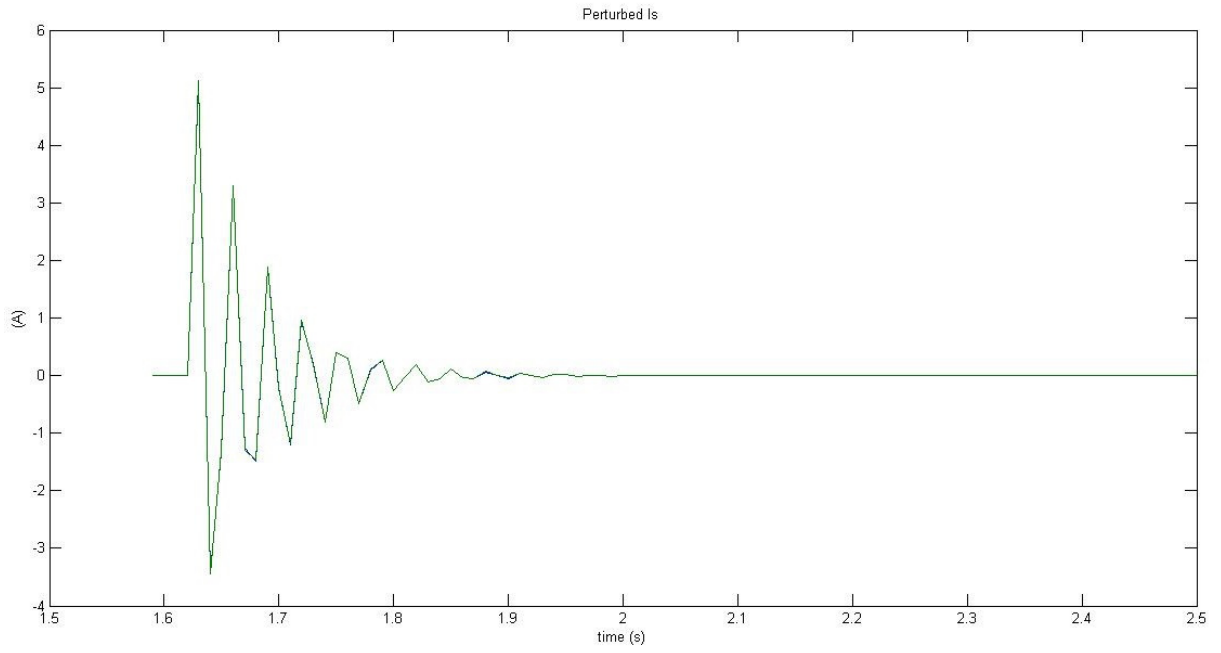Figure 3-6, Figure 3-7, and Figure 3-8 show the sampled perturbed capacitor voltage $\tilde{V}_c$ and line current $\tilde{I}_s$, after that a +1% step change has been applied in peak voltage along d-axis at $t = 1,605s$ at the maximum of voltage source, when the system is in steady-state operation for the three different conduction angle of the TCR, $\sigma_d = 15°, 30°, 45°$ respectively. Our expectations have been confimed: there is a good agreement between the waveforms at the sampled instants obtained by the linear discrete state space model (blue line) and PSIM (green line) in all the three modes of operation of the TCR. Now, focus on Figure 3-7 and Figure 3-8 and in particular on the behavior of $\tilde{V}_c$: it reaches a new steady-state operation, consistent with the magnitude of the perturbation applied. This occurs also for $\tilde{I}_s$: it is not visible in Figure 3-7 because of the scale of y axis that is choosen to show the whole transient associated to the perturbation applied, while it is just visible in Figure 3-8, at the end of the transient. At steady-state operation both perturbed quantities changed in sign at each sampling time due to the fact that a single-phase SVC is studied.

Figure 3-6 Perturbed line current Is and capacitor voltage Vc to a +1% step change in peak voltage along d-axis for σ = 15°. Green line for PSIM model and blue line for linear one.

Figure 3-7 Perturbed line current Is and capacitor voltage Vc to a +1% step change in peak voltage along d-axis for σ = 30°. Green line for PSIM model and blue line for linear one.

Figure 3-8 Perturbed line current Is and capacitor voltage Vc to a +1% step change in peak voltage along d-axis for $\sigma = 45°$. Green line for PSIM model and blue line for linear one.

The following Figure 3-9, Figure 3-10 and Figure 3-11 show the sampled perturbed capacitor voltage $\tilde{V}_c$ and line current $\tilde{I}_s$, after that a +1% step change has been applied in peak voltage along q-axis at $t = 1,605s$ at the maximum of voltage source, when the system is in steady-state operation, for the three different conduction angle of the TCR, $\sigma_d = 15°, 30°, 45°$ respectively. Also in this case our expectations have been confimed: there is a good agreement between the waveforms at the sampled instants obtained by the linear discrete state space model (blue line) and PSIM (green line) in all the three modes of operation of the TCR. Now, focus on Figure 3-10 and 3-11: here it is more explicit that both perturbed variables reach a new steady-state operation, consistent with the magnitude of the perturbation applied. At steady-state operation both perturbed quantities changed in sign at each sampling time due to the fact that a single-phase SVC is studied.
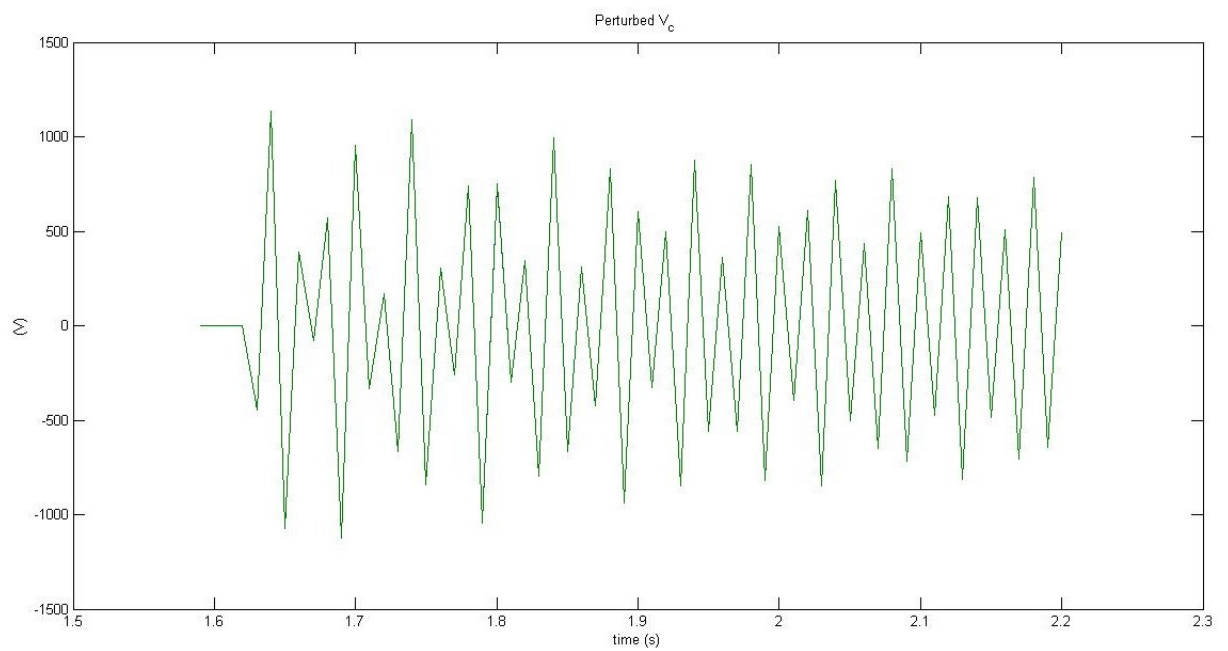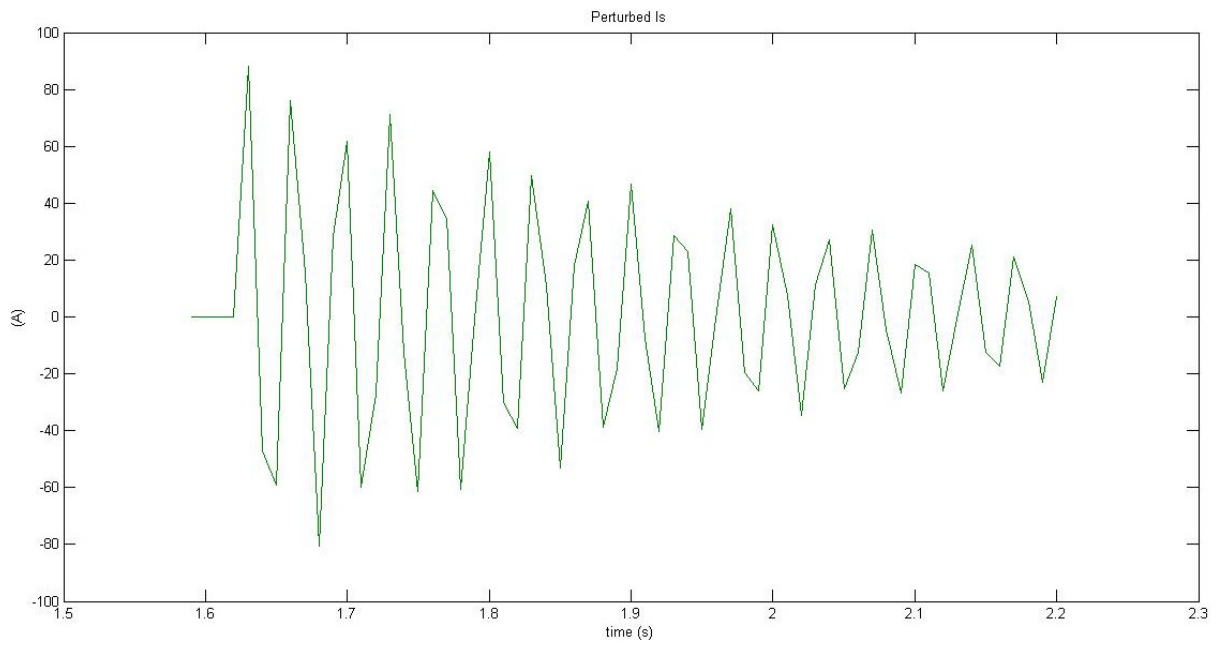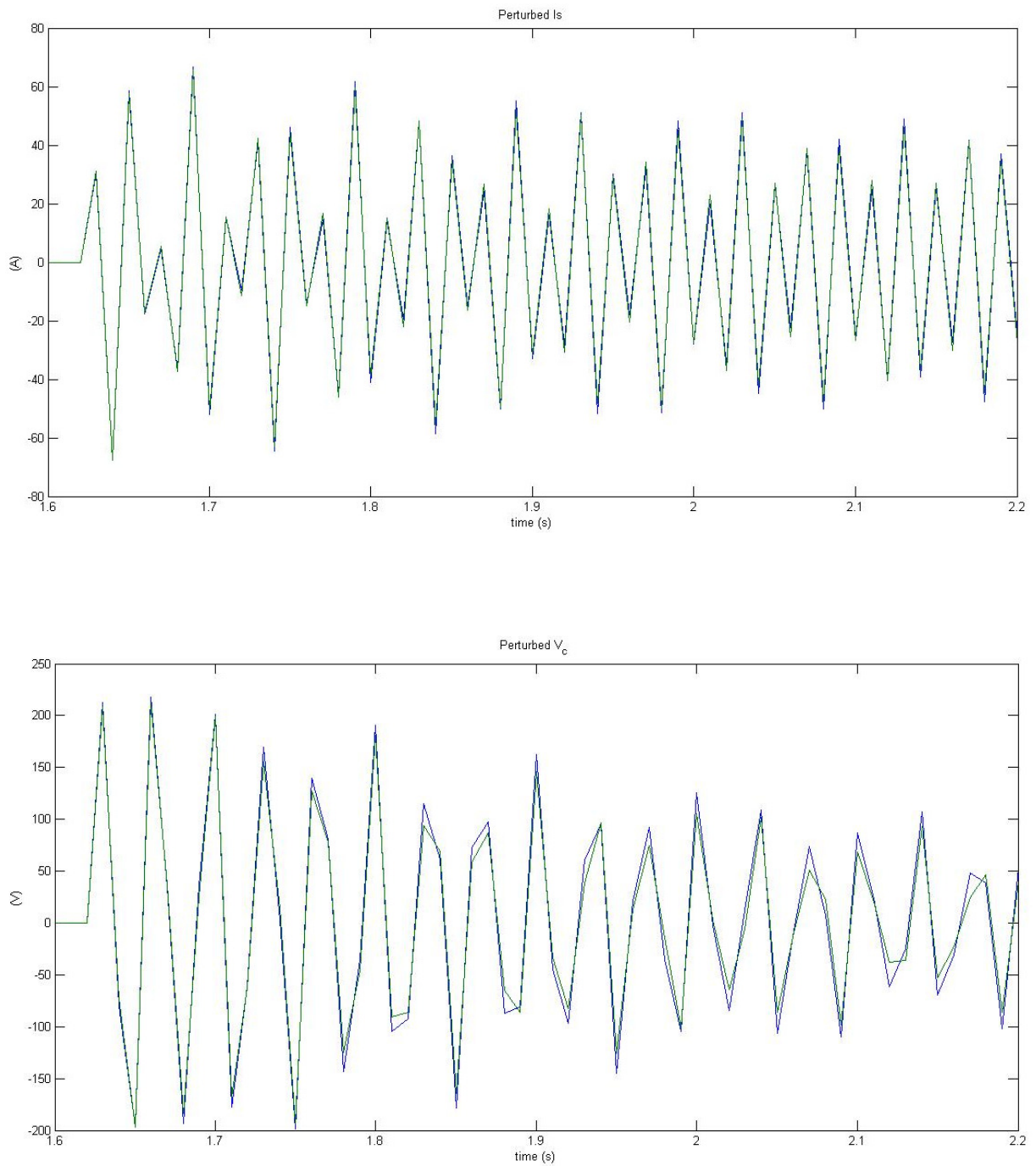
Figure 3-9 Perturbed line current Is and capacitor voltage Vc to a +1% step change in peak voltage along q-axis for $\sigma = 15°$. Green line for PSIM model and blue line for linear one.
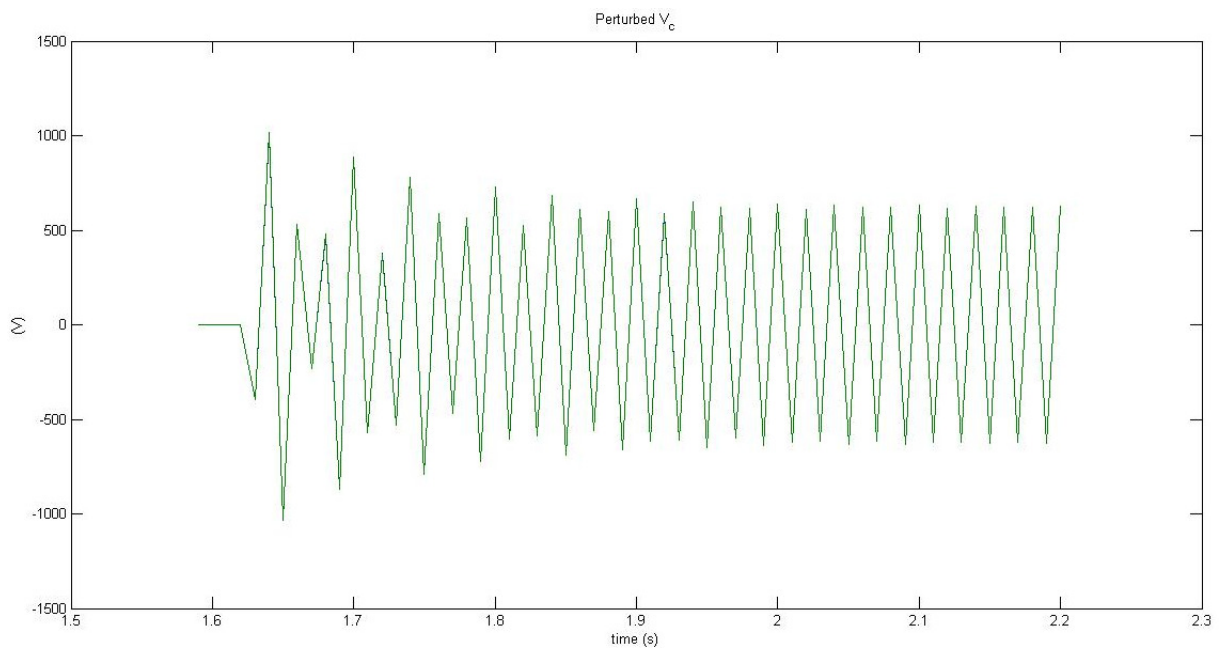
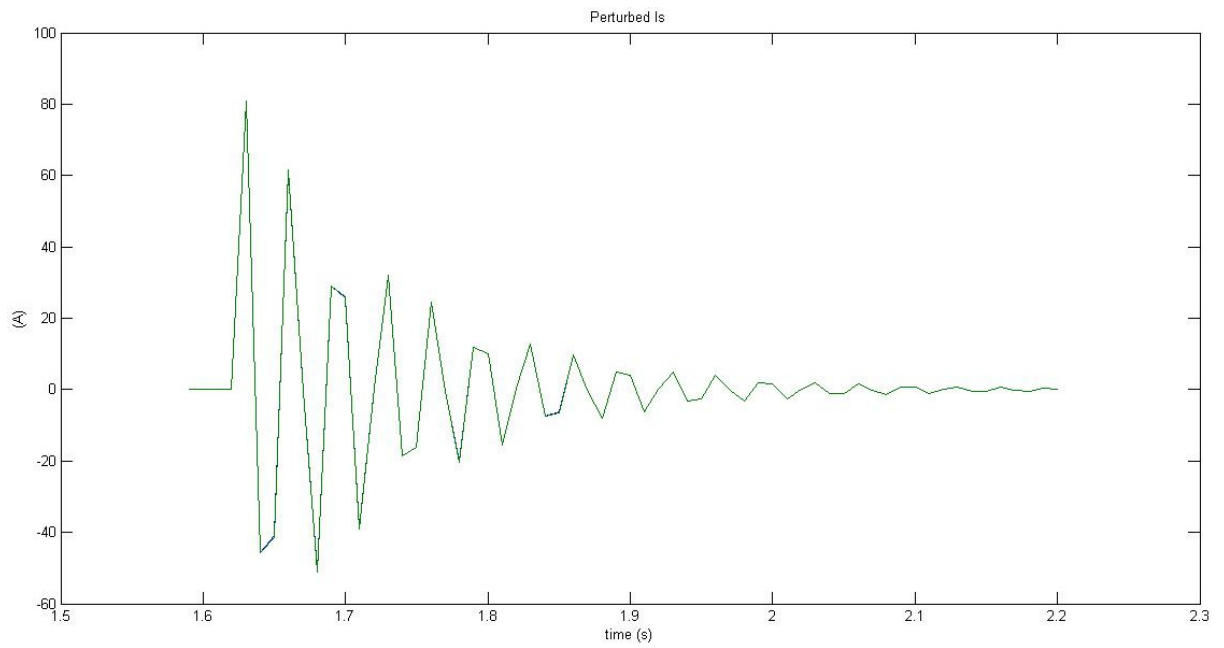*Figure 3-10 Perturbed line current Is and capacitor voltage Vc to a +1% step change in peak voltage along q-axis for $\sigma = 30°$. Green line for PSIM model and blue line for linear one.*
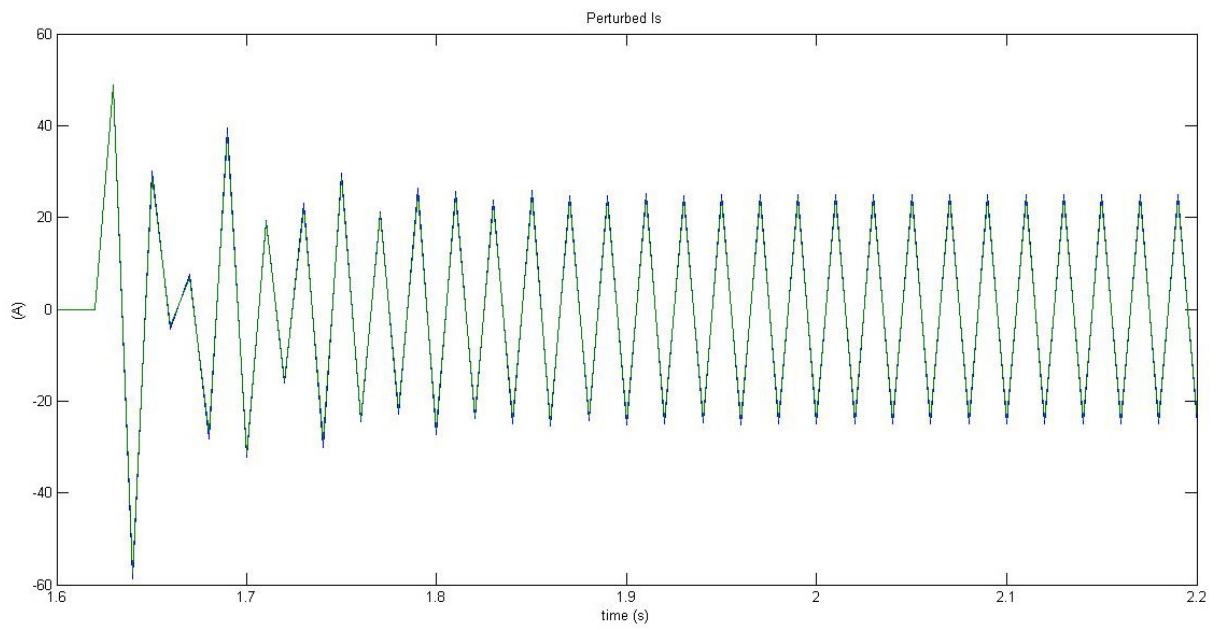
Figure 3-11 Perturbed line current Is and capacitor voltage Vc to a +1% step change in peak voltage along q-axis for $\sigma = 45°$. Green line for PSIM model and blue line for linear one.

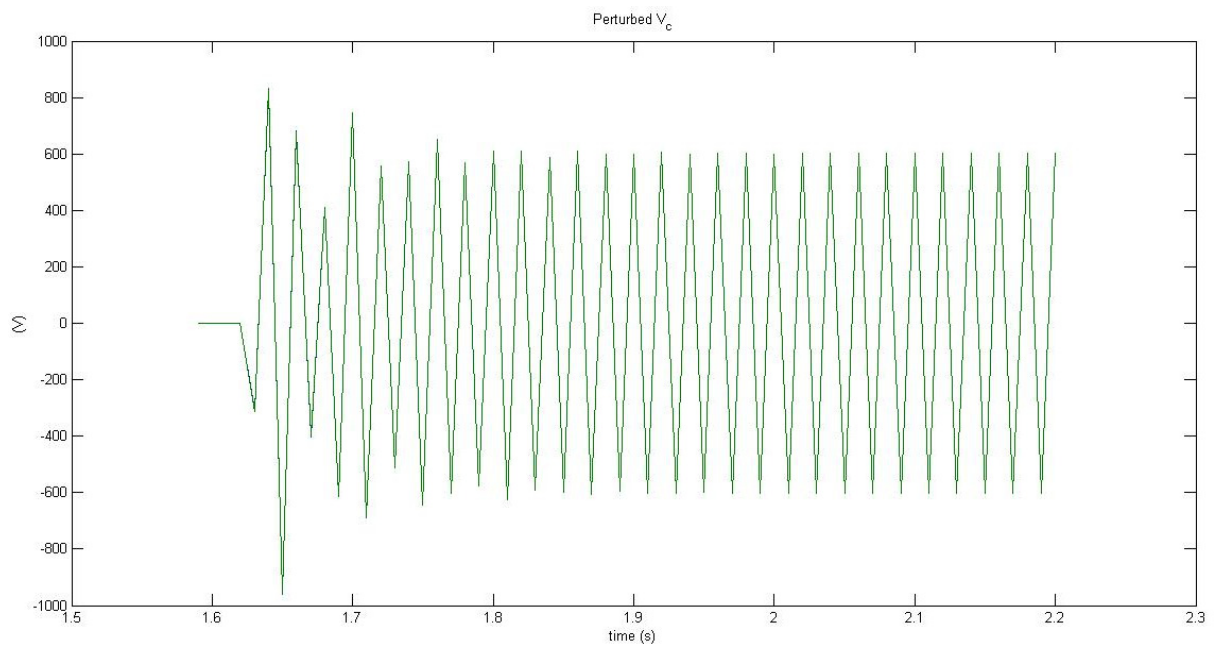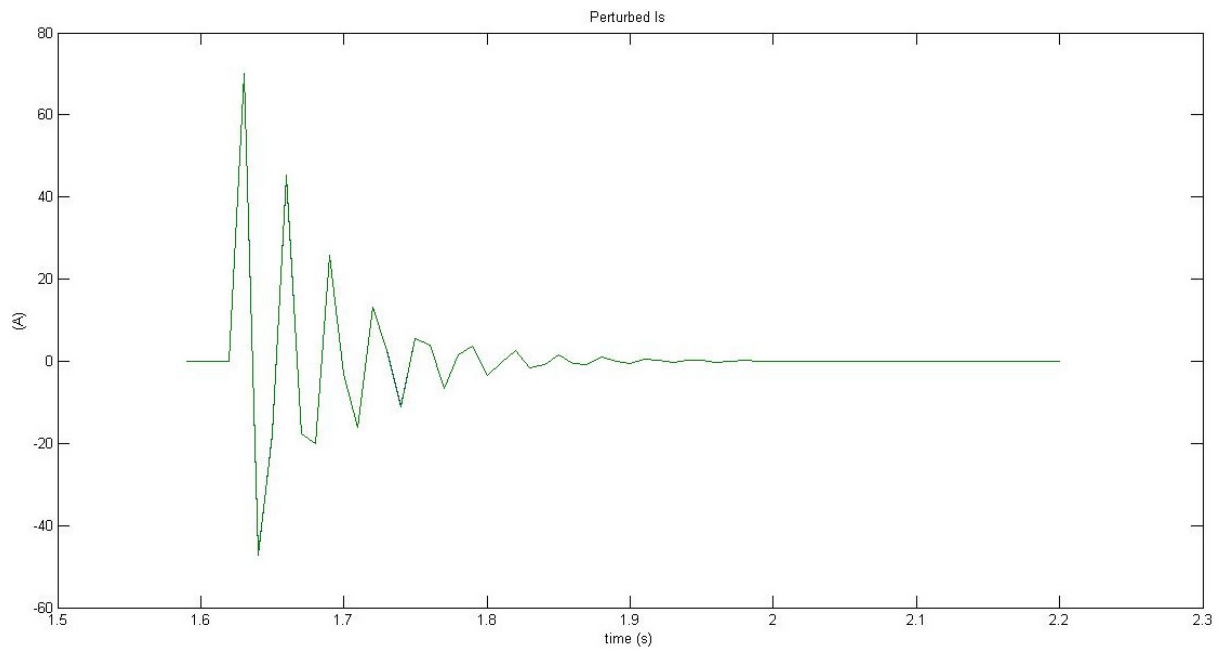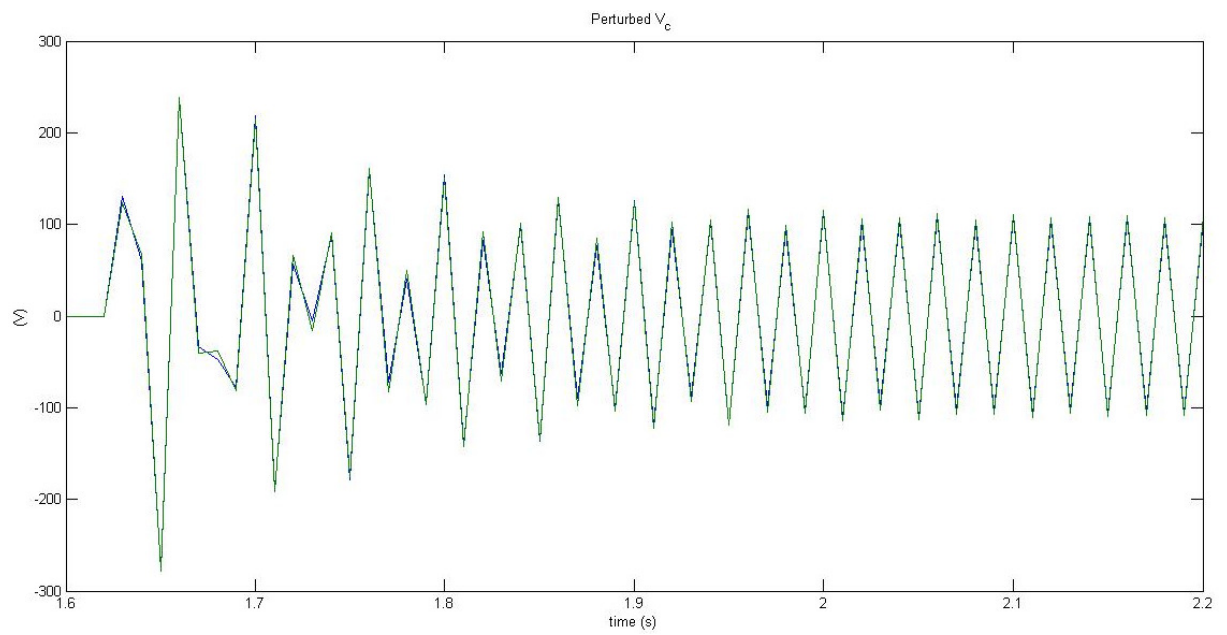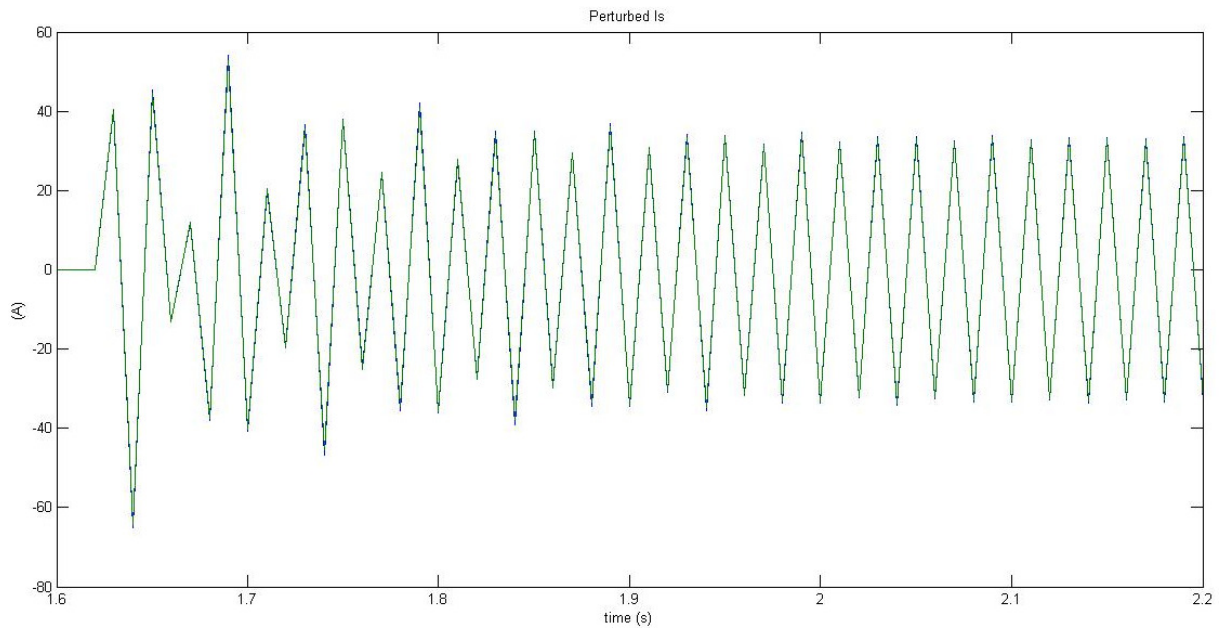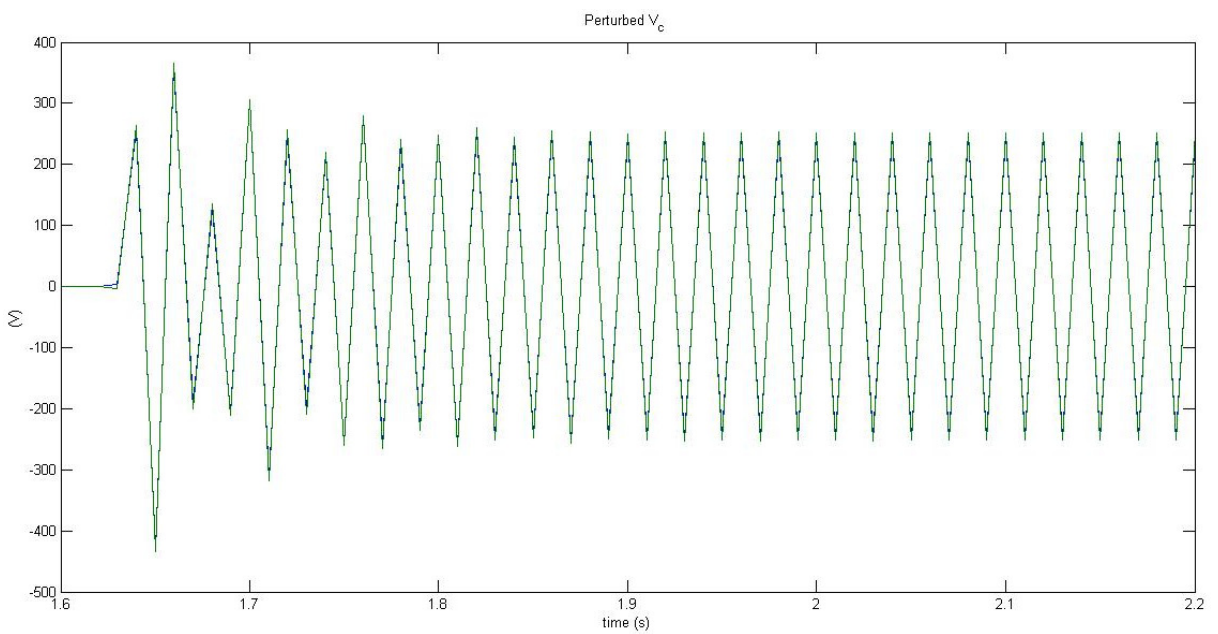## 3.2   System modelling in a three-phase SVC application

Three single-phase SVC systems displaced by 120° has been considered for the development of the discrete state space model for the three phase system with the TCR in star configuration (see Figure 3-12(a)), as it has been approached in [1]. Figure 3-12(b) depicts the TCR branch current waveforms associated with three-phase operation: each phase has been sampled over half-cycle $(0, T_s)$. Each of the three Poincarè maps is analogous to the single-phase map (3.14), so formulas (3.11) and (3.12) have been applied for a sample period referred to each phase with steady-state turn-on instants, turn-off instants and inputs depicted in Table 3-2.

Table 3-2 Turn-on instants, turn-off instants and inputs associated with three-phase operation of the SVC.

Phase	Map	Φ_d	τ_d	$W(t)$	
a	H_a	$\dfrac{\pi}{2} - \sigma_d/2$	$\dfrac{\pi}{2} + \sigma_d/2$	$(\cos\omega t$	$-\sin\omega t)$
b	H_b	$\dfrac{\pi}{6} - \sigma_d/2$	$\dfrac{\pi}{6} + \sigma_d/2$	$(\cos\left(\omega t - \dfrac{2\pi}{3}\right)$	$-\sin\left(\omega t - \dfrac{2\pi}{3}\right))$
c	H_c	$\dfrac{5\pi}{6} - \sigma_d/2$	$\dfrac{5\pi}{6} + \sigma_d/2$	$(\cos\left(\omega t + \dfrac{2\pi}{3}\right)$	$-\sin\left(\omega t + \dfrac{2\pi}{3}\right))$

In order to write a unique linear model also for three-phase operation, the state vectors at sampling instant T_s of each phase $\tilde{y}_a$, $\tilde{y}_b$ and $\tilde{y}_c$ (related to the respective maps) have been rearranged inside the vector $\tilde{y}_{abc}$, using matrix S:

$$\tilde{y}_{abc} = \begin{pmatrix} \tilde{\imath}_{s\_abc} \\ \tilde{v}_{r\_abc} \end{pmatrix} = S \cdot \begin{pmatrix} \tilde{y}_a \\ \tilde{y}_b \\ \tilde{y}_c \end{pmatrix} \qquad (3.19)$$

$$\begin{pmatrix} \tilde{y}_a \\ \tilde{y}_b \\ \tilde{y}_c \end{pmatrix} = S' \cdot \begin{pmatrix} \tilde{\imath}_{s\_abc} \\ \tilde{v}_{r\_abc} \end{pmatrix} \qquad (3.20)$$

where

$$S = \begin{bmatrix} 1 & 0 & 0 & 0 & 0 & 0 \\ 0 & 0 & 1 & 0 & 0 & 0 \\ 0 & 0 & 0 & 0 & 1 & 0 \\ 0 & 1 & 0 & 0 & 0 & 0 \\ 0 & 0 & 0 & 1 & 0 & 0 \\ 0 & 0 & 0 & 0 & 0 & 1 \end{bmatrix} \qquad (3.21)$$
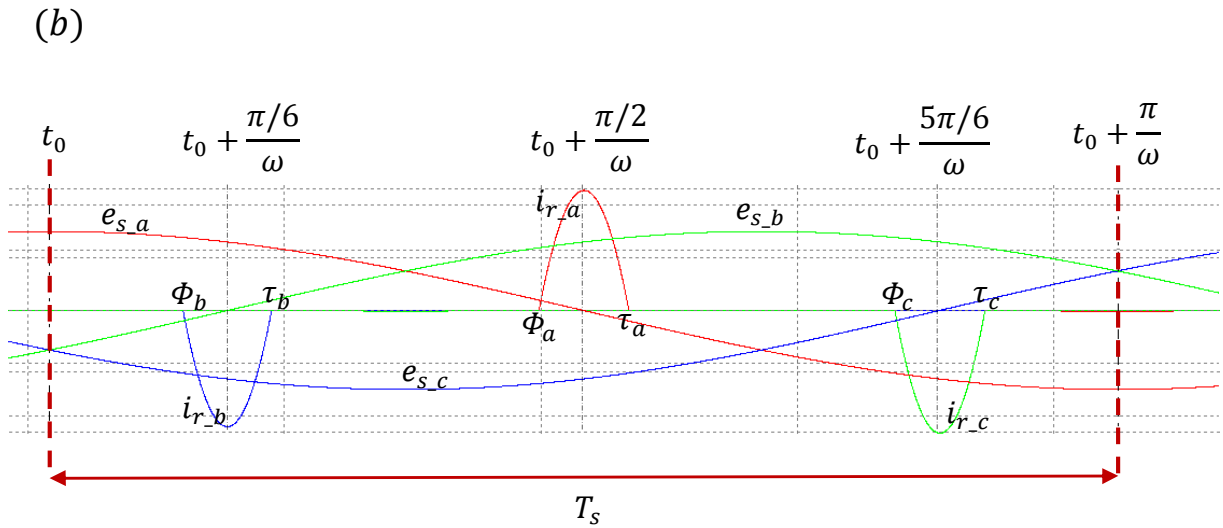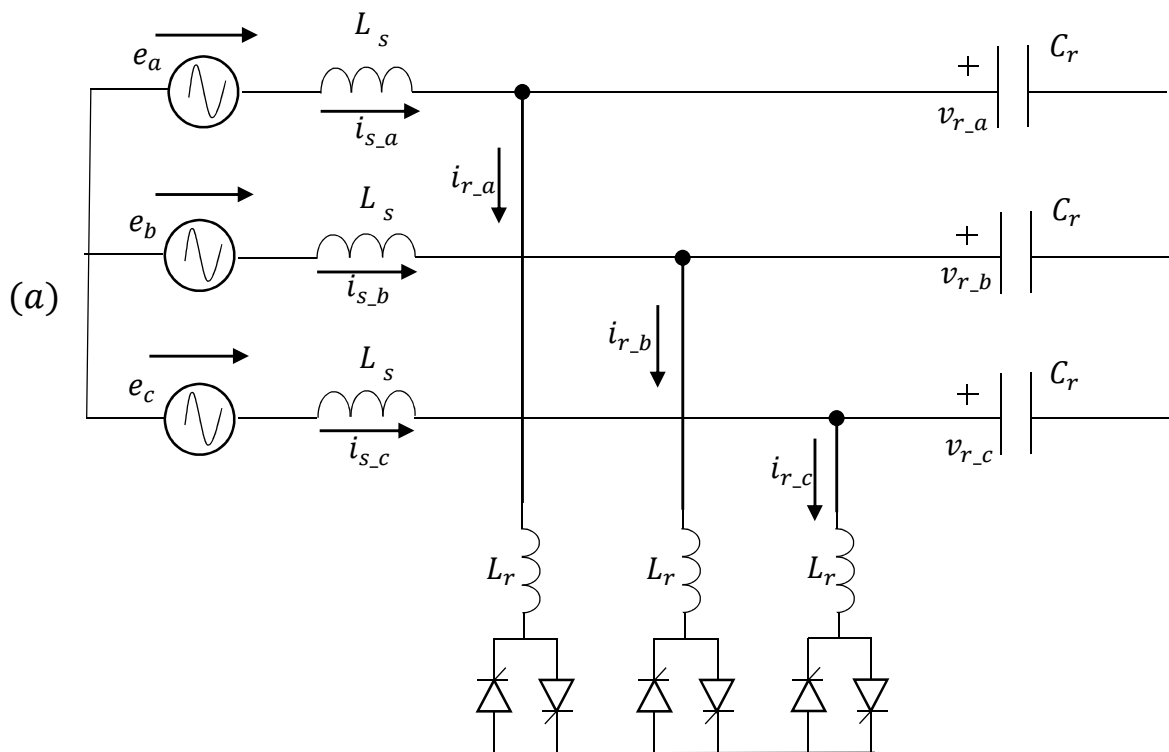
Figure 3-12 Three phase SVC system (a) circuit diagram (b) TCR branch current waveforms: it is highlighted the sampling period Ts referred to phase a.

The linearized three-phase model can be written as (3.14) considering the new state vector $\breve{y}_{abc}$:

$$\breve{y}_{abc}((k+1)T_s) = \Psi_{abc}\breve{y}_{abc}(kT_s) + (-1)^k \cdot \left\{ \Gamma_{\Phi abc}\widetilde{\Phi}(kT_s) + \Gamma_{u abc}\breve{u}_{dq}(kT_s) \right\}$$

(3.22)

where

$$\Psi_{abc} = S \begin{bmatrix} \Psi_a & 0 & 0 \\ 0 & \Psi_b & 0 \\ 0 & 0 & \Psi_c \end{bmatrix} S' \qquad \Gamma_{\Phi abc} = S \begin{bmatrix} \Gamma_{\Phi a} \\ \Gamma_{\Phi b} \\ \Gamma_{\Phi c} \end{bmatrix}$$

(3.23)

$$\Gamma_{u abc} = S \begin{bmatrix} \Gamma_{u_a} \\ \Gamma_{u_b} \\ \Gamma_{u_c} \end{bmatrix}$$

are expressed in terms of (3.15) (3.16) (3.17) with appropriate substitution according to Table 3-2. The above SVC model is time-varying (because of $(-1)^k$), consequently the transformation to the $dq\gamma$- reference frame has been used. Park's transformation associated with the orientation of the inputs defined in Table 3-2 are

$$V(t) = \frac{2}{3} \begin{bmatrix} cos\omega t & \cos(\omega t - \frac{2}{3}\pi) & \cos(\omega t + \frac{2}{3}\pi) \\ -sin\omega t & -\sin(\omega t - \frac{2}{3}\pi) & -\sin(\omega t + \frac{2}{3}\pi) \\ 1/2 & 1/2 & 1/2 \end{bmatrix}$$

(3.24)

$$W(t) = \begin{bmatrix} W_a(t) & 1 \\ W_b(t) & 1 \\ W_c(t) & 1 \end{bmatrix} = \begin{bmatrix} cos\omega t & -sin\omega t & 1 \\ \cos(\omega t - \frac{2}{3}\pi) & -\sin(\omega t - \frac{2}{3}\pi) & 1 \\ \cos(\omega t + \frac{2}{3}\pi) & -\sin(\omega t + \frac{2}{3}\pi) & 1 \end{bmatrix}$$

(3.25)

where $V(\theta)$ projects stationary *abc* variables onto the rotating $dq\gamma$- reference frame and $W(\theta)$ projects $dq\gamma$- reference frame variables onto the stationary *abc*-reference frame.

Defining

$$\mho(t) = \begin{bmatrix} V(t) & 0 \\ 0 & V(t) \end{bmatrix} \qquad \Russian(t) = \begin{bmatrix} W(t) & 0 \\ 0 & W(t) \end{bmatrix}$$

(3.26)

it's possible to pass from a time-varying model expressed by Poincarè map (3.22) to a linearized *time-invariant* model only if values in the columns of Ψ that refers to zero sequence

42

component, are changed in sign as shown in (3.28). For this reason, the linear time invariant model is expressed in $dq0$- frame:

$$\breve{y}_{dq0}\big((k+1)T_s\big) = \Psi \breve{y}_{dq0}(kT_s) + \Gamma_\Phi \widetilde{\Phi}(kT_s) + \Gamma_u \breve{u}_{dq}(kT_s)$$

$$(\,3.27\,)$$

where

$$\Psi = -\mho(0)\Psi_{abc}\,\Sha(0)$$

$$\Psi(n,3) = -\Psi(n,3), \quad \Psi(n,6) = -\Psi(n,6) \text{ with } n \in [1,6]$$

$$\Gamma_\Phi = -\mho(0)\Gamma_{\Phi_{abc}}$$

$$\Gamma_u = -\mho(0)\Gamma_{u_{abc}}$$

$$(\,3.28\,)$$

The following demonstration aims to show how it is possible to pass from a time-varyng model to the *time-invariant* model, applying Park's transformation to (3.22). To simplify the demonstration, it is considered a general vector state $\breve{x}_{abc}$ of three variables *abc* (that can be voltages or currents), instaed of the whole vector $\breve{y}_{abc}$. The Poincaré map written for the new state vector $\breve{x}_{abc}$ is (the sampling time is omitted, for example k is used instead of kT_s and matrices are denoted with accent "$-$"):

$$\breve{x}_{abc}(k+1) = \bar{\Psi}\breve{x}_{abc}(k) + (-1)^k \cdot \big\{ \bar{\Gamma}_\Phi \widetilde{\Phi}(k) + \bar{\Gamma}_u \breve{u}_{dq}(k) \big\}$$

$$(\,3.29\,)$$

Then it's useful to divide the matrixes (3.24) and (3.25) as follows, distinguishing the first two rows of $V(t)$ and the first two columns of $W(t)$ from the last row and column respectively:

$$V(t) = \frac{2}{3}\begin{bmatrix} V_{dq}(t) \\ V_\gamma \end{bmatrix}$$

$$(\,3.30\,)$$

$$W(t) = [W_{dq}(t) \quad W_\gamma]$$

$$(\,3.31\,)$$

In this way dq components are considered separately from the zero sequence one: this allows deriving a time-invariant model.

Multiplying both members of (3.29) for $V((k+1)T_s)$, and considering $W(kT_s)$ that projects $dq\gamma$- reference frame variables onto the stationary *abc*-reference frame, it is obtained (always omitting the sampling time):

$$\check{x}_{dq\gamma}(k+1) = V(k+1)\check{x}_{abc}(k+1)$$

$$= V(k+1)\overline{\Psi}W(k)\cdot\check{x}_{dq\gamma}(k) + V(k+1)(-1)^k \tag{3.32}$$

$$\cdot\left\{\overline{\Gamma}_\Phi\widetilde{\Phi}(k) + \overline{\Gamma}_u\check{u}_{dq}(k)\right\}$$

Now, it's possible to consider separately dq and γ components, introducing (3.30) and (3.31) in (3.29).

For dq components,

$$\check{x}_{dq}(k+1) = V_{dq}(k+1)\overline{\Psi}W_{dq}(k)\cdot\check{x}_{dq}(k) + V_{dq}(k+1)\overline{\Psi}W_\gamma(k)\cdot\check{x}_\gamma(k)$$

$$+ V_{dq}(k+1)(-1)^k\cdot\left\{\overline{\Gamma}_\Phi\widetilde{\Phi}(k) + \overline{\Gamma}_u\check{u}_{dq}(k)\right\} \tag{3.33}$$

And the zero sequence component results:

$$\check{x}_\gamma(k+1) = V_\gamma(k+1)\overline{\Psi}W_{dq}(k)\cdot\check{x}_{dq}(k) + V_\gamma(k+1)\overline{\Psi}W_\gamma(k)\cdot\check{x}_\gamma(k)$$

$$+ V_\gamma(k+1)\cdot(-1)^k\cdot\left\{\overline{\Gamma}_\Phi\widetilde{\Phi}(k) + \overline{\Gamma}_u\check{u}_{dq}(k)\right\} \tag{3.34}$$

Considering the following properties:

$$V_{dq}(k) = (-1)^k\cdot V_{dq}(0)$$

$$V_\gamma(k) = V_\gamma(0)$$

$$W_{dq}(k) = (-1)^k\cdot W_{dq}(0) \tag{3.35}$$

$$W_\gamma(k) = W_\gamma(0)$$

Some coefficients of (3.33) result time invariant:

$$V_{dq}(k+1)\overline{\Psi}W_{dq}(k) = (-1)^{k+1}\cdot V_{dq}(0)\overline{\Psi}(-1)^k\cdot W_{dq}(0)$$

$$= (-1)\cdot V_{dq}(0)\overline{\Psi}\cdot W_{dq}(0) \tag{3.36}$$

$$V_{dq}(k+1)(-1)^k = (-1)^{k+1}\cdot V_{dq}(0)\cdot(-1)^k = (-1)\cdot V_{dq}(0)$$

while the coefficients related to the zero sequence component are still time variant.

Therefore multiplying (3.34) by $(-1)^k$ and substituting W_{dq} and V_{dq} with the properties expressed in (3.35), it yields:

$$(-1)^k\cdot\check{x}_\gamma(k+1)$$

$$= (-1)^k\cdot V_\gamma(0)\overline{\Psi}(-1)^k\cdot W_{dq}(0)\cdot\check{x}_{dq}(k) + (-1)^k$$

$$\cdot V_\gamma(0)\overline{\Psi}W_\gamma(0)\cdot\check{x}_\gamma(k) + (-1)^k\cdot V_\gamma(0)\cdot(-1)^k \tag{3.37}$$

$$\cdot\left\{\overline{\Gamma}_\Phi\widetilde{\Phi}(k) + \overline{\Gamma}_u\check{u}_{dq}(k)\right\}$$

Defining a new state variable:

$$\check{x}_0(k+1) = (-1)^k \cdot \check{x}_\gamma(k+1)$$

$$\check{x}_0(k) = (-1)^{k-1} \cdot \check{x}_\gamma(k) \qquad (3.38)$$

The equation (3.38) results:

$$\check{x}_0(k+1) = V_\gamma(0)\overline{\Psi} \cdot W_{dq}(0) \cdot \check{x}_{dq}(k) + (-1)^k \cdot V_\gamma(0)\overline{\Psi}W_\gamma(0) \cdot (-1)^{-k+1}$$
$$\cdot \check{x}_0(k) + V_\gamma(0) \cdot \{\overline{\Gamma}_\Phi \widetilde{\Phi}(k) + \overline{\Gamma}_u \check{u}_{dq}(k)\} \qquad (3.39)$$

Obtaining the final time invariant form for the new zero sequence component:

$$\check{x}_0(k+1) = V_\gamma(0)\overline{\Psi} \cdot W_{dq}(0) \cdot \check{x}_{dq}(k) - V_\gamma(0)\overline{\Psi}W_\gamma(0) \cdot \check{x}_0(k) + V_\gamma(0)$$
$$\cdot \{\overline{\Gamma}_\Phi \widetilde{\Phi}(k) + \overline{\Gamma}_u \check{u}_{dq}(k)\} \qquad (3.40)$$

and substituting $\check{x}_\gamma$ by $\check{x}_0$ in (3.33) and considering the coefficients of (3.35), it yields a time invariant system for dq components:

$$\check{x}_{dq}(k+1) = (-1) \cdot V_{dq}(0)\overline{\Psi} \cdot W_{dq}(0) \cdot \check{x}_{dq}(k) + V_{dq}(0)\overline{\Psi}W_\gamma(0) \cdot \check{x}_0(k)$$
$$+ (-1) \cdot V_{dq}(0) \cdot \{\overline{\Gamma}_\Phi \widetilde{\Phi}(k) + \overline{\Gamma}_u \check{u}_{dq}(k)\} \qquad (3.41)$$

Note that it's possible to write a time invariant model only if a new zero component is defined as in (3.35) and, consequently, the column of $\overline{\Psi}$ that refers to the new zero sequence component are changed in sign. So the linearized time invariant model in $dq\gamma$- frame is:

$$\check{x}((k+1)T_s) = \overline{\Psi}\check{x}(kT_s) + \overline{\Gamma}_\Phi \widetilde{\Phi}(kT_s) + \overline{\Gamma}_\Phi \check{u}_{dq}(kT_s) \qquad (3.42)$$

That has the same form of (3.27) previous used and is consistent with the form of LTI discrete-state space model for thyristor-based static switching circuit expressed in Chapter 2.1.

Figure 3-13,Figure 3-14, Figure 3-15,Figure 3-16,Figure 3-18 andFigure 3-17 compare the SVC perturbed capacitor voltage response of the LTI model (green line) with PSIM model (blue line) for a +5% step change in the power system d-axis voltage u_d for the operating mode $\sigma_d = 45°$, in the discrete-time domain. The SVC is operating in steady-state and at time $t_0 = 1.605\ s$ the step change is applied. The linearized model captures the dynamic response of the SVC associated with the transient process leading from one cyclic mode to the next.
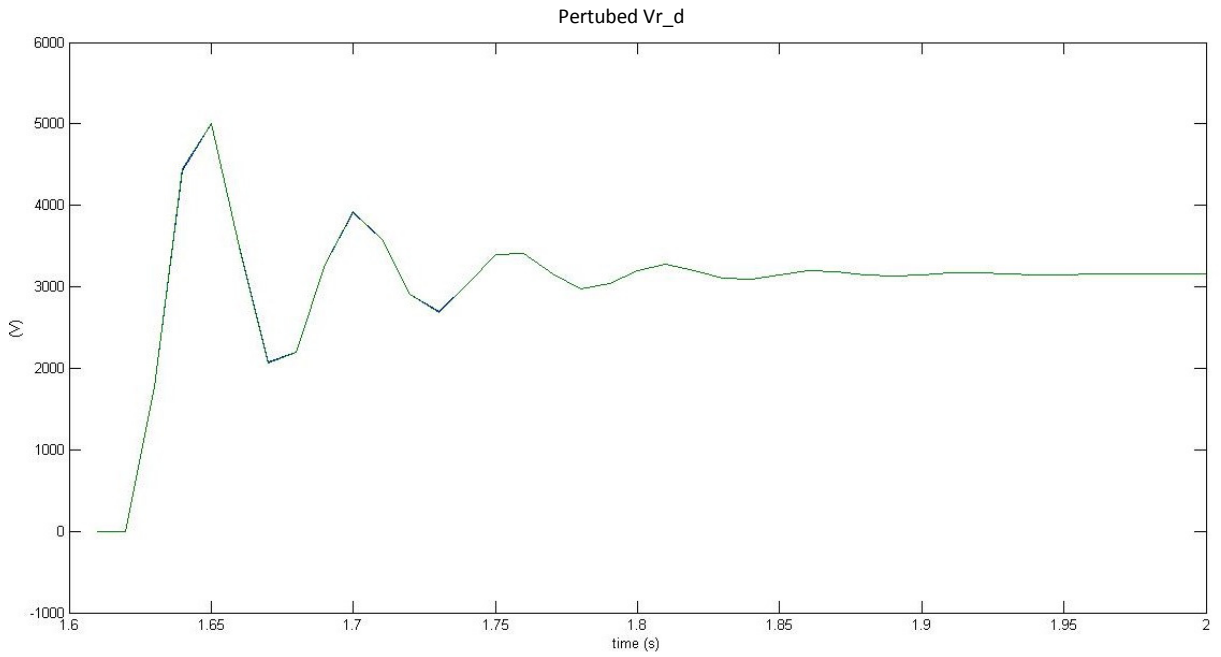
Figure 3-13. Perturbed capacitor voltage Vr_d response in the dqγ--frame to a 5% step change in peak source voltage along d-axis for $\sigma = 45°$. Green line for LTI model and blue line for PSIM one.
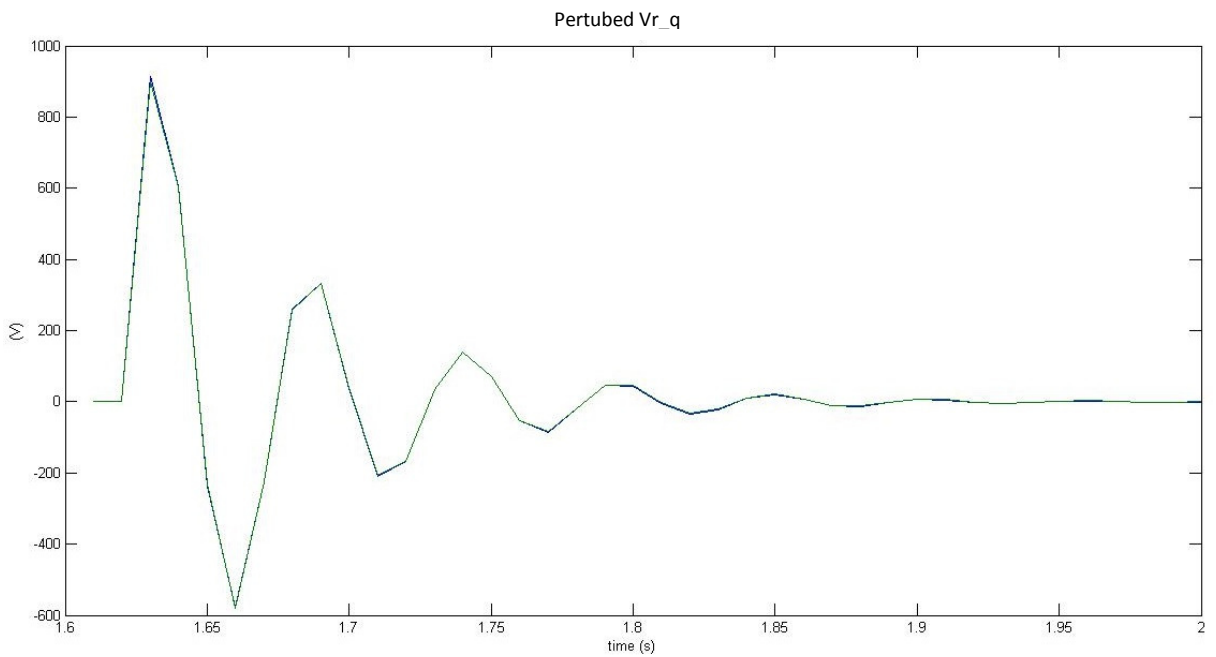
Figure 3-14 Perturbed capacitor voltage Vr_q response in the dqγ--frame to a 5% step change in peak source voltage along d-axis for $\sigma = 45°$. Green line for LTI model and blue line for PSIM one.
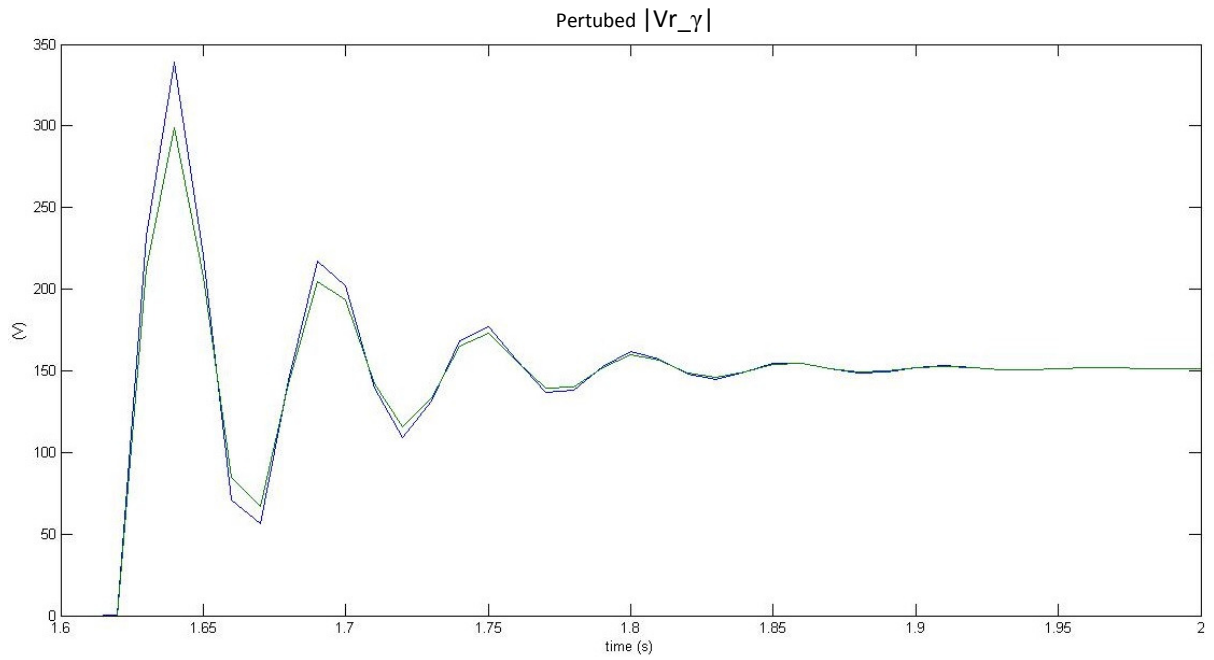
Figure 3-15 Perturbed zero sequence capacitor voltage response in the dqγ -frame to a 5% step change in peak source voltage along d-axis for σ = 45°. Green line for |Vr_0| (computed with LTI model) and blue line for |Vr_γ| (PSIM).
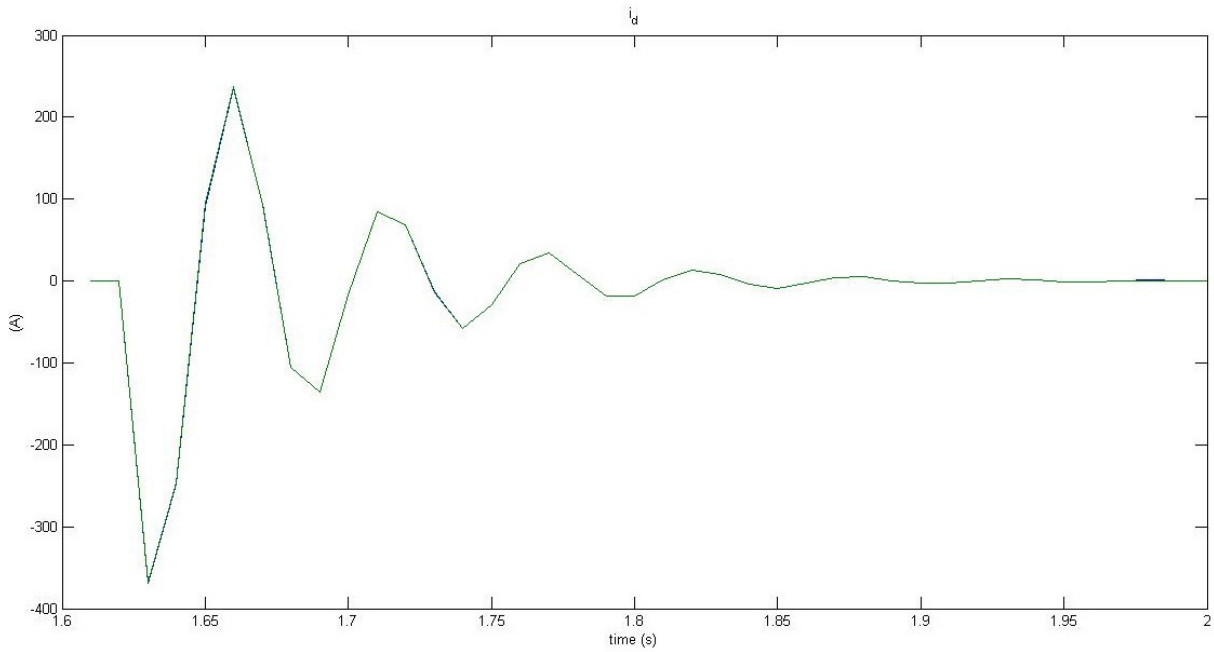
Figure 3-16 Perturbed line current is_d response in the dqγ-frame to a 5% step change in peak source voltage along d-axis for σ = 45°. Green line for LTI model and blue line for PSIM one.
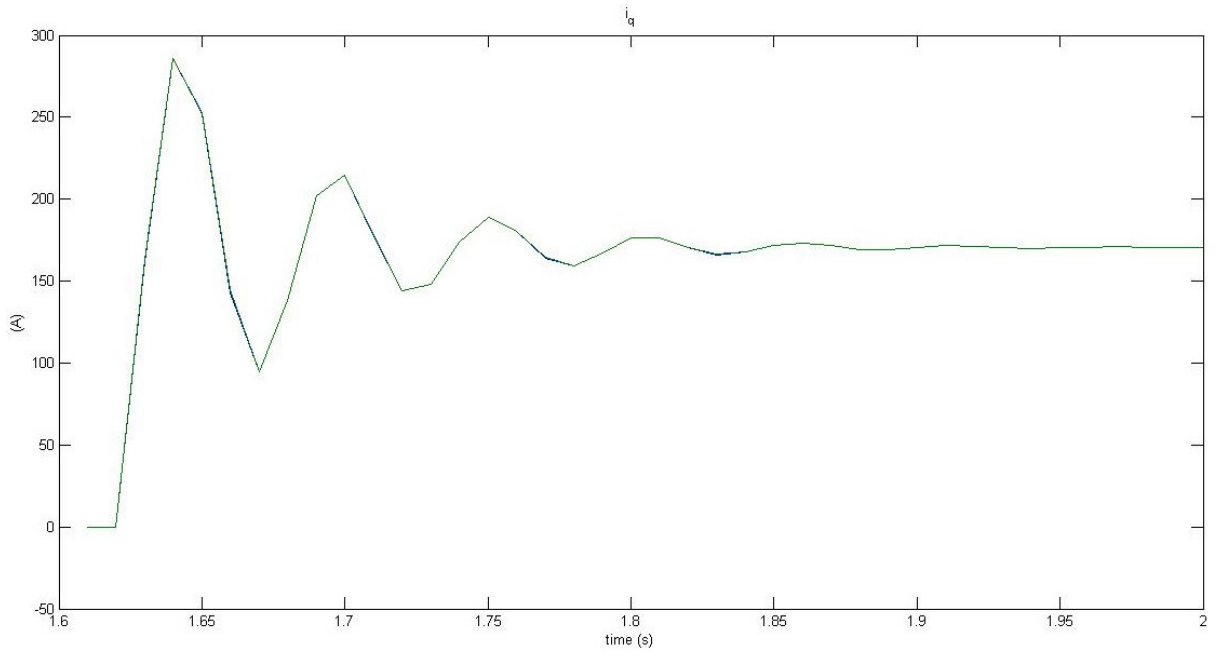
Figure 3-17 Perturbed line current is_q response in the dqγ-frame to a 5% step change in peak source voltage along d-axis for σ = 45°. Green line for LTI model and blue line for PSIM one.
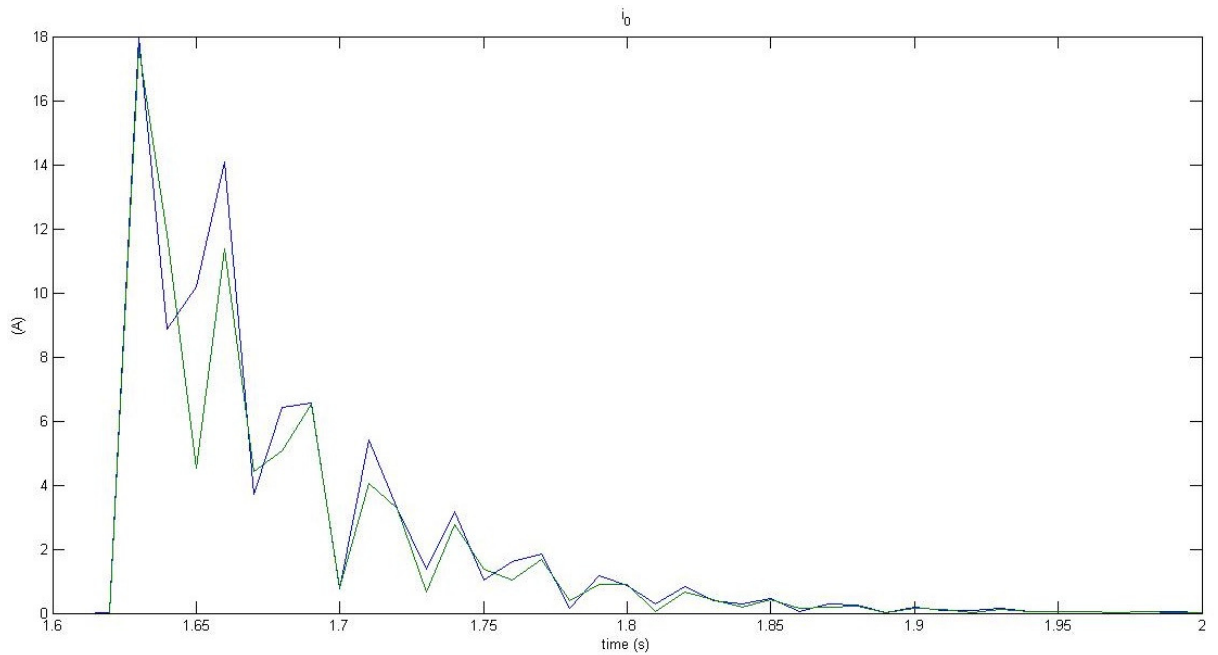
Figure 3-18 Perturbed zero sequence line current response in the dqγ -frame to a 5% step change in peak source voltage along d-axis for σ = 45°. Green line for |is_0| (computed with LTI model) and blue line for |is_γ| (PSIM).

There is a very good matching between the two models for all the components of perturbed capacitor voltage and line current: for zero sequence component of capacitor voltage and line current the difference between the two models is more visible than the other plots because of the different scale of y axis. Moreover, it is highlighted that the absolute value of zero sequence component "0" of the model has been plotted because it changes sign at each odd cycle respect to the "real" γ component, as it is shown in (3.38). The "real" zero sequence component of perturbed capacitor voltage $\tilde{V}r\_\gamma$ has periodic behavior, so when it is sampled at T_s and, then, its absolute value is calculated, the sampling gives out always the same value at steady state operation. For this reason in Figure 3-15 the absolute value $|\tilde{V}r\_\gamma|$, represented by PSIM results (blue line) and $|\tilde{V}r\_0|$ (green line, computed with LTI discrete-state space model) stabilizes at about 150V at steady state operation.

4 Three-phase delta-connected TCR of ITER experimental reactor

In this chapter a discrete state space model of three-phase delta-connected TCR of ITER experimental reactor (highlighted in Figure 2-3) referring to the circuit shown in Figure 4-2(a) has been developed and compare with the continuous model developed in [2].

Differently from the previous chapter, a model with a reduced sampling time has been developed, equivalent to 60 electrical degrees instead of 180 degrees, that corresponds to the operation of the three-phase TCR. This allows to extend the frequency range of accuracy of the discrete state space model.

The discrete state space models have been developed for the conduction angle of the thyristors of the TCR smaller than 60 and between 60 and 120 electrical degrees, that means one and two conducting TCR respectively on a sampling period. The case of the conduction angle included between 120 and 180 electrical degree, has been neglected because is similar to the one 60-120.

4.1 *System modelling for conduction angle $\sigma \in (0, 60°)$*

In this section a discrete state space model has been developed considering the interval $[t_0, t_1]$ (Figure 4-1) when only a TCR conducts (in this case the thyristor between the phases a and b, see Figure 4-2(b)), because the conduction angle of the TCR is minor than the angle equivalent to the sampling time (i.e. 60 electrical degree). This analysis is the same of one carried out in Section 3.1, but limited to the interval $[t_0, t_1]$, where only the TCR a-b is switched on, as it has been already said. So, to simplify the description, some consideration is neglected. Then, this analysis has been easily extended by dq transformation to the other time intervals with the switching of other TCRs as shown in the next sections, thus obtaining a LTI discrete state-space model independent from the considered time interval.

Considering a sample period $[t_0, t_1]$ referred to TCR ab (see Figure 4-1), when either thyristor is in its conduction mode, the state vector of the circuit is:

$$x = (i_1 \quad i_2 \quad v_1 \quad v_2 \quad v_3 \quad i_r)^t \tag{4.1}$$

and the system dynamics are described by

$$\dot{x} = Ax + Bu_s \qquad (4.2)$$

The equations of the circuit in Figure 4-2(b) are:

$$
\begin{cases}
e_a - L_s \dfrac{di_1}{dt} - v_1 + v_3 - L_s \dfrac{di_1}{dt} - L_s \dfrac{di_2}{dt} - e_c = 0 \\[2mm]
e_b - L_s \dfrac{di_2}{dt} - v_2 + v_3 - L_s \dfrac{di_1}{dt} - L_s \dfrac{di_2}{dt} - e_c = 0 \\[2mm]
\dfrac{dv_1}{dt} = \dfrac{1}{C_r}(i_1 - i_r) \\[2mm]
\dfrac{dv_2}{dt} = \dfrac{1}{C_r}(i_2 + i_r) \\[2mm]
\dfrac{dv_3}{dt} = \dfrac{1}{C_r}(-i_1 - i_2) \\[2mm]
\dfrac{di_r}{dt} = \dfrac{1}{L_r}(v_1 - v_2)
\end{cases}
\qquad (4.3)
$$

It is necessary to rearrange the first two equations in the system above to obtain the matrixes A and B, resulting:

$$
\begin{bmatrix} 2 & 1 \\ 1 & 2 \end{bmatrix} L_s
\begin{bmatrix} \dfrac{di_1}{dt} \\[2mm] \dfrac{di_2}{dt} \end{bmatrix}
=
\begin{pmatrix} 0 & 0 & -1 & 0 & 1 \\ 0 & 0 & 0 & -1 & 1 \end{pmatrix}
\begin{bmatrix} i_1 \\ i_2 \\ v_1 \\ v_2 \\ v_3 \end{bmatrix}
+
\begin{pmatrix} 1 & 0 & -1 \\ 0 & 1 & -1 \end{pmatrix}
\begin{bmatrix} e_a \\ e_b \\ e_c \end{bmatrix}
\qquad (4.4)
$$

So:

$$
\begin{bmatrix} \dfrac{di_1}{dt} \\[2mm] \dfrac{di_2}{dt} \end{bmatrix}
=
\dfrac{1}{L_s}\begin{bmatrix} 2 & 1 \\ 1 & 2 \end{bmatrix}^{-1}
\left(
\begin{pmatrix} 0 & 0 & -1 & 0 & 1 \\ 0 & 0 & 0 & -1 & 1 \end{pmatrix}
\begin{bmatrix} i_1 \\ i_2 \\ v_1 \\ v_2 \\ v_3 \end{bmatrix}
+
\begin{pmatrix} 1 & 0 & -1 \\ 0 & 1 & -1 \end{pmatrix}
\begin{bmatrix} e_a \\ e_b \\ e_c \end{bmatrix}
\right)
\qquad (4.5)
$$

Adding at the end a columns of zeros for the TCR current i_r, from the system (4.3) it yields,

$$
A =
\begin{bmatrix}
0 & 0 & -2/(3Ls) & 1/(3Ls) & 1/(3Ls) & 0 \\
0 & 0 & 1/(3Ls) & -2/(3Ls) & 1/(3Ls) & 0 \\
1/C & 0 & 0 & 0 & 0 & -1/C \\
0 & 1/C & 0 & 0 & 0 & 1/C \\
-1/C & -1/C & 0 & 0 & 0 & 0 \\
0 & 0 & 1/Lr & -1/Lr & 0 & 0
\end{bmatrix},
\qquad (4.6)
$$

$$
B = \begin{bmatrix} \frac{2}{3Ls} & \frac{-1}{3Ls} & \frac{-1}{3Ls} \\ \frac{-1}{3Ls} & \frac{2}{3Ls} & \frac{-1}{3Ls} \\ 0 & 0 & 0 \\ 0 & 0 & 0 \\ 0 & 0 & 0 \\ 0 & 0 & 0 \end{bmatrix} \ , \quad u_s = \begin{bmatrix} e_a \\ e_b \\ e_c \end{bmatrix}.
$$

The vector c that allows to express thyristor current as linear combination of the state vector (see Section I.1 in Appendix I) results:

$$
i_r = cx = (0 \quad 0 \quad 0 \quad 0 \quad 0 \quad 1)x \tag{4.7}
$$

And the projection and injection matrices associated with the thyristor are:

$$
Q = \begin{bmatrix} 1 & 0 & 0 & 0 & 0 \\ 0 & 1 & 0 & 0 & 0 \\ 0 & 0 & 1 & 0 & 0 \\ 0 & 0 & 0 & 1 & 0 \\ 0 & 0 & 0 & 0 & 1 \\ 0 & 0 & 0 & 0 & 0 \end{bmatrix} \qquad P = Q' \tag{4.8}
$$

Thus, in nonconduction mode $i_r = 0$ and the system state vector is composed by only five variables:

$$
y = Px = \begin{bmatrix} i_1 \\ i_2 \\ v_1 \\ v_2 \\ v_3 \end{bmatrix} \tag{4.9}
$$

with system dynamics described by

$$
\dot{y} = PAQy + PBu_s \tag{4.10}
$$

In Figure 4-1 it's possible to distinguish conduction mode and non-conduction mode inside the sample period $T_s = \frac{\pi/3}{\omega}$ referred to TCR_ab.
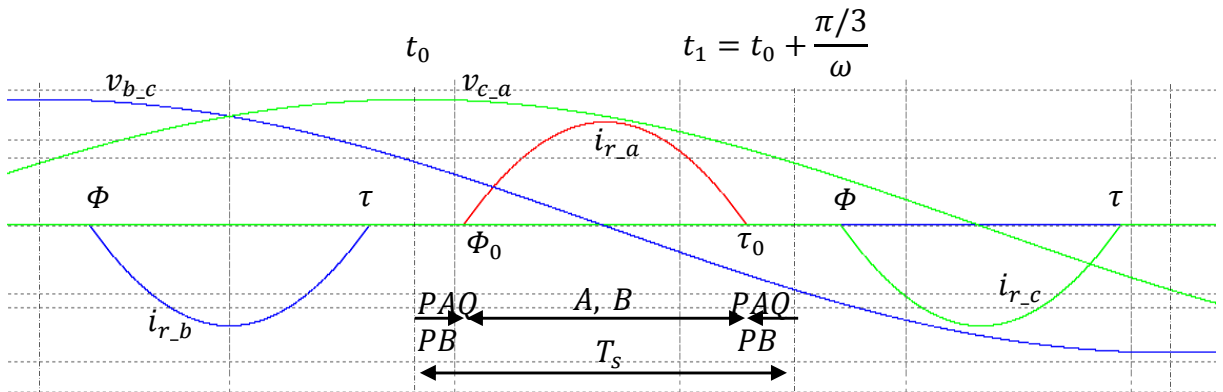
Figure 4-1 Three phase TCR branch current waveforms

52
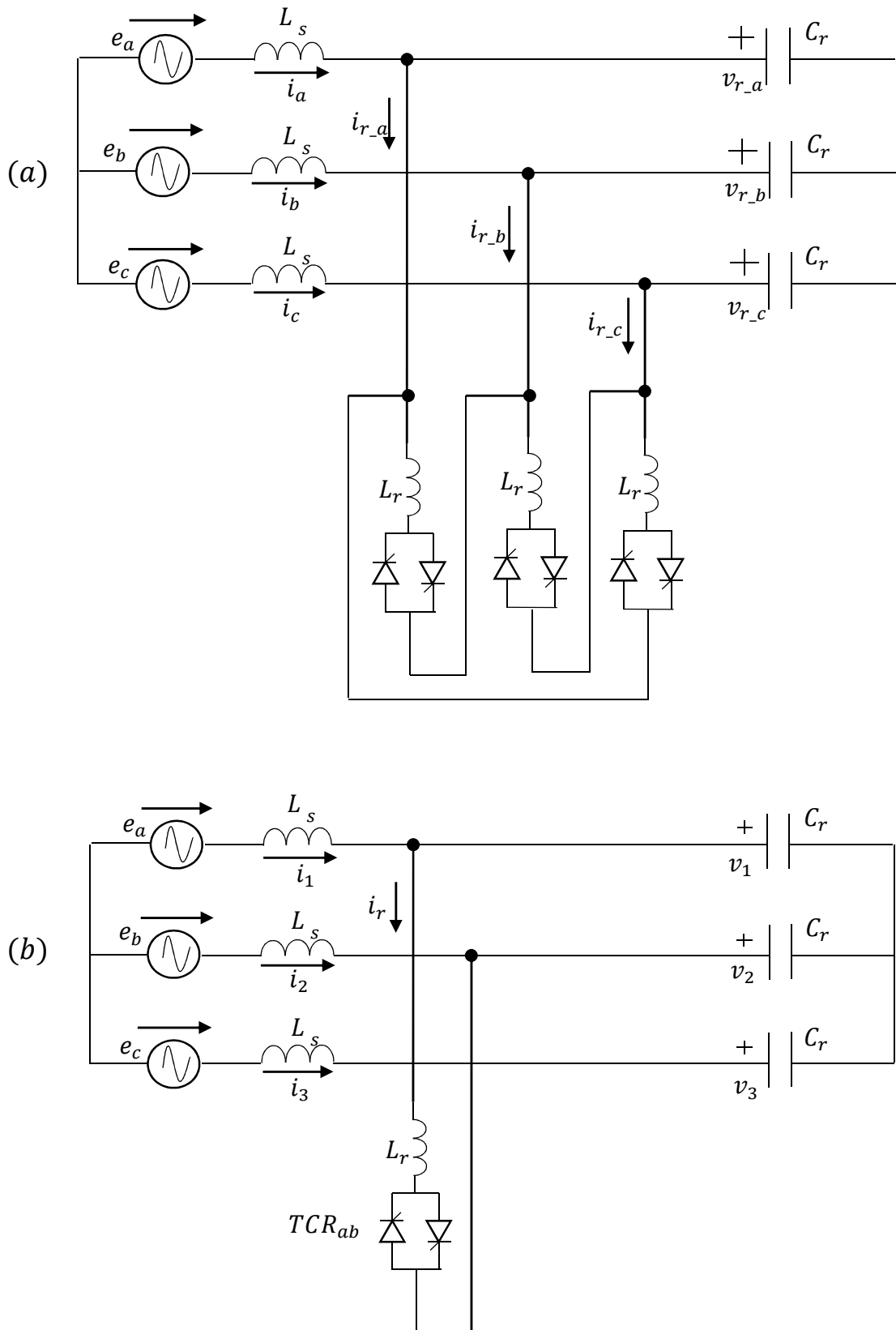
Figure 4-2 (a) Three-phase delta-connection SVC (b) Three-phase SVC considering only TCR a-b

4.1.1 Three-phase non-linear model

If it is defined

$$W(t) = \begin{bmatrix} \cos(\omega t + \frac{\pi}{6}) & -sen(\omega t + \frac{\pi}{6}) \\ \cos(\omega t - \frac{\pi}{2}) & -sen(\omega t - \frac{\pi}{2}) \\ \cos(\omega t - \frac{7\pi}{6}) & -sen(\omega t - \frac{7\pi}{6}) \end{bmatrix}$$

the source voltages may be written:

$$u_s(t) = W(t) \cdot u_{dq}, \quad u_{dq} = \begin{pmatrix} u_d \\ u_q \end{pmatrix} \tag{4.11}$$

where u_d and u_q are the direct and quadrature voltages respectively for a given reference frame. Figure 4-1(b) describes the system dynamics as the circuit evolves over a period. The representation of the state at thyristor turn-on and turn-off are

$$x(\Phi^+) = Qy(\Phi^-) \quad \text{and} \quad y(\tau^+) = Px(\tau^-) \tag{4.12}$$

respectively. The Poincarè map H_1 that projects the circuit state over the first cycle of reference, starting from instant $t_0 = 0$ (choosen as the instant when phase-to-phase voltage is maximum and the system is in steady state operation) to $t_1 = t_0 + T_s$, is

$$H_1: \quad y(0) \to y_1 = y(T_s) \tag{4.13}$$

is obtained by integrating (4.2) and (4.10) with mode transitions represented by (4.12). Let y_0 the state vector at steady state operating point at a general instant t_0. On the assumption that u_{dq} is constant over a sampling period, this yields, over the first cycle $T_s = \frac{\pi/3}{\omega}$:

$$y(\Phi) = e^{PAQ \, \Phi} y_0 + \int_0^{\Phi} e^{PAQ \, (\Phi - \xi)} PB \, W_a(\xi) d\xi u_d$$

$$x(\Phi) = Qy(\Phi)$$

$$x(\tau) = e^{A(\tau - \Phi_0)} x(\Phi) + \int_{\Phi}^{\tau} e^{A(\tau - \xi)} B \, W_a(\xi) d\xi u_d \tag{4.14}$$

$$y(\tau) = Px(\tau)$$

$$y(T_s) = e^{PAQ \, (T_s - \tau)} y(\tau) + \int_{\tau}^{T_s} e^{PAQ \, (T_s - \xi)} PB \, W_a(\xi) d\xi u_d$$

Relations in (4.14) are written for a generic instant of thyristor turn-on Φ and turn-off τ.

As already explained in Section 3.1, starting from the first relation of (4.14) and substituting in sequence previous formula into the next one, it yields to a non-linear Poincarè map H_1 over the first cycle of reference:

$$y(T_s) = e^{PAQ\ (T_s-\tau)} P e^{A(\tau-\Phi)} Q e^{PAQ\ \Phi} \cdot y_0 + h_1(\Phi, u_{dq})$$

(4.15)

where

$$h_1(\Phi, u_{dq}) = e^{PAQ\ (T_s-\tau)} P$$
$$\cdot \left\{ e^{A(\tau-\Phi)} Q \int_0^\Phi e^{PAQ\ (\Phi-\xi)} PB\ W_a(\xi) d\xi u_{dq} \right.$$
$$\left. + \int_\Phi^\tau e^{A(\tau-\xi)} B\ W_a(\xi) d\xi u_{dq} \right\} + \int_\tau^{T_s} e^{PAQ\ (T_s-\xi)} PB\ W_a(\xi) d\xi u_{dq}\ .$$

(4.16)

4.1.2   Three-phase linear model

In order to investigate small signal stability of the system, it is necessary to linearize (4.15) to a first order approximation, under the assumption that the inputs u_{dq} and Φ are constant over the sample period T_s. Indeed, considering a perturbation from the nominal steady-state operation generally expressed by (4.15), the perturbed inputs and outputs (denoted with tilde) for the first cycle can be related by the Poicarè map H_1 of (4.13) in the form:

$$\tilde{y}_1 = \Psi \cdot \tilde{y}(0) + \left\{ \Gamma_\Phi \tilde{\Phi}(0) + \Gamma_u \breve{u}_{dq}(0) \right\}$$

(4.17)

Matrix Ψ represents the Jacobian $\frac{\partial H}{\partial y_0}$ of the Poincarè map (4.15) rewritten considering the steady-state conduction angle $\sigma_t = \tau - \Phi$:

$$\Psi = \frac{\partial H_1}{\partial y_0} = e^{PAQ\ (T_s-\sigma_t)/2} P e^{A\sigma_t} Q e^{PAQ(T_s-\sigma_t)/2}$$

(4.18)

Now differentiating (4.15) with respect to the firing instant (as it is reported in Section I.2.1), always considering the steady-state conduction angle σ_t:

$$\Gamma_\Phi = \left.\frac{\partial H_1}{\partial \Phi}\right|_{\Phi_0} = \left.\frac{\partial h_1(\Phi, u_{dq})}{\partial \Phi}\right|_{\Phi_0}$$

$$= e^{PAQ\frac{T_s - \sigma_t}{2}} P e^{A\sigma_t}\{Q\dot{y}(\Phi_0) - Ax(\Phi_0) - Bu_s(\Phi_0)\} \tag{4.19}$$

$$= e^{PAQ\frac{T_s - \sigma_t}{2}} P e^{A\sigma_t}\{QP - I\}\dot{x}(\Phi_0) = -e^{PAQ\frac{T_s - \sigma_t}{2}} P e^{A\sigma} c^t c \dot{x}(\Phi_0)$$

where $\{QP - I\} = c^t c$ from the properties of projection and injection matrices. Note that $c\dot{x}(\Phi_0)$ is the gradient of the thyristor current at turn-on. Finally

$$\Gamma_{u\_d} = \frac{\partial H_1}{\partial u_{dq}} = \frac{\partial h_1(\Phi_0, u_{dq})}{\partial u_{dq}} = h_1(\Phi_0, u_{dq}), with\ u_{dq} = \begin{pmatrix} 1 \\ 0 \end{pmatrix}$$

$$\tag{4.20}$$

$$\Gamma_{u_q} = \frac{\partial H_1}{\partial u_{dq}} = \frac{\partial h_1(\Phi_0, u_{dq})}{\partial u_{dq}} = h_1(\Phi_0, u_{dq}), with\ u_{dq} = \begin{pmatrix} 0 \\ 1 \end{pmatrix}$$

$$\Gamma_u = (\Gamma_{u\_d} \quad \Gamma_{u\_q})$$

In order to find a LTI discrete model it's necessary to transform the state vector of five variables, developed considering a sampling period where TCR_ab is conducting, into a state vector expressed in the abc −frame in the same sampling period of reference. Considering the topology of the grid (see Figure 4-2(a)) the currents $(i_1 \quad i_2)^t$ has been linked to currents $(i_a \quad i_b \quad i_c)^t$ through a matrix $C_{12\to abc}$ finding:

$$\begin{bmatrix} i_a \\ i_b \\ i_c \end{bmatrix} = \begin{bmatrix} 1 & 0 \\ 0 & 1 \\ -1 & -1 \end{bmatrix} \begin{bmatrix} i_1 \\ i_2 \end{bmatrix}, \qquad C_{12\to abc} = \begin{bmatrix} 1 & 0 \\ 0 & 1 \\ -1 & -1 \end{bmatrix} \tag{4.21}$$

$$\begin{bmatrix} i_1 \\ i_2 \end{bmatrix} = \begin{bmatrix} 0 & -1 & -1 \\ -1 & 0 & -1 \end{bmatrix} \begin{bmatrix} i_a \\ i_b \\ i_c \end{bmatrix}, \qquad C_{abc\to 12} = \begin{bmatrix} 0 & -1 & -1 \\ -1 & 0 & -1 \end{bmatrix} \tag{4.22}$$

while for capacitor voltage $[v_1 \quad v_2 \quad v_3]^t = [v_{r\_a} \quad v_{r\_b} \quad v_{r\_c}]^t$. This allows to transform Poincaré Map (4.17) based on a state vector (tilde that denotes perturbed quantities is omitted for variables inside the vectors):

$$\tilde{y} = (i_1 \quad i_2 \quad v_1 \quad v_2 \quad v_3)^t$$

into a map written for the new state vector

$$\tilde{y}_{abc} = (i_a \quad i_b \quad i_c \quad v_{r\_a} \quad v_{r\_b} \quad v_{r\_c})^t$$

Since the transformation refers only to line current, while the capacitor voltages remain the same, it's necessary to divide the matrix Ψ in four sub-matrixes, writing the Poincare map only in the first step. So, denoting with subscript "1"rewriting (4.17) in extended form and

$$
\begin{bmatrix} i_1 \\ i_2 \\ - \\ v_1 \\ v_2 \\ v_3 \end{bmatrix} = \begin{bmatrix} \Psi_{1,1} & | & \Psi_{1,2} \\ - & | & - \\ \Psi_{2,1} & | & \Psi_{2,2} \end{bmatrix} \begin{bmatrix} i_1 \\ i_2 \\ - \\ v_1 \\ v_2 \\ v_3 \end{bmatrix} + \left\{ \begin{bmatrix} \Gamma_{\Phi_1} \\ - \\ \Gamma_{\Phi_2} \end{bmatrix} \widetilde{\Phi}(0) + \begin{bmatrix} \Gamma_{u_1} \\ - \\ \Gamma_{u_2} \end{bmatrix} \breve{u}_{dq}(0) \right\}
\tag{4.23}
$$

The subsystem that refers to current line $(i_1 \quad i_2)^t$ has been considered separately from capacitor voltages $(v_1 \quad v_2 \quad v_3)^t$: multipling the previous equation for $C_{12 \to abc}$ it is obtained

$$
C_{12 \to abc} \begin{bmatrix} i_1 \\ i_2 \end{bmatrix} = C_{12 \to abc} [\Psi_{1,1}] \begin{bmatrix} i_1 \\ i_2 \end{bmatrix} + C_{12 \to abc} [\Psi_{1,2}] \begin{bmatrix} v_1 \\ v_2 \\ v_3 \end{bmatrix}
$$
$$
+ \left\{ C_{12 \to abc} [\Gamma_{\Phi_1}] \widetilde{\Phi} + C_{12 \to abc} [\Gamma_{u_1}] \breve{u}_{dq} \right\}
\tag{4.24}
$$

Finally, considering (4.21) and (4.22)

$$
\begin{bmatrix} i_a \\ i_b \\ i_c \end{bmatrix} = C_{12 \to abc} [\Psi_{1,1}] C_{abc \to 12} \begin{bmatrix} i_a \\ i_b \\ i_c \end{bmatrix} + C_{12 \to abc} [\Psi_{1,2}] \begin{bmatrix} v_{r\_a} \\ v_{r\_b} \\ v_{r\_c} \end{bmatrix}
$$
$$
+ \left\{ C_{12 \to abc} [\Gamma_{\Phi_1}] \widetilde{\Phi} + C_{12 \to abc} [\Gamma_{u_1}] \breve{u}_{dq} \right\}
\tag{4.25}
$$

From which it is derived:

$$
[\Psi_{abc_{1,1}}] = C_{12 \to abc} [\Psi_{1,1}] C_{abc \to 12}
$$

$$
[\Psi_{abc_{1,2}}] = C_{12 \to abc} [\Psi_{1,2}]
$$

$$
[\Gamma_{\Phi 1_{abc}}] = C_{12 \to abc} [\Gamma_{\Phi_1}]
\tag{4.26}
$$

$$
[\Gamma_{u1_{abc}}] = C_{12 \to abc} [\Gamma_{u_1}]
$$

For capacitor voltages:

$$
\begin{bmatrix} v_{r\_a} \\ v_{r\_b} \\ v_{r\_c} \end{bmatrix} = [\Psi_{2,1}] C_{abc \to 12} \begin{bmatrix} i_a \\ i_b \\ i_c \end{bmatrix} + [\Psi_{2,2}] \begin{bmatrix} v_{r\_a} \\ v_{r\_b} \\ v_{r\_c} \end{bmatrix} + \left\{ [\Gamma_{\Phi_2}] \widetilde{\Phi} + [\Gamma_{u_2}] \breve{u}_{dq} \right\}
\tag{4.27}
$$

Hence:

$$[\Psi_{abc_{2,1}}] = [\Psi_{2,1}]C_{abc\rightarrow 12}$$

$$[\Psi_{abc_{2,2}}] = [\Psi_{2,2}]$$

$$[\Gamma_{\Phi 2_{abc}}] = [\Gamma_{\Phi 2}]$$

$$[\Gamma_{u2_{abc}}] = [\Gamma_{u2}]$$

(4.28)

Finally, the Poincarè map in abc −frame for the first cycle of reference is

$$\begin{bmatrix} i_a \\ i_b \\ i_c \\ v_{r\_a} \\ v_{r\_b} \\ v_{r\_c} \end{bmatrix} = \begin{bmatrix} \Psi_{abc\_1,1} & | & \Psi_{abc\_1,2} \\ - & | & - \\ \Psi_{abc\_2,1} & | & \Psi_{abc\_2,2} \end{bmatrix} \begin{bmatrix} i_a \\ i_b \\ i_c \\ v_{r\_a} \\ v_{r\_b} \\ v_{r\_c} \end{bmatrix} + \left\{ \begin{bmatrix} \Gamma_{\Phi 1_{abc}} \\ - \\ \Gamma_{\Phi 2_{abc}} \end{bmatrix} \tilde{\Phi}(0) + \begin{bmatrix} \Gamma_{u1_{abc}} \\ - \\ \Gamma_{u2_{abc}} \end{bmatrix} \check{u}_{dq}(0) \right\}$$

(4.29)

In order to develop LTI model to reproduce the operation of the whole circuit of Figure 4-2(a), it's possible to take as reference the state vector calculated in (4.29). To simplify the demonstration, a new state vector x of three variables abc (that can be voltages or currents) is defined instead of the whole vector $\tilde{y}_{abc}$. Hence the Poincaré map for the first cycle written in this new notation (denoted by accent "=") is:

$$\check{x}_{abc}(T_s) = \bar{\bar{\Psi}} \cdot \check{x}_{0\_abc} + \{\overline{\Gamma_\Phi} \cdot \tilde{\Phi}(0) + \bar{\Gamma}_u \cdot \check{u}_{dq}(0)\}$$

(4.30)

It's possible to relate state vectors at each sampling time with state vector from the first cycle $\check{x}_{abc}(T_s)$ over a period of operation throughout adattive matrices S_k and $T_k = S^t{}_k$ depicted in Table 4-1.

Table 4-1. Adattive matrices of state vector at each time sampling

k	TCR ON	S_k	T_k
0	a-b	$\begin{pmatrix} 1 & 0 & 0 \\ 0 & 1 & 0 \\ 0 & 0 & 1 \end{pmatrix}$	$\begin{pmatrix} 1 & 0 & 0 \\ 0 & 1 & 0 \\ 0 & 0 & 1 \end{pmatrix}$
1	a-c	$\begin{pmatrix} 0 & -1 & 0 \\ 0 & 0 & -1 \\ -1 & 0 & 0 \end{pmatrix}$	$\begin{pmatrix} 0 & 0 & -1 \\ -1 & 0 & 0 \\ 0 & -1 & 0 \end{pmatrix}$
2	b-c	$\begin{pmatrix} 0 & 0 & 1 \\ 1 & 0 & 0 \\ 0 & 1 & 0 \end{pmatrix}$	$\begin{pmatrix} 0 & 1 & 0 \\ 0 & 0 & 1 \\ 1 & 0 & 0 \end{pmatrix}$

3	a-b	$\begin{pmatrix} -1 & 0 & 0 \\ 0 & -1 & 0 \\ 0 & 0 & -1 \end{pmatrix}$	$\begin{pmatrix} -1 & 0 & 0 \\ 0 & -1 & 0 \\ 0 & 0 & -1 \end{pmatrix}$
4	a-c	$\begin{pmatrix} 0 & 1 & 0 \\ 0 & 0 & 1 \\ 1 & 0 & 0 \end{pmatrix}$	$\begin{pmatrix} 0 & 0 & 1 \\ 1 & 0 & 0 \\ 0 & 1 & 0 \end{pmatrix}$
5	b-c	$\begin{pmatrix} 0 & 0 & -1 \\ -1 & 0 & 0 \\ 0 & -1 & 0 \end{pmatrix}$	$\begin{pmatrix} 0 & -1 & 0 \\ 0 & 0 & -1 \\ -1 & 0 & 0 \end{pmatrix}$

Fixed:

$$\check{x}_{abc\_REF} = \check{x}_{0\_abc} \tag{4.31}$$

So, for a generic cycle k:

$$\check{x}_{k\_abc} = S_k \cdot \check{x}_{abc\_REF}, \qquad \check{x}_{abc\_REF} = T_k \cdot \check{x}_{k\_abc} \tag{4.32}$$

For a generic sample period, multiplying both members of (4.30) for S_k and denoting with $\check{x}_{k\_abc}(k+1) = S_k \cdot \check{x}_{abc}(k+1)$, where the sampling time is omitted (for example k is used instead of kT_s), Poincarè map is:

$$\check{x}_{k\_abc}(k+1) = S_k \cdot \overline{\overline{\Psi}} \cdot T_k \cdot \check{x}_{k\_abc}(k) + S_k \cdot \{\overline{\overline{\Gamma_\Phi}} \cdot \widetilde{\Phi}(k) + \overline{\overline{\Gamma_u}} \cdot \check{u}_{dq}(k)\} \tag{4.33}$$

In order to have a time invariant model in dq- reference, matrices V and W that describe Park's transformation associated with the orientation of the inputs defined in (4.11), are expressed by

$$V(t) = \frac{2}{3} \begin{bmatrix} \cos\left(\omega t + \frac{\pi}{6}\right) & \cos\left(\omega t - \frac{\pi}{2}\right) & \cos\left(\omega t - \frac{7\pi}{6}\right) \\ -\sin\left(\omega t + \frac{\pi}{6}\right) & -\sin\left(\omega t - \frac{\pi}{2}\right) & -\sin\left(\omega t - \frac{7\pi}{6}\right) \end{bmatrix} \tag{4.34}$$

$$W(t) = \begin{bmatrix} W_a(t) \\ W_b(t) \\ W_c(t) \end{bmatrix} = \begin{bmatrix} \cos\left(\omega t + \frac{\pi}{6}\right) & -\sin\left(\omega t + \frac{\pi}{6}\right) \\ \cos\left(\omega t - \frac{\pi}{2}\right) & -\sin\left(\omega t - \frac{\pi}{2}\right) \\ \cos\left(\omega t - \frac{7\pi}{6}\right) & -\sin\left(\omega t - \frac{7\pi}{6}\right) \end{bmatrix} \tag{4.35}$$

$V(t)$ projects stationary abc variables onto the rotating dq- reference frame and $W(t)$ projects dq- reference frame variables onto the stationary abc-reference frame. In this case it's not necessary to take into account the zero sequence component because at the sampling instant no TCR is conducting and it has delta-connected configuration.

Denoting with $V(k)$ and $W(k)$ matrices (4.34) and (4.35) calculated at each sampling instant and multiplying both members for $V(k+1)$, it is obtained:

$$\check{x}_{dq}(k+1) = V(k+1) \cdot \check{x}_{abc}(k+1)$$
$$= V(k+1) \cdot S_k \cdot \overline{\overline{\Psi}} \cdot T_k \cdot W(k) \cdot \check{x}_{dq}(k) + V(k+1) \cdot S_k$$
$$\cdot \{\Gamma_\Phi \cdot \tilde{\Phi}(k) + \Gamma_u \cdot \check{u}_{dq}(k)\} \qquad (4.36)$$

It's easy to verify that

$$V(k+1) \cdot S_k = V(1) \cdot S_0$$
$$T_k \cdot W(k) = T_0 \cdot W(0) \qquad (4.37)$$

Finding a LTI model in dq- reference written with a general state vector $\check{x}_{dq}$.

To apply this result to (4.29), following matrices are defined

$$\mho(t) = \begin{bmatrix} V(t) & 0 \\ 0 & V(t) \end{bmatrix} \qquad \text{Ш}(t) = \begin{bmatrix} W(t) & 0 \\ 0 & W(t) \end{bmatrix} \qquad (4.38)$$

it's possible to write a LTI discrete-time model over a general sampling period T_s

$$\check{y}_{dq}\big((k+1)T_s\big) = \Psi \check{y}_{dq}(kT_s) + \Gamma_\Phi \cdot \tilde{\Phi}(kT_s) + \Gamma_u \cdot \check{u}_{dq}(kT_s) \qquad (4.39)$$

where

$$\Psi = \mho(T_s) \cdot \Psi_{abc} \cdot \text{Ш}(0)$$
$$\Gamma_\Phi = \mho(T_s)\Gamma_{\Phi\_abc}$$
$$\Gamma_{u\_d} = \mho(T_s)\Gamma_{u\_d\_abc} \qquad (4.40)$$
$$\Gamma_{u\_q} = \mho(T_s)\Gamma_{u\_q\_abc}$$
$$\Gamma_u = (\Gamma_{u\_d} \quad \Gamma_{u\_q})$$

In Figure 4-3,Figure 4-4,Figure 4-6, Figure 4-5, Figure 4-8,Figure 4-7,Figure 4-10,Figure 4-9 the response of the system to different perturbations of source voltages and firing angle at instant $t_0 = 0.71\,s$ is given, with operation mode $\sigma_d = 45°$: the green line represents the linear discrete state space model, while the blue one is PSIM output.
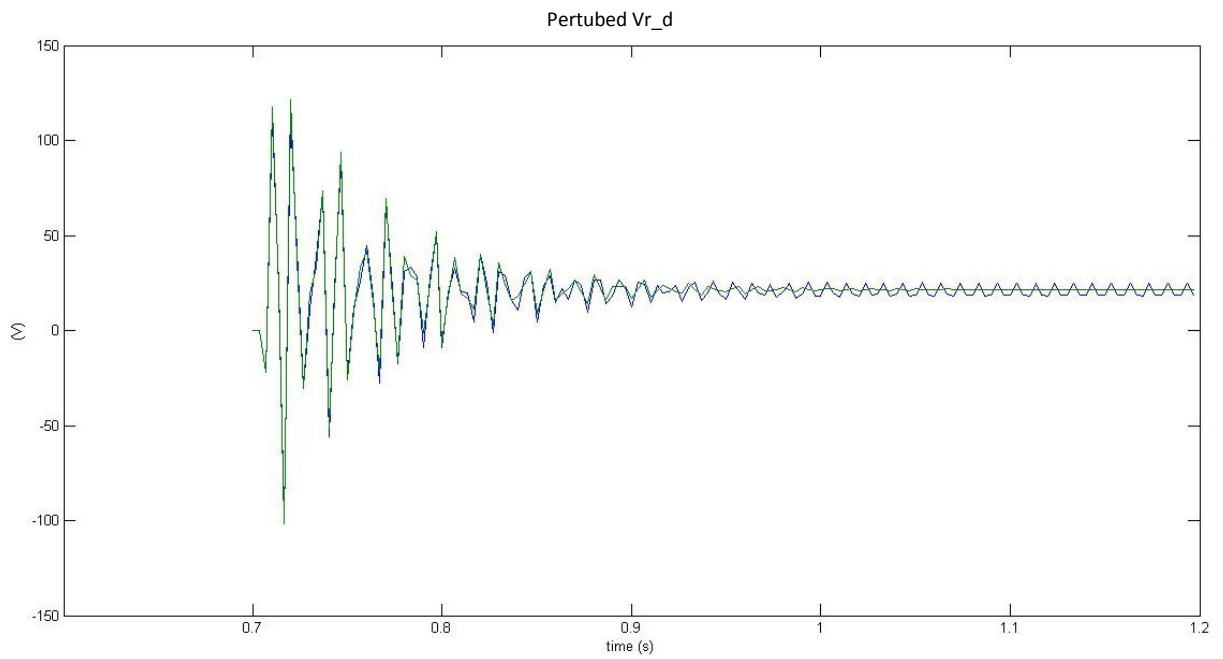
Figure 4-3 Perturbed capacitor voltage Vr_d response to a +1° step change in the firing angle. Green line for LTI discrete-time model and blue line for PSIM one
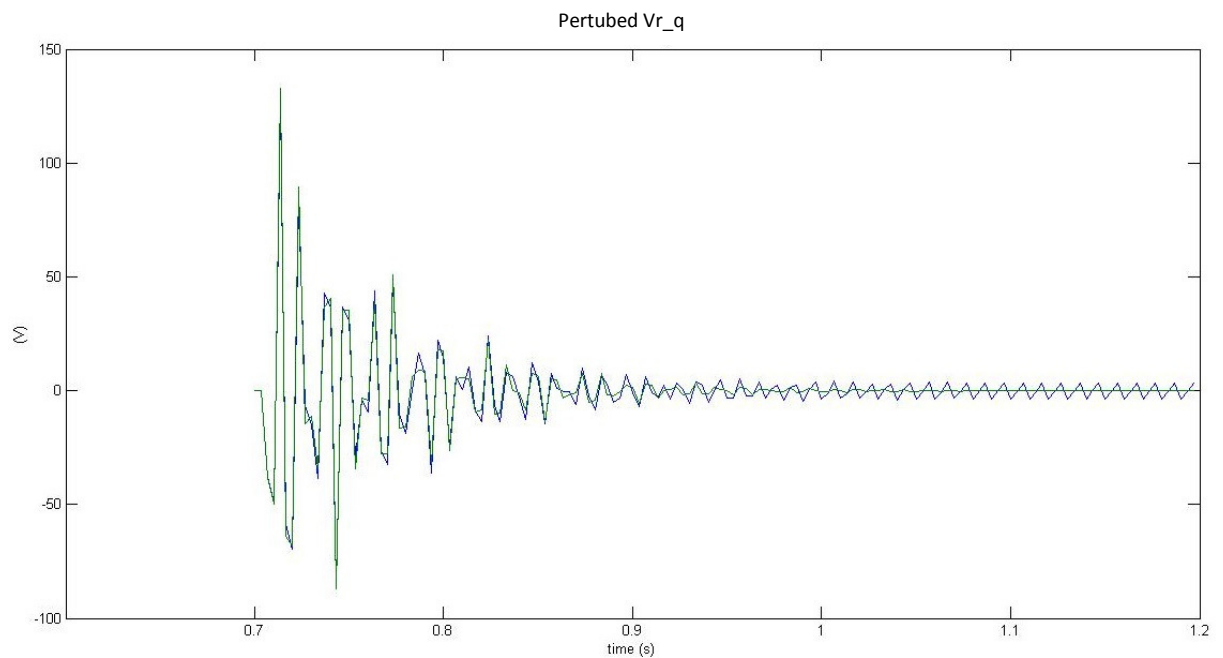
Figure 4-4 Perturbed capacitor voltage Vr_q response to a +1° step change in the firing angle. Green line for LTI discrete-time model and blue line for PSIM one
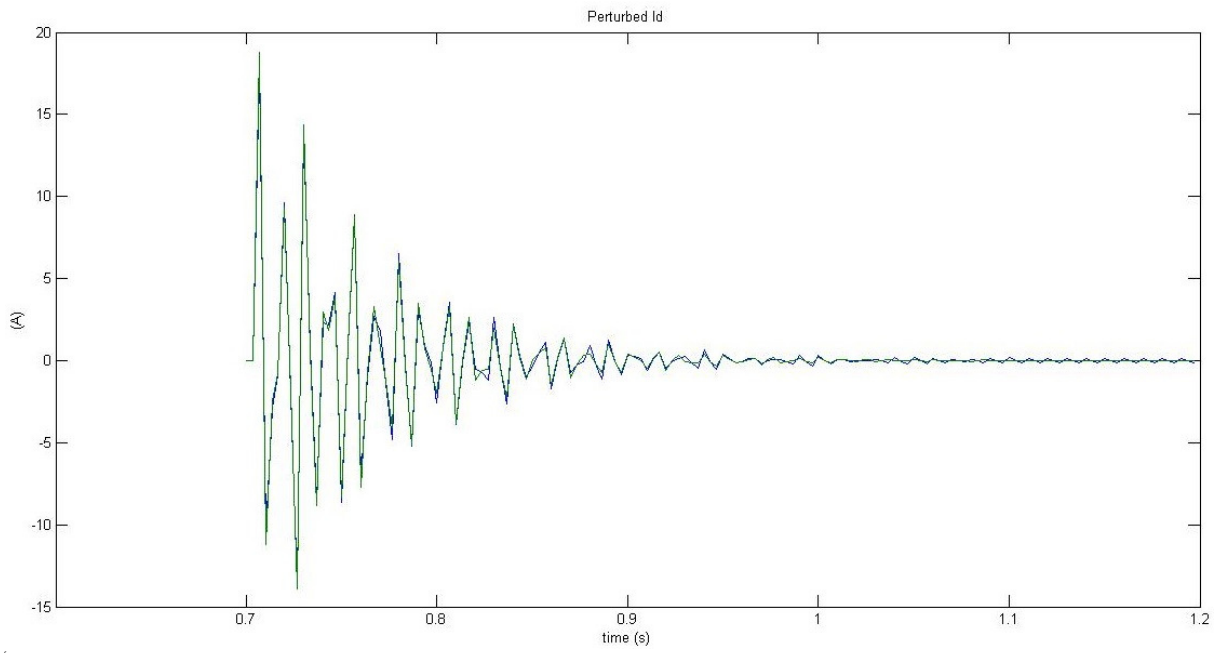
Figure 4-5 Perturbed line current i_d response to a +1° step change in the firing angle. Green line for LTI discrete-time model and blue line for PSIM one.
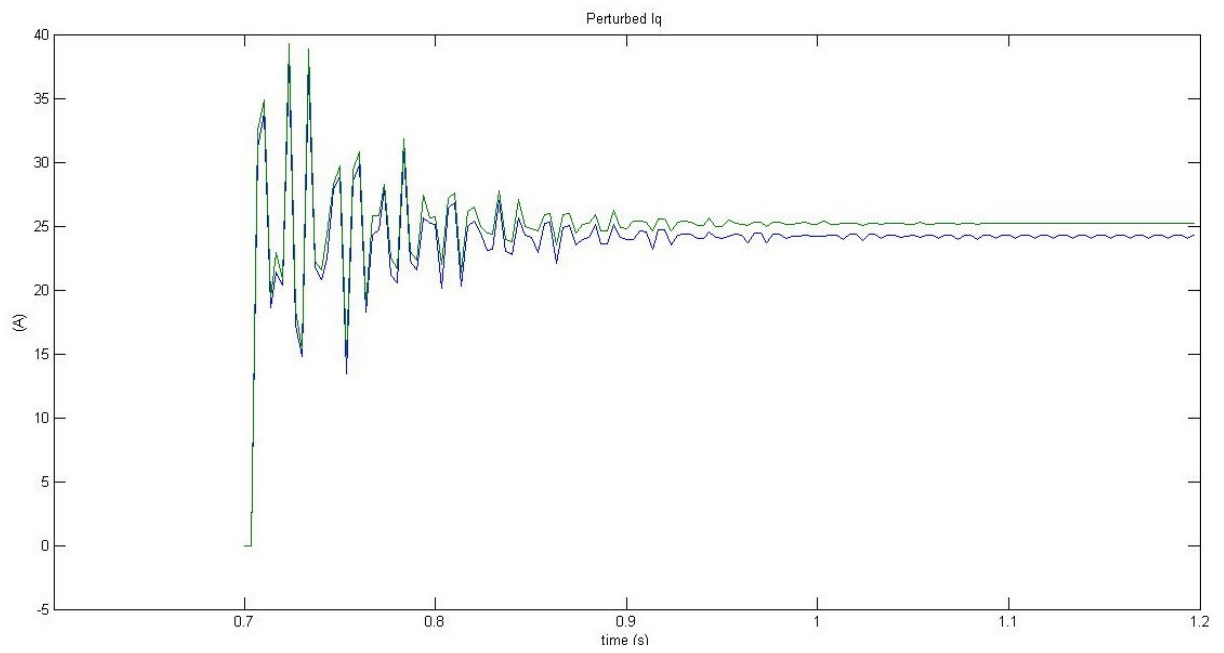
Figure 4-6 Perturbed line current i_q response to a +1° step change in the firing angle. Green line for LTI discrete-time model and blue line for PSIM one
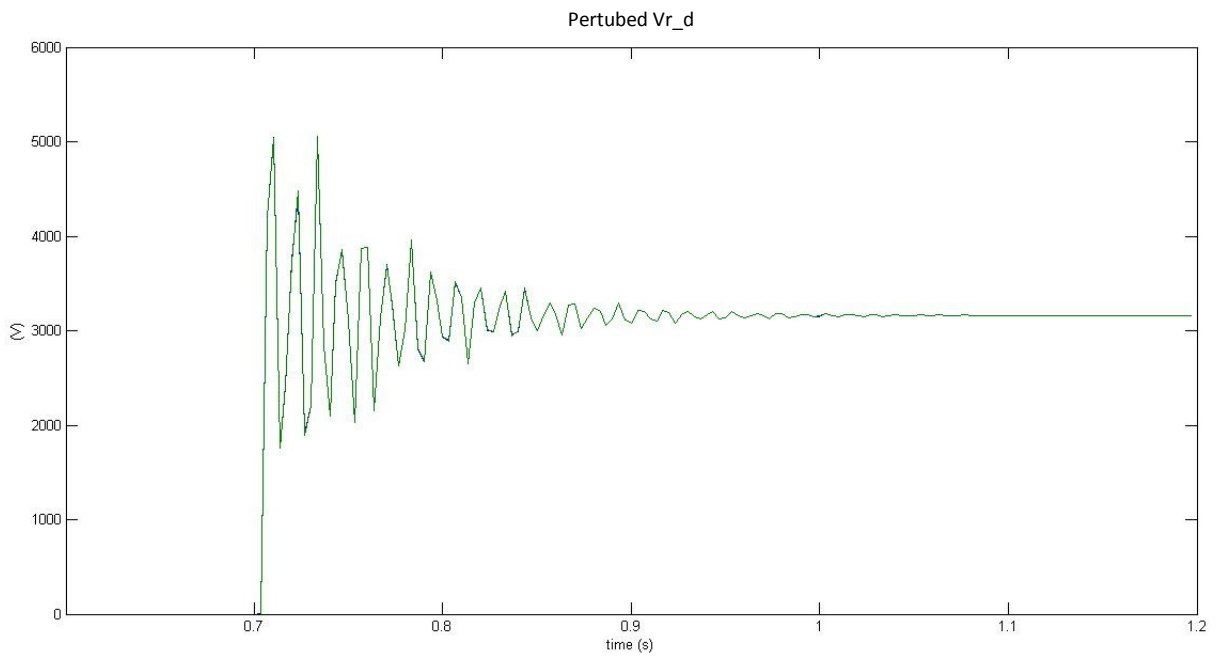
Figure 4-7 Perturbed capacitor voltage Vr_d response to a +5% step change in peak source voltage along d-axis. Green line for LTI discrete-time model and blue line for PSIM one
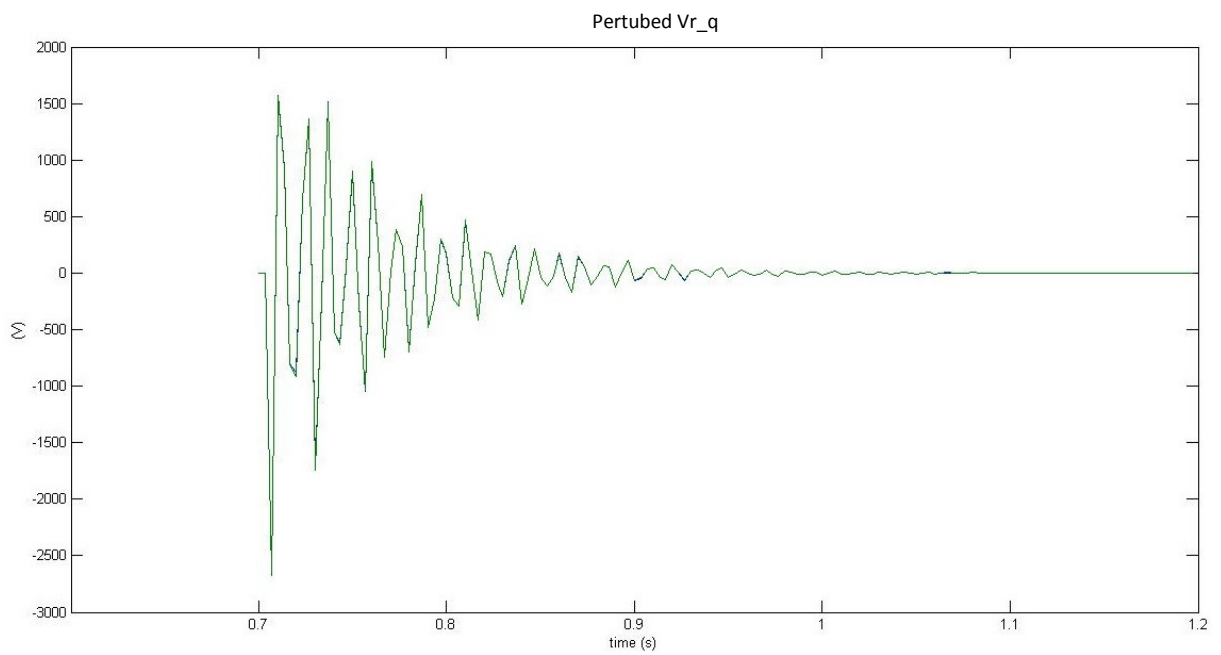
Figure 4-8 Perturbed capacitor voltage Vr_q response to a +5% step change in peak source voltage along d-axis. Green line for LTI discrete-time model and blue line for PSIM one
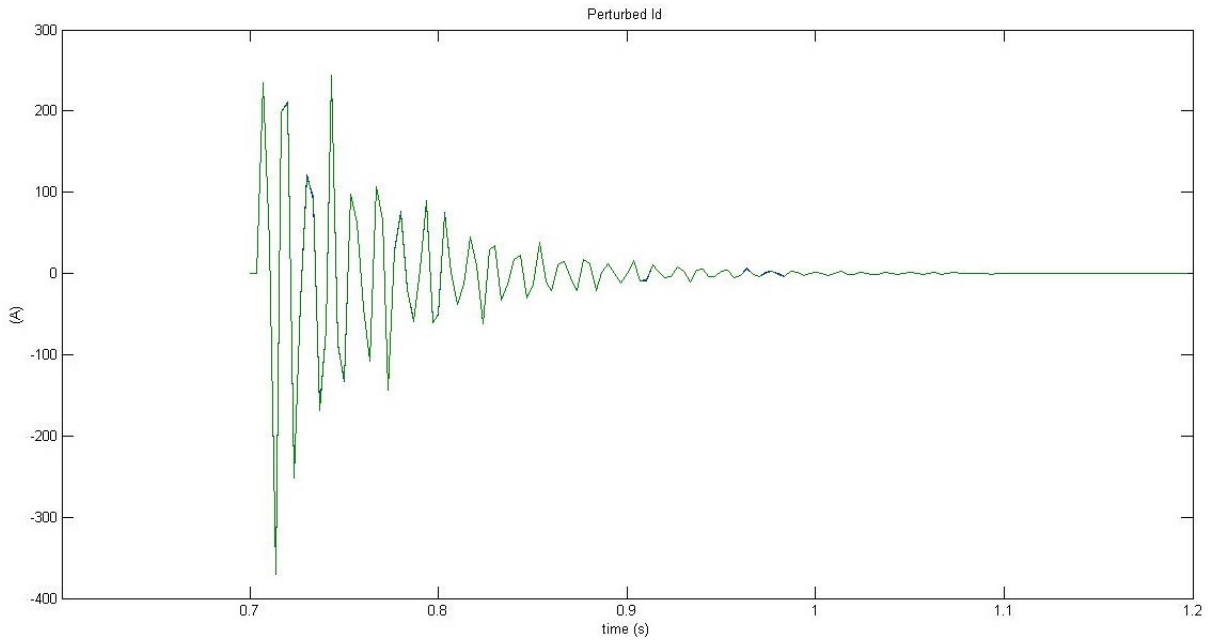
Figure 4-9 Perturbed line current i_d response to a 5% step change in peak source voltage along d-axis. Green line for LTI discrete time model and blue line for PSIM one
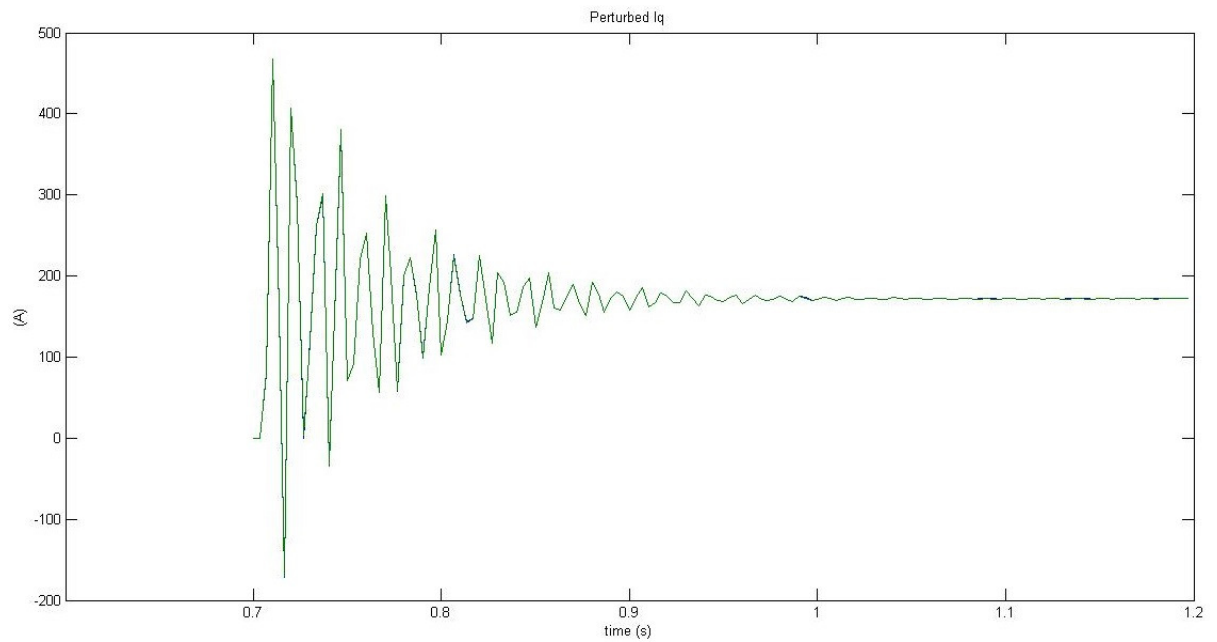
Figure 4-10 Perturbed line current i_q response to a 5% step change in peak source voltage along d-axis. Green line for LTI discrete time model and blue line for PSIM one

There is a very good matching between the two models in the two different perturbations for all the components of perturbed capacitor voltage and line current. In all case, after the perturbation, the system reach a new steady state operating point. Figure 4-3 andFigure 4-4 that respectively depict the perturbed capacitor voltage component Vr_d and Vr_q to a +1° step change in the firing angle, show that PSIM response swings around the steady state operation, while LTI response seems more stable, because of numerical errors due to the very small perturbation in the firing angle. This swing is minus visible in the perturbed line currents component i_d and i_q, show in Figure 4-5 and Figure 4-6, though still it remains. Also the small difference between the new steady state operating points of i_q reached by the two models may be due to numerical errors of the software. Finally, the perturbed capacitor voltage component Vr_d response to a 5% step change in peak source voltage along d-axis reaches a new equilibrium point compatible with the quantity of the perturbation given.

4.2   System modelling for conduction angle $\sigma \,\epsilon\, (60° - 120°)$

Respect to the previous section, the operating condition of the TCR is with a conduction angle of the thyristor included between 60 and 120 degrees, maintaining the same previous sample period of 60° electrical degree. It's considered a steady state operation point at instant t_0, synchronized with respect to the positive maximum of thyristor current when TCR_ab is conducting (see Figure 4-11). So taking as reference the interval between two sampling instants $[t_0, t_1]$, at t_0 TCR_ab is ON (other TCRs OFF), while at t_1 TCR_ac is ON (other TCRs OFF). When thyristors of both TCRs are conducting (interval $[\Phi_2, \tau_1]$) the circuit has state vector

$$x = \begin{pmatrix} i_1 & i_2 & v_1 & v_2 & v_3 & i_{r\_1} & i_{r\_2} \end{pmatrix}^t \qquad (4.41)$$

and the system dynamics are described by

$$\dot{x} = Ax + Bu_s \qquad (4.42)$$

The equations of the circuit in Figure 4-12(b) are:

$$\begin{cases} e_a - L_s\dfrac{di_1}{dt} - v_1 + v_3 - L_s\dfrac{di_1}{dt} - L_s\dfrac{di_2}{dt} - e_c = 0 \\[2mm] e_b - L_s\dfrac{di_2}{dt} - v_2 + v_3 - L_s\dfrac{di_1}{dt} - L_s\dfrac{di_2}{dt} - e_c = 0 \\[2mm] \dfrac{dv_1}{dt} = \dfrac{1}{C_r}(i_1 - i_{r\_1} + i_{r\_2}) \\[2mm] \dfrac{dv_2}{dt} = \dfrac{1}{C_r}(i_2 + i_{r\_1}) \\[2mm] \dfrac{dv_3}{dt} = \dfrac{1}{C_r}(-i_1 - i_2 - i_{r\_2}) \\[2mm] \dfrac{di_{r\_1}}{dt} = \dfrac{1}{L_r}(v_1 - v_2) \\[2mm] \dfrac{di_{r\_2}}{dt} = \dfrac{1}{L_r}(-v_1 - v_3) \end{cases} \qquad (4.43)$$

It is necessary to rearrange the first two equations in the system above to obtain the matrixes A and B, resulting:

$$\begin{bmatrix} 2 & 1 \\ 1 & 2 \end{bmatrix} L_s \begin{bmatrix} \dfrac{di_1}{dt} \\ \dfrac{di_2}{dt} \end{bmatrix} = \begin{pmatrix} 0 & 0 & -1 & 0 & 1 \\ 0 & 0 & 0 & -1 & 1 \end{pmatrix} \begin{bmatrix} i_1 \\ i_2 \\ v_1 \\ v_2 \\ v_3 \end{bmatrix} + \begin{pmatrix} 1 & 0 & -1 \\ 0 & 1 & -1 \end{pmatrix} \begin{bmatrix} e_a \\ e_b \\ e_c \end{bmatrix} \qquad (4.44)$$

So:

$$\begin{bmatrix} \dfrac{di_1}{dt} \\ \dfrac{di_2}{dt} \end{bmatrix} = \dfrac{1}{L_s}\begin{bmatrix} 2 & 1 \\ 1 & 2 \end{bmatrix}^{-1} \left(\begin{pmatrix} 0 & 0 & -1 & 0 & 1 \\ 0 & 0 & 0 & -1 & 1 \end{pmatrix} \begin{bmatrix} i_1 \\ i_2 \\ v_1 \\ v_2 \\ v_3 \end{bmatrix} + \begin{pmatrix} 1 & 0 & -1 \\ 0 & 1 & -1 \end{pmatrix} \begin{bmatrix} e_a \\ e_b \\ e_c \end{bmatrix} \right) \qquad (4.45)$$

On the right of the first matrix of the sum in (4.45), two columns of zeros have been added because of the TCR currents i_{r_1} and i_{r_2}, obtaining the first two rows of matrix A and B of system (4.42). The others rows have been built considering the state equation for capacitors and TCR inductors. So,

$$A = \begin{bmatrix} 0 & 0 & -2/(3Ls) & 1/(3Ls) & 1/(3Ls) & 0 & 0 \\ 0 & 0 & 1/(3Ls) & -2/(3Ls) & 1/(3Ls) & 0 & 0 \\ 1/C & 0 & 0 & 0 & 0 & -1/C & 1/C \\ 0 & 1/C & 0 & 0 & 0 & 1/C & 0 \\ -1/C & -1/C & 0 & 0 & 0 & 0 & -1/C \\ 0 & 0 & 1/Lr & -1/Lr & 0 & 0 & 0 \\ 0 & 0 & -1/Lr & 0 & 1/Lr & 0 & 0 \end{bmatrix}, \qquad (4.46)$$

$$B = \begin{bmatrix} 2/(3Ls) & -1/(3Ls) & -1/(3Ls) \\ -1/(3Ls) & 2/(3Ls) & -1/(3Ls) \\ 0 & 0 & 0 \\ 0 & 0 & 0 \\ 0 & 0 & 0 \\ 0 & 0 & 0 \\ 0 & 0 & 0 \end{bmatrix}, \quad u_s = \begin{bmatrix} e_a \\ e_b \\ e_c \end{bmatrix}.$$

In the interval $[t_0, \Phi_2]$ the projection and injection matrices associated with thyristor switching-on of TCR_ac (the notation "_2" highlights this association, as thyristor current in TCR_ac is named i_{r_2}) are

$$P\_2 = \begin{bmatrix} 1 & 0 & 0 & 0 & 0 & 0 & 0 \\ 0 & 1 & 0 & 0 & 0 & 0 & 0 \\ 0 & 0 & 1 & 0 & 0 & 0 & 0 \\ 0 & 0 & 0 & 1 & 0 & 0 & 0 \\ 0 & 0 & 0 & 0 & 1 & 0 & 0 \\ 0 & 0 & 0 & 0 & 0 & 1 & 0 \end{bmatrix} \qquad Q\_2 = P\_2' \tag{4.47}$$

The current in the conducting thyristor TCR_ab can be express as a linear combination of the state variable, defining a vector c_1 (for more detail see Section I.1 of Appendix I):

$$i_{r\_1} = c_1 x = \begin{pmatrix} 0 & 0 & 0 & 0 & 0 & 1 & 0 \end{pmatrix} x \tag{4.48}$$

The circuit has dynamic equations

$$\dot{y} = P\_2 \cdot A \cdot Q\_2 \cdot y + P\_2 \cdot B u_s \tag{4.49}$$

In the interval $[\tau_1, t_1]$ the projection and injection matrices associated with TCR_ab (the notation "_1" highlights this association, as thyristor current in TCR_ab i_{r_1} is going to zero) are:

$$P\_1 = \begin{bmatrix} 1 & 0 & 0 & 0 & 0 & 0 & 0 \\ 0 & 1 & 0 & 0 & 0 & 0 & 0 \\ 0 & 0 & 1 & 0 & 0 & 0 & 0 \\ 0 & 0 & 0 & 1 & 0 & 0 & 0 \\ 0 & 0 & 0 & 0 & 1 & 0 & 0 \\ 0 & 0 & 0 & 0 & 0 & 0 & 1 \end{bmatrix} \qquad Q\_1 = P\_1' \tag{4.50}$$

The current in the new conducting thyristor can be express as a linear combination of the state variable, defining a vector c_2 (for more detail see Section I.1 of Appendix I):

$$i_{r\_2} = c_2 x = \begin{pmatrix} 0 & 0 & 0 & 0 & 0 & 0 & 1 \end{pmatrix} x \tag{4.51}$$

with system dynamics described by

$$\dot{y} = P\_1 \cdot A \cdot Q\_1 \cdot y + P\_1 \cdot Bu_s \qquad\qquad (4.52)$$

In Figure 4-11 it's possible to distinguish the two different conduction modes inside a sample period $T_s = \frac{\pi/3}{\omega}$. The period of interest begins at t_0 when i_{r_1} is on its maximum: TCR_ab is ON, while the other two are OFF. Then, while TCR_ab is conducting there is the thyristor turn-on transition of TCR_ac at instant Φ_2 and after while TCR_ac is conducting there is the thyristor switching -off of TCR_ab at instant τ_1. Finally, the sample period T_s finishes when i_{r_2} reaches its maximum. Finally, generic instants of turn-on transition Φ and turn-off τ are highlighted, referred to the behaviour of thyristor currents according system dynamic.
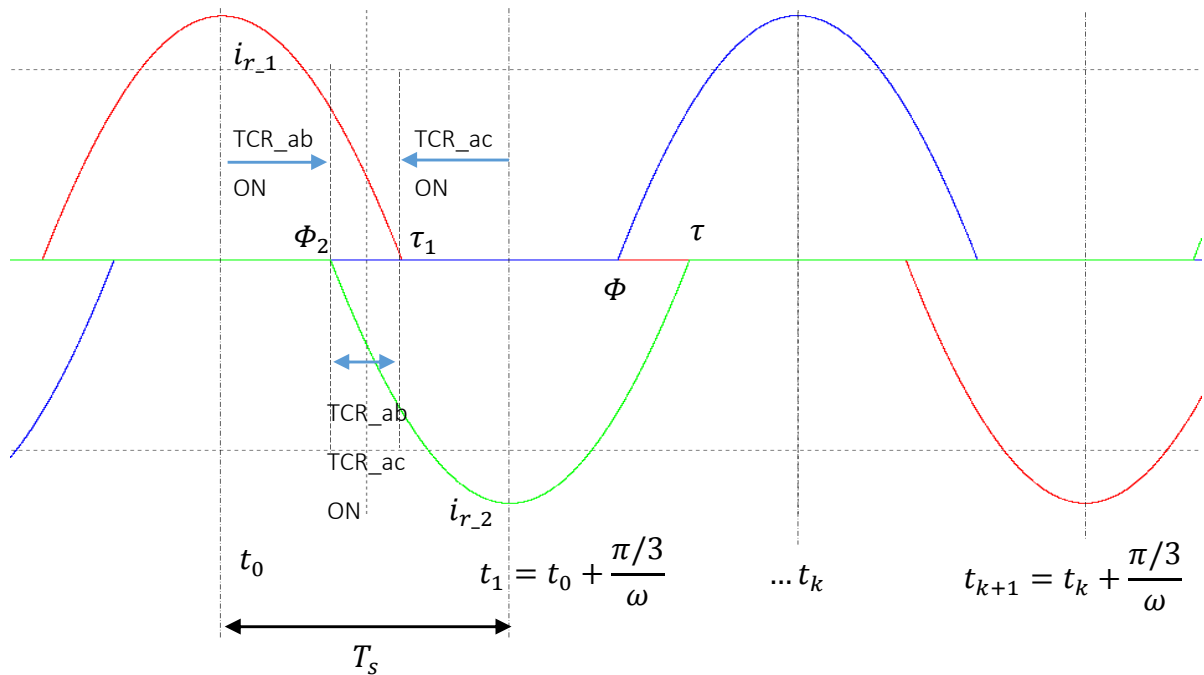
Figure 4-11 Three phase TCR branch current waveforms
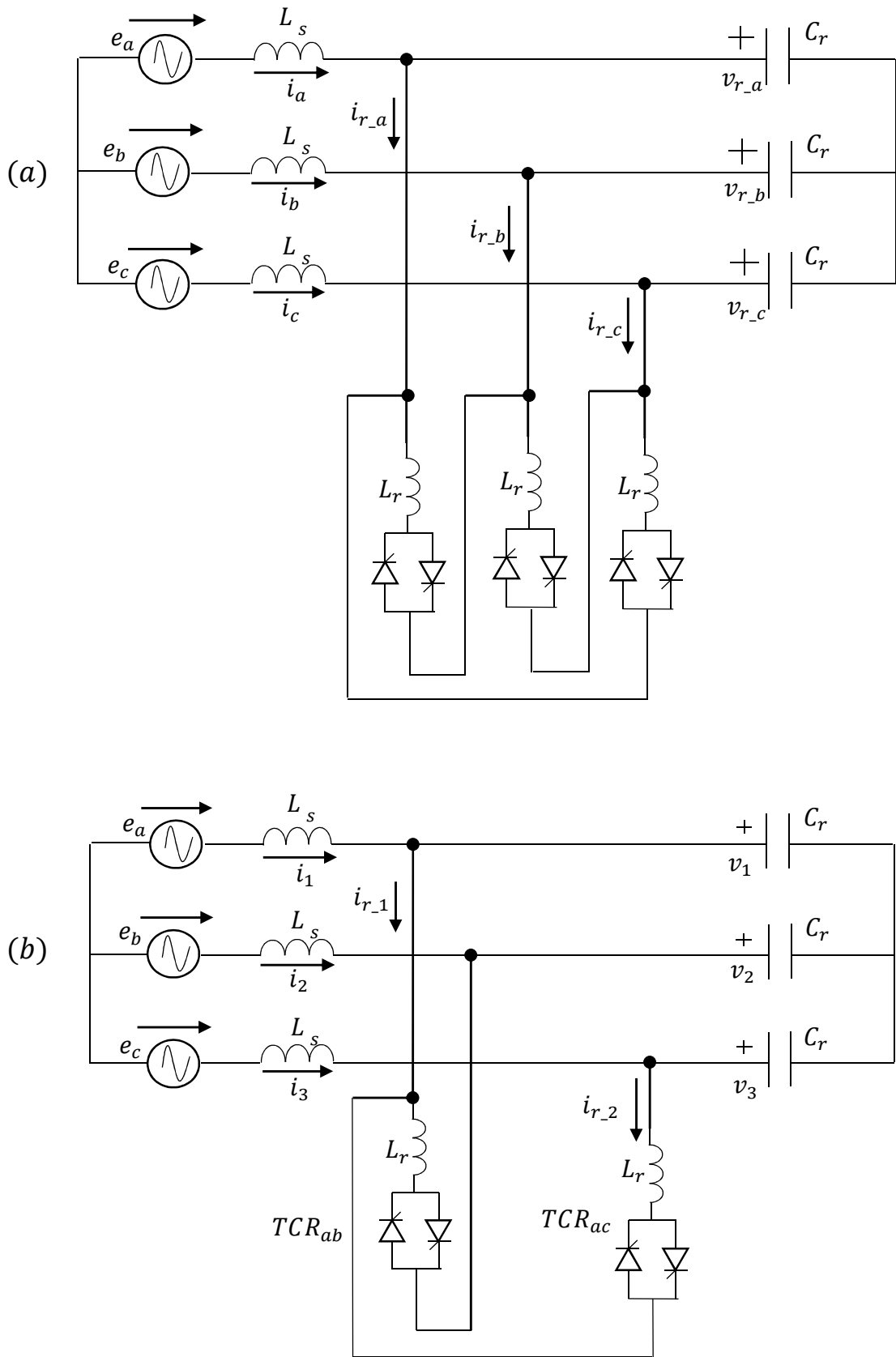
Figure 4-12 (a) Three-phase delta-connection SVC (b) Three-phase SVC with TCR_ab and TCR_ac ON

4.2.1 Three-phase non-linear model

If it is defined

$$W(t) = \begin{bmatrix} \cos(\omega t + \frac{\pi}{6}) & -sen(\omega t + \frac{\pi}{6}) \\ \cos(\omega t - \frac{\pi}{2}) & -sen(\omega t - \frac{\pi}{2}) \\ \cos(\omega t - \frac{7\pi}{6}) & -sen(\omega t - \frac{7\pi}{6}) \end{bmatrix}$$

the source voltages may be written:

$$u_s(t) = W(t) \cdot u_{dq}, \qquad u_{dq} = \begin{pmatrix} u_d \\ u_q \end{pmatrix} \tag{4.53}$$

where u_d and u_q are the direct and quadrature voltages respectively for a given reference frame. Figure 4-11(b) describes the system dynamics as the circuit evolves over a period. The representation of the state at thyristor turn-on and turn-off are

$$x(\Phi^+) = Q\_2 \cdot y(\Phi^-) \quad \text{and} \quad y(\tau^+) = P\_1 \cdot x(\tau^-) \tag{4.54}$$

respectively. The Poincarè map H_1 that projects the circuit state over the first cycle of reference, starting from instant $t_0 = 0$ (choosen as the maximum of i_{r_1}) to $t_1 = t_0 + T_s$, is

$$H_1: \quad \tilde{y}(0) \rightarrow y_1 = y(T_s) \tag{4.55}$$

is obtained by integrating (4.42), (4.49) and (4.52) in their own interval with mode transitions represented by (4.54). Let y_0 the state vector at steady state operating point at a general instant t_0. On the assumption that u_{dq} is constant over a general sampling period $T_s = \frac{\pi/3}{\omega}$, this yields:

$$y(\Phi) = e^{P\_2AQ\_2\,\Phi}y_0 + \int_0^{\Phi} e^{P\_2AQ\_2\,(\Phi - \xi)} P\_2B\, W_a(\xi)d\xi u_d$$

$$x(\Phi) = Q\_2 \cdot y(\Phi)$$

$$x(\tau) = e^{A(\tau - \Phi)}x(\Phi) + \int_{\Phi}^{\tau} e^{A(\tau - \xi)} B\, W_a(\xi)d\xi u_d \tag{4.56}$$

$$y(\tau) = P\_1 \cdot x(\tau)$$

$$y(T_s) = e^{P\_1AQ\_1\,(T_s - \tau)}y(\tau) + \int_{\tau}^{T_s} e^{P\_1AQ\_1\,(T_s - \xi)} P\_1B\, W_a(\xi)d\xi u_d$$

Relations in (4-56) are written for a generic instant of thyristor turn-on Φ, turn-off τ. As already explained in previous chapter, starting from the first relation of (4.56) and substituting in

sequence a formula into the next one, it yields to a non-linear Poincarè map over a general sample period T_s:

$$y(T_s) = e^{P\_1AQ\_1\,(T_s-\tau)}P\_1e^{A(\tau-\Phi)}Q\_2e^{P\_2AQ\_2\,\Phi} \cdot y_0 + h_1(\Phi, u_{dq})$$

(4.57)

where

$$h_1(\Phi, u_{dq}) = e^{P\_1AQ\_1\,(T_s-\tau)}P\_1$$

$$\cdot \left\{ e^{A(\tau-\Phi)}Q\_2 \int_0^\Phi e^{P\_2AQ\_2\,(\Phi-\xi)}P\_2B\,W_a(\xi)d\xi u_{dq} \right.$$

$$+ \int_\Phi^\tau e^{A(\tau-\xi)}B\,W_a(\xi)d\xi u_{dq} \right\}$$

(4.58)

$$+ \int_\tau^{T_s} e^{P\_1AQ\_1\,(T_s-\xi)}P\_1B\,W_a(\xi)d\xi u_{dq} \,.$$

4.2.2 Three-phase linear model

In order to investigate small signal stability of the system, it is necessary to linearize (4.59) to a first order approximation, under the assumption that the inputs u_{dq} and Φ are constant over the sample period T_s. Indeed, considering a perturbation from the nominal steady-state operation generally expressed by (4.57), the perturbed inputs and outputs (denoted with tilde) for the first cycle can be related by the Poincarè map H_1 in the form:

$$\tilde{y}_1 = \Psi \cdot \tilde{y}(0) + \left\{ \Gamma_\Phi \tilde{\Phi}(0) + \Gamma_u \breve{u}_{dq}(0) \right\}$$

(4.59)

Matrix Ψ represents the Jacobian $\dfrac{\partial H}{\partial y_0}$ of the Poincarè map (4.57) rewritten considering the steady-state conduction angle $\sigma_t = \tau - \Phi$:

$$\Psi = \frac{\partial H_1}{\partial y_0} = e^{P\_1AQ\_1\,(T_s-\frac{\sigma_t}{2})}P\_1e^{A(\sigma_t-T_s)}Q\_2e^{P\_2AQ\_2(T_s-\frac{\sigma_t}{2})}$$

(4.60)

Now differentiating (4.57) with respect to the firing instant (as it is reported in Section I.2.1), always considering the steady-state conduction angle σ_t:

$$\Gamma_\Phi = \left.\frac{\partial H_1}{\partial \Phi}\right|_{\Phi_2} = \left.\frac{\partial h_1(\Phi, u_{dq})}{\partial \Phi}\right|_{\Phi_2}$$

$$= e^{P\_1 A Q\_1 \left(T_s - \frac{\sigma_t}{2}\right)} P\_1 e^{A(\sigma_t - T_s)}\{Q\_2 \dot{y}(\Phi_2) - Ax(\Phi_2) - Bu_s(\Phi_2)\} \qquad (4.61)$$

$$= e^{P\_1 A Q\_1 \left(T_s - \frac{\sigma_t}{2}\right)} P\_1 e^{A(\sigma_t - T_s)}\{Q\_2 \cdot P\_2 - I\}\dot{x}(\Phi_2)$$

$$= -e^{P\_1 A Q\_1 \left(T_s - \frac{\sigma_t}{2}\right)} P\_1 e^{A(\sigma_t - T_s)} c_2{}^t c_2 \dot{x}(\Phi_2)$$

where $\{Q\_2 \cdot P\_2 - I\} = c_2{}^t c_2$ from the properties of projection and injection matrices (see Section I.1 of Appendix I for more details). Note that $c_2 \dot{x}(\Phi_2)$ is the gradient of the thyristor current i_{r_2} at turn-on. Finally

$$\Gamma_{u\_d} = \frac{\partial H_1}{\partial u_{dq}} = \frac{\partial h_1(\Phi_2, u_{dq})}{\partial u_{dq}} = h_1(\Phi_2, u_{dq}), with\ u_{dq} = \begin{pmatrix}1\\0\end{pmatrix}$$

$$\qquad (4.62)$$

$$\Gamma_{u\_q} = \frac{\partial H_1}{\partial u_{dq}} = \frac{\partial h_1(\Phi_2, u_{dq})}{\partial u_{dq}} = h_1(\Phi_2, u_{dq}), with\ u_{dq} = \begin{pmatrix}0\\1\end{pmatrix}$$

$$\Gamma_u = (\Gamma_{u\_d} \quad \Gamma_{u\_q})$$

In order to find a LTI model it's necessary to transform the state vector of five variables, developed considering a sample period where TCR_ab is conducting, into a state vector expressed in the abc −frame in the same sample period of reference. Considering the topology of the grid (see Figure 4-12(a)) the currents $(i_1 \quad i_2)^t$ are linked to currents $(i_a \quad i_b \quad i_c)^t$ through a matrix $C_{12 \to abc}$ finding:

$$\begin{bmatrix}i_a\\i_b\\i_c\end{bmatrix} = \begin{bmatrix}1 & 0\\0 & 1\\-1 & -1\end{bmatrix}\begin{bmatrix}i_1\\i_2\end{bmatrix}, \qquad C_{12 \to abc} = \begin{bmatrix}1 & 0\\0 & 1\\-1 & -1\end{bmatrix} \qquad (4.63)$$

$$\begin{bmatrix}i_1\\i_2\end{bmatrix} = \begin{bmatrix}0 & -1 & -1\\-1 & 0 & -1\end{bmatrix}\begin{bmatrix}i_a\\i_b\\i_c\end{bmatrix}, \qquad C_{abc \to 12} = \begin{bmatrix}0 & -1 & -1\\-1 & 0 & -1\end{bmatrix} \qquad (4.64)$$

while for capacitor voltage $[v_1 \quad v_2 \quad v_3]^t = [v_{r\_a} \quad v_{r\_b} \quad v_{r\_c}]^t$. This allows to transform Poincaré Map (4.59) based on a state vector (from now tilde that denotes perturbed quantities is omitted for variables inside the vectors):

$$\tilde{y} = (i_1 \quad i_2 \quad v_1 \quad v_2 \quad v_3 \quad i_r)^t$$

into a map written for the new state vector

$$\tilde{y}_{abc} = (i_a \quad i_b \quad i_c \quad v_{r\_a} \quad v_{r\_b} \quad v_{r\_c} \quad i_{r\_a} \quad i_{r\_b} \quad i_{r\_c})^t$$

The matrix Ψ is divided in nine sub-matrixes. So, rewriting (4.59) in extended form, omitting the sample instants "0" in which the initial state vector is valutated and "1" for the state vector obtained consequently, it is given:

$$
\begin{bmatrix} i_1 \\ i_2 \\ - \\ v_1 \\ v_2 \\ v_3 \\ - \\ i_r \end{bmatrix} = \begin{bmatrix} \Psi_{1,1} & | & \Psi_{1,2} & | & \Psi_{1,3} \\ - & | & - & | & - \\ \Psi_{2,1} & | & \Psi_{2,2} & | & \Psi_{2,3} \\ - & | & - & | & - \\ \Psi_{3,1} & | & \Psi_{3,2} & | & \Psi_{3,3} \end{bmatrix} \begin{bmatrix} i_1 \\ i_2 \\ - \\ v_1 \\ v_2 \\ v_3 \\ - \\ i_r \end{bmatrix} + \left\{ \begin{bmatrix} \Gamma_{\Phi 1} \\ - \\ \Gamma_{\Phi 2} \\ - \\ \Gamma_{\Phi 3} \end{bmatrix} \tilde{\Phi}(0 + \begin{bmatrix} \Gamma_{u1} \\ - \\ \Gamma_{u2} \\ - \\ \Gamma_{u3} \end{bmatrix} \check{u}_{dq}(0) \right\}
\qquad (\,4.65\,)
$$

Consider separately the subsystem of line currents $(i_1 \quad i_2)^t$, capacitor voltages $[v_1 \quad v_2 \quad v_3]^t$ and TCR currents (i_r).

For line currents multiplying the previous equation for $C_{12 \to abc}$ it is obtained

$$
C_{12 \to abc} \begin{bmatrix} i_1 \\ i_2 \end{bmatrix} = C_{12 \to abc} [\Psi_{1,1}] \begin{bmatrix} i_1 \\ i_2 \end{bmatrix} + C_{12 \to abc} [\Psi_{1,2}] \begin{bmatrix} v_1 \\ v_2 \\ v_3 \end{bmatrix} + C_{12 \to abc} [\Psi_{1,3}][i_r]
$$
$$
+ \left\{ C_{12 \to abc} [\Gamma_{\Phi 1}] \tilde{\Phi} + C_{12 \to abc} [\Gamma_{u1}] \check{u}_{dq} \right\}
\qquad (\,4.66\,)
$$

Considering (4.63) and (4.64), from (4.66) it is obtained

$$
\begin{bmatrix} i_a \\ i_b \\ i_c \end{bmatrix} = C_{12 \to abc} [\Psi_{1,1}] C_{abc \to 12} \begin{bmatrix} i_a \\ i_b \\ i_c \end{bmatrix} + C_{12 \to abc} [\Psi_{1,2}] \begin{bmatrix} v_{r\_a} \\ v_{r\_b} \\ v_{r\_c} \end{bmatrix} + C_{12 \to abc} [\Psi_{1,3}][i_r]
$$
$$
+ \left\{ C_{12 \to abc} [\Gamma_{\Phi 1}] \tilde{\Phi} + C_{12 \to abc} [\Gamma_{u1}] \check{u}_{dq} \right\}
\qquad (\,4.67\,)
$$

From which it can be derive:

$$
[\Psi_{abc_{1,1}}] = C_{12 \to abc} [\Psi_{1,1}] C_{abc \to 12}
$$

$$
[\Psi_{abc_{1,2}}] = C_{12 \to abc} [\Psi_{1,2}]
$$

$$
[\Psi_{abc_{1,3}}] = \left[\left(C_{12 \to abc} [\Psi_{1,3}] \right) \begin{matrix} 0 & 0 \\ 0 & 0 \\ 0 & 0 \end{matrix} \right]
\qquad (\,4.68\,)
$$

$$
[\Gamma_{\Phi 1_{abc}}] = C_{12 \to abc} [\Gamma_{\Phi 1}]
$$

$$\left[\Gamma_{u_{1abc}}\right] = C_{12 \to abc}\left[\Gamma_{u_1}\right]$$

For capacitor voltages:

$$\begin{bmatrix} v_a \\ v_b \\ v_c \end{bmatrix} = [\Psi_{2,1}]C_{abc \to 12}\begin{bmatrix} i_a \\ i_b \\ i_c \end{bmatrix} + [\Psi_{2,2}]\begin{bmatrix} v_{r\_a} \\ v_{r\_b} \\ v_{r\_c} \end{bmatrix} + [\Psi_{2,3}][i_r] + \{[\Gamma_{\Phi_2}]\tilde{\Phi} + [\Gamma_{u_2}]\breve{u}_{dq}\} \qquad (4.69)$$

Hence:

$$\left[\Psi_{abc_{2,1}}\right] = [\Psi_{2,1}]C_{abc \to 12}$$

$$\left[\Psi_{abc_{2,2}}\right] = [\Psi_{2,2}]$$

$$\left[\Psi_{abc_{2,3}}\right] = \left[\left([\Psi_{2,3}]\right)\begin{matrix} 0 & 0 \\ 0 & 0 \\ 0 & 0 \end{matrix}\right] \qquad (4.70)$$

$$\left[\Gamma_{\Phi_2{}_{abc}}\right] = [\Gamma_{\Phi_2}]$$

$$\left[\Gamma_{u_2{}_{abc}}\right] = [\Gamma_{u_2}]$$

For TCR currents to find the submatrices related, it's necessary to add two rows of zeros in the $[\Psi_{3,1}]$ $[\Psi_{3,2}]$ $[\Psi_{3,3}]$ that corresponds to the zero currents in TCRs that are OFF in the sample instant. So,

$$\left[\Psi_{abc_{3,1}}\right] = \left[\Psi_{abc_{3,1}}\right] = \begin{bmatrix} 0 & 0 & 0 \\ [& \Psi_{3,1}C_{abc \to 12} &] \\ 0 & 0 & 0 \end{bmatrix}$$

$$\left[\Psi_{abc_{3,2}}\right] = \begin{bmatrix} 0 & 0 & 0 \\ [& \Psi_{3,2} &] \\ 0 & 0 & 0 \end{bmatrix}$$

$$\left[\Psi_{abc_{3,3}}\right] = \begin{bmatrix} 0 & 0 & 0 \\ [\Psi_{3,3}] & 0 & 0 \\ 0 & 0 & 0 \end{bmatrix} \qquad (4.71)$$

$$\left[\Gamma_{\Phi_3{}_{abc}}\right] = \begin{bmatrix} 0 \\ \Gamma_{\Phi_3} \\ 0 \end{bmatrix}$$

$$\left[\Gamma_{u3\,abc}\right] = \begin{bmatrix} 0 \\ \Gamma_{u3} \\ 0 \end{bmatrix}$$

Finally, the Poincarè map H_1 in abc −frame for the first cycle of reference is

$$H_1: \begin{bmatrix} i_a \\ i_b \\ i_c \\ v_{r\_a} \\ v_{r\_b} \\ v_{r\_c} \\ i_{r\_a} \\ i_{r\_b} \\ i_{r\_c} \end{bmatrix} = \begin{bmatrix} \Psi_{abc\_1,1} & | & \Psi_{abc\_1,2} & | & \Psi_{abc\_1,3} \\ - & | & - & | & - \\ \Psi_{abc\_2,1} & | & \Psi_{abc\_2,2} & | & \Psi_{abc\_2,3} \\ - & | & - & | & - \\ \Psi_{abc\_3,1} & | & \Psi_{abc\_3,2} & | & \Psi_{abc\_3,3} \end{bmatrix} \begin{bmatrix} i_a \\ i_b \\ i_c \\ v_{r\_a} \\ v_{r\_b} \\ v_{r\_c} \\ i_{r\_a} \\ i_{r\_b} \\ i_{r\_c} \end{bmatrix}$$

$$+ \left\{ \begin{bmatrix} \Gamma_{\Phi 1_{abc}} \\ - \\ \Gamma_{\Phi 2_{abc}} \\ - \\ \Gamma_{\Phi 3_{abc}} \end{bmatrix} \tilde{\Phi}(0) + \begin{bmatrix} \Gamma_{u1_{abc}} \\ - \\ \Gamma_{u2_{abc}} \\ - \\ \Gamma_{u3_{abc}} \end{bmatrix} \breve{u}_{dq}(0) \right\}$$

(4.72)

The task is to have a LTI model to study the evolution of the whole system of Figure 4-12(a). in discrete-time domain, so transformation to the dq- reference frame is necessary. Park's transformation associated with the orientation of the inputs defined in (4.53)

$$V(t) = \frac{2}{3} \begin{bmatrix} \cos\left(\omega t + \frac{\pi}{6}\right) & \cos\left(\omega t - \frac{\pi}{2}\right) & \cos\left(\omega t - \frac{7\pi}{6}\right) \\ -\sin\left(\omega t + \frac{\pi}{6}\right) & -\sin\left(\omega t - \frac{\pi}{2}\right) & -\sin\left(\omega t - \frac{7\pi}{6}\right) \end{bmatrix}$$

(4.73)

$$W(t) = \frac{3}{2} \begin{bmatrix} W_a(t) \\ W_b(t) \\ W_c(t) \end{bmatrix} = \frac{3}{2} \begin{bmatrix} \cos\left(\omega t + \frac{\pi}{6}\right) & -\sin\left(\omega t + \frac{\pi}{6}\right) \\ \cos\left(\omega t - \frac{\pi}{2}\right) & -\sin\left(\omega t - \frac{\pi}{2}\right) \\ \cos\left(\omega t - \frac{7\pi}{6}\right) & -\sin\left(\omega t - \frac{7\pi}{6}\right) \end{bmatrix}$$

(4.74)

where $V(t)$ projects stationary abc variables onto the rotating dq- reference frame and $W(t)$ projects dq- reference frame variables onto the stationary abc-reference frame.

A conduction angle σ ∈ (60°, 120°) in a delta-connected TCR implies a zero sequence current i_γ with period $T = 120°$ flowing <u>only</u> in the triangle of TCR: it exhibits odd halfwave symmetry. To take into account this, it's necessary to consider $abc \rightarrow dq\gamma$ transformation only for TCR currents, modifying (4.73) (4.74) as follows:

75

$$V_{dq\gamma}(t) = \frac{2}{3}\begin{bmatrix} \cos\left(\omega t + \frac{\pi}{6}\right) & \cos\left(\omega t - \frac{\pi}{2}\right) & \cos\left(\omega t - \frac{7\pi}{6}\right) \\ -\sin\left(\omega t + \frac{\pi}{6}\right) & -\sin\left(\omega t - \frac{\pi}{2}\right) & -\sin\left(\omega t - \frac{7\pi}{6}\right) \\ 1/2 & 1/2 & 1/2 \end{bmatrix} \qquad (4.75)$$

$$W_{dq\gamma}(t) = \frac{3}{2}\begin{bmatrix} W_a(t) \\ W_b(t) \\ W_c(t) \end{bmatrix} = \frac{3}{2}\begin{bmatrix} \cos\left(\omega t + \frac{\pi}{6}\right) & -\sin\left(\omega t + \frac{\pi}{6}\right) & 1 \\ \cos\left(\omega t - \frac{\pi}{2}\right) & -\sin\left(\omega t - \frac{\pi}{2}\right) & 1 \\ \cos\left(\omega t - \frac{7\pi}{6}\right) & -\sin\left(\omega t - \frac{7\pi}{6}\right) & 1 \end{bmatrix} \qquad (4.76)$$

A linear time-invariant model in dq- frame can be calculated as in the previous chapter. Defining

$$\mho(\theta) = \begin{bmatrix} V(t) & 0 & 0 \\ 0 & V(t) & 0 \\ 0 & 0 & V_{dq\gamma}(t) \end{bmatrix} \qquad \mathrm{III}(t) = \begin{bmatrix} W(t) & 0 & 0 \\ 0 & W(t) & 0 \\ 0 & 0 & W_{dq\gamma}(t) \end{bmatrix} \qquad (4.77)$$

Now, as deeply shown in Chapter 3, it's possible to pass from a time-varying model expressed by Poincarè map (4.72) for the first reference cycle to a LTI model only if values in the columns of Ψ that refers to zero sequence component of TCR currents are chaged in sign. For this reason, the linear time invariant model is expressed in this new $dq0$- frame:

$$\widecheck{y}_{dq0}\big((k+1)T_s\big) = \Psi\widecheck{y}_{dq0}(kT_s) + \Gamma_\Phi\widetilde{\Phi}(0) + \Gamma_u\widecheck{u}_{dq}(0) \qquad (4.78)$$

where

$$\begin{aligned} \Psi &= \mho(T_s)\,\Psi_{abc}\,\mathrm{III}(0) \\ \Psi(n,7) &= -\Psi(n,7), \text{ with } n \in [1,7] \\ \Gamma_\Phi &= \mho(T_s)\,\Gamma_{\Phi\_abc} \\ \Gamma_{ud} &= \mho(T_s)\,\Gamma_{ud\_abc} \\ \Gamma_{uq} &= \mho(T_s)\,\Gamma_{uq\_abc} \\ \Gamma_u &= (\Gamma_{u\_d} \quad \Gamma_{u\_q}) \end{aligned} \qquad (4.79)$$

Figure 4-13, Figure 4-14, Figure 4-15, Figure 4-16, Figure 4-18, Figure 4-17 and Figure 4-19 compare the perturbed state variables response of the LTI model (green line) with PSIM model (blue line) for a +1° step change in the firing angle for the operating mode $\sigma_d = 75°$, in the discrete-time domain. The SVC is operating in steady-state and at time $t_0 = 0.71\ s$, the step change is applied. The linearized model captures the dynamic response of the SVC associated with the transient process leading from one cyclic mode to the next.

Figure 4-13 Perturbed capacitor voltage Vr_d response to a +1° step change in the firing angle. Green line for LTI discrete-time model and blue line for PSIM one.

Figure 4-14 Perturbed capacitor voltage Vr_q response to a +1° step change in the firing angle. Green line for LTI discrete-time model and blue line for PSIM one.
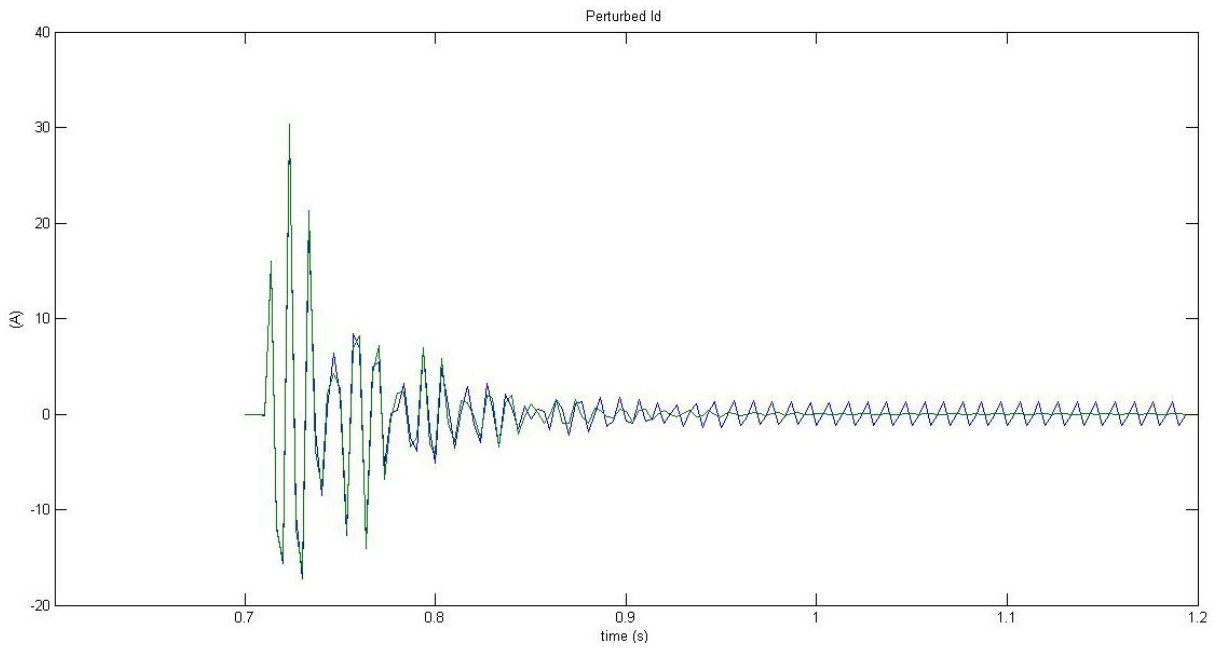
Figure 4-15 Perturbed line current i_d response to a +1° step change in the firing angle. Green line for LTI discrete-time model and blue line for PSIM one.
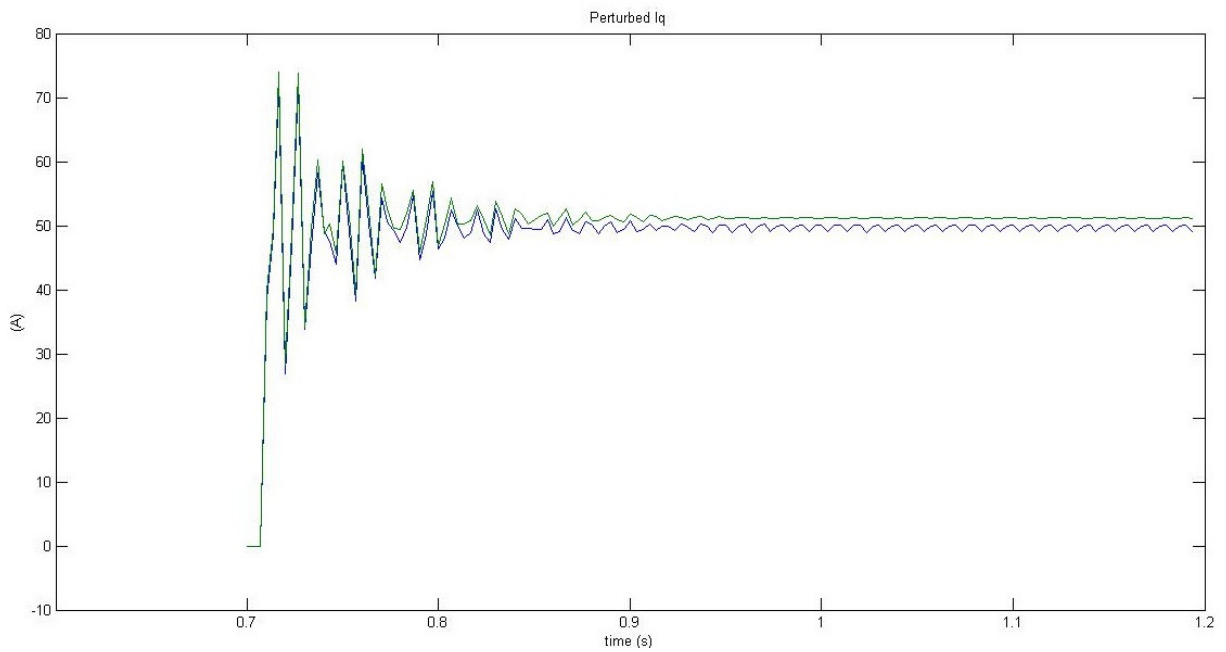
Figure 4-16 Perturbed line current i_q response to a +1° step change in the firing angle. Green line for LTI discrete-time model and blue line for PSIM one.
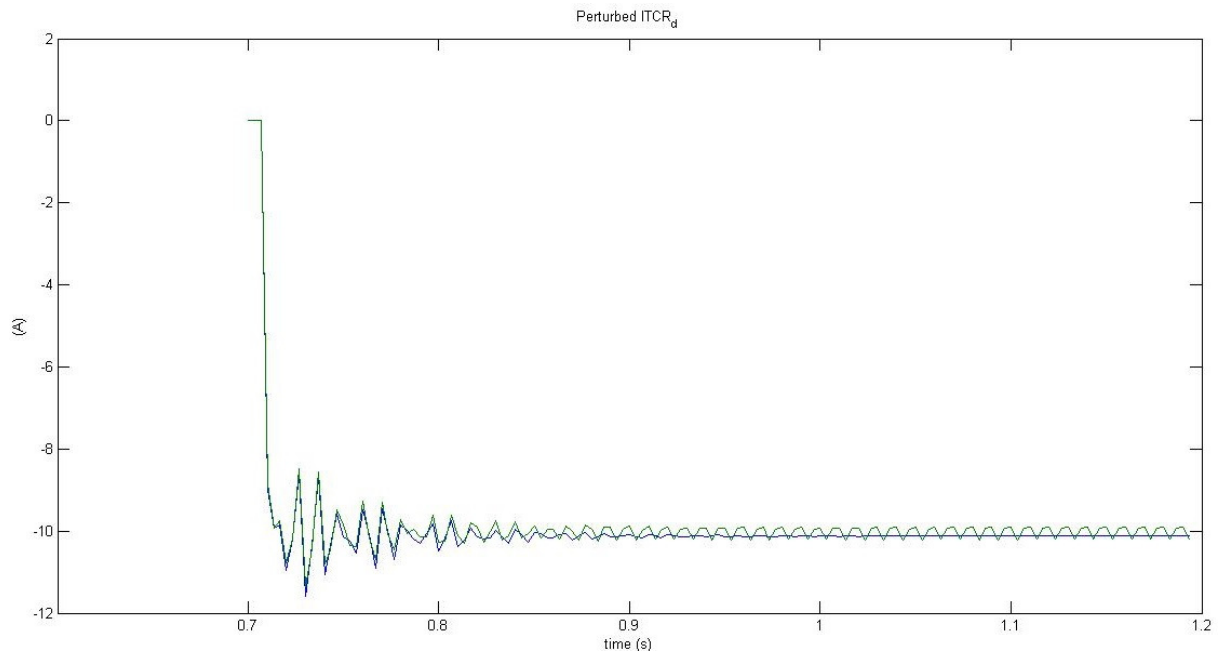
Figure 4-17 Perturbed thyristor current iTCR_d response to a +1° step change in the firing angle. Green line for LTI discrete-time model and blue line for PSIM one.
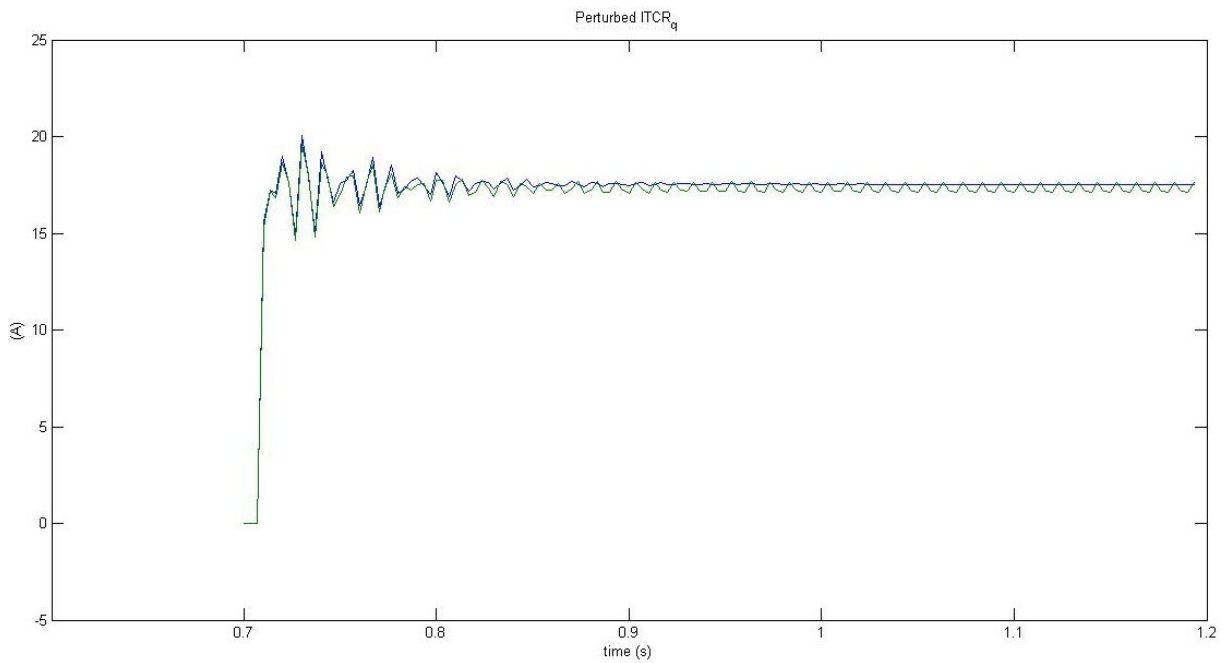
Figure 4-18 Perturbed thyristor current iTCR_q response to a +1° step change in the firing angle. Green line for LTI discrete-time model and blue line for PSIM one.

79
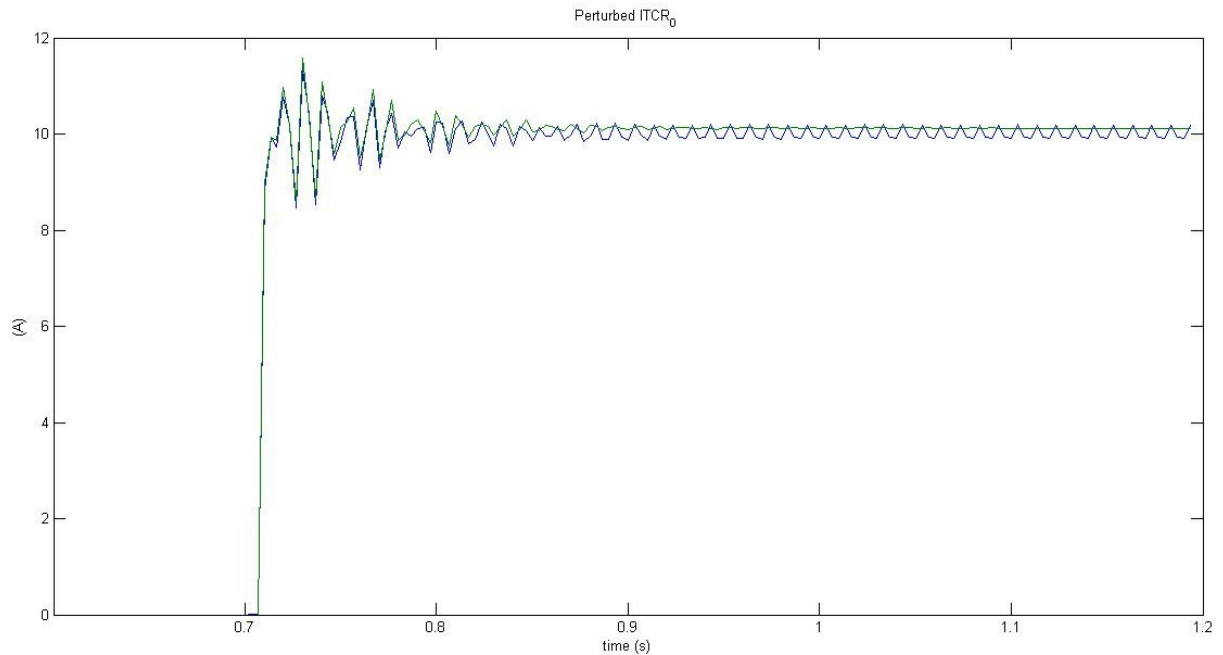
Figure 4-19 Perturbed thyristor current |iTCR_0| response to a +1° step change in the firing angle. Green line for LTI discrete-time model and blue line for PSIM one.

There is a very good matching between the two models for all the components of perturbed capacitor voltage and line current and after the perturbation in the firing angle the system reaches a new steady steate operation point. Moreover, it is highlighted that the absolute value of zero sequence component "0" of the TCR current has been plotted because it changes sign at each odd cycle respect to the "real" γ component as also happened for the zero sequence component of the line current in the star-connected TCR studied in Chapter 3. The swing around the operating point for PSIM response is compatible with software numerical errors due to the quantity of the perturbation.

Figure 4-20, Figure 4-21, Figure 4-23, Figure 4-22, Figure 4-25, Figure 4-24 and Figure 4-26 compare the perturbed state variables response of the LTI model (green line) with PSIM model (blue line) for a +5% step change to peak sorce voltage along d-axis for the operating mode $\sigma_d = 45°$, in the discrete-time domain. The SVC is operating in steady-state and at time $t_0 = 0.71\ s$, the step change is applied. The linearized model captures the dynamic response of the SVC associated with the transient process leading from one cyclic mode to the next.
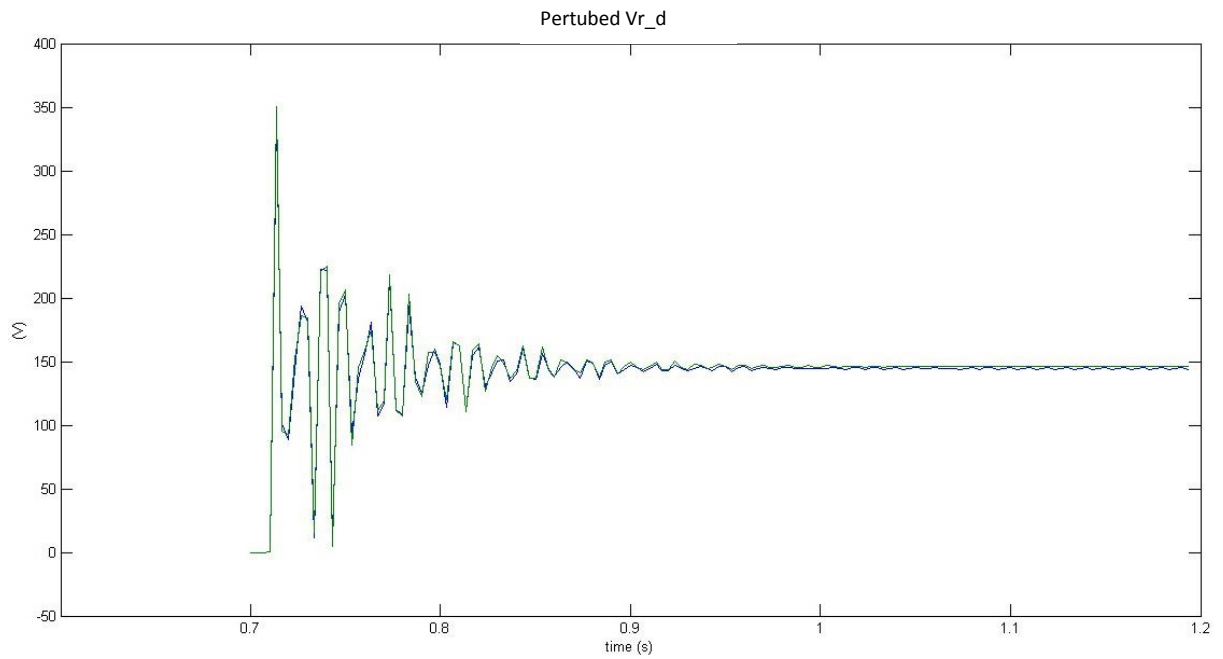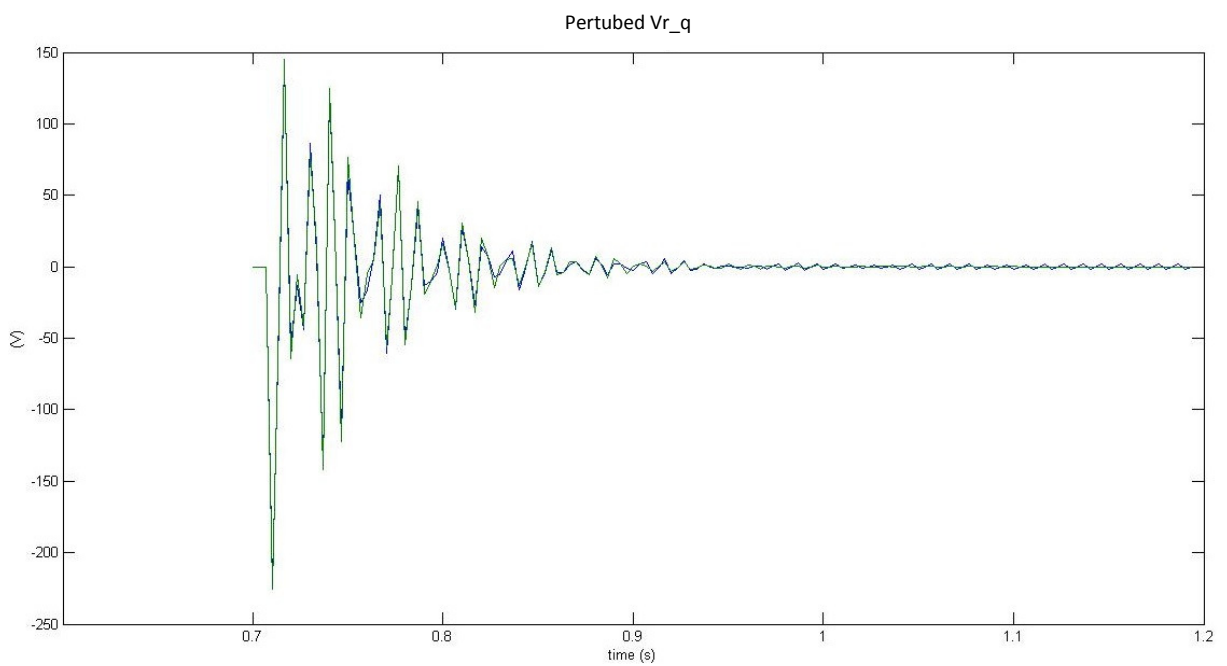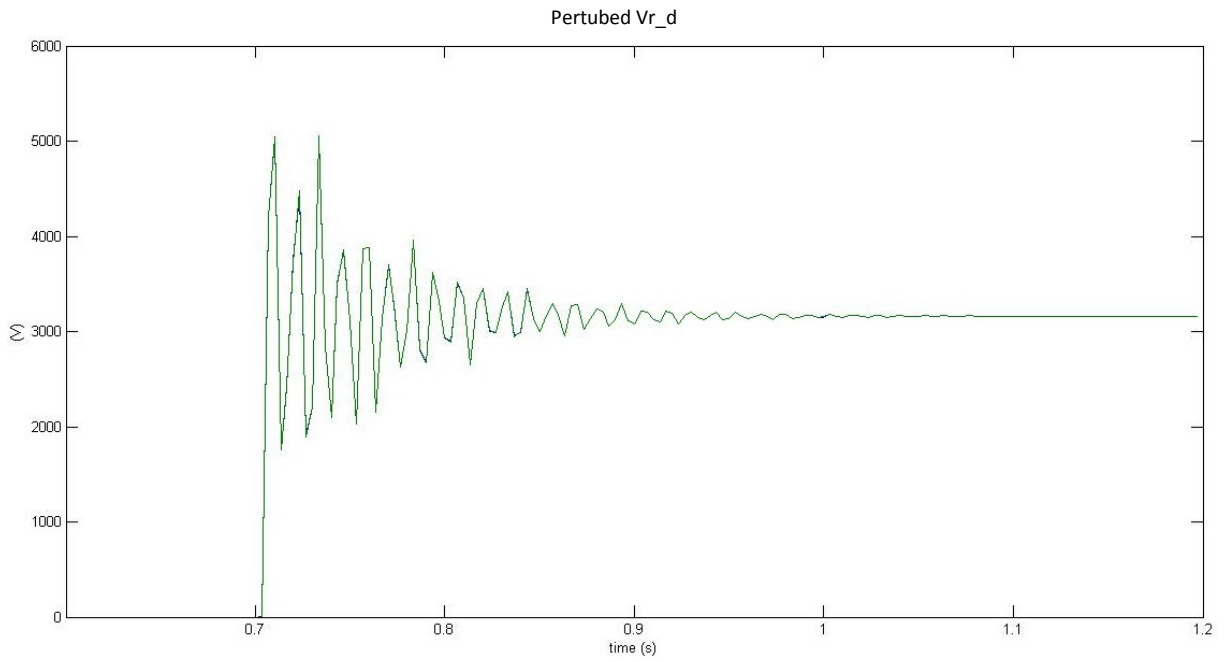
Figure 4-20 Perturbed capacitor voltage Vr_d response to a +5% step change in peak source voltage along d-axis. Green line for LTI discrete-time model and blue line for PSIM one.
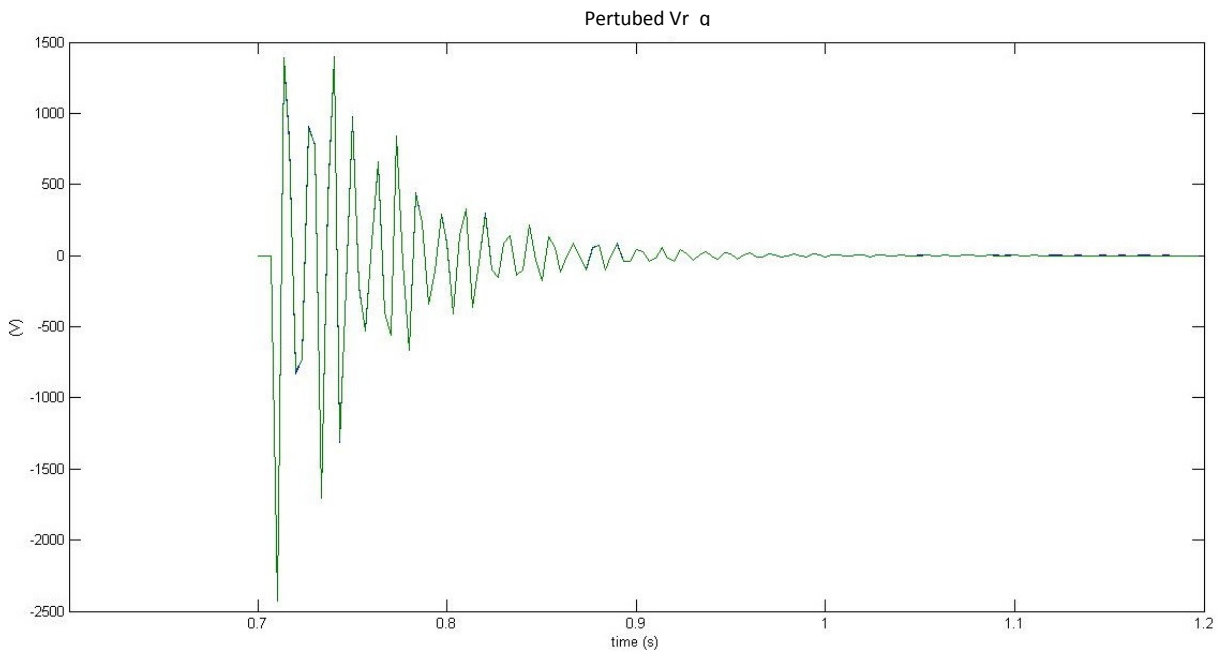
Figure 4-21 Perturbed capacitor voltage Vr_q response to a +5% step change in peak source voltage along d-axis. Green line for LTI discrete-time model and blue line for PSIM one.
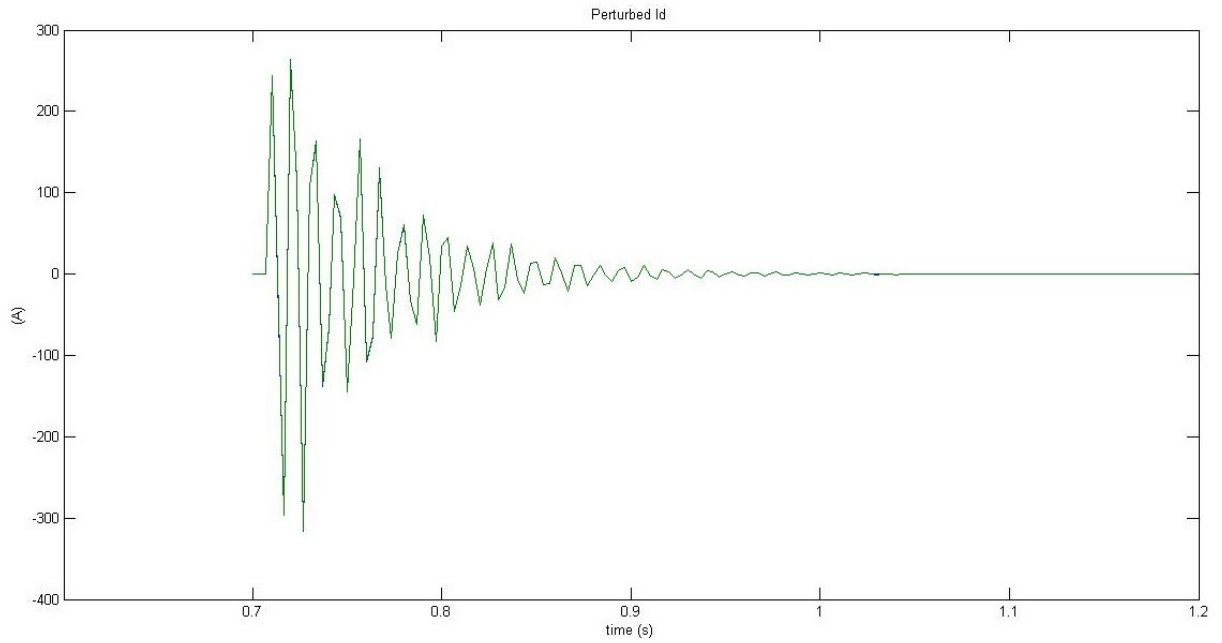
Figure 4-22 Perturbed line current i_d response to a +5% step change in peak source voltage along d-axis. Green line for LTI discrete-time model and blue line for PSIM one.
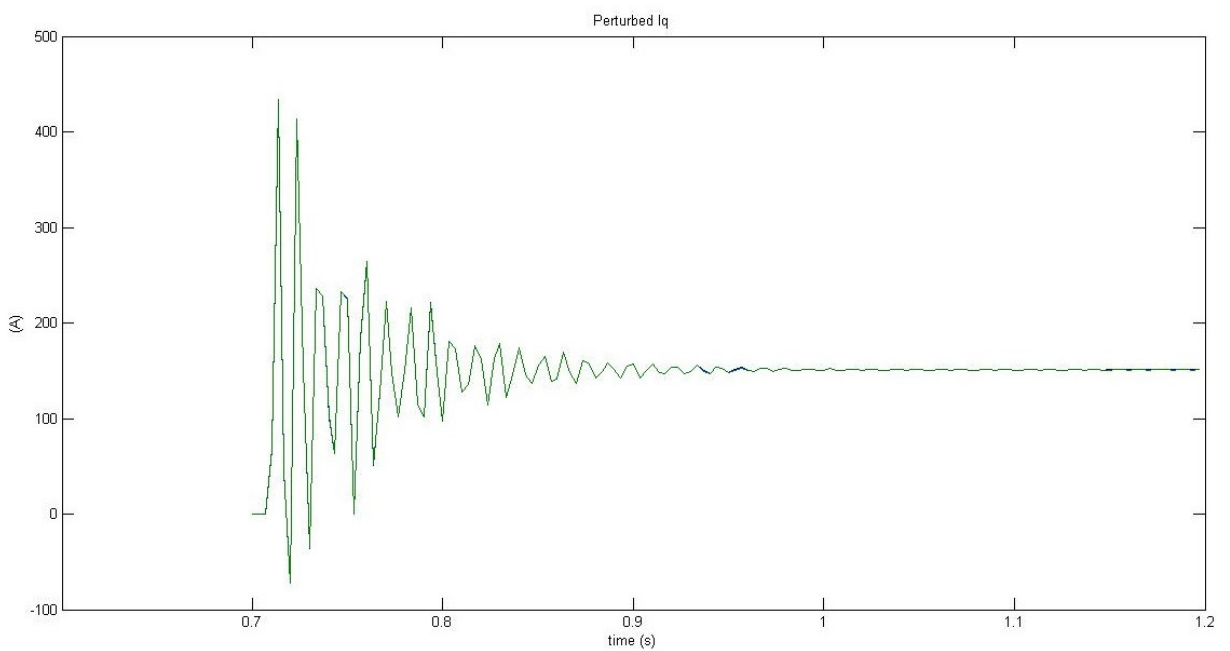
Figure 4-23 Perturbed line current i_q response to a +5% step change in peak source voltage along d-axis. Green line for LTI discrete-time model and blue line for PSIM one.
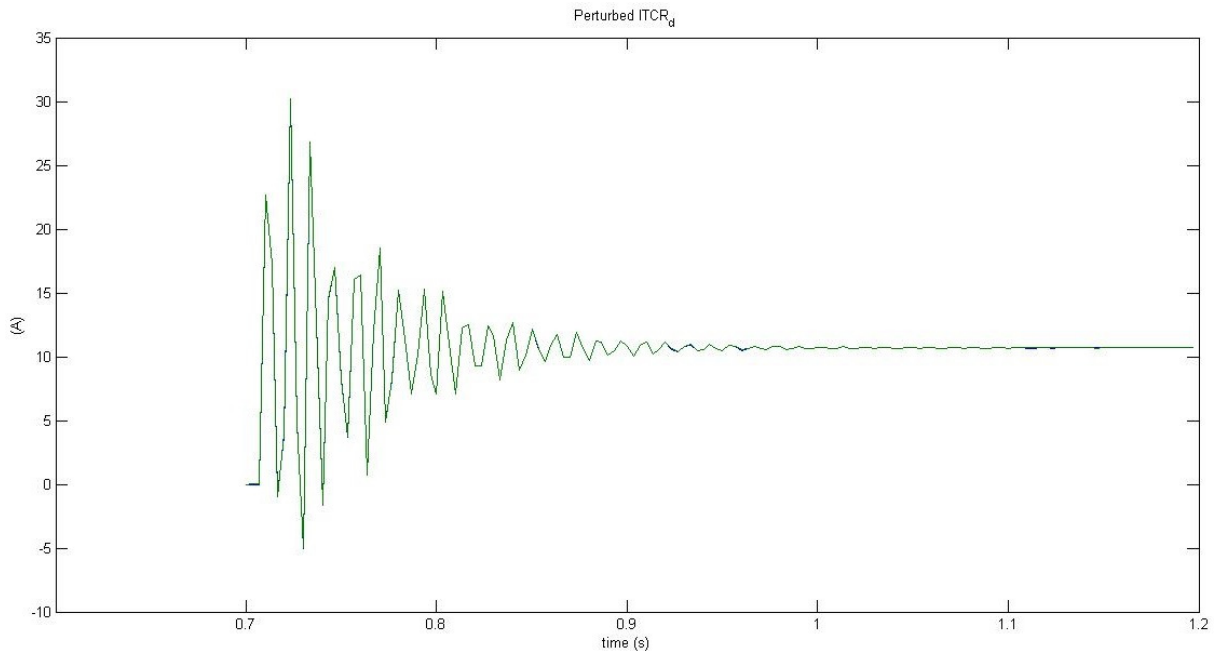
Figure 4-24 Perturbed TCR current iTCR_d response to a +5% step change in peak source voltage along d-axis. Green line for LTI discrete-time model and blue line for PSIM one.
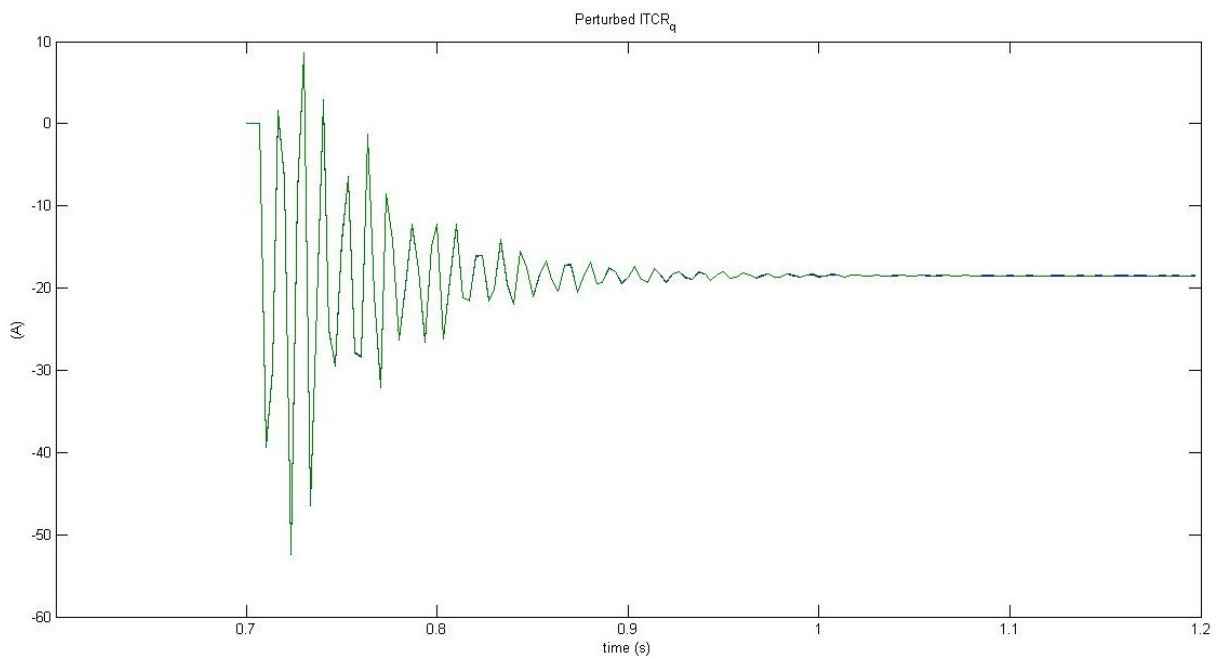
Figure 4-25 Perturbed TCR current iTCR_q response to a +5% step change in peak source voltage along d-axis. Green line for LTI discrete-time model and blue line for PSIM one.
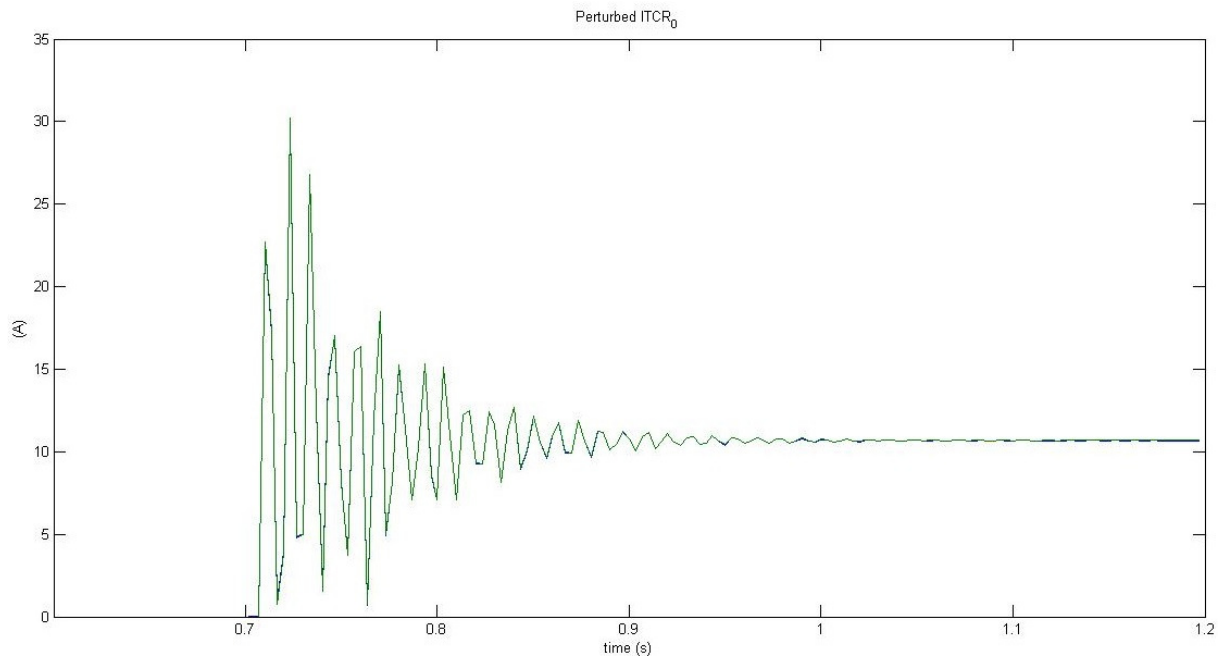
Figure 4-26 Perturbed TCR current |iTCR_0| response to a +5% step change in peak source voltage along d-axis. Green line for LTI discrete-time model and blue line for PSIM one.

There is a very good matching between the two models for all the components of perturbed capacitor voltage and line current and after the perturbation in source voltage along d-axis the system reaches a new steady steate operation point. Moreover, it is highlighted that the absolute value of zero sequence component "0" of the TCR current has been plotted because it changes sign at each odd cycle respect to the "real" γ component as also happened for the zero sequence component of the line current in the star-connected TCR studied in Chapter 3. Figure 4-20 shows that the new operating point reached at steady state is consistent with the quantity of the perturbation applied to source voltage along d-axis.

4.3 Comparison between Equivalent Discrete-time and Continuous-time Model

In the previous sections the analytical approach synthesized in Section 2.2 has been developed in order to have a LTI discrete state-space model of delta-connected TCR in the SVC system of ITER. In this chapter the LTI continuous-time model has been derived from the discete one, developed in the simplest case of conduction angle $\sigma_d \epsilon$ (0,60°) (see Section 4.1.2): for this reason it has been called Equivalent Discrete-time Model (EDM). The transformation in continuous-time domain is necessary to compare it with another Continuous Model (CM), derived by an innovative approach presented in [2], in term of accurancy. In CM suitable transfer functions were worked out to reproduce the dynamic behavior for each static conversion subsystems of ITER Static Var compensator, in this way it presents the advantage of a modular approach: each subsystem can be studied separately and then, considering all models toghether, the whole system. In this case a little resistance is put in series to the inductance L_s to avoid oscillating behavior, probably due to the ideal circuit without damping components. The comparison has been made in time and frequency domain.

To compare these two models a common continuous-time frame is necessary and it is considered the operating mode $\sigma_d = 45°$. The LTI discrete-time state space model as given in (4.39) is reported below for clarity of presentation:

$$\breve{y}_{dq}\big((k+1)T_s\big) = \Psi \breve{y}_{dq}(kT_s) + \Gamma_\Phi \cdot \widetilde{\Phi}(kT_s) + \Gamma_u \cdot \breve{u}_{dq}(kT_s) \qquad (4.80)$$

From dynamical system theory (see Section II in Appendix I) LTI discrete-time model (4.80) can be expressed in a continuous time frame as follows:

$$\frac{d\tilde{y}_{dq}}{dt} = \hat{A}\tilde{y}_{dq} + \hat{B}_\Phi \widetilde{\Phi} + \hat{B}_u \tilde{u}_{dq} \qquad (4.81)$$

(4.81) is the equivalent continuous time model to the discrete one (4.80), so called "EDM": its response matches the other one of (4.80) at the sample-instants with attention to aliasing. On the assumption that the inputs Φ and u_{dq} are constant in a sample period, the coefficients of (4.81) are related to those of (4.80) by following formulas (for the demonstration see Section II in Appendix I):

$$\Psi = e^{\hat{A}T_s} \qquad \Gamma_\Phi = \int_0^{T_s} e^{\hat{A}\xi} \, d\xi \hat{B}_\Phi \qquad \Gamma_u = \int_0^{T_s} e^{\hat{A}\xi} \, d\xi \hat{B}_u \qquad (4.82)$$

Considering the first one of (4.82), it' possible to diagonalize Ψ by the similarity transform S so that $\Psi = S\Lambda S^{-1}$ and find $\hat{A}$ as follows:

$$log(\Psi) = \hat{A}T_s$$

$$S \cdot log(\Lambda) \cdot S^{-1} = \hat{A}T_s$$

$$\hat{A} = \frac{1}{T_s} S\{log\Lambda \pm jn\pi I\} S^{-1} \qquad (4.83)$$

where n is chosen so that the model parameters for $\sigma \to 0$ are consistent with those at $\sigma_d = 0°$, which is simply the LTI system that results when both thyristors are in blocking mode. So to compute n for the operating mode of interest ($\sigma_d = 45°$), formerly it's necessary to find $\hat{A}$ when $\sigma_d = 0°$, studying the circuit when no thyristor is conducting. This configuration is depicted in Figure 4-27 below.
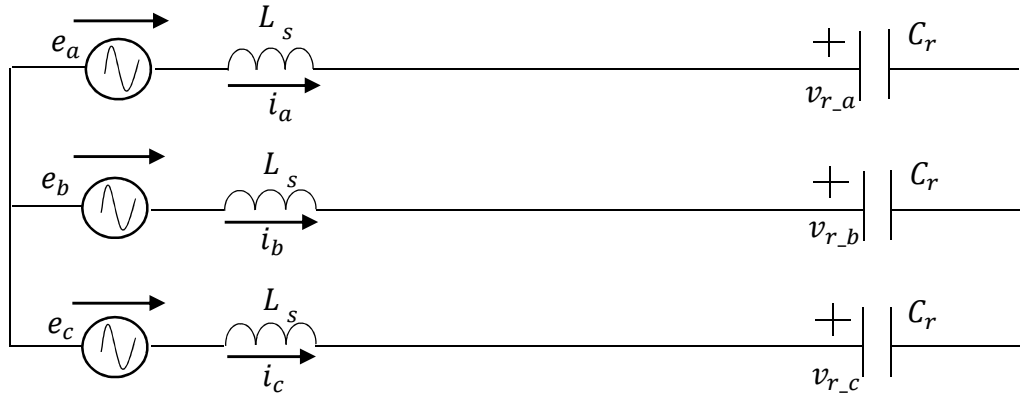
Figure 4-27 Three-phase circuit when all thyristors (of each TCR) are in blocking mode

The equation that describes its steady state operation in a continuous-time frame is

$$L_s \frac{d[i]_{abc}}{dt} = [u_s]_{abc} - [v_r]_{abc} \qquad (4.84)$$

where

$$[i]_{abc} = \begin{bmatrix} i_a \\ i_b \\ i_c \end{bmatrix}, \qquad [u_s]_{abc} = \begin{bmatrix} e_a \\ e_a \\ e_a \end{bmatrix}, \qquad [v_r]_{abc} = \begin{bmatrix} v_{r\_a} \\ v_{r\_b} \\ v_{r\_c} \end{bmatrix} \qquad (4.85)$$

It's necessary to write (4.84) in a dq reference frame, in order to find $\hat{A}$ consistent with the model expression in (4.81). $[abc \rightarrow dq]$ transformation defined in (4.86) for a generic tern of variables x_{abc} is previously applied to derivates of line currents in (4.84): (note that that zero sequence component is neglected because of delta connected TCR)

$$\begin{bmatrix} x_d \\ x_q \end{bmatrix} = \frac{2}{3} \cdot [abc \rightarrow dq] \cdot \begin{bmatrix} x_a \\ x_b \\ x_c \end{bmatrix}$$

$$[abc \rightarrow dq] = \begin{bmatrix} cos(\omega t) & cos\left(\omega t - \frac{2}{3}\pi\right) & cos\left(\omega t - \frac{4}{3}\pi\right) \\ -sen(\omega t) & -sen\left(\omega t - \frac{2}{3}\pi\right) & -sen\left(\omega t - \frac{4}{3}\pi\right) \end{bmatrix}$$

(4.86)

it yields:

$$[abc \rightarrow dq] \cdot \frac{d[i]_{abc}}{dt} = \frac{d}{dt}\left([abc \rightarrow dq] \cdot \begin{bmatrix} i_a \\ i_b \\ i_c \end{bmatrix}\right) =$$

$$= \frac{d[i]_{dq}}{dt} - \frac{2}{3} \cdot \begin{bmatrix} -\omega sen(\omega t) & -\omega sen\left(\omega t - \frac{2}{3}\pi\right) & -\omega sen\left(\omega t - \frac{4}{3}\pi\right) \\ -\omega cos(\omega t) & -\omega cos\left(\omega t - \frac{2}{3}\pi\right) & -\omega cos\left(\omega t - \frac{4}{3}\pi\right) \end{bmatrix} \cdot \begin{bmatrix} i_a \\ i_b \\ i_c \end{bmatrix}$$

(4.87)

$$= \frac{d[i]_{dq}}{dt} - \begin{bmatrix} \omega & 0 \\ 0 & -\omega \end{bmatrix} \cdot \begin{bmatrix} i_q \\ i_d \end{bmatrix} = \frac{d[i]_{dq}}{dt} - \begin{bmatrix} 0 & -\omega \\ \omega & 0 \end{bmatrix} \cdot \begin{bmatrix} i_q \\ i_d \end{bmatrix}$$

while applying (4.86) to both members of (4.84) yields

$$L_s \frac{d[i]_{dq}}{dt} + L_s \begin{bmatrix} 0 & -\omega \\ \omega & 0 \end{bmatrix} [i]_{dq} = [u_s]_{dq} - [v_r]_{dq}$$

(4.88)

$$L_s \frac{d[i]_{dq}}{dt} = -\begin{bmatrix} 0 & -\omega \\ \omega & 0 \end{bmatrix} [i]_{dq} + \frac{1}{L_s}[u_s]_{dq} - \frac{1}{L_s}[v_r]_{dq}$$

(4.89)

and for the voltage capacitor $[v_r]_{abc}$

$$C_r \frac{d[v_r]_{abc}}{dt} = [i]_{abc}$$

(4.90)

$$C_r \frac{d[v_r]_{dq}}{dt} + C \begin{bmatrix} 0 & -\omega \\ \omega & 0 \end{bmatrix} [v_r]_{dq} = [i]_{dq}$$

(4.91)

$$C_r \frac{d[v_r]_{dq}}{dt} = -\begin{bmatrix} 0 & -\omega \\ \omega & 0 \end{bmatrix} [v_r]_{dq} + \frac{1}{C} [i]_{dq}$$

(4.92)

So, when $\sigma_d = 0°$, $\hat{A}$ and $\hat{B}_u$ (4.89) and (4.92) can be are given together in the matrix form (note that it can be written either perturbed or whole state variables):

$$\frac{d}{dt}\begin{bmatrix} i_d \\ i_q \\ v_{r\_d} \\ v_{r\_q} \end{bmatrix} = \begin{bmatrix} 0 & \omega & -\frac{1}{L_s} & 0 \\ -\omega & 0 & 0 & -\frac{1}{L_s} \\ \frac{1}{C} & 0 & 0 & \omega \\ 0 & \frac{1}{C} & -\omega & 0 \end{bmatrix} \begin{bmatrix} i_d \\ i_q \\ v_{r\_d} \\ v_{r\_q} \end{bmatrix} + \begin{bmatrix} \frac{1}{L_s} & 0 \\ 0 & \frac{1}{L_s} \\ 0 & 0 \\ 0 & 0 \end{bmatrix} \begin{bmatrix} u_{s\_d} \\ u_{s\_q} \end{bmatrix}$$

(4.93)

Knowing $\hat{A}$, it's now possible to find n from (3.83). In the case under consideration $n = 2$ for capacitor voltage and $n = 0$ for line current.

It remains to find $\hat{B}$ with relations below (see Section II of Appendix I)

$$\hat{B}_\Phi = (\Psi - I)^{-1} \hat{A} \Gamma_\Phi \qquad \hat{B}_u = (\Psi - I)^{-1} \hat{A} \Gamma_u$$

(4.94)

4.3.1 Comparison in the time domain

In Figure 4-28, Figure 4-29, Figure 4-30 and Figure 4-31 the waveforms of the different models (blue line for the PSIM, green line for EDM and red line for CM) describe the response to a step function of +1° degree on the firing angle. The PSIM model shows oscillating waveforms probably due to the too little perturbation comparable with the numerical errors.

However, for the first cycles from the instant t_0 there is a good matching between PSIM response and EDM. In CM, a low-pass filter has been used to consider the average time delay in the response to a variation of firing angle due to the switching of the thyristor which occur at about every 60 electrical degrees; nevertheless this assumption limits its accuracy in high frequency range.
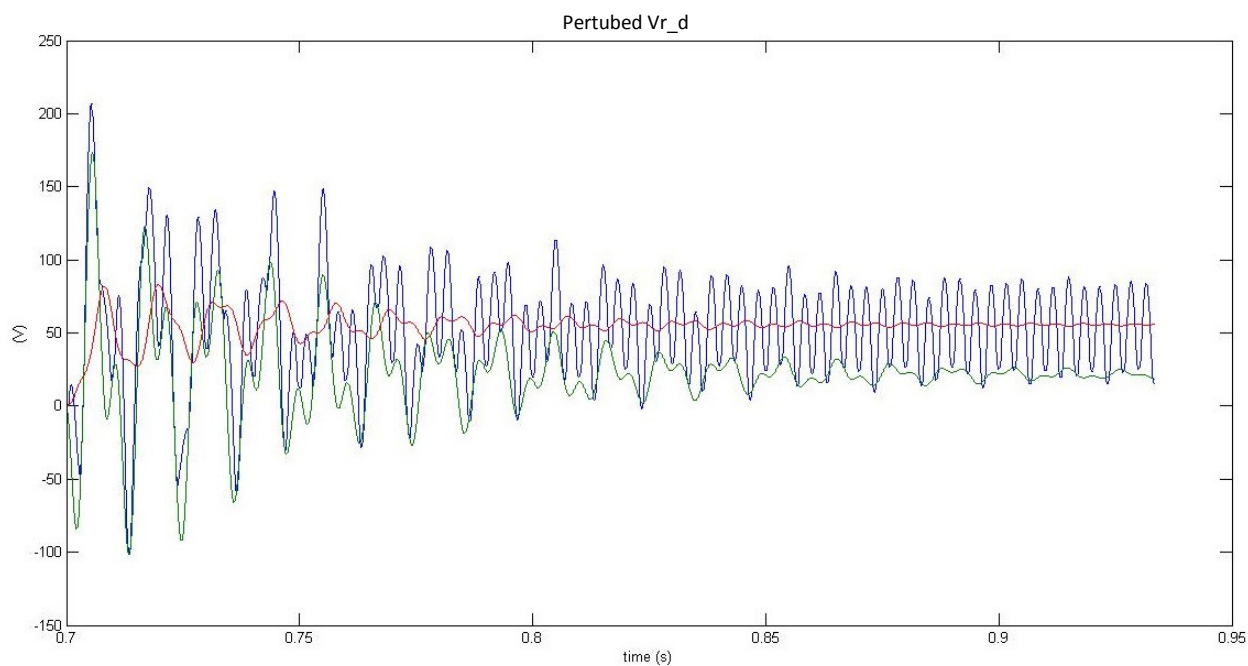
Figure 4-28 Perturbed capacitor voltage Vr_d response to a +1° step change in the firing angle. Blue line for PSIM, green line for EDM and red line for CM.
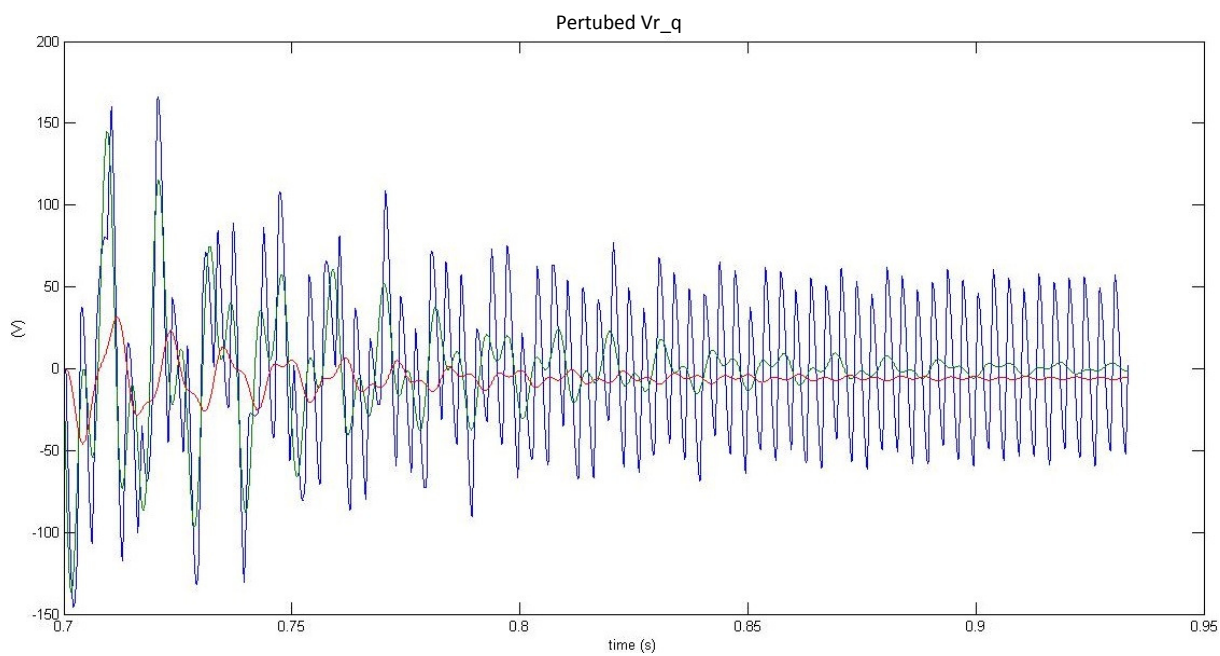
Figure 4-29 Perturbed capacitor voltage Vr_q response to a +1° step change in the firing angle. Blue line for PSIM, green line for EDM and red line for CM.

89
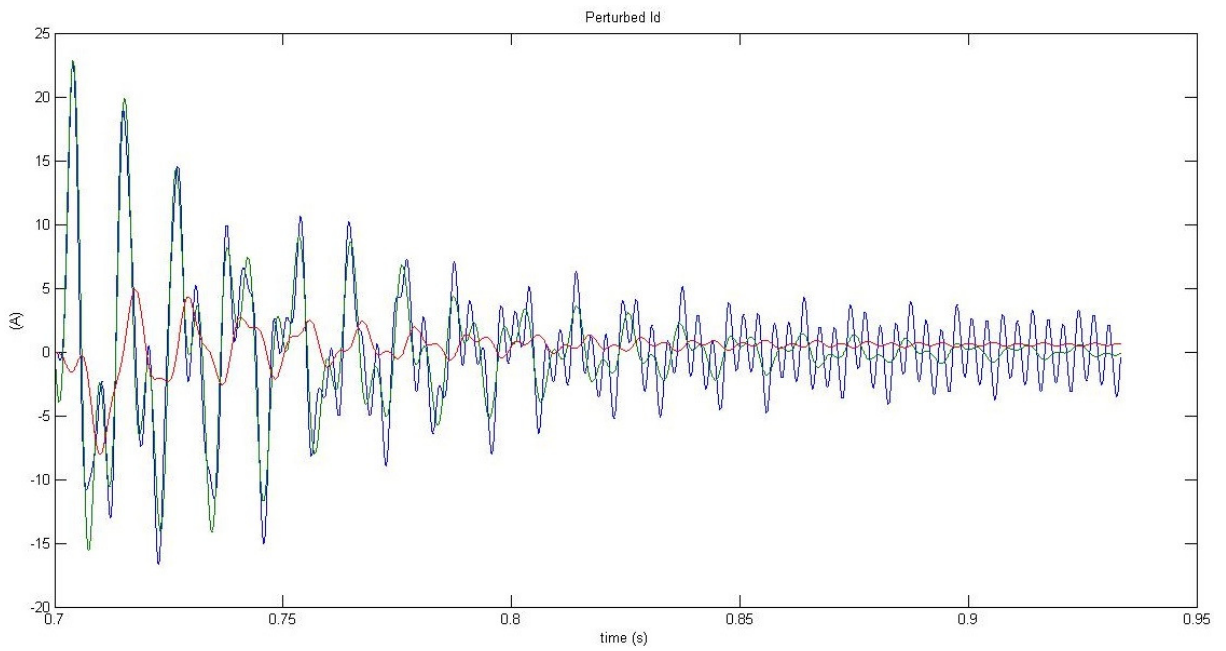
Figure 4-30 Perturbed line current i_d response to a +1° step change in the firing angle. Blue line for PSIM, green line for EDM and red line for CM.
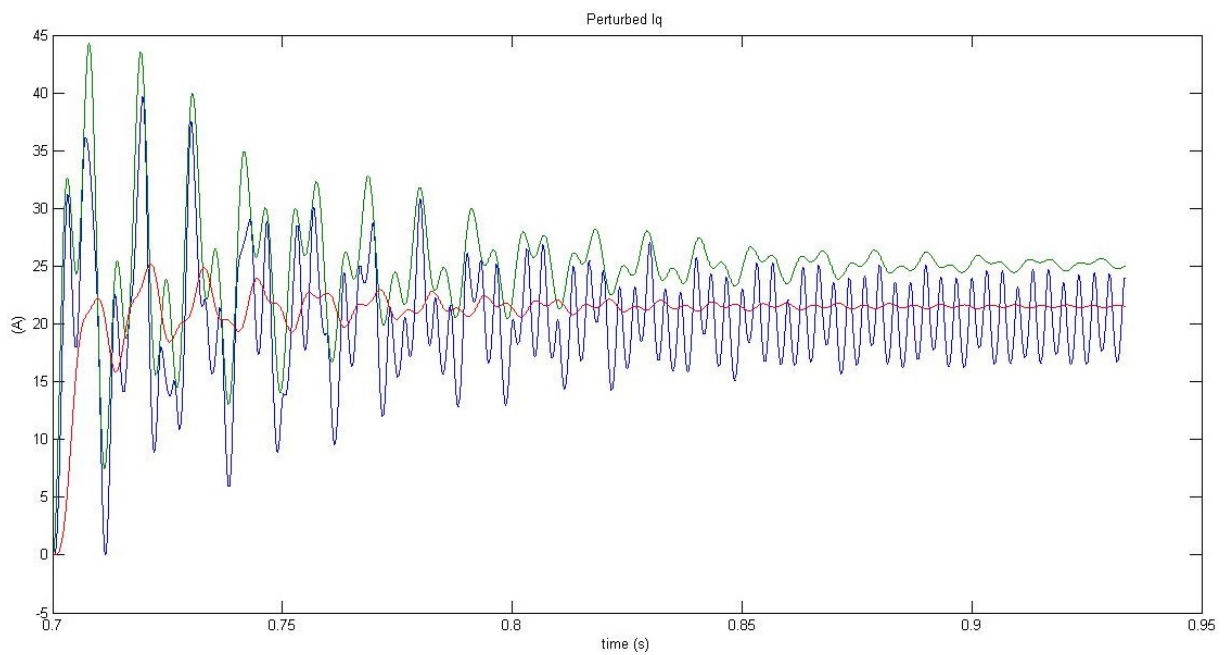
Figure 4-31 Perturbed line current i_q response to a +1° step change in the firing angle. Blue line for PSIM, green line for EDM and red line for CM.
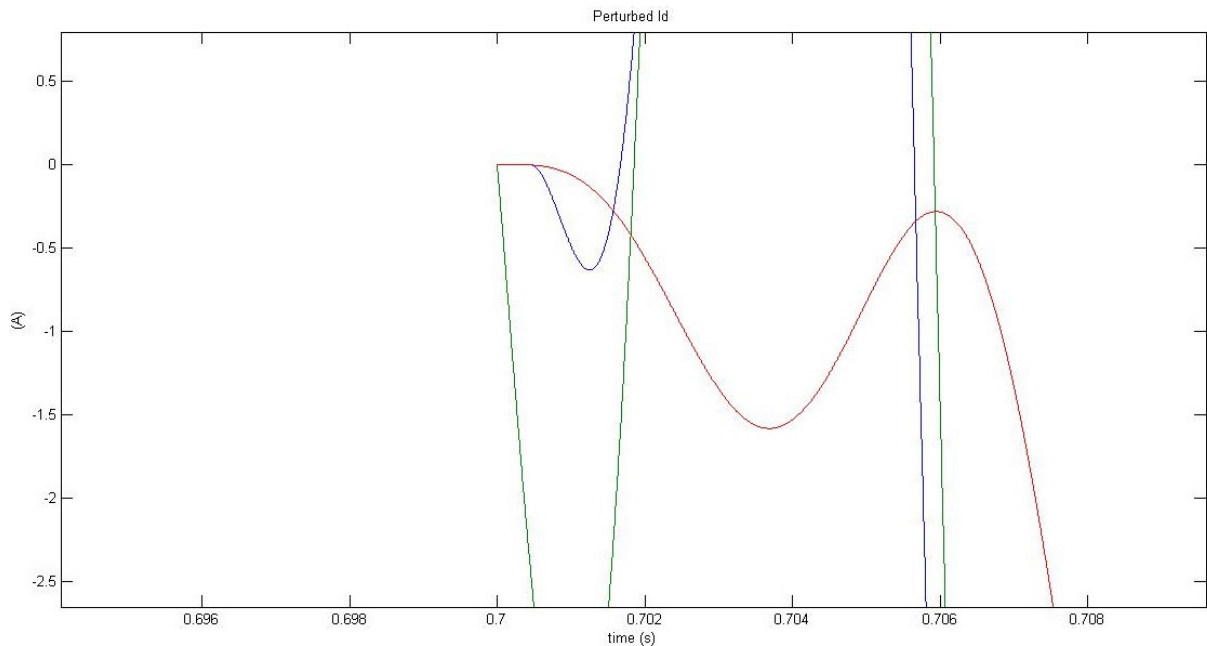
Figure 4-32 Zoom in of i_d response to a +1° step change in the firing angle at the perturbation instant. Blue line for PSIM, green line for EDM and red line for CM.

Figure 4-32 shows, for example, a zoom of the d-component of current line at the beginning of the perturbation. The PSIM model (blue line) has a latency of few hundreds of micro seconds, and it is related to the switching of the thyristor; CM (red line) considers this latency by introducing a low pass filter as discussed before; EDM based on discrete-time approach (green line) shows no latency.

In Figure 4-33,Figure 4-34,Figure 4-35 and Figure 4-36 the resulting waveforms of perturbed components of voltage and current of the three models after a step perturbation of +5% in the d-component of source voltage are shown: there is a good matching for all the three different responses. The same results are also valid for a step change +5% in the q-component of source voltage (shown in Figure 4-37,Figure 4-38,Figure 4-39 and Figure 4-40).
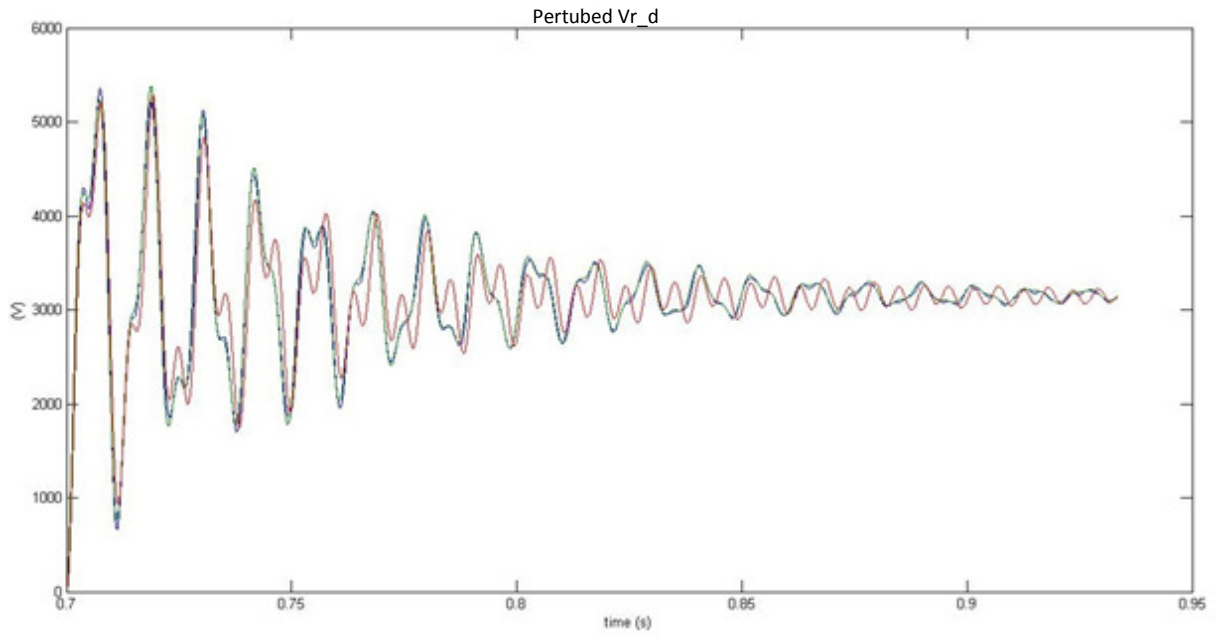
Figure 4-33 Perturbed capacitor voltage Vr_d response to a +5% step change in in the d-component of source voltage. Blue line for PSIM, green line for EDM and red line for CM.
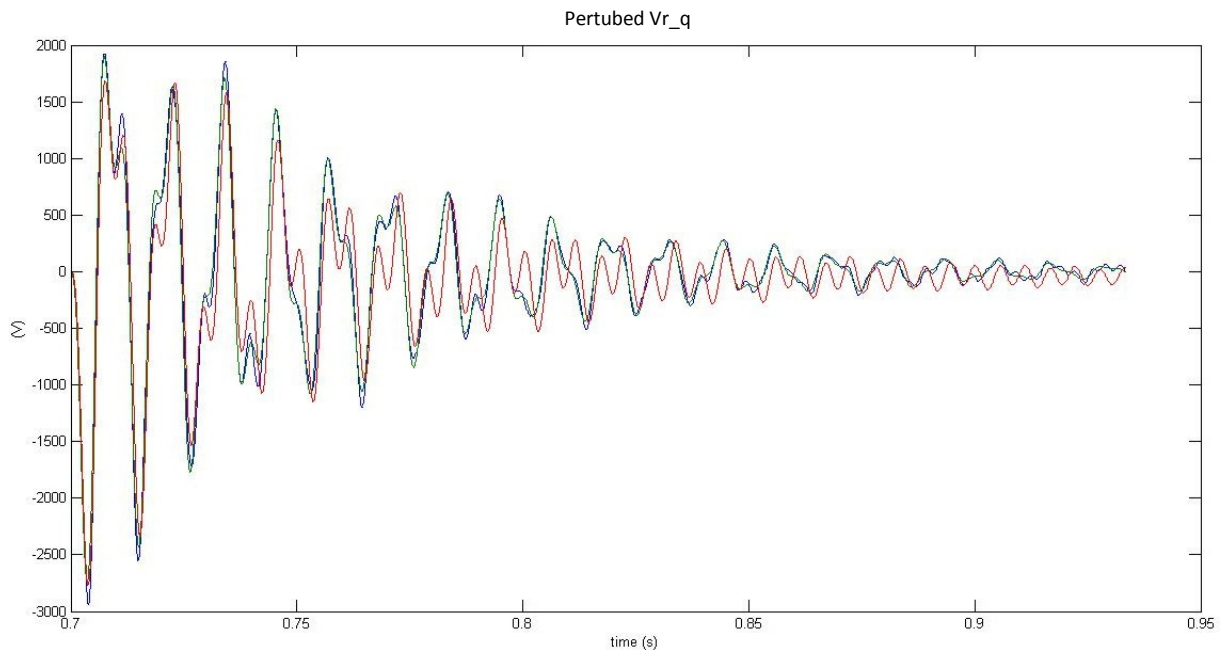
Figure 4-34 Perturbed capacitor voltage Vr_q response to a +5% step change in in the d-component of source voltage. Blue line for PSIM, green line for EDM and red line for CM.
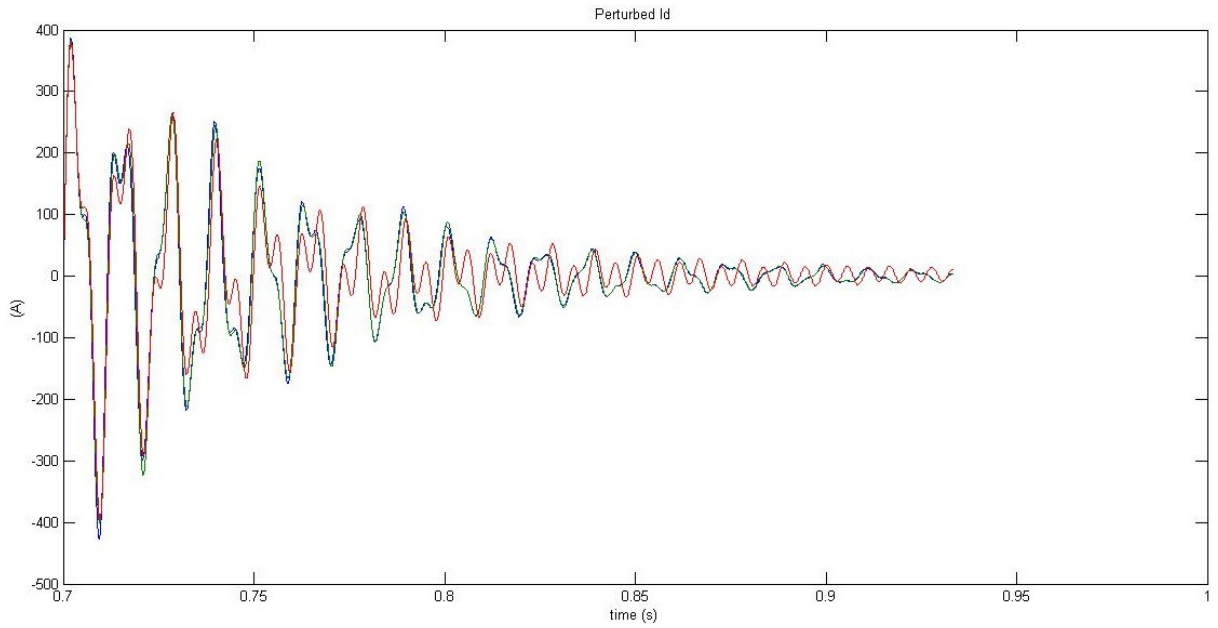
Figure 4-35 Perturbed line current i_d response to a +5% step change in in the d-component of source voltage. Blue line for PSIM, green line for EDM and red line for CM.
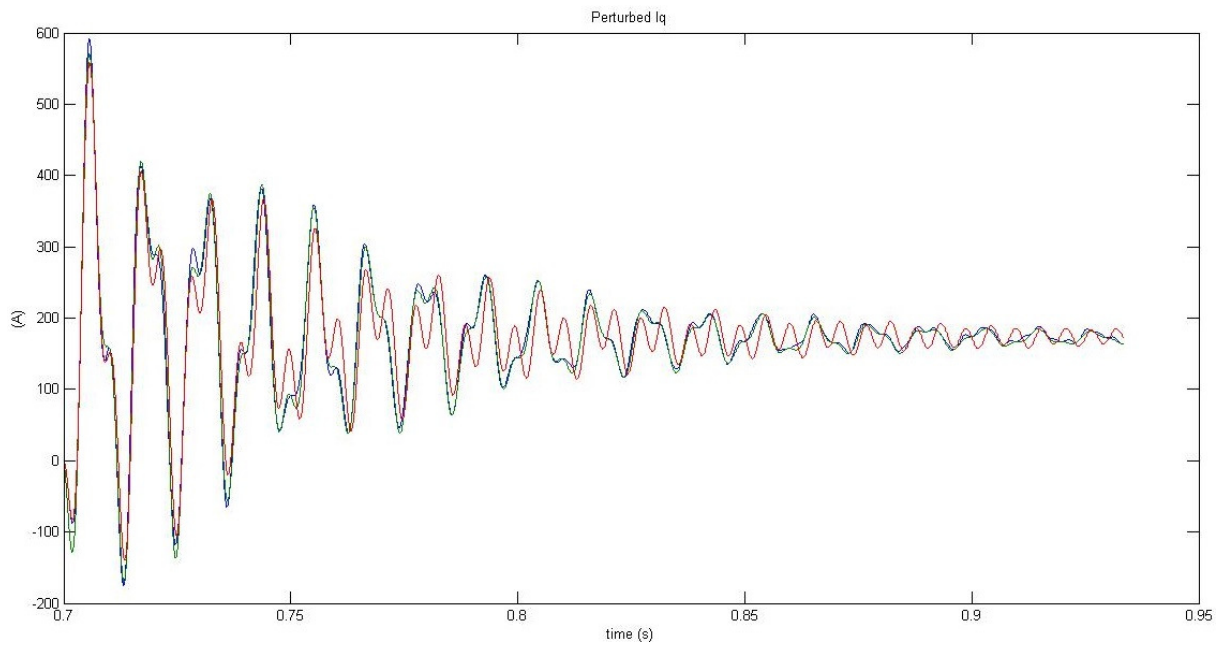
Figure 4-36 Perturbed line current i_q response to a +5% step change in in the d-component of source voltage. Blue line for PSIM, green line for EDM and red line for CM.
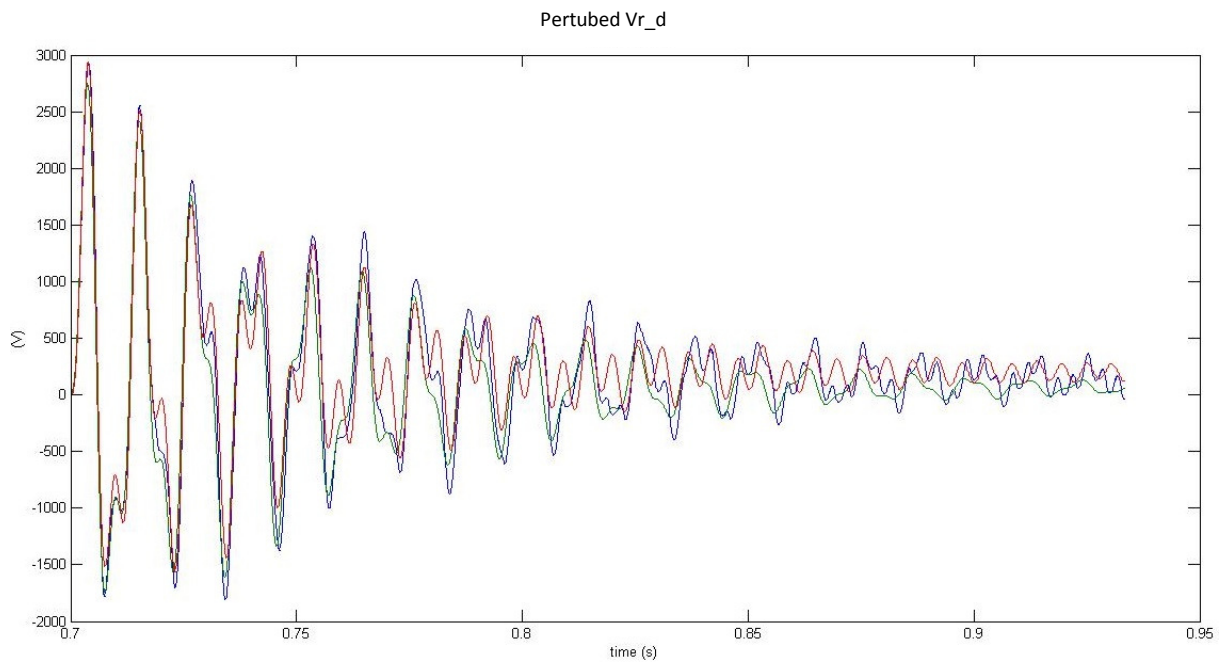
Figure 4-37 Perturbed capacitor voltage Vr_d response to a +5% step change in the q-component of source voltage. Blue line for PSIM, green line for EDM and red line for CM.
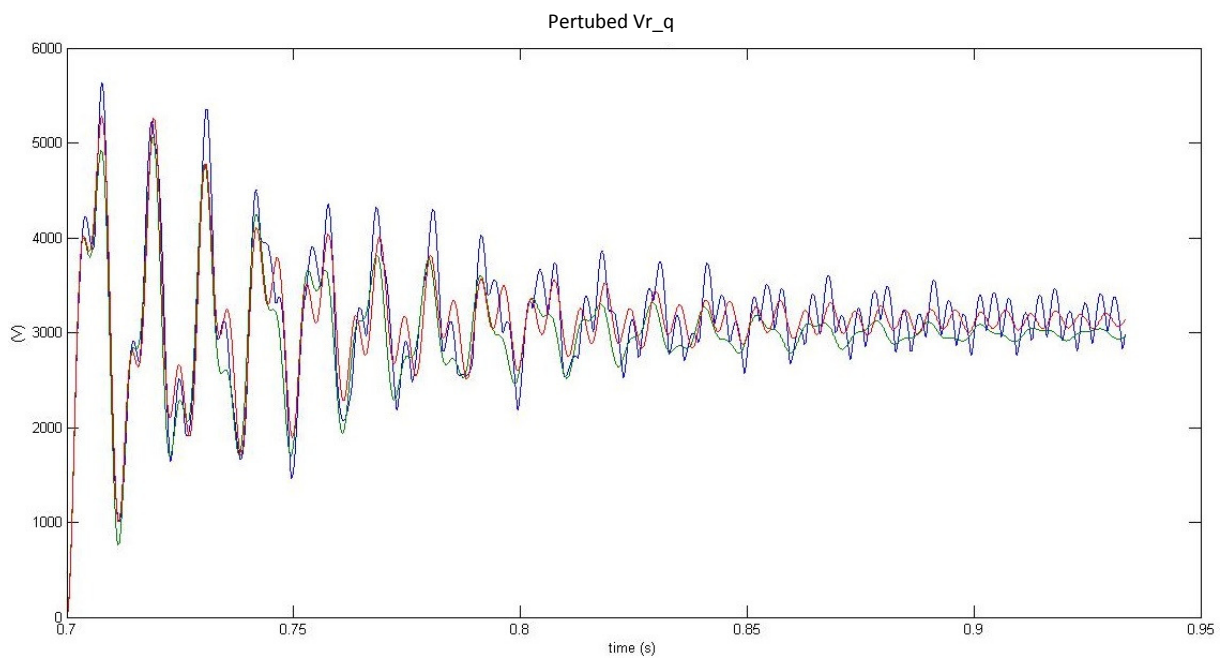
Figure 4-38 Perturbed capacitor voltage Vr_q response to a +5% step change in the q-component of source voltage. Blue line for PSIM, green line for EDM and red line for CM.

94
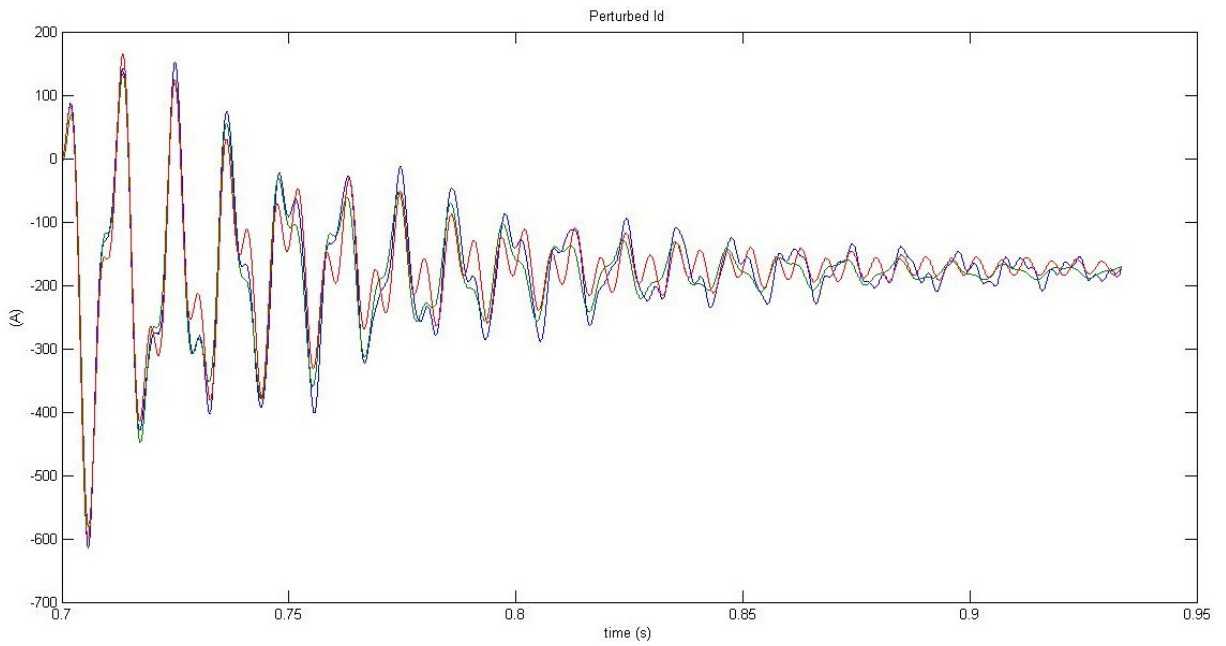
Figure 4-39 Perturbed line current i_d response to a +5% step change in in the q-component of source voltage. Blue line for PSIM, green line for EDM and red line for CM.
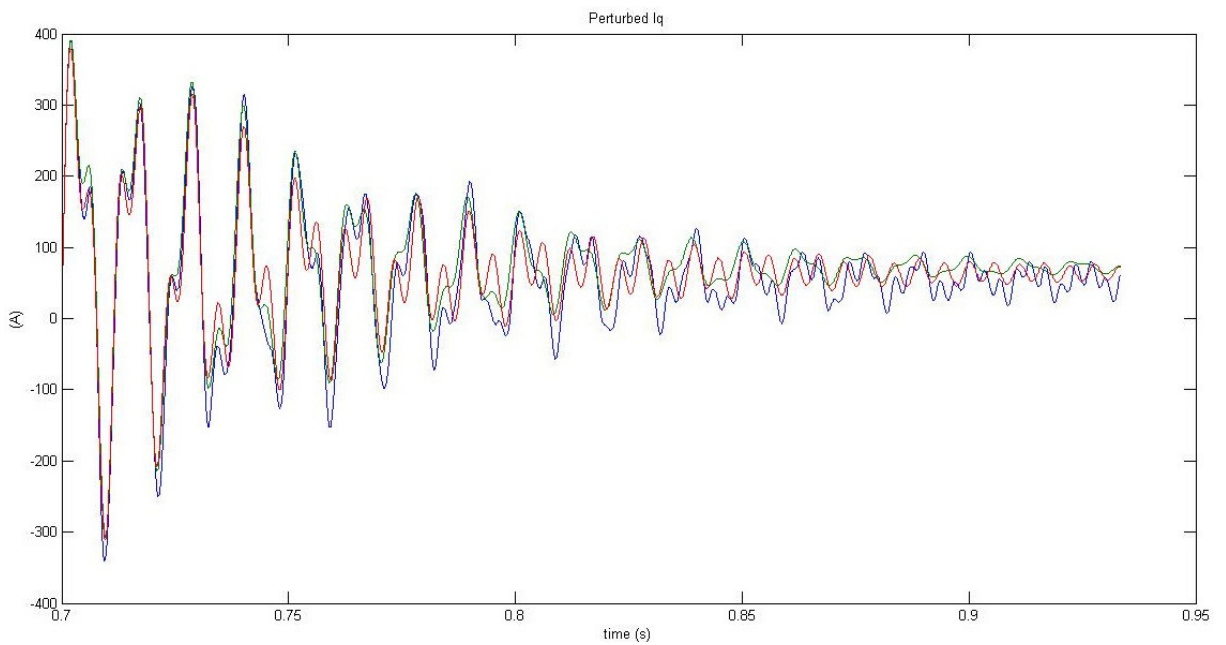
Figure 4-40 Perturbed line current i_q response to a +5% step change in in the q-component of source voltage. Blue line for PSIM, green line for EDM and red line for CM.

From all previous figures it can be noted that discrete-time approach is more accurate than the dynamic model.

Moreover, it is highlighted that in the previous cases the step perturbation has been applied at an instant time synchronized with the sampling instants used to develop the LTI discrete state space model. Figure 4-41 shows the case in which the perturbation is applied between two sampling instants, at t_1; it may be noted that the accuracy of the EDM derived from the discrete one is less accurate respect the case depicted in Figure 4-37.
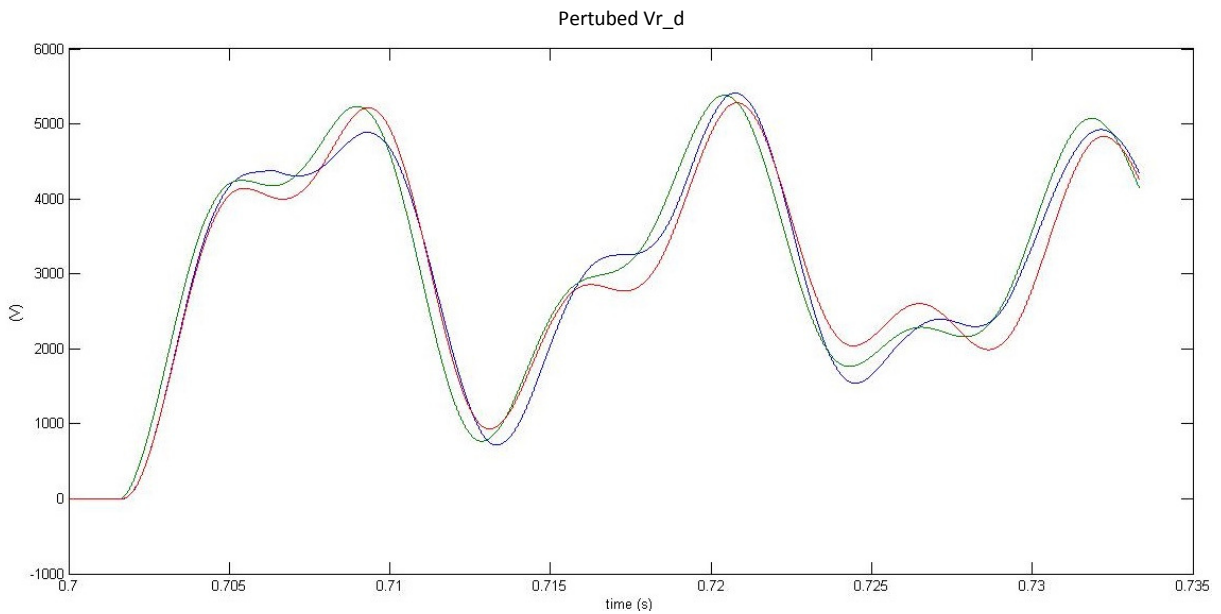
Figure 4-41 Perturbed capacitor voltage Vr_d response to a +5% step change in the d-component of source voltage applied at instant t_1. Blue line for PSIM, green line for EDM and red line for CM.

4.3.2 Comparison in the frequency domain

In this section a comparison in frequency domain between EDM and CM has been carried out. Therefore a perturbation to the dq voltages has been applied, given by these equations

$$\Delta e_{s\_d} = 0.05 \sqrt{\frac{2}{3}} \cdot U_s \cos(2\pi f_s t)$$

$$\Delta e_{s\_q} = 0.05 \sqrt{\frac{2}{3}} \cdot U_s \cos(2\pi f_s t)$$

(4.95)

96

where f_s is the frequency of the perturbation. PSIM response is taken as reference, thus the magnitude ratio and the phase error defined below has been calculated for both models.

For EDM, the magnitude ratios are:

$$|V_{r\_d}| = 20\log\left(\frac{V_{r_{d\,EDM}}}{V_{r_{d\,PSIM}}}\right), \quad |V_{r\_q}| = 20\log\left(\frac{V_{r_{q\,EDM}}}{V_{r_{q\,PSIM}}}\right)$$

$$|i_d| = 20\log\left(\frac{i_{d\,EDM}}{i_{d\,PSIM}}\right), \quad |i_q| = 20\log\left(\frac{i_{q\,EDM}}{i_{q\,PSIM}}\right)$$

$$(\,4.96\,)$$

and the phase errors are

$$phase(V_{r\_d}) = phase\left(V_{r_{d\,EDM}}\right) - phase\left(V_{r_{d\,PSIM}}\right)$$

$$phase(V_{r\_q}) = phase\left(V_{r_{q\,EDM}}\right) - phase\left(V_{r_{q\,PSIM}}\right)$$

$$phase(i_d) = phase(i_{d\,EDM}) - phase(i_{d\,PSIM})$$

$$phase(i_q) = phase\left(i_{q\,EDM}\right) - phase\left(i_{q\,PSIM}\right)$$

$$(\,4.97\,)$$

For CM, the magnitude ratios are:

$$|V_{r\_d}| = 20\log\left(\frac{V_{r_{d\,CM}}}{V_{r_{d\,PSIM}}}\right), \quad |V_{r\_q}| = 20\log\left(\frac{V_{r_{q\,CM}}}{V_{r_{q\,PSIM}}}\right)$$

$$|i_d| = 20\log\left(\frac{i_{d\,CM}}{i_{d\,PSIM}}\right), \quad |i_q| = 20\log\left(\frac{i_{q\,CM}}{i_{q\,PSIM}}\right)$$

$$(\,4.98\,)$$

and the phase errors are

$$phase(V_{r\_d}) = phase\left(V_{r_{d\,CM}}\right) - phase\left(V_{r_{d\,PSIM}}\right)$$

$$phase(V_{r\_q}) = phase\left(V_{r_{q\,CM}}\right) - phase\left(V_{r_{q\,PSIM}}\right)$$

$$phase(i_d) = phase(i_{d\,CM}) - phase(i_{d\,PSIM})$$

$$phase(i_q) = phase\left(i_{q\,CM}\right) - phase\left(i_{q\,PSIM}\right)$$

$$(\,4.99\,)$$

In all the figures the results are good enough for both models up to a frequency of 150 Hz, even if EDM shows better results than the CM. The frequency at 150 Hz is half of the sampling frequency at 300 Hz and for the Nyquist–Shannon sampling theorem it has been considered the upper theoretical limit of the accuracy of the continuous time model due to the zero order hold assumption used for the development of the model.

At $f_s = 80\ Hz$ both models have a big error. The reason is that the resonance of the line inductor and the capacitor is at 80 Hz in dq frame and 130 Hz in abc frame, so the small signal perturbation becomes a large perturbation at this frequency, and the models are not more so valid. However these are preliminary results, because TCR operation with conducting angle larger than 45 electrical degrees should be also verified.
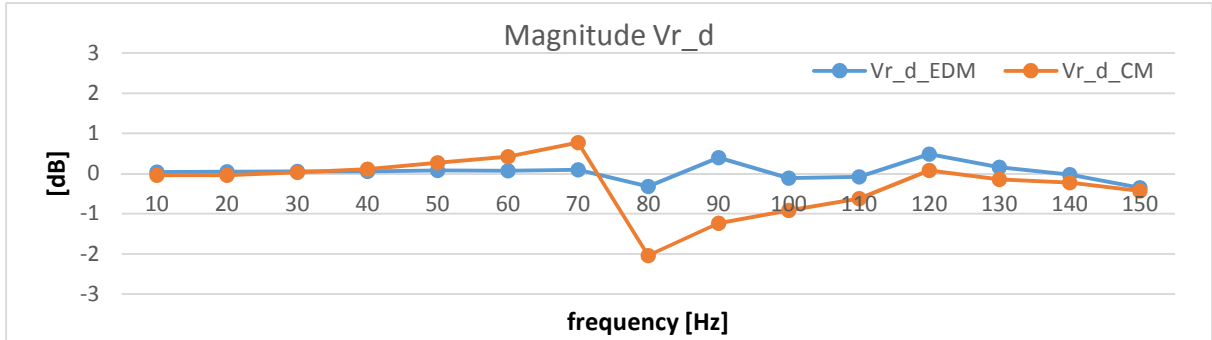
Figure 4-42 Magnitude of Vr_d in relation to frequency
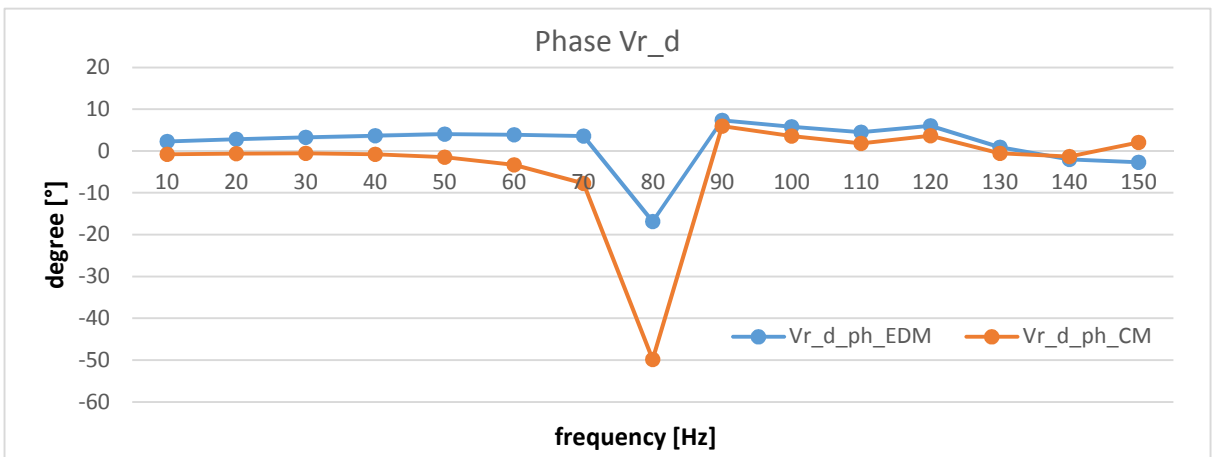
Figure 4-43 Phase of Vr_d in relation to frequency
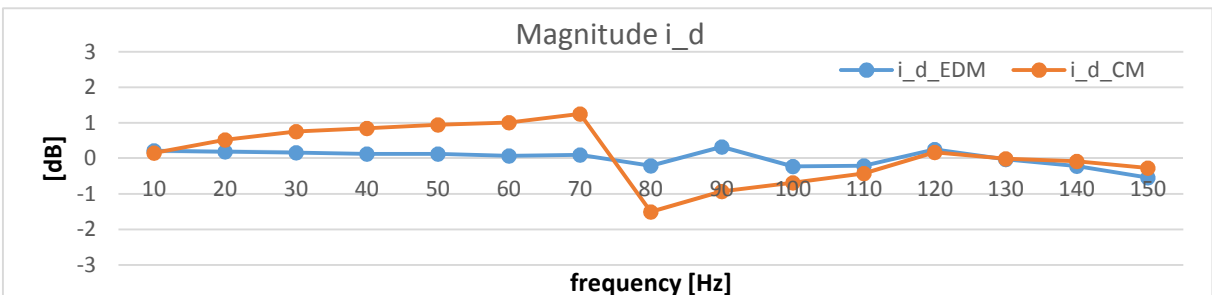
Figure 4-44 Magnitude of i_d in relation to frequency
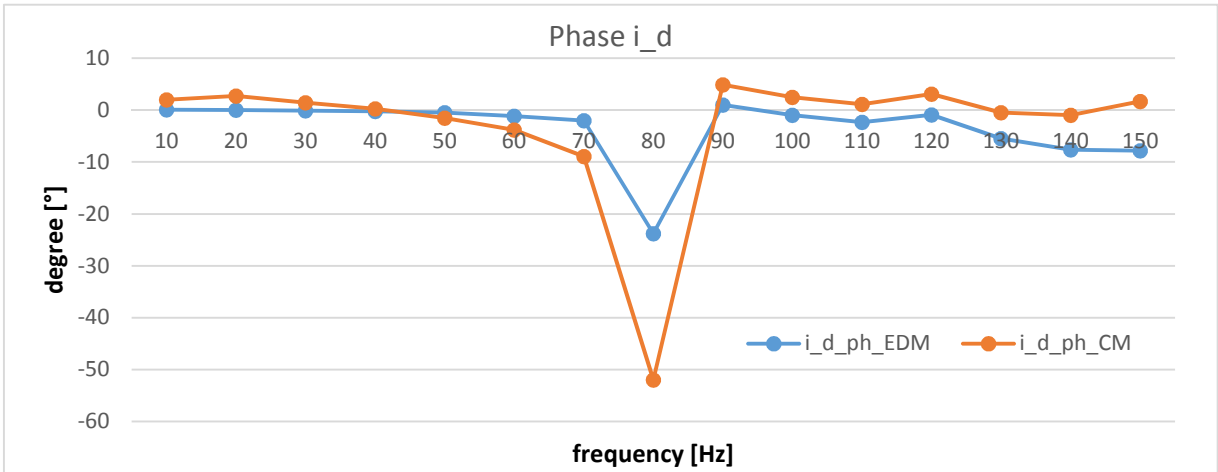
Figure 4-45 Phase of i_d in relation to frequency
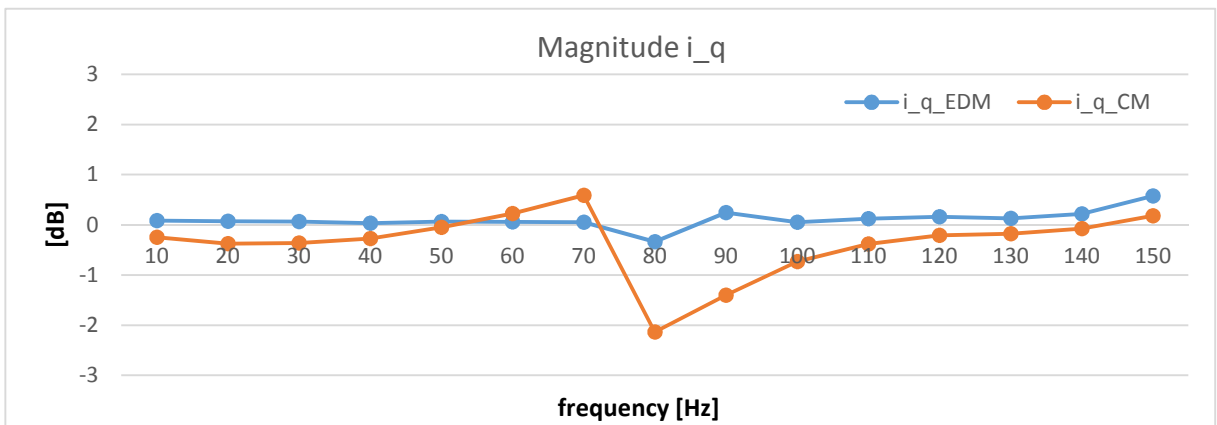
Figure 4-46 Magnitude of i_q in relation to frequency
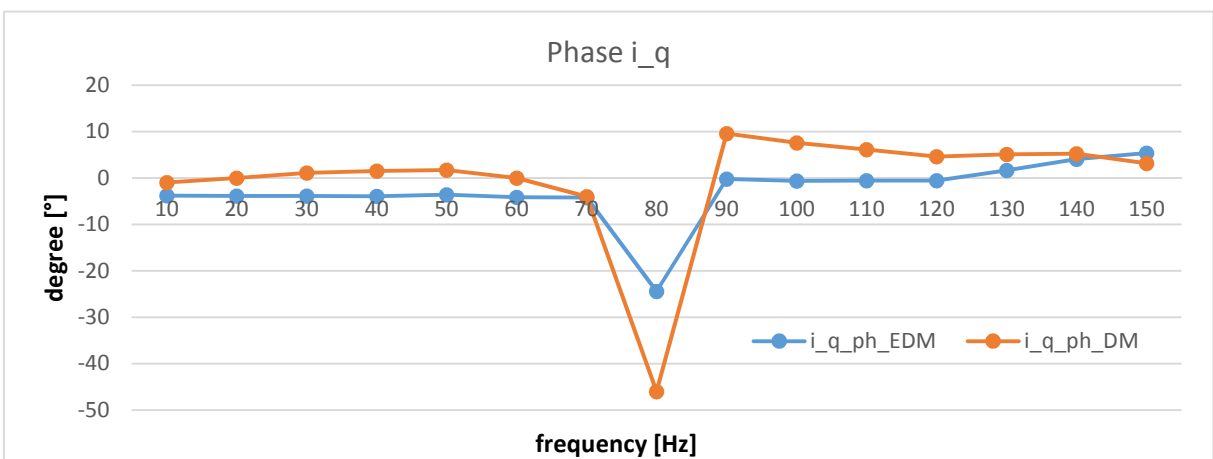
Figure 4-47 Phase of i_q in relation to frequency
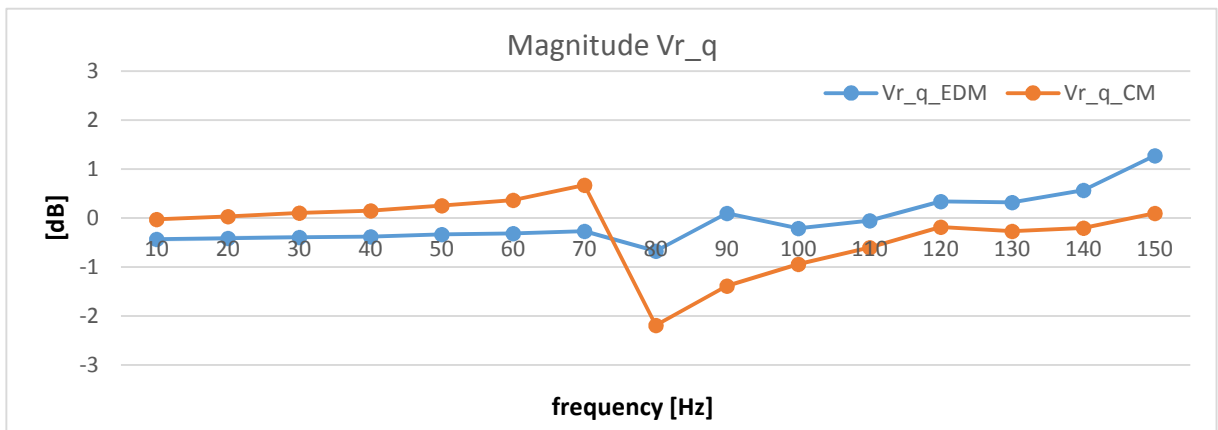
Figure 4-48 Magnitude of Vr_q in relation to frequency
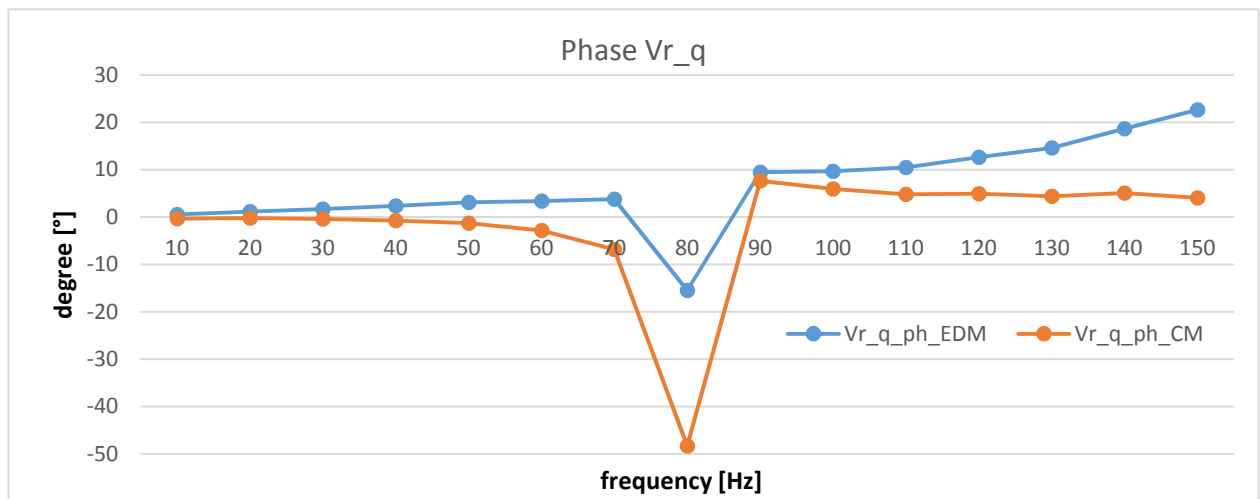
Figure 4-49 Phase of Vr_q in relation to frequency

5   Conclusions and future works

In this work an analytical Linear Time invariant (LTI) discrete-time model of the Static Var Compensation System of the ITER power supply system based on Thyristor Controlled Reactor (TCR) has been developed, and validated in time and frequency domain by comparison with PSIM program [11], which reproduces instantaneous voltage and current profiles.

Starting from studies already presented in literature (i.e. [1] [12]), the Poincarè Map of single phase SVC system has been built and then linearized. Then moving to a three phase SVC system with the TCR in star configuration, a LTI discrete-time model has been obtained by the dqγ transformation of state variables (capacitor voltages and line currents), manipulating the equations related to the γ components to eliminate its non periodic behavior respect to the choosen sampling time, equivalent to 180 electrical degrees, obtaining a new periodic zero sequence component (with subscript 0). This device allows finding a time-invariant model. A good agreement has been obtained by comparison with PSIM model in both cases.

Then, the previous model developed has been applied to SVC system of ITER experimental reactor with delta-connected TCR, reducing the sampling time. Two modes of operation have been considered: the first one with conduction angle $\sigma \in (0°, 60°)$ and the second with $\sigma \in (60°, 120°)$. Applying the same device of previous case, a LTI model has been developed in dq0 frame: the model results show a good agreement with the PSIM one. As future work it may be interesting to analyze also another operation mode with $\sigma \in (120°, 180°)$: in this case zero sequence component of thyristor current presents again odd half-wave symmetry, so the same solution (i.e transform γ component into a new one "0") used in previous cases may be applied to obtain a LTI discrete-time model.

Finally the continuous-time model has been developed from the discrete one to compare it in time and frequency domain with the response from another different continuous-time model presented in [2]. The results of numerical simulations given by PSIM have been used as reference. To do this only conduction angle $\sigma \in (0°, 60°)$ has been taken into account. In all the figures the results are good enough for both models in time and frequency domain, even if the discrete-time approach is more accurate than the continuous one: for a frequency perturbation $f_s = 80\ Hz$ on d and q components, both models have a big error due to the

resonance of line inductor and the capacitor, even if for the model here developed with a discrete-time approach remains little, while for the other is bigger. On the other hand, the first one is more complex to build, especially if there are a large number of variables to take into account, for example if harmonic filters have been considered. Finally, if discrete-time approach has to be applied studying the whole SVC system, the continuous one presents the advantage of a modular approach, as it has already explained in last Section.

Acknowledgement

Abbreviations and notation

SVC	Static Var Compensator
LTI	Linear, Time-Invariant
P	Projection matrix relating state vectors at thyristor turn-off
Q	Injection matrix relating state vectors at thyristor turn-on
$\hat{A}$	Matrix that refers to a LTI continuous-time model
$V(t), W(t)$	Parks' transformations
x	state vector for a discrete-time state space model
$\check{x}$	Perturbation from nominal steady-state quantity
Φ	Firing instant at which a thyristor makes a turn-on transition
τ	Extinction instant at which a thyristor makes a turn-off transition
σ_t, σ_d	Conduction angle associated with SVC circuit (expressed in time or degree unit)
θ	$\theta = \omega t$, electrical degree
ω	$\omega = 2\pi f$, angular frequency

REFERENCES

[1] B. K. Perkins, *Dynamic modelling of thyristor-based staic switching circuits with application to power systems,* University of Toronto, 1997.

[2] C. Finotti, *Studies on the impact of the ITER Pulsed Power Supply System on the Pulsed Power Electrical Network,* Padova, 2012.

[3] « ITER,» [Online]. Available: http://www.iter.org.

[4] H. Tan, J. Tao, I. Benfatto, J. K. Goff, A. Mankani, F. Milani, I. Song, H. Tan e J. Thomsen, «ITER Coil Power Supply and Distribution System,» in *IEEE/NPSS 24th Symposium on Fusion Engineering (SOFE)*, 2011.

[5] A. Mankani, I. Benfatto, J. Tao, J. K. Goff, J. Hourtoule, J. Gascon, D. Cardoso-Rodrigues e B. Gadeau, «The ITER reactive power compensation and harmonic filtering (RPC & HF) system: Stability & performance,» in *IEEE/NPSS 24th Symposium on Fusion Engineering (SOFE)*, 2011.

[6] G. F. Franklin, J. D. Powel, I. Michael e L. Workman, Digital Control of Dynamic Systems, Addison-Wesley Series in Electrical and Computer Engineering: Control Engineering.

[7] «IEA key world energy statistics 2011».

[8] R. Rutherford, J. Goldston e P. H, Introduction to plasma Physics, Institute of Physics Publishing Bristol and Philadelphia, 1995.

[9] S. Weston, Fusion, Wiley VCH Verlag, 2010.

[10] J. Wesson e Campbell, Tokamaks, Oxford, Clarendon.

[11] *PSIM simulation program.*

[12] S. G. Jalali, R. H. Lasseter e I. Dobson, *Dynamic response of Thyristor Controlled Switched Capacitor,* IEEE Transaction on Power Delivery, Vol.9, No.3, 1994.

[13] I. Dobson, "Stability of ideal thyristor and diode switching circuits," September 1995, pp. 517-529.

[14] J. Kassakian, M. Schlet e G. Verghese, Principles of Power Electronics, New York: N.Y: Addinson-Wesley, 1991.

[15] MathWorks, *MatLab and Simulink program.*

[16] A. Foussat, «Overview of the ITER Correction Coils Design,» *IEEE Transaction on Applied Superconductivity,* vol. 20, n. 3, June 2010..

[17] I. Dobson, S. Jalali e R. Rajaraman, *Damping and resonance in a high power switching circuit,* Electrical and Computer Engineering Department, University of Wisconsin, 1995.

[18] I. Dobson e S. Jalali, *Surprising simplification of the jacobian of diode switching circuits,* Electrical and Computer Engineering Dept. University of Wisconsin.

[19] J. T. Thompson e H. B. Stewart, Non linear Dynamics and chaos: geometrical methods for scientists and enigneers, London: John Wiley, 1987.

[20] N. Mitchell, A. Devred, P. Libeyre, B. Lim e F. Savary, «The ITER Magnets: Design and Construction Status,» *IEEE Transactions on Applied Superconductivity.*

[21] N. Mitchell, P. Bauer, R. Gallix, P. Libeyre, B. Lim, A. Sahu , F. Simon, D. Bessette, A. Devred, C. Jong e J. Knaster, «Status of the ITER magnets,» in *Fusion Engineering and Design, vol.84,,* June 2009, pp. pp. 113-121.

Appendix

I. Background of discrete-time analytical models of thyristor-based switching circuits

The theory presented in this appendix for illustrative purposes is given in [1], [6], [12], rearranging the notation as used in this thesis.

I.1. Projection and injection matrices

In a thyristor-based static switching circuit the topology of the system changes, according to the commutation of the switching components. Each interval is described by a LTI system: to join the different systems in order to describe the evolution over a sample period, projection and injection matrices are used.

For example, consider the single-phase controlled rectifier shown in Figure I-2 where the switching elements are ideal thyristors. The operating point of the rectifier can be controlled by varying the firing instant called Φ. The thyristor turn-off instant, denoted τ, represents an uncontrolled switching event that depends on circuit state. For continuous current operation the circuit has three possible modes: a commutation mode in which all thyristors are conducting and two modes associated with conduction of two different couple of thyrisotrs Q1/ Q2, Q3/Q4. Denote i_α and i_β as the currents associated with conduction in each leg of the bridge as depicted in Figure I-1. Note that in commutation mode the circuit has state vector $(i_\alpha \quad i_\beta)^t \in \mathrm{R}^2$ otherwise the circuit has state vectors described by $i_\alpha \in R^1$ or $i_\beta \in R^1$. Projection and injection matrices relate the state vectors between modes. The following development represents a simplification of the more general presented in [13].

Consider a mode in which a particular thyristor is conducting with circuit dynamics described by the linear system

$$\dot{x} = Ax + Bu \qquad\qquad I.1$$

where $x \in R^n$ is the state vector and $u \in R^m$ is a vector of time-periodic functions representing the sources.

Now let i_r denote the current associated with a particular thyristor. For the circuits under consideration the thyristor current can be expressed as a linear combination of the state so that $i_r = cx$, where c is a row vector. When the particular thyristor is nonconducting $i_r = cx = 0$, therefore the vector state x is constrained to lie in the $n-1$ dimensional hyperplane with normal

vector c. Let the columns of $Q \in R^{n \times (n-1)}$ form a basis for vectors in the hyperplane: the coordinates $y \in R^{n-1}$, that express the circuit state when a particular thyristor is not conducting, are related to the original coordinates for R^n by $x = Qy$. Finally, since c is normal to any vector in the hyperplane expressed by Q, the product cQ is equal to zero. Let v_r represent the voltage across the particular thyristor when it is in its nonconducting state (see Figure I-1)

$$\dot{x} = Ax + Bu + dv_r \qquad (I.2)$$

where $d \in R^n$ is a column vector assumed not to lie in the hyperplane with normal vector c, i.e. $cd \neq 0$. Consequently d can be scaled so that $cd = 1$. It follows that the matrix $(Q \quad d)$ is full rank. Define $P \in R^{(n-1) \times n}$ so that

$$\begin{pmatrix} P \\ c \end{pmatrix} (Q \quad d) = \begin{pmatrix} PQ & Pd \\ cQ & cd \end{pmatrix} = \begin{pmatrix} I_{n-1} & 0 \\ 0 & 1 \end{pmatrix} = I_n \qquad (I.3)$$

It follows that P has rank $n-1$, i.e. $n-1$ columns linearly indipendent, and so $Pd = 0$. Consequently, P can be determined from

$$\begin{pmatrix} P \\ c \end{pmatrix} = (Q \quad d)^{-1} \qquad (I.4)$$

Left multiplying by $(Q \quad d)$ yields the useful relation

$$(Q \quad d) \begin{pmatrix} P \\ c \end{pmatrix} = QP + dc = I_n \qquad (I.5)$$

Note that $Px = PQy = y$, thus P can be interpreted as the projection of x onto the hyperplane. Now writing (I.1) in the y coordinates yields

$$\dot{y} = PAQy + PBu \qquad (I.6)$$

describing the system with the thyristor under consideration in its nonconducting state. Furthermore, the vector states associated with a particular thyristor turn-on or turn-off transition can be related through the above projection and injection matrices as follows:

$$x(\Phi^+) = Qy(\Phi^-), \qquad Q \in R^{n \times (n-1)} \qquad (I.7)$$

$$y(\tau^+) = Px(\tau^-), \qquad P \in R^{(n-1) \times n} \qquad (I.8)$$

where Φ denotes the turn-on or and τ denotes the turn-off instant. The superscript denotes the left or right-hand limit associated with the switching process. Q is the injection matrix that allows to switch from non-conduction mode to conduction mode of the thyristor (i.e. from (I.1) to (I.6)), so it is related with the firing instant, while P allows the opposite switching (i.e. from (I.6) to (I.1)), transforming state vector x into y at turn-off instant.
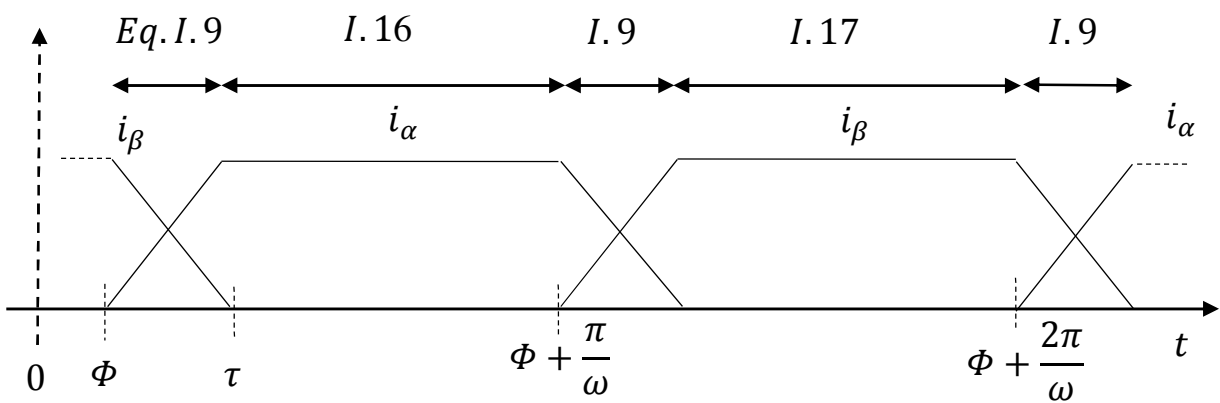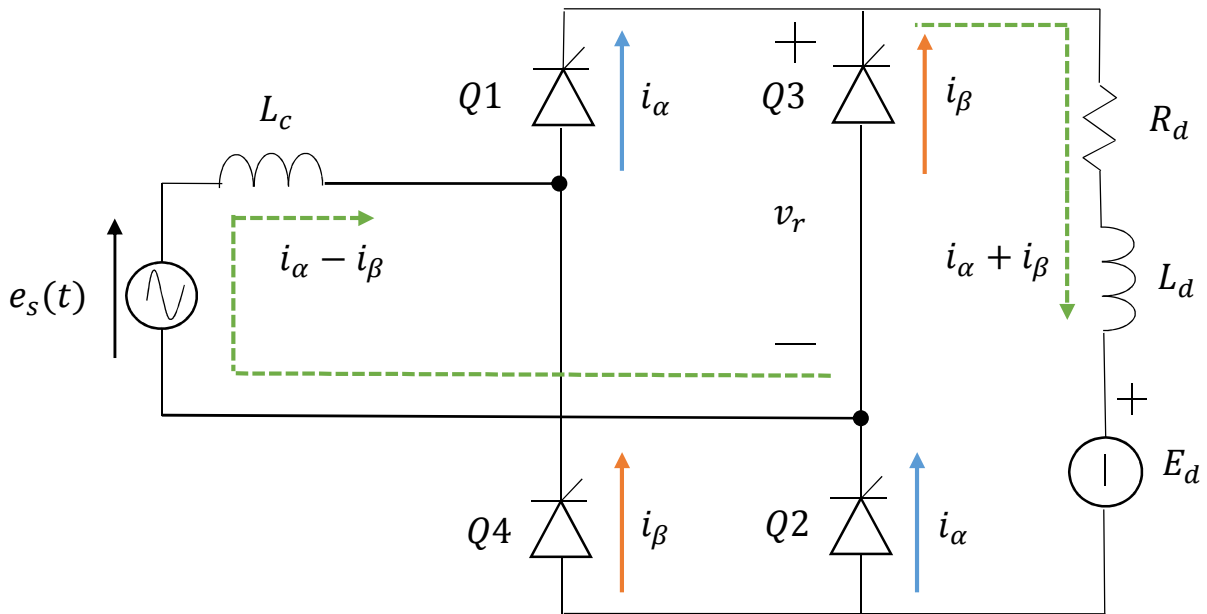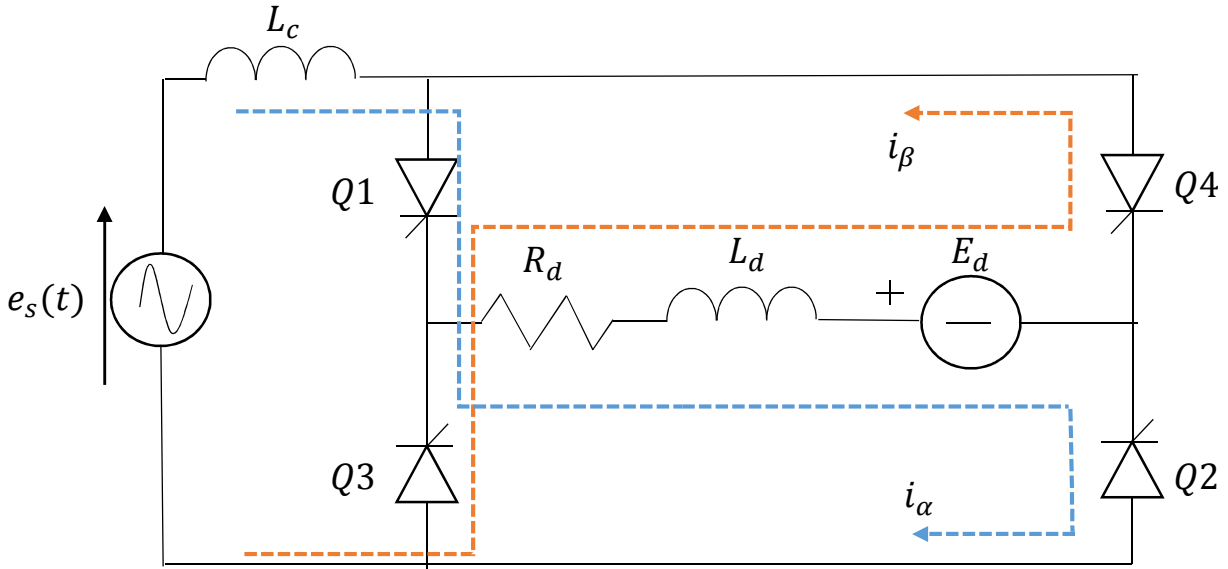
Figure I-1 Single-phase full wave rectifier with commutation reactance (a) circuit diagram (b) waveforms associated with circuit operation

Each thyristor transition has its associated injection and projection matrices which can be determined from the general circuit equations and elementary linear algebra. For example, consider the single-phase rectifier of Figure I-1(a). During commutation both legs of the bridge circuit conduct, consequently the state vector is $x = (i_\alpha \quad i_\beta)^t$ with the system dynamics described by

$$\dot{x} = Ax + B_s e_s + B_d E_d$$

To find the values of A, B_s, B_d we consider the two independent loop in the circuit writing Kirchhoff current law (KCL) on them:

$$\begin{cases} e_s = L_c \dfrac{d(i_\alpha - i_\beta)}{dt} \\ 0 = R_d(i_\alpha + i_\beta) + L_d \dfrac{d(i_\alpha + i_\beta)}{dt} + E_d \end{cases}$$

Resolving the system, it is obtained

$$\begin{cases} \dfrac{di_\alpha}{dt} = -\dfrac{R_d}{2L_d}(i_\alpha + i_\beta) + \dfrac{e_s}{2L_c} - \dfrac{E_d}{2L_d} \\ \dfrac{di_\beta}{dt} = -\dfrac{R_d}{2L_d}(i_\alpha + i_\beta) - \dfrac{e_s}{2L_c} - \dfrac{E_d}{2L_d} \end{cases}$$

Finally,

$$A = -\frac{R_d}{2L_d}\begin{pmatrix} 1 & 1 \\ 1 & 1 \end{pmatrix}, \quad B_s = \frac{1}{2L_c}\begin{pmatrix} 1 \\ -1 \end{pmatrix}, \quad B_d = -\frac{1}{2L_d}\begin{pmatrix} 1 \\ 1 \end{pmatrix}$$

Consider first a commutation interval which finishes when $i_\beta = 0$ leaving only thyristor pair Q1/Q2 (denoted α) conducting, while Q3/Q4 has been switched off. Indeed $i_r = cx$ with $c = (0 \quad 1)$ represent the current through the thyristor pair Q3/Q4 when it is conducting. It follows that the injection matrix $Q_\alpha = (1 \quad 0)^t$ relates the commutation interval which has state vector $(i_\alpha \quad i_\beta)^t$ with thyristor pair Q1/Q2 conducting mode which has state vector i_α. To obtain d let v_r represent the voltage across thyristor pair Q3/Q4 in their non-conducting state (see Figure I-1). Writing KCL on the same previous rings of the circuit it is obtained:

$$\begin{cases} e_s = L_c \dfrac{d(i_\alpha - i_\beta)}{dt} + v_r \\ v_r = R_d(i_\alpha + i_\beta) + L_d \dfrac{d(i_\alpha + i_\beta)}{dt} + E_d \end{cases} \tag{I.13}$$

$$\begin{cases} \dfrac{di_\alpha}{dt} = -\dfrac{R_d}{2L_d}(i_\alpha + i_\beta) + \dfrac{e_s}{2L_c} - \dfrac{E_d}{2L_d} + \left(\dfrac{L_c - L_d}{2L_cL_d}\right)v_r \\ \dfrac{di_\beta}{dt} = -\dfrac{R_d}{2L_d}(i_\alpha + i_\beta) - \dfrac{e_s}{2L_c} - \dfrac{E_d}{2L_d} + \left(\dfrac{L_c + L_d}{2L_cL_d}\right)v_r \end{cases} \tag{I.14}$$

Comparing (I.11) and (I.14) we have $d_\alpha = \frac{1}{2L_dL_c}(L_c - L_d \quad L_c + L_d)^t$. We can scale d in order to

have $cd_\alpha = 1$: this yields to $d_\alpha = \left(\frac{L_c-L_d}{L_c+L_d} \quad 1\right)^t$. Now

$$\begin{pmatrix} P_\alpha \\ c \end{pmatrix} = (Q_\alpha \quad d_\alpha)^{-1} = \begin{pmatrix} 1 & \dfrac{L_d - L_c}{L_c + L_d} \\ 0 & 1 \end{pmatrix} \tag{I.15}$$

So $P_\alpha = \left(1 \quad \frac{L_d-L_c}{L_c+L_d}\right)$ and $c = (0 \quad 1)$ as stated. Consequently, the circuit equation when thyristor

pair $\boldsymbol{\alpha}$ is conducting is

$$\frac{di_\alpha}{dt} = P_\alpha A Q_\alpha i_\alpha + P_\alpha B_s e_s + P_\alpha B_d E_d = -\frac{R_d}{L_c + L_d} i_\alpha + \frac{1}{L_c + L_d} e_s - \frac{1}{L_c + L_d} E_d$$

$$= P_\alpha A Q_\alpha i_\alpha + P_\alpha \left((B_s \quad B_d) \begin{pmatrix} e_s \\ E_d \end{pmatrix} \right) = P_\alpha A Q_\alpha i_\alpha + P_\alpha B u. \tag{I.16}$$

which is consistent with the circuit topology associated with this mode and with the general form

expressed in (I.6).

Now consider a commutation interval which terminates when $i_\alpha = 0$ leaving only thyristor pair

Q3/Q4 (denoted $\boldsymbol{\beta}$) conducting, while Q1/Q2 has been switched off. A similar exercise yields $c =$

$(1 \quad 0)$, injection matrix $Q_\beta = (0 \quad 1)^t$ and a normalized $d_\beta = \left(1 \quad \frac{L_d-L_c}{L_c+L_d}\right)^t$ so that $cd_\beta = 1$. The

associated projection matrix is $P_\beta = \left(\frac{L_d-L_c}{L_c+L_d} \quad 1\right)$. Consequently, the circuit equations when thyristor

pair $\boldsymbol{\beta}$ is conducting is

$$\frac{di_\beta}{dt} = P_\beta A Q_\beta i_\beta + P_\beta B_s u + P_\beta B_d E_d = -\frac{R_d}{L_c + L_d} i_\beta + \frac{1}{L_c + L_d} u - \frac{1}{L_c + L_d} E_d =$$

$$= P_\beta A Q_\beta i_\beta + P_\beta \left((B_s \quad B_d) \begin{pmatrix} e_s \\ E_d \end{pmatrix} \right) = P_\beta A Q_\beta i_\beta + P_\beta B u. \qquad (I.17)$$

which is consistent with the circuit topology associated with this mode and with the general form expressed in (I.6).

I.2. Analysis of an interval containing a single thyristor transition

This section formulates analytical expressions for the calculation of the Jacobian of the state variables respect a perturbation applied to the system over a time interval in which a thyristor makes a turn-on or a turn-off transition. Thyristor turn-on is controlled by varying the firing instant. Thyristor turn-off, on the other hand, is an uncontrolled switching process governed by the circuit: this is the main problem in the analysis of thyristor-based circuits. To stress the difficulties associated with obtaining the Jacobian over a time interval in which a thyristor transition occurs, consider the rectifier system introduced in the previous paragraph. First consider an interval that spans a thyristor turn-on transition which initiates commutation in the circuit. Two Jacobians are of interest: the Jacobian with respect to the initial state on the interval and the Jacobian with respect to the firing instant. Figure I-2 illustrates the basic mechanism for the example. On the interval (t_1, Φ) the vector state is $y = i_\beta \in R^1$ while on the interval $(\Phi, \ t_2)$ is $x = (i_\alpha \quad i_\beta)^t \in R^2$. The solid lines depict nominal circuit trajectories while the dashed lines represent circuit trajectories associated with perturbations to the initial state and to the firing instant, respectively, of the nominal trajectory. The Jacobians over the interval either (1) relates the final state perturbation to the initial state perturbation or (2) relates the final state perturbation to the perturbation in the firing instant. In general, the Jacobians are expressed mathematically as

$$(1) \quad \frac{\partial x(t_2)}{\partial y(t_1)} \epsilon R^{n \times (n-1)} \qquad\qquad (2) \quad \frac{\partial x(t_2)}{\partial \Phi} \epsilon R^n \qquad (I.18)$$

respectively.

Now consider an interval that spans a thyristor turn-off transition which for the example under consideration terminates commutation in the circuit. Figure I-2(b) illustrates the basic mechanism. On the interval (t_1, τ) the vector state is $x = (i_\alpha \quad i_\beta)^t \in R^2$ while on the interval $(\tau, \ t_2)$ is $y = i_\alpha \in R^1$. Once again the solid line depicts a nominal circuit trajectory and the dashed line represents

8

a circuit trajectory associated with a perturbation in the initial state on the interval. The Jacobian over the interval relates the final state perturbation to the initial state perturbation with particular attention to the variation in the turn-off instant which admits no external control. The Jacobian is expected to have the form

$$\left(\frac{\partial y(t_2)}{\partial x(t_1)}\right)_\tau + \frac{\partial y(t_2)}{\partial \tau} \cdot \frac{\partial \tau}{\partial x(t_1)} \epsilon\, R^{(n-1)\times n}$$

(I.19)

where the first term represents the variation in $y(t_2)$ assuming unperturbed turn-off instant τ and the second term accounts for the variation in the thyristor turn-off instant due to its implicit dependence on the initial state on the interval.

(a)

(b)
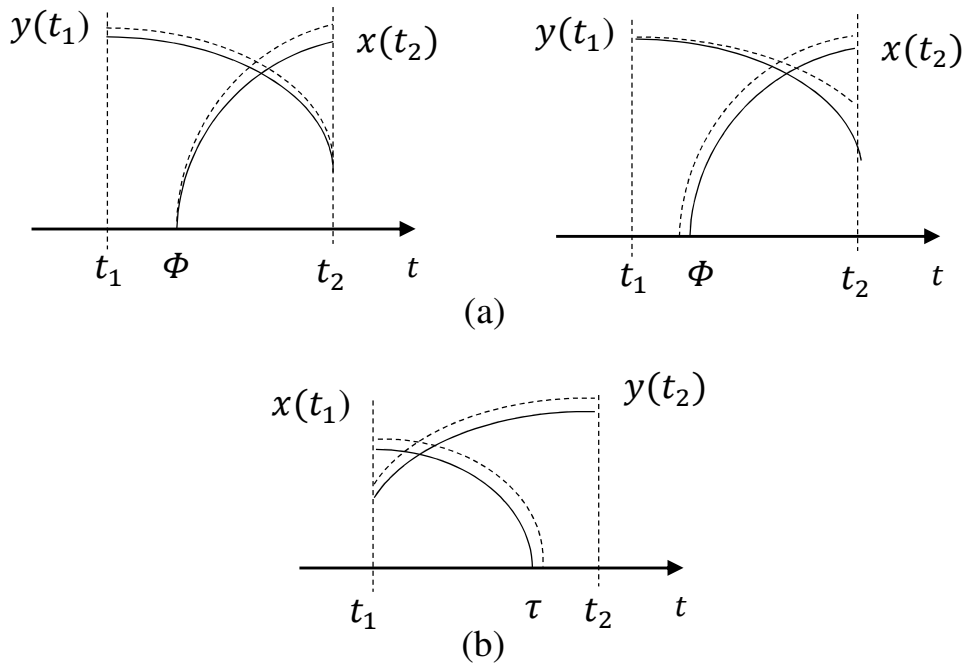
Figure I-2 Illustration of nominal (continuous line) and perturbed (dashed line) trajectories associated with a single-phase controlled rectifier on an interval containing a thyristor (a) turn-on transition and (b) turn-off transition

The subsequent development for thyristor-based circuits is based on the result presented in [13] for diode-based circuits.

I.2.1. Analysis of an interval containing a thyristor turn-on transition

Consider a time interval that contains a thyristor turn-on transition at $\Phi \in (t_1,\ t_2)$ and no other transitions. The thyristor is nonconducting in the interval $(t_1,\ \Phi)$ where the circuit is described by

$$\dot{y} = PAQy + PBu$$

(I.20)

As discussed in Section I. For example, integrating from t_1 to Φ yields

9

$$y(\Phi) = e^{PAQ(\Phi-t_1)}y(t_1) + \int_{t_1}^{\Phi} e^{PAQ(\Phi-\xi)}PBu(\xi)d\xi$$

where $y(t_1)$ is the initial state on the interval. The thyristor is subsequently conducting in the interval $(\Phi,\ t_2)$ where the circuit is described by

$$\dot{x} = Ax + Bu$$

As discussed in Section Section I. Integrating from Φ to t_2, yields

$$x(t_2) = e^{A(t_2-\Phi)}x(\Phi) + \int_{\Phi}^{t_2} e^{A(t_2-\Phi)}Bu(\xi)d\xi.$$

The injection matrix introduced in Section I relates the initial state on the conduction interval to the final state on the non-conduction interval as follows $x(\Phi^+) = Qy(\Phi^-)$. Consequently, the final state can be expressed

$$x(t_2) = e^{A(t_2-\Phi)}Qe^{PAQ(\Phi-t_1)}y(t_1)$$

$$+ e^{A(t_2-\Phi)}Q\int_{t_1}^{\Phi} e^{PAQ(\Phi-\xi)}PBu(\xi)d\xi + \int_{\Phi}^{t_2} e^{A(t_2-\xi)}Bu(\xi)d\xi.$$

The Jacobian with respect to the initial state on the interval is simply

$$\frac{\partial x(t_2)}{\partial y(t_1)} = e^{A(t_2-\Phi)}Qe^{PAQ(\Phi-t_1)}$$

which corresponds to the result associated with diode-based circuits presented in [13]. The Jacobian with respect to the firing instant on the interval yields with some simplification

$$\frac{\partial x(t_2)}{\partial \Phi} = e^{A(t_2-\Phi)}(QP - I)$$

$$\cdot \left\{ AQ\left(e^{PAQ(\Phi-t_1)}y(t_1) + \int_{t_1}^{\Phi} e^{PAQ(\Phi-\xi)}PBu(\xi)d\xi \right) + Bu(\Phi) \right\}.$$

where the fundamental theorem of calculus is used in differentiating the integrals. Substituting $x(\Phi) = Qy(\Phi)$ and $\dot{x}(\Phi) = Ax(\Phi) + Bu(\Phi)$ yields

$$\frac{\partial x(t_2)}{\partial \Phi} = -e^{A(t_2-\Phi)}dc\{AQy(\Phi) + Bu(\Phi)\} = -e^{A(t_2-\Phi)}dc\{AQy(\Phi) + Bu(\Phi)\}$$

$$= -e^{A(t_2-\Phi)}dc\dot{x}(\Phi)$$

<div align="right">(I.27)</div>

where $c\dot{x}(\Phi)$ represents the gradient of the thyristor current at turn-on.

I.2.2. Analysis of an interval containing a thyristor turn-off transition

Consider a time interval that contains a thyristor turn-off transition at $\tau \in (t_1, t_2)$ and no other transitions. The thyristor is conducting in the interval (t_1, τ) where the circuit is described by

$$\dot{x} = Ax + Bu$$

<div align="right">(I.28)</div>

As discussed in Section I. Integrating from t_1 to τ yields

$$x(\tau) = e^{A(\tau-t_1)}x(t_1) + \int_{t_1}^{\tau} e^{A(\tau-\xi)}Bu(\xi)d\xi.$$

<div align="right">(I.29)</div>

where $x(t_1)$ is the initial state on the interval. The thyristor is subsequently nonconducting on the interval (τ, t_2) where the circuit is described by

$$\dot{y} = PAQy + PBu$$

<div align="right">(I.30)</div>

As discussed in Section I. Integrating from τ to t_2 yields

$$y(t_2) = e^{PAQ(t_2-\tau)}y(\tau) + \int_{\tau}^{t_2} e^{PAQ(t_2-\xi)}PBu(\xi)d\xi.$$

<div align="right">(I.31)</div>

The projection matrix introduced in Section I relates the initial state on the non-conduction interval to the final state on the conduction interval as follows $y(\tau^+) = Px(\tau^-)$. Consequently, the final state on the interval can be expressed

$$y(t_2) = e^{PAQ(t_2-\tau)}Pe^{A(\tau-t_1)}x(t_1)$$

$$+ e^{PAQ(t_2-\tau)}P \int_{t_1}^{\tau} e^{A(\tau-\xi)}Bu(\xi)d\xi + \int_{\tau}^{t_2} e^{PAQ(t_2-\xi)}PBu(\xi)d\xi.$$

<div align="right">(I.32)</div>

Now taking the Jacobian with respect to the initial state noting that τ is an implicit function of the interval's initial state yields

<div align="right">11</div>

$$\frac{\partial y(t_2)}{\partial x(t_1)} = e^{PAQ(t_2-\tau)}Pe^{A(\tau-t_1)} + \frac{\partial y(t_2)}{\partial \tau} \cdot \frac{\partial \tau}{\partial x(t_1)}$$

<div align="right">(I.33)</div>

with some simplification

$$\frac{\partial y(t_2)}{\partial \tau} = e^{PAQ(t_2-\tau)}PA(I-QP) \cdot \left\{ e^{A(\tau-t_1)}x(t_1) + \int_{t_1}^{\tau} e^{A(\tau-\xi)}Bu(\xi)d\xi \right\}$$

<div align="right">I.34)</div>

where the fundamental theorem of calculus is used in differentiating the integrals. Substituting $I - QP = dc$ and (I.29) yields

$$\frac{\partial y(t_2)}{\partial \tau} = e^{PAQ(t_2-\tau)}PAdcx(\tau) = I$$

<div align="right">(I.35)</div>

where $cx(\tau) = 0$ represents the thyristor turn-off instant. Consequently we have the simple expression for the Jacobian with respect to the initial state

$$\frac{\partial x(t_2)}{\partial x(t_1)} = e^{PAQ(t_2-\tau)}Pe^{A(\tau-t_1)}$$

<div align="right">(I.36)</div>

This result is identical to that associated with a diode turn-off transition presented in [13].

I.3. Analysis of an interval containing a turn-on and turn-off transition

In the previous sections the trajectory and its associated Jacobian over a time interval that contains a single thyristor transition is obtained. In this section the Jacobian associated with a time interval containing both a turn-on and a turn-off thyristor transition is obtained.

First consider an interval in which a thyristor makes a turn-on followed by a turn-off transition. That is $t_1 < \Phi < \tau < t_2$, consequently the thyristor is non-conducting at t_1 and t_2. Applying the chain rule to the result of the last sections yields an analytical expression for the Jacobian with respect to the initial condition on the interval

$$\frac{\partial y(t_2)}{\partial y(t_1)} = e^{PAQ(t_2-\tau)}Pe^{A(\tau-\Phi)}Qe^{PAQ(\Phi-t_1)} \in R^{(n-1)\times(n-1)}$$

<div align="right">(I.37)</div>

The expression for the Jacobian with respect to the firing instant is

<div align="right">12</div>

$$\frac{\partial y(t_2)}{\partial \Phi} = -e^{PAQ(t_2-\tau)}Pe^{A(\tau-\Phi)}dc\dot{x}(\Phi) \in R^{(n-1)}$$

<div align="right">(I.38)</div>

where $c\dot{x}(\Phi)$ represents the gradient of the thyristor current at turn-on.

Now consider an interval in which a thyristor makes a turn-off followed by a turn-on transition. That is $t_1 < \tau < \Phi < t_2$, consequently the thyristor is conducting at t_1 and t_2. Again applying the chain rule to the result of the last sections yields an analytical expression for the Jacobian with respect to the initial condition on the interval

$$\frac{\partial x(t_2)}{\partial x(t_1)} = e^{A(t_2-\Phi)}Qe^{PAQ(\Phi-\tau)}Pe^{A(\tau-t_1)} \in R^{n \times n}$$

<div align="right">(I.39)</div>

The expression for the Jacobian with respect to the firing instant is

$$\frac{\partial x(t_2)}{\partial \Phi} = -e^{A(t_2-\Phi)}dc\dot{x}(\Phi) \in R^n$$

<div align="right">(I.40)</div>

where $c\dot{x}(\Phi)$ represents the gradient of the thyristor current at turn-on.

As an illustrative example, suppose that the rectifier already introduced in Section I is operating in the periodic steady-state – that is the circuit waveforms, sources and switching processes are periodic with period $T_d = 2\pi$ (letter "d" denotes a time interval expressed in [rad]). Note, however, that the dc load current is periodic with period $T_d/2$ corresponding to half cycle of the supply frequency. Consequently, consider the Jacobian with respect to the initial state on an interval spanning half a cycle $T_s = \frac{T_d}{2\omega}$ of circuit operation. Specifically, consider the interval $(\Phi, \ \Phi + T_s)$ which contains a commutation mode that terminates when $i_\beta(\tau) = 0$. Consequently, the initial state on the interval is $i_\beta(\Phi)$ and the final state on the interval is $i_\alpha(\Phi + T_s) = i_\beta(\Phi)$. Both represent the dc load current at the onset of a commutation interval. From the result on Section 2.2 the Jacobian with respect to the initial state on the interval is

$$\frac{\partial i_\alpha(\Phi + T_s)}{\partial i_\beta(\Phi)} = e^{P_\beta AQ_\beta(T_s+\Phi-\tau)}P_\beta e^{A(\tau-\Phi)}Q_\alpha \in R^1$$

<div align="right">(I.41)</div>

where Q_α is the injection matrix associated with the turn-on transition of thyristor pair Q1/Q2 and P_β is the projection matrix associated with the turn-off transition of thyristor pair Q3/Q4. Define the commutation interval $\mu = \tau - \Phi$. Evaluating the above yields the scalar

$$\frac{\partial i_\alpha(\Phi + T_s)}{\partial i_\beta(\Phi)} = e^{-\frac{R_d}{L_c+L_d}(T_s-\mu)} \frac{L_d - L_c e^{-\frac{R_d}{L_d}\mu}}{L_d + L_c} \qquad (I.42\ )$$

which gives a measure of the damping of a perturbation to the initial state (the dc load current just prior to initiating a commutation interval) effected over a half cycle of operation. Note that for typical parameters the Jacobian varies little with operating point characterized by the commutation interval μ. In particular, for $R_d = 0$ the Jacobian becomes

$$\frac{\partial i_\alpha(\Phi + T_s)}{\partial i_\beta(\Phi)} = \frac{L_d - L_c}{L_d + L_c} \qquad (I.43\ )$$

which is independent of operating point. A similar result associated with a six-pulse diode rectifier is obtained in [13].

Now consider the classical approach to the dynamic analysis of the single-phase controlled rectifier. Classical steady-state analysis is based on the assumption of constant ripple-free load current [14].
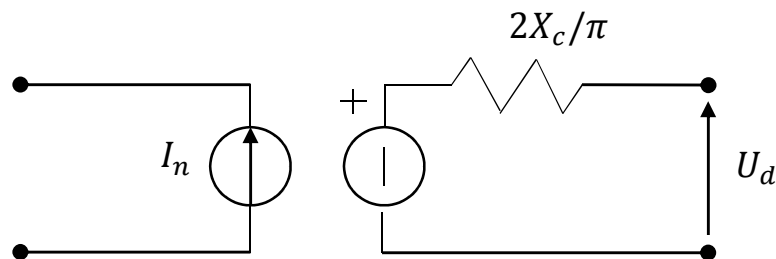
Figure I-3 Classical model of the single-phase full-wave rectifier

The steady-state model is often represented as in Figure I-3 which decouples the ac and dc circuits. The phasor I_n represent harmonic currents injected into the ac system and U_d represents the controlled dc voltage. The resistance models the dc voltage regulation due to the commutation reactance $X_c = \omega L_c$.

The classical approach to dynamic analysis is based on this phasor model. Suppose the dc side is connected to an R-L-E load as in the example, then the dynamics of the dc side assuming unperturbated inputs u and E_d are governed by

$$L_d \frac{d\breve{\imath}_d}{dt} = -\left(\frac{2X_c}{\pi} + R_d\right)\breve{\imath}_d$$

<div align="right">(I.44)</div>

where $\breve{\imath}_d$ represents perturbations from the steady-state dc load current.

We now show the near equivalence of both dynamic models for parameter values characterized by $R_d = 0$ and $L_c \ll L_d$. The continuous-time eigenvalue $\lambda = -\frac{2X_c}{\pi L_d}$ associated with the classical model becomes the sampled-data characteristic multiplier

$$\Psi = e^{\lambda\frac{\pi}{\omega}} = e^{-\frac{2l_c}{L_d}} \approx 1 - \frac{2L_c}{L_d}$$

<div align="right">(I.45)</div>

based on a half-cycle sample interval. The characteristic multiplier characterizes the evolution of a perturbation to the dc load current over the half cycle. Note that Φ closely corresponds to the characteristic multiplier

$$\frac{\partial i_\alpha(\Phi + T_s)}{\partial i_\beta(\Phi)} = \frac{L_d - L_c}{L_d + L_c} = 1 - \frac{2L_c}{L_c + L_d}$$

<div align="right">(I.46)</div>

for the stated assumption $L_c \ll L_d$. This justifies the current practice of using the phasor model for linearized dynamic analysis.

II. Basic concepts of LTI state-space model

In this Chapter taken from [6], readapted with the notation used here, briefly introduces how can be related LTI discrete-state space model to continuous one, because often it is useful to change the reference frame, also to carry out frequency analysis for a discrete-time model written in a continuous-time reference.

A continuous, linear, constant-coefficient system of differential equations that can always be expressed as a set of first-order matrix differential equations:

$$\dot{x} = \hat{A}x + \hat{B}u$$

(II.1)

where u is the control input to the system. The output can be expressed as a linear combination of the state x and the input u:

$$v = \hat{C}x + \hat{J}u$$

(II.2)

It is studied the case in which $\hat{J}$ is zero and $\hat{C} = I$. To relate the samples of the output v_k to the samples of the control u_k (II.1) has to be solved. It is begun by solving the equation with only initial conditions and no external input. This is the homogeneous equation

$$\dot{x}_h = \hat{A}x_h(t), \quad x_h(t) = x_0$$

(II.3)

It can be shown that the solution given below is unique and given by:

$$x_h(t) = e^{\hat{A}(t-t_0)}x(t_0)$$

(II.4)

where $e^{\hat{A}(t-t_0)}$ is the $n \times n$ matrix obtained by exponentiating $\hat{A}$. It is defined by the convergent series as follow

$$e^{\hat{A}(t-t_0)} = \left[I + \hat{A}(t-t_0)^2 + \frac{\hat{A}^2(t-t_0)^2}{2} + \frac{\hat{A}^3(t-t_0)^3}{6} + \cdots \right]$$

(II.5)

The particular solution when u is not zero is obtained by using the method of variation of parameters. The solution must be in the form

$$x_p(t) = e^{\hat{A}(t-t_0)}z(t)$$

(0I.6)

where $z(t)$ is a vector of variable parameters to be determined. Substituting (II.6) into (II.1), it is obtained

16

$$\hat{A}e^{\hat{A}(t-t_0)}z + e^{\hat{A}(t-t_0)}\dot{z} = \hat{A}e^{\hat{A}(t-t_0)}z + \hat{B}u \qquad (OI.7)$$

and it is solved for $\dot{x}$ as

$$\dot{z}(t) = e^{-\hat{A}(t-t_0)}\hat{B}u(t) \qquad (OI.8)$$

Assuming that the control $u(t)$ is zero $t < t_0$, it's possible to integrate $\dot{z}$ from t_0 to t obtaining

$$z(t) = \int_{t_0}^{t} e^{-\hat{A}(\tau-t_0)}\hat{B}u(\tau)d\tau \qquad (II.9)$$

Hence, from (I.6)

$$x_p(t) = e^{\hat{A}(t-t_0)} \int_{t_0}^{t} e^{-\hat{A}(\tau-t_0)}\hat{B}u(\tau)d\tau \qquad (II.10)$$

and simplifying it is obtained the particular solution (convolution)

$$x_p(t) = \int_{t_0}^{t} e^{\hat{A}(t-\tau)}\hat{B}u(\tau)d\tau \qquad (II.11)$$

The total solution is the sum of (II.11) and (II.4):

$$x(t) = e^{\hat{A}(t-t_0)}x(t_0) + \int_{t_0}^{t} e^{\hat{A}(t-\tau)}\hat{B}u(\tau)d\tau \qquad (II.12)$$

Using this solution over one sample period to obtain a difference equation and juggling the notation a bit (let $t = kT_s + T_s$ and $t_0 = kT_s$) it yields a particular version of (II.12):

$$x(kT_s + T_s) = e^{\hat{A}T_s}x(kT) + \int_{kT_s}^{kT_s+T_s} e^{\hat{A}(kT_s+T_s-\tau)}\hat{B}u(\tau)d\tau \qquad (II.13)$$

This result is not dependent on the type of hold because u is specified in terms of its continuous time history, $u(t)$, over the sample interval. It's possible to assume that

$$u(\tau) = u(kT_s), \qquad kT_s \leq \tau < kT_s + T_s \qquad (II.14)$$

Changing variables in the integral from τ to η such that

$$\eta = kT_s + T_s - \tau \qquad (II.15)$$

It is obtained

$$x(kT_s + T_s) = e^{\hat{A}T}x(kT_s) + \int_0^{T_s} e^{\hat{A}\eta}d\eta \hat{B}u(kT_s) \qquad (II.16)$$

If it's defined

$$\Psi = e^{\hat{A}T_s} \qquad (II.17)$$

$$\Gamma = \int_0^{T_s} e^{\hat{A}\eta}d\eta \hat{B} \qquad (II.18)$$

Eq. (II.1) and (II.2) reduce to difference equations in standard form (with $\Sigma = \hat{C} = I$):

$$x(k+1) = \Psi x(k) + \Gamma u(k)$$

$$y(k) = \Sigma x(k) \qquad (II.19)$$

That is the discrete state-space form of the linear continuous-time modelexpressed by (II.1).

Now the task is to derive the continuous time model from the discrete one (II.19). From (I.66), consider the similarity transform S that diagonalizes $\Psi = S\Lambda S^{-1}$ so

$$\hat{A} = \frac{1}{T_s}S\{log\Lambda \pm jn\pi I\}S^{-1} \qquad (II.20)$$

where n is chosen with attention to aliasing, comparing the evolution of state variables with the discrete and continuous time approach.

The Ψ series expansion (II.5) can be rewritten

$$\Psi = e^{\hat{A}T_s} = \left[I + AT_s + \frac{\hat{A}^2T_s^2}{2} + \frac{\hat{A}^3T_s^3}{6} + \cdots\right] \qquad (II.21)$$

can also be written

$$\Psi = I + \hat{A}T_s\Omega \qquad (II.22)$$

where

$$\Omega = I + \frac{\hat{A}T_s}{2!} + \frac{\hat{A}^2T_s^2}{3!} + \cdots \qquad (0I.23)$$

while Γ integral (I.18) can be evaluated term by term to give

$$\Gamma = \sum_{k=0}^{\infty} \frac{\hat{A}^k T_s^{k+1}}{(k+1)!} \hat{B} = \sum_{k=0}^{\infty} \frac{\hat{A}^k T_s^{k}}{(k+1)!} T\hat{B} = (\Omega T_s)\hat{B} \qquad (\mathit{0I.24})$$

Comparing (II.22) and (II.24) we have

$$(T_s\Omega) = \hat{A}^{-1}(\Psi - I) = \Gamma \hat{B}^{-1} \qquad (\mathit{II.25})$$

So on the assumption that A is invertible

$$\hat{B} = (\Psi - I)^{-1}\hat{A}\Gamma \qquad (\mathit{0I.26})$$

The eigenvalues of $\hat{A}$ matrix in the continuous state space form (II.1) define the stability of the steady-state operation: the system is exponentially stable if the eigenvalues of $\hat{A}$ have negative real part. Considering (II.19), in the discrete form this is equal to say that the eigenvalues of Ψ lie strictly inside the unit circle: a pole inside the unit circle has positive damping and a pole outside the unit circle implies instability.

III.   List of programs

Below there are the list of the programs used to carry out the simulations in this work using [15].

III.1.   *Single-phase case study*

The list below refers to simulations presented in Section 3.1.3.

```
%-------------------------- dati input-------------------------------
w=2*pi*50; %[Hz]
T=2*pi/w;
t=linspace(0,1,1e06);
sigma=[15 30 45]*pi/180;
n_el=size(sigma,2);
Lr=112.174e-3/3; %[H]
Cr=183e-06; %[F]
Ls=8.278e-3; %[H]
Rs=0.9e-03; %[ohm]
u=53889;
%----------------------------matrici---------------------------------
A=[0 -1/Ls 0
   1/Cr 0 -1/Cr
    0 1/Lr 0];
B=[1/Ls 0 0]';
P=[1 0 0
   0 1 0];
Q=P';
c=[0 0 1];
%---------------------------Program----------------------------------
clc
close all
SVC_dati_input_Perkins_ex
[V,Ad] = eig(A);
PAQ=P*A*Q;
[C,PAQd] = eig(PAQ);
n=size(A);
m=size(PAQ);
u_d=[1 0]';
u_q=[0 1]';
for k=1:n_el
        for i=1:n
            exp_A_sigma(i,i)=exp(Ad(i,i)*(sigma(k)/w));
        end
        exp_A_sigma_1=V*exp_A_sigma*inv(V);
        for i=1:m
            exp_PAQ_pi_sigma(i,i)=exp(PAQd(i,i)*(pi-sigma(k))/(2*w));
        end
        exp_PAQ_pi_sigma_1=C*exp_PAQ_pi_sigma*inv(C);
        DH(:,:,k)=exp_PAQ_pi_sigma_1*P*exp_A_sigma_1*Q*exp_PAQ_pi_sigma_1;
        DH(1:2,1:2,k)=DH(:,:,k);
        E(:,k)=eig(DH(:,:,k));
        figure (1)
        title ('Posizione degli autovalori di DH nel piano complesso al variare
di sigma');
        plot (real(E(:,k)),imag(E(:,k)),'*');
```

```matlab
    hold on
% calcolo del primo integrale nell'intervallo [0, phi] con passo
% d'integrazione relativo di 1/10000 (cioè prendendo 10000 campioni)
    csi=linspace(0,(pi-sigma(k))/2,1e4);
    for kk=1:1e4
    Wa=[cos(csi(kk)) -sin(csi(kk))];
        for i=1:m
            exp_PAQ_phi_csi(i,i)=exp(PAQd(i,i)*((pi-sigma(k))/2-csi(kk))/w);
        end
    exp_PAQ_phi_csi_1=C*exp_PAQ_phi_csi*inv(C);
    int_1_d(:,:,kk)=exp_PAQ_phi_csi_1*P*B*u*Wa*u_d;
    M_1_d(kk,1)= int_1_d(1,1,kk);
    M_1_d(kk,2)= int_1_d(2,1,kk);
    int_1_q(:,:,kk)=exp_PAQ_phi_csi_1*P*B*u*Wa*u_q;
    M_1_q(kk,1)= int_1_q(1,1,kk);
    M_1_q(kk,2)= int_1_q(2,1,kk);
    end
INT_1_d(1,1,k)=trapz(csi/w,M_1_d(:,1));
INT_1_d(2,1,k)=trapz(csi/w,M_1_d(:,2));
INT_1_q(1,1,k)=trapz(csi/w,M_1_q(:,1));
INT_1_q(2,1,k)=trapz(csi/w,M_1_q(:,2));
    for i=1:m
        exp_PAQ_phi(i,i)=exp(PAQd(i,i)*((pi-sigma(k))/2)/w);
    end
exp_PAQ_phi_1=C*exp_PAQ_phi*inv(C);
_phi(:,k)=exp_PAQ_phi_1*y_0(:,k)+INT_1_d(:,1,k);
x_phi(:,k)=Q*y_phi(:,k);
% calcolo dH/dphi
 x_punto_phi(:,k)=A*x_phi(:,k)+B*(u*cos((pi-sigma(k))/2));
 dH_dphi(:,k)=-exp_PAQ_pi_sigma_1*P*exp_A_sigma_1*c'*c*x_punto_phi(:,k);
%----------------------------------------------------------------------
% calcolo del secondo integrale nell'intervallo [phi, tau]
csi=linspace((pi-sigma(k))/2,((pi+sigma(k))/2),1e4);
for kk=1:1e4
    Wa=[cos(csi(kk)) -sin(csi(kk))];
        for i=1:n
            exp_A_tau_csi(i,i)=exp(Ad(i,i)*((pi+sigma(k))/2-csi(kk))/w);
        end
    exp_A_tau_csi_1=V*exp_A_tau_csi*inv(V);
    int_2_d(:,:,kk)=exp_A_tau_csi_1*B*u*Wa*u_d;
    int_2_q(:,:,kk)=exp_A_tau_csi_1*B*u*Wa*u_q;
    M_2_d(kk,1)= int_2_d(1,1,kk);
    M_2_d(kk,2)= int_2_d(2,1,kk);
    M_2_d(kk,3)= int_2_d(3,1,kk);
    M_2_q(kk,1)= int_2_q(1,1,kk);
    M_2_q(kk,2)= int_2_q(2,1,kk);
    M_2_q(kk,3)= int_2_q(3,1,kk);
end
INT_2_d(1,1,k)=trapz(csi/w,M_2_d(:,1));
INT_2_d(2,1,k)=trapz(csi/w,M_2_d(:,2));
INT_2_d(3,1,k)=trapz(csi/w,M_2_d(:,3));
INT_2_q(1,1,k)=trapz(csi/w,M_2_q(:,1));
INT_2_q(2,1,k)=trapz(csi/w,M_2_q(:,2));
INT_2_q(3,1,k)=trapz(csi/w,M_2_q(:,3));
    for i=1:n
        exp_A_tau_phi(i,i)=exp(Ad(i,i)*(sigma(k)/w));
    end
exp_A_tau_phi_1=V*exp_A_tau_phi*inv(V);
x_tau(:,k)=exp_A_tau_phi_1*x_phi(:,k)+INT_2_d(:,1,k);
y_tau(:,k)=P*x_tau(:,k);
%----------------------------------------------------------------------
% calcolo del terzo integrale nell'intervallo [tau, pi]
```

```matlab
csi=linspace(((pi+sigma(k))/2),pi,1e4);
for kk=1:1e4
    Wa=[cos(csi(kk)) -sin(csi(kk))];
        for i=1:m
            exp_PAQ_pi_csi(i,i)=exp(PAQd(i,i)*(pi-csi(kk))/w);
        end
    exp_PAQ_pi_csi_1=C*exp_PAQ_pi_csi*inv(C);
    int_3_d(:,:,kk)=exp_PAQ_pi_csi_1*P*u*B*Wa*u_d;
    int_3_q(:,:,kk)=exp_PAQ_pi_csi_1*P*u*B*Wa*u_q;
    M_3_d(kk,1)= int_3_d(1,1,kk);
    M_3_d(kk,2)= int_3_d(2,1,kk);
    M_3_q(kk,1)= int_3_q(1,1,kk);
    M_3_q(kk,2)= int_3_q(2,1,kk);
end
INT_3_d(1,1,k)=trapz(csi/w,M_3_d(:,1));
INT_3_d(2,1,k)=trapz(csi/w,M_3_d(:,2));
INT_3_q(1,1,k)=trapz(csi/w,M_3_q(:,1));
INT_3_q(2,1,k)=trapz(csi/w,M_3_q(:,2));
    for i=1:m
        exp_PAQ_pi_tau(i,i)=exp(PAQd(i,i)*((pi-sigma(k))/2)/w);
    end
  exp_PAQ_pi_tau_1=C*exp_PAQ_pi_tau*inv(C);
y_pi(:,k)=exp_PAQ_pi_tau_1*y_tau(:,k)+INT_3_d(:,1,k);
h_phi_ud(:,k)=exp_PAQ_pi_tau_1*P*(exp_A_tau_phi_1*Q*INT_1_d(:,1,k)/u+INT_2_d(:,1
,k)/u)+INT_3_d(:,1,k)/u;
h_phi_uq(:,k)=exp_PAQ_pi_tau_1*P*(exp_A_tau_phi_1*Q*INT_1_q(:,1,k)/u+INT_2_q(:,1
,k)/u)+INT_3_q(:,1,k)/u;
% perturbazione del firing angle (0.1 gradi) mantenendo sorgente U(s)
% invariata: variazione dello stato del sistema utilizzando la mappa di Poicarè.
Y_0=[0 0 0; 0 0 0];
for i=0:(n_cycles-2)
    Y(:,k)=DH(:,:,k)*Y_0(:,k)+(-1)^i*(dH_dphi(:,k)*0.1/100/180);  % a seconda
dell'asse in
% cui è data la perturbazione in ampiezza bisogna scegliere h_phi_ud o
% h_phi_uq.
    Is_tilde(i+1,k)=Y(1,k);
    Vc_tilde(i+1,k)=Y(2,k);
    Y_0(:,k)=Y(:,k);
end
DH_15(:,:)=real(DH(:,:,1));
dH_dphi_15(:,1)=real(dH_dphi(:,1));
h_phi_u_15(:,:)=real([h_phi_ud(:,1) h_phi_uq(:,1)]);
DH_30(:,:)=real(DH(:,:,2));
dH_dphi_30(:,1)=real(dH_dphi(:,2));
h_phi_u_30(:,:)=real([h_phi_ud(:,2) h_phi_uq(:,2)]);
DH_45(:,:)=real(DH(:,:,3));
dH_dphi_45(:,1)=real(dH_dphi(:,3));
h_phi_u_45(:,:)=real([h_phi_ud(:,3) h_phi_uq(:,3)]);
figure (1)
plot (i_s_angle.time, i_s_angle.signals.values, '- ' );
title ('Perturbed Is ');
xlabel('time (s)');
ylabel('(A)');
figure (2)
plot (V_c_angle.time, V_c_angle.signals.values, '- ' );
title ('Perturbed V_c ');
xlabel('time (s)');
ylabel('(V)');
% --------lettura dati da PSIM-----------------------------------------
%clear all
% clc
nomefile1 = fopen( 'inputTCRMAT_angle_30.txt','r');
```

```
inputsPSIM = fscanf ( nomefile1 , '%g %g %g %g %g %g' , [6 inf] );
%Time    Ud1_Ud    Uq1_Uq    alphaTCR        Vr1-Vr    Is1-Is
fclose(nomefile1);
inputsPSIM_v=inputsPSIM';
tstart1=inputsPSIM_v(1,1);
tstart=ceil(tstart1*(100))*1/(100)
inputsPSIM_v(:,1)=inputsPSIM_v(:,1)+(tstart-tstart1);
tend=inputsPSIM_v(end,1)
```
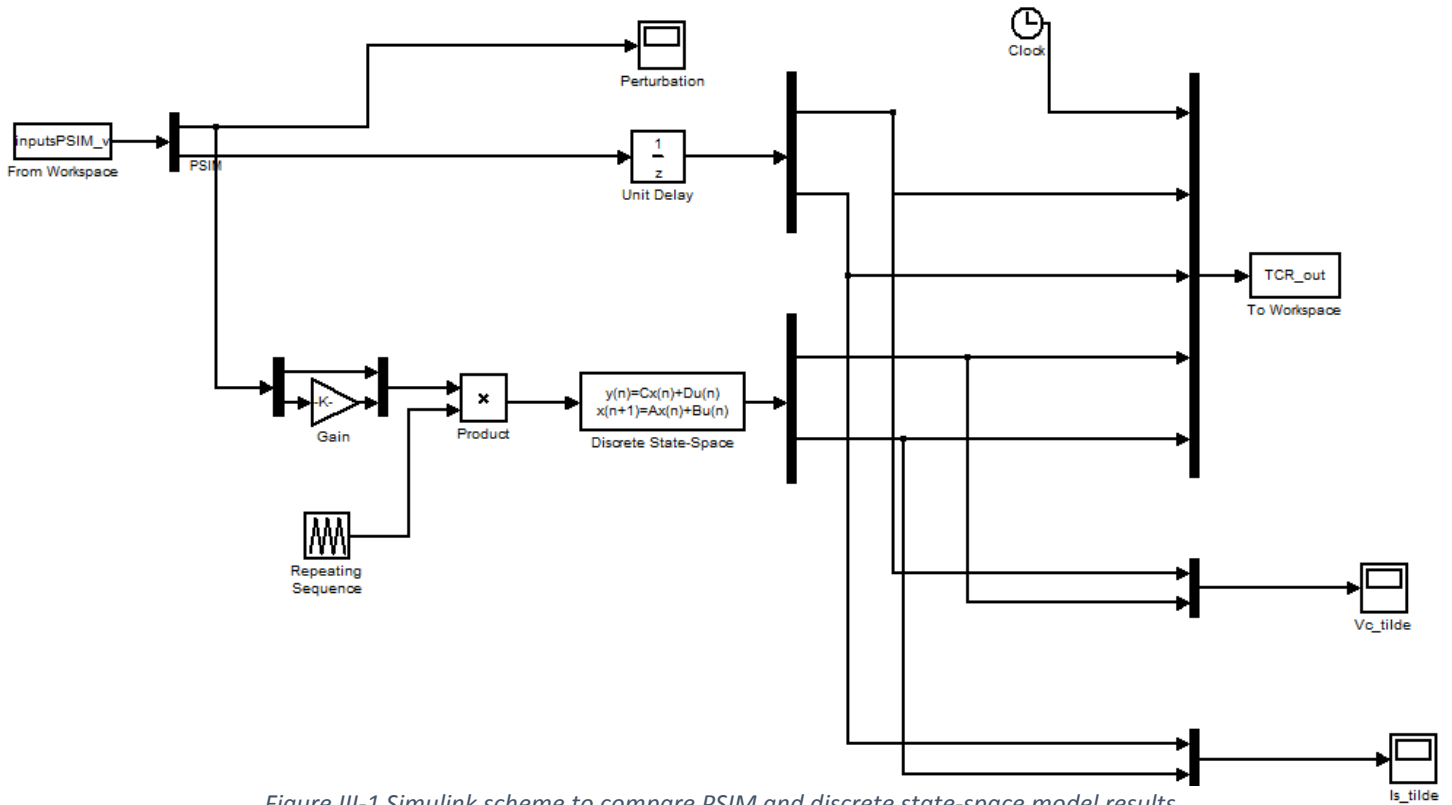

Figure III-1 Simulink scheme to compare PSIM and discrete state-space model results
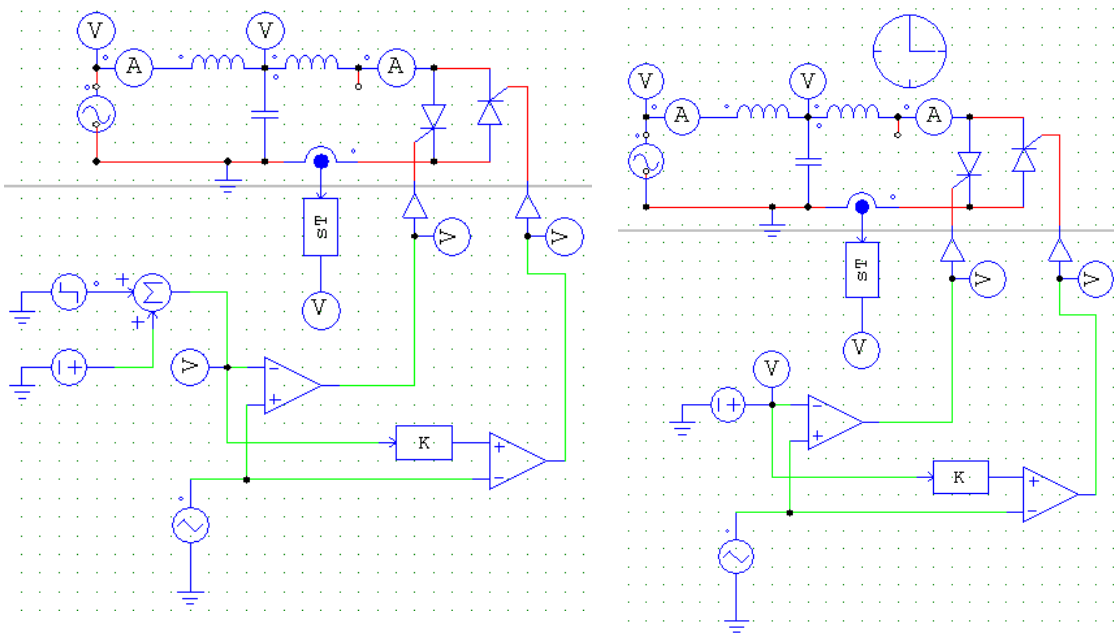
Figure III-2 PSIM circuits to simulate steady state and perturbed mode of operation

III.2. Three-phase star-connected TCR with $\sigma \epsilon$ $(0, 60°)$

The list below refers to simulations presented in Section 3.2.

```
%------------------------ dati input-------------------------------
w=2*pi*50; %[Hz]
T=2*pi/w;
t=linspace(0,1,1e06);
sigma=[0.00001 15 30 45]*pi/180;
n_el=size(sigma,2);
Lr=112.174e-3/3; %[H]
Cr=183e-06; %[F]
Ls=8.278e-3; %[H]
u=53889;
%--------------------------matrici---------------------------------
A=[0 -1/Ls 0
   1/Cr 0 -1/Cr
    0 1/Lr 0];
B=[1/Ls 0 0]';
P=[1 0 0
   0 1 0];
Q=P';
c=[0 0 1];
% da PSIM
%y_0=[is(0) is(15) is(30)  is(45)
%     Vr(0) Vr(15) Vr(30)  Vr(45)]

y_0_a=[3.7137e3          0            0              0
       6.354e+004  6.3237327e+004    6.2426174e+004  6.0137043e+004];

y_0_b=[1.6e3    3.1427919e+003   3.0962824e+003  2.9533682e+003
      -5.389e4  -3.1752442e+004  -3.2530991e+004  -3.4608536e+004];

y_0_c=[-1.6e3     -3.1420207e+003  -3.0962905e+003  -2.9533756e+003
       -5.389e4    -3.1807548e+004  -3.2530941e+004  -3.4608492e+004];
n_cycles=10;
S=[1 0 0 0 0 0; 0 0 1 0 0 0; 0 0 0 0 1 0; 0 1 0 0 0 0; 0 0 0 1 0 0; 0 0 0 0 0
1];
V_0=2/3*[cos(0) cos(0-2*pi/3) cos(0+2*pi/3)
       -sin(0) -sin(0-2*pi/3) -sin(0+2*pi/3)
       1/2     1/2            1/2];
W_0=[cos(0)         -sin(0)        1;
    cos(0-2*pi/3)  -sin(0-2*pi/3)  1;
    cos(0+2*pi/3)  -sin(0+2*pi/3)  1];
NI_0=[V_0 zeros(3,3); zeros(3,3) V_0];
DOUBLE_NI_0=[W_0 zeros(3,3); zeros(3,3) W_0];
V_180=2/3*[cos(pi) cos(pi-2*pi/3) cos(pi+2*pi/3)
       -sin(pi) -sin(pi-2*pi/3) -sin(pi+2*pi/3)
       1/2     1/2            1/2];
W_180=[cos(pi)         -sin(pi)         1;
    cos(pi-2*pi/3)  -sin(pi-2*pi/3)  1;
    cos(pi+2*pi/3)  -sin(pi+2*pi/3)  1];
I_180=[V_180 zeros(3,3); zeros(3,3) V_180];
DOUBLE_NI_180=[W_180 zeros(3,3); zeros(3,3) W_180];

%---------------------------Program--------------------------------
close all
clc
SVC_dati_input_Perkins_ex_0
```

```matlab
[V,Ad] = eig(A);
PAQ=P*A*Q;
[C,PAQd] = eig(PAQ);

n=size(A);
m=size(PAQ);

u_d=[1 0]';
u_q=[0 1]';

for k=1:n_el
      for i=1:n
          exp_A_sigma(i,i)=exp(Ad(i,i)*(sigma(k)/w));
      end
      exp_A_sigma_1=V*exp_A_sigma*inv(V);
      for i=1:m
          exp_PAQ_pi_sigma_mezzi(i,i)=exp(PAQd(i,i)*(pi-sigma(k))/(2*w));
          exp_PAQ_pi_sigma_mezzi_pi_3(i,i)=exp(PAQd(i,i)*((pi-
sigma(k))/2+pi/3)/(w));
          exp_PAQ_pi_sigma_mezzi__pi_3(i,i)=exp(PAQd(i,i)*((pi-sigma(k))/2-
pi/3)/(w));
      end
      exp_PAQ_pi_sigma_mezzi_1=C*exp_PAQ_pi_sigma_mezzi*inv(C);
      exp_PAQ_pi_sigma_mezzi_pi_3_1=C*exp_PAQ_pi_sigma_mezzi_pi_3*inv(C);
      exp_PAQ_pi_sigma_mezzi__pi_3_1=C*exp_PAQ_pi_sigma_mezzi__pi_3*inv(C);

DH_a(:,:,k)=exp_PAQ_pi_sigma_mezzi_1*P*exp_A_sigma_1*Q*exp_PAQ_pi_sigma_mezzi_1;

DH_b(:,:,k)=exp_PAQ_pi_sigma_mezzi_pi_3_1*P*exp_A_sigma_1*Q*exp_PAQ_pi_sigma_mez
zi__pi_3_1;

DH_c(:,:,k)=exp_PAQ_pi_sigma_mezzi__pi_3_1*P*exp_A_sigma_1*Q*exp_PAQ_pi_sigma_me
zzi_pi_3_1;
      nulla(:,:,k)=zeros(2);
      PHI_signed(:,:,k)=S*real([DH_a(:,:,k) nulla(:,:,k) nulla(:,:,k);
nulla(:,:,k) DH_b(:,:,k) nulla(:,:,k); nulla(:,:,k) nulla(:,:,k)
DH_c(:,:,k)])*S';

% calcolo del primo integrale

    csi_a=linspace(0,(pi-sigma(k))/2,1e4);
    csi_b=linspace(0,(pi-sigma(k))/2-pi/3,1e4);
    csi_c=linspace(0,(pi-sigma(k))/2+pi/3,1e4);

  for kk=1:1e4
   Wa_a=[cos(csi_a(kk)) -sin(csi_a(kk))];
   Wa_b=[cos(csi_b(kk)-2*pi/3) -sin(csi_b(kk)-2*pi/3)];
   Wa_c=[cos(csi_c(kk)+2*pi/3) -sin(csi_c(kk)+2*pi/3)];
      for i=1:m
          exp_PAQ_phi_csi_a(i,i)=exp(PAQd(i,i)*((pi-sigma(k))/2-csi_a(kk))/w);
          exp_PAQ_phi_csi_b(i,i)=exp(PAQd(i,i)*((pi-sigma(k))/2-pi/3-
csi_b(kk))/w);
          exp_PAQ_phi_csi_c(i,i)=exp(PAQd(i,i)*((pi-sigma(k))/2+pi/3-
csi_c(kk))/w);
      end
    exp_PAQ_phi_csi_1_a=C*exp_PAQ_phi_csi_a*inv(C);
    exp_PAQ_phi_csi_1_b=C*exp_PAQ_phi_csi_b*inv(C);
    exp_PAQ_phi_csi_1_c=C*exp_PAQ_phi_csi_c*inv(C);
    int_1_d_a(:,:,kk)=exp_PAQ_phi_csi_1_a*P*B*u*Wa_a*u_d;
    int_1_d_b(:,:,kk)=exp_PAQ_phi_csi_1_b*P*B*u*Wa_b*u_d;
    int_1_d_c(:,:,kk)=exp_PAQ_phi_csi_1_c*P*B*u*Wa_c*u_d;
```

```
    M_1_d_a(kk,1)= int_1_d_a(1,1,kk);
    M_1_d_a(kk,2)= int_1_d_a(2,1,kk);
    M_1_d_b(kk,1)= int_1_d_b(1,1,kk);
    M_1_d_b(kk,2)= int_1_d_b(2,1,kk);
    M_1_d_c(kk,1)= int_1_d_c(1,1,kk);
    M_1_d_c(kk,2)= int_1_d_c(2,1,kk);

    int_1_q_a(:,:,kk)=exp_PAQ_phi_csi_1_a*P*B*u*Wa_a*u_q;
    int_1_q_b(:,:,kk)=exp_PAQ_phi_csi_1_b*P*B*u*Wa_b*u_q;
    int_1_q_c(:,:,kk)=exp_PAQ_phi_csi_1_c*P*B*u*Wa_c*u_q;

    M_1_q_a(kk,1)= int_1_q_a(1,1,kk);
    M_1_q_a(kk,2)= int_1_q_a(2,1,kk);
    M_1_q_b(kk,1)= int_1_q_b(1,1,kk);
    M_1_q_b(kk,2)= int_1_q_b(2,1,kk);
    M_1_q_c(kk,1)= int_1_q_c(1,1,kk);
    M_1_q_c(kk,2)= int_1_q_c(2,1,kk);
  end

    INT_1_d_a(1,1,k)=trapz(csi_a/w,M_1_d_a(:,1));
    INT_1_d_a(2,1,k)=trapz(csi_a/w,M_1_d_a(:,2));
    INT_1_d_b(1,1,k)=trapz(csi_b/w,M_1_d_b(:,1));
    INT_1_d_b(2,1,k)=trapz(csi_b/w,M_1_d_b(:,2));
    INT_1_d_c(1,1,k)=trapz(csi_c/w,M_1_d_c(:,1));
    INT_1_d_c(2,1,k)=trapz(csi_c/w,M_1_d_c(:,2));

    INT_1_q_a(1,1,k)=trapz(csi_a/w,M_1_q_a(:,1));
    INT_1_q_a(2,1,k)=trapz(csi_a/w,M_1_q_a(:,2));
    INT_1_q_b(1,1,k)=trapz(csi_b/w,M_1_q_b(:,1));
    INT_1_q_b(2,1,k)=trapz(csi_b/w,M_1_q_b(:,2));
    INT_1_q_c(1,1,k)=trapz(csi_c/w,M_1_q_c(:,1));
    INT_1_q_c(2,1,k)=trapz(csi_c/w,M_1_q_c(:,2));

    for i=1:m
        exp_PAQ_phi_a(i,i)=exp(PAQd(i,i)*((pi-sigma(k))/2)/w);
        exp_PAQ_phi_b(i,i)=exp(PAQd(i,i)*((pi-sigma(k))/2-pi/3)/w);
        exp_PAQ_phi_c(i,i)=exp(PAQd(i,i)*((pi-sigma(k))/2+pi/3)/w);
    end

exp_PAQ_phi_1_a=C*exp_PAQ_phi_a*inv(C);
exp_PAQ_phi_1_b=C*exp_PAQ_phi_b*inv(C);
exp_PAQ_phi_1_c=C*exp_PAQ_phi_c*inv(C);

y_phi_a(:,k)=exp_PAQ_phi_1_a*y_0_a(:,k)+INT_1_d_a(:,1,k);
x_phi_a(:,k)=Q*y_phi_a(:,k);
y_phi_b(:,k)=exp_PAQ_phi_1_b*y_0_b(:,k)+INT_1_d_b(:,1,k);
x_phi_b(:,k)=Q*y_phi_b(:,k);
y_phi_c(:,k)=exp_PAQ_phi_1_c*y_0_c(:,k)+INT_1_d_c(:,1,k);
x_phi_c(:,k)=Q*y_phi_c(:,k);

% calcolo dH/dphi

x_punto_phi_a(:,k)=A*x_phi_a(:,k)+B*(u*cos((pi-sigma(k))/2));
x_punto_phi_b(:,k)=A*x_phi_b(:,k)+B*(-u*cos((pi-sigma(k))/2));
x_punto_phi_c(:,k)=A*x_phi_c(:,k)+B*(-u*cos((pi-sigma(k))/2));
dH_dphi_a(:,:,k)=-
exp_PAQ_pi_sigma_mezzi_1*P*exp_A_sigma_1*c'*c*x_punto_phi_a(:,k);
dH_dphi_b(:,:,k)=-
exp_PAQ_pi_sigma_mezzi_pi_3_1*P*exp_A_sigma_1*c'*c*x_punto_phi_b(:,k);
```

```matlab
dH_dphi_c(:,:,k)=-
exp_PAQ_pi_sigma_mezzi__pi_3_1*P*exp_A_sigma_1*c'*c*x_punto_phi_c(:,k);

%-------------------------------------------------------------------------
% calcolo del secondo integrale

csi_a=linspace((pi-sigma(k))/2,((pi+sigma(k))/2),1e4);
csi_b=linspace((pi-sigma(k))/2-pi/3,pi/6+sigma(k)/2,1e4);
csi_c=linspace((pi-sigma(k))/2+pi/3,5*pi/6+sigma(k)/2,1e4);

for kk=1:1e4
    Wa_a=[cos(csi_a(kk)) -sin(csi_a(kk))];
    Wa_b=[cos(csi_b(kk)-2*pi/3) -sin(csi_b(kk)-2*pi/3)];
    Wa_c=[cos(csi_c(kk)+2*pi/3) -sin(csi_c(kk)+2*pi/3)];
        for i=1:n
            exp_A_tau_csi_a(i,i)=exp(Ad(i,i)*((pi+sigma(k))/2-csi_a(kk))/w);
            exp_A_tau_csi_b(i,i)=exp(Ad(i,i)*(pi/6+sigma(k)/2-csi_b(kk))/w);
            exp_A_tau_csi_c(i,i)=exp(Ad(i,i)*(5*pi/6+sigma(k)/2-csi_c(kk))/w);
        end
    exp_A_tau_csi_1_a=V*exp_A_tau_csi_a*inv(V);
    exp_A_tau_csi_1_b=V*exp_A_tau_csi_b*inv(V);
    exp_A_tau_csi_1_c=V*exp_A_tau_csi_c*inv(V);

    int_2_d_a(:,:,kk)=exp_A_tau_csi_1_a*B*u*Wa_a*u_d;
    int_2_d_b(:,:,kk)=exp_A_tau_csi_1_b*B*u*Wa_b*u_d;
    int_2_d_c(:,:,kk)=exp_A_tau_csi_1_c*B*u*Wa_c*u_d;

    int_2_q_a(:,:,kk)=exp_A_tau_csi_1_a*B*u*Wa_a*u_q;
    int_2_q_b(:,:,kk)=exp_A_tau_csi_1_b*B*u*Wa_b*u_q;
    int_2_q_c(:,:,kk)=exp_A_tau_csi_1_c*B*u*Wa_c*u_q;

    M_2_d_a(kk,1)= int_2_d_a(1,1,kk);
    M_2_d_a(kk,2)= int_2_d_a(2,1,kk);
    M_2_d_a(kk,3)= int_2_d_a(3,1,kk);

    M_2_d_b(kk,1)= int_2_d_b(1,1,kk);
    M_2_d_b(kk,2)= int_2_d_b(2,1,kk);
    M_2_d_b(kk,3)= int_2_d_b(3,1,kk);

    M_2_d_c(kk,1)= int_2_d_c(1,1,kk);
    M_2_d_c(kk,2)= int_2_d_c(2,1,kk);
    M_2_d_c(kk,3)= int_2_d_c(3,1,kk);

    M_2_q_a(kk,1)= int_2_q_a(1,1,kk);
    M_2_q_a(kk,2)= int_2_q_a(2,1,kk);
    M_2_q_a(kk,3)= int_2_q_a(3,1,kk);

    M_2_q_b(kk,1)= int_2_q_b(1,1,kk);
    M_2_q_b(kk,2)= int_2_q_b(2,1,kk);
    M_2_q_b(kk,3)= int_2_q_b(3,1,kk);

    M_2_q_c(kk,1)= int_2_q_c(1,1,kk);
    M_2_q_c(kk,2)= int_2_q_c(2,1,kk);
    M_2_q_c(kk,3)= int_2_q_c(3,1,kk);
end

INT_2_d_a(1,1,k)=trapz(csi_a/w,M_2_d_a(:,1));
INT_2_d_b(1,1,k)=trapz(csi_b/w,M_2_d_b(:,1));
INT_2_d_c(1,1,k)=trapz(csi_c/w,M_2_d_c(:,1));
```

```matlab
INT_2_d_a(2,1,k)=trapz(csi_a/w,M_2_d_a(:,2));
INT_2_d_b(2,1,k)=trapz(csi_b/w,M_2_d_b(:,2));
INT_2_d_c(2,1,k)=trapz(csi_c/w,M_2_d_c(:,2));
INT_2_d_a(3,1,k)=trapz(csi_a/w,M_2_d_a(:,3));
INT_2_d_b(3,1,k)=trapz(csi_b/w,M_2_d_b(:,3));
INT_2_d_c(3,1,k)=trapz(csi_c/w,M_2_d_c(:,3));


INT_2_q_a(1,1,k)=trapz(csi_a/w,M_2_q_a(:,1));
INT_2_q_b(1,1,k)=trapz(csi_b/w,M_2_q_b(:,1));
INT_2_q_c(1,1,k)=trapz(csi_c/w,M_2_q_c(:,1));
INT_2_q_a(2,1,k)=trapz(csi_a/w,M_2_q_a(:,2));
INT_2_q_b(2,1,k)=trapz(csi_b/w,M_2_q_b(:,2));
INT_2_q_c(2,1,k)=trapz(csi_c/w,M_2_q_c(:,2));
INT_2_q_a(3,1,k)=trapz(csi_a/w,M_2_q_a(:,3));
INT_2_q_b(3,1,k)=trapz(csi_b/w,M_2_q_b(:,3));
INT_2_q_c(3,1,k)=trapz(csi_c/w,M_2_q_c(:,3));


    for i=1:n
        exp_A_tau_phi(i,i)=exp(Ad(i,i)*(sigma(k)/w));
    end

exp_A_tau_phi_1=V*exp_A_tau_phi*inv(V);

x_tau_a(:,k)=exp_A_tau_phi_1*x_phi_a(:,k)+INT_2_d_a(:,1,k);
x_tau_b(:,k)=exp_A_tau_phi_1*x_phi_b(:,k)+INT_2_d_b(:,1,k);
x_tau_c(:,k)=exp_A_tau_phi_1*x_phi_c(:,k)+INT_2_d_c(:,1,k);
y_tau_a(:,k)=P*x_tau_a(:,k);
y_tau_b(:,k)=P*x_tau_b(:,k);
y_tau_c(:,k)=P*x_tau_c(:,k);


%-------------------------------------------------------------------------
% calcolo del terzo integrale nell'intervallo [tau, pi]

csi_a=linspace(((pi+sigma(k))/2),pi,1e4);
csi_b=linspace(pi/6+sigma(k)/2,pi,1e4);
csi_c=linspace(5*pi/6+sigma(k)/2,pi,1e4);

for kk=1:1e4
    Wa_a=[cos(csi_a(kk)) -sin(csi_a(kk))];
    Wa_b=[cos(csi_b(kk)-2*pi/3) -sin(csi_b(kk)-2*pi/3)];
    Wa_c=[cos(csi_c(kk)+2*pi/3) -sin(csi_c(kk)+2*pi/3)];
        for i=1:m
            exp_PAQ_pi_csi_a(i,i)=exp(PAQd(i,i)*(pi-csi_a(kk))/w);
            exp_PAQ_pi_csi_b(i,i)=exp(PAQd(i,i)*(pi-csi_b(kk))/w);
            exp_PAQ_pi_csi_c(i,i)=exp(PAQd(i,i)*(pi-csi_c(kk))/w);
        end
    exp_PAQ_pi_csi_1_a=C*exp_PAQ_pi_csi_a*inv(C);
    exp_PAQ_pi_csi_1_b=C*exp_PAQ_pi_csi_b*inv(C);
    exp_PAQ_pi_csi_1_c=C*exp_PAQ_pi_csi_c*inv(C);
    int_3_d_a(:,:,kk)=exp_PAQ_pi_csi_1_a*P*u*B*Wa_a*u_d;
    int_3_d_b(:,:,kk)=exp_PAQ_pi_csi_1_b*P*u*B*Wa_b*u_d;
    int_3_d_c(:,:,kk)=exp_PAQ_pi_csi_1_c*P*u*B*Wa_c*u_d;

    int_3_q_a(:,:,kk)=exp_PAQ_pi_csi_1_a*P*u*B*Wa_a*u_q;
    int_3_q_b(:,:,kk)=exp_PAQ_pi_csi_1_b*P*u*B*Wa_b*u_q;
    int_3_q_c(:,:,kk)=exp_PAQ_pi_csi_1_c*P*u*B*Wa_c*u_q;

    M_3_d_a(kk,1)= int_3_d_a(1,1,kk);
    M_3_d_a(kk,2)= int_3_d_a(2,1,kk);
    M_3_d_b(kk,1)= int_3_d_b(1,1,kk);
```

```
        M_3_d_b(kk,2)= int_3_d_b(2,1,kk);
        M_3_d_c(kk,1)= int_3_d_c(1,1,kk);
        M_3_d_c(kk,2)= int_3_d_c(2,1,kk);

        M_3_q_a(kk,1)= int_3_q_a(1,1,kk);
        M_3_q_a(kk,2)= int_3_q_a(2,1,kk);
        M_3_q_b(kk,1)= int_3_q_b(1,1,kk);
        M_3_q_b(kk,2)= int_3_q_b(2,1,kk);
        M_3_q_c(kk,1)= int_3_q_c(1,1,kk);
        M_3_q_c(kk,2)= int_3_q_c(2,1,kk);
    end

    INT_3_d_a(1,1,k)=trapz(csi_a/w,M_3_d_a(:,1));
    INT_3_d_b(1,1,k)=trapz(csi_b/w,M_3_d_b(:,1));
    INT_3_d_c(1,1,k)=trapz(csi_c/w,M_3_d_c(:,1));
    INT_3_d_a(2,1,k)=trapz(csi_a/w,M_3_d_a(:,2));
    INT_3_d_b(2,1,k)=trapz(csi_b/w,M_3_d_b(:,2));
    INT_3_d_c(2,1,k)=trapz(csi_c/w,M_3_d_c(:,2));

    INT_3_q_a(1,1,k)=trapz(csi_a/w,M_3_q_a(:,1));
    INT_3_q_b(1,1,k)=trapz(csi_b/w,M_3_q_b(:,1));
    INT_3_q_c(1,1,k)=trapz(csi_c/w,M_3_q_c(:,1));
    INT_3_q_a(2,1,k)=trapz(csi_a/w,M_3_q_a(:,2));
    INT_3_q_b(2,1,k)=trapz(csi_b/w,M_3_q_b(:,2));
    INT_3_q_c(2,1,k)=trapz(csi_c/w,M_3_q_c(:,2));

        for i=1:m
            exp_PAQ_pi_tau_a(i,i)=exp(PAQd(i,i)*((pi-sigma(k))/2)/w);
            exp_PAQ_pi_tau_b(i,i)=exp(PAQd(i,i)*((5*pi/6-sigma(k)/2)/w));
            exp_PAQ_pi_tau_c(i,i)=exp(PAQd(i,i)*((pi/6-sigma(k)/2)/w));
        end

    exp_PAQ_pi_tau_1_a=C*exp_PAQ_pi_tau_a*inv(C);
    exp_PAQ_pi_tau_1_b=C*exp_PAQ_pi_tau_b*inv(C);
    exp_PAQ_pi_tau_1_c=C*exp_PAQ_pi_tau_c*inv(C);

    y_pi_a(:,k)=exp_PAQ_pi_tau_1_a*y_tau_a(:,k)+INT_3_d_a(:,1,k);
    y_pi_b(:,k)=exp_PAQ_pi_tau_1_b*y_tau_a(:,k)+INT_3_d_b(:,1,k);
    y_pi_c(:,k)=exp_PAQ_pi_tau_1_c*y_tau_a(:,k)+INT_3_d_c(:,1,k);

    h_phi_ud_a(:,:,k)=exp_PAQ_pi_tau_1_a*P*(exp_A_tau_phi_1*Q*INT_1_d_a(:,1,k)/u+INT
    _2_d_a(:,1,k)/u)+INT_3_d_a(:,1,k)/u;
    h_phi_ud_b(:,:,k)=exp_PAQ_pi_tau_1_b*P*(exp_A_tau_phi_1*Q*INT_1_d_b(:,1,k)/u+INT
    _2_d_b(:,1,k)/u)+INT_3_d_b(:,1,k)/u;
    h_phi_ud_c(:,:,k)=exp_PAQ_pi_tau_1_c*P*(exp_A_tau_phi_1*Q*INT_1_d_c(:,1,k)/u+INT
    _2_d_c(:,1,k)/u)+INT_3_d_c(:,1,k)/u;

    h_phi_uq_a(:,:,k)=exp_PAQ_pi_tau_1_a*P*(exp_A_tau_phi_1*Q*INT_1_q_a(:,1,k)/u+INT
    _2_q_a(:,1,k)/u)+INT_3_q_a(:,1,k)/u;
    h_phi_uq_b(:,:,k)=exp_PAQ_pi_tau_1_b*P*(exp_A_tau_phi_1*Q*INT_1_q_b(:,1,k)/u+INT
    _2_q_b(:,1,k)/u)+INT_3_q_b(:,1,k)/u;
    h_phi_uq_c(:,:,k)=exp_PAQ_pi_tau_1_c*P*(exp_A_tau_phi_1*Q*INT_1_q_c(:,1,k)/u+INT
    _2_q_c(:,1,k)/u)+INT_3_q_c(:,1,k)/u;

    h_phi_u_a(:,:,k)=[h_phi_ud_a(:,:,k) h_phi_uq_a(:,:,k)];
    h_phi_u_b(:,:,k)=[h_phi_ud_b(:,:,k) h_phi_uq_b(:,:,k)];
    h_phi_u_c(:,:,k)=[h_phi_ud_c(:,:,k) h_phi_uq_c(:,:,k)];

    DELTA_phi_signed(:,:,k)=S*real([dH_dphi_a(:,:,k); dH_dphi_b(:,:,k);
    dH_dphi_c(:,:,k)]);
```

```matlab
DELTA_U_signed(:,:,k)=S*real([h_phi_u_a(:,:,k); h_phi_u_b(:,:,k);
h_phi_u_c(:,:,k)]);


DELTA_phi(:,:,k)=NI_180*DELTA_phi_signed(:,:,k);
DELTA_U(:,:,k)=NI_180*DELTA_U_signed(:,:,k);
PHI(:,:,k)=NI_180*PHI_signed(:,:,k)*DOUBLE_NI_0;
PHI(:,3,k)=-PHI(:,3,k);
PHI(:,6,k)=-PHI(:,6,k);

Y_0=[0 0 0 0              % Is_d
     0 0 0 0              % Is_q
     0 0 0 0              % Vr_d
     0 0 0 0
     0 0 0 0
     0 0 0 0];           % Vr_q
for i=0:(n_cycles-2)
    Y(:,:,k)=PHI(:,:,k)*Y_0(:,k)+DELTA_U(:,:,k)*u_d*5/100*u;
    Is_tilde_d(i+1,k)=Y(1,k);
    Is_tilde_q(i+1,k)=Y(2,k);
    Vc_tilde_d(i+1,k)=Y(3,k);
    Vc_tilde_q(i+1,k)=Y(4,k);
    Y_0(:,k)=Y(:,:,k)
end
end


A_3f_dq=[0 w -1/Ls 0;-w 0 0 -1/Ls;1/Cr 0 0 w; 0 1/Cr -w 0];

B_3f_dq=[1/Ls  0
         0     1/Ls
         0     0
         0     0];

[A_3f_dq_v,A_3f_dq_diag] = eig(A_3f_dq);


PHI_45=PHI(:,:,4);
DELTA_U_45=DELTA_U(:,1,4);
DELTA_phi_45=DELTA_phi(:,1,4);
% [S_45,PHId_45] = eig(PHI_45);

% %Vr
figure(1)
plot (e_d.time, e_d.signals.values)
title('Vr_d');
xlabel('time (s)');
ylabel('(V)');
figure(2)
plot (e_q.time, e_q.signals.values)
title('Vr_q');
xlabel('time (s)');
ylabel('(V)');
figure(3)
plot (e_0.time, e_0.signals.values)
title('Vr_0');
xlabel('time (s)');
ylabel('(V)');

%Is
figure(4)
```

30

```
plot (i_d.time, i_d.signals.values)
title('i_d');
xlabel('time (s)');
ylabel('(A)');
figure(5)
plot (i_q.time, i_q.signals.values)
title('i_q');
xlabel('time (s)');
ylabel('(A)');
figure(6)
plot (i_0.time, i_0.signals.values)
title('i_0');
xlabel('time (s)');
ylabel('(A)');
```
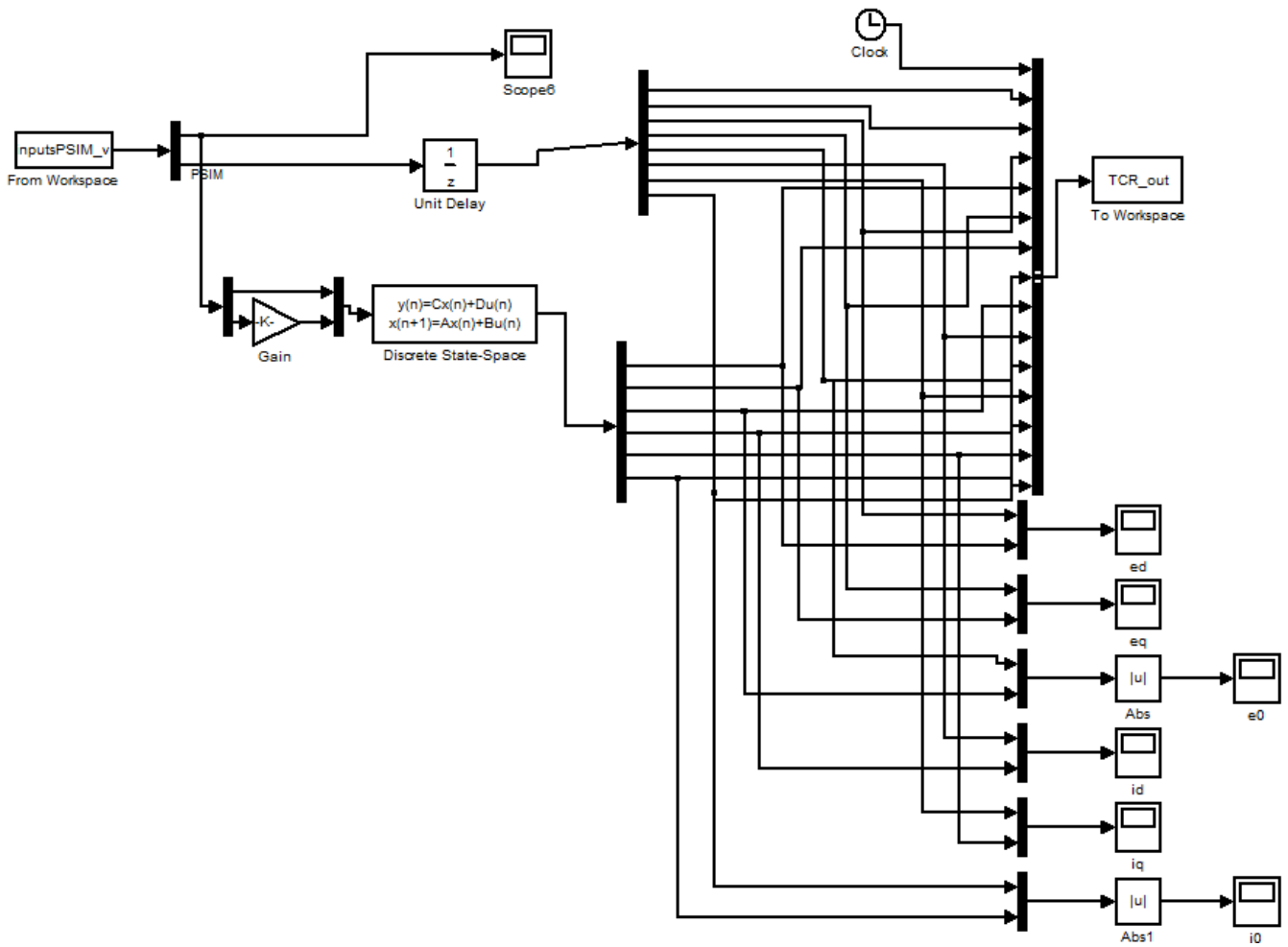

Figure III-3 Simulink scheme to compare PSIM response and LTI discrete-time model.
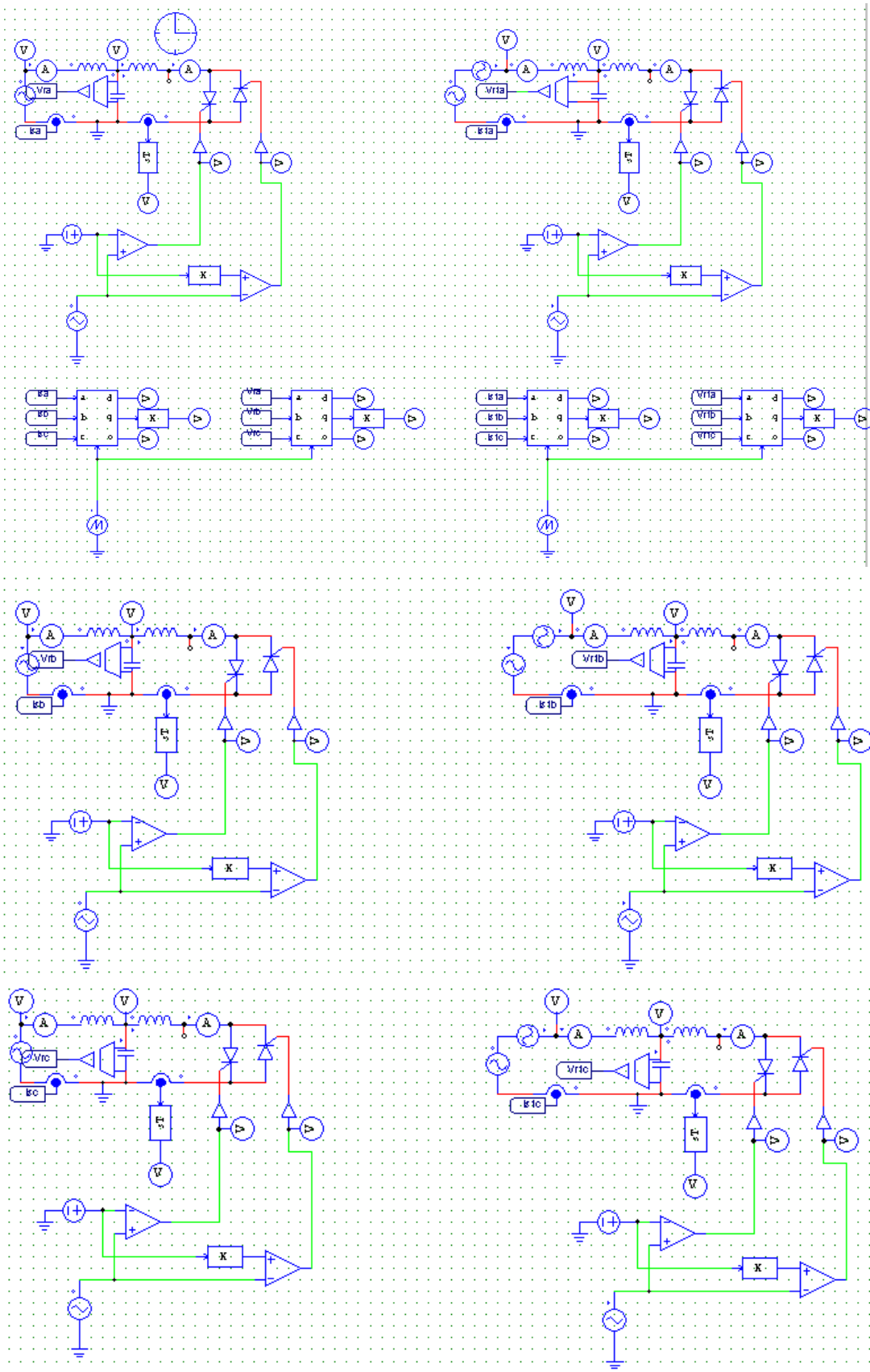
Figure III-4 PSIM circuits to simulate steady state and perturbed mode of operation

III.3.   *Three-phase delta-connected TCR with $\sigma \epsilon$ $(0, 60°)$*

The list below refers to simulations presented in Section 4.1.2 and 4.3 when EDM is derived. PSIM scheme used is presented in [2], so here is omitted.

```
%------------------------- dati input------------------------------------
-
w=2*pi*50; %[Hz]
T=2*pi/w;
t=linspace(0,1,1e06);
sigma=[0.0001 15 45]*pi/180;
n_el=size(sigma,2);
Lr=112.174e-3; %[H]
Cr=183e-06; %[F]
Ls=8.278e-3; %[H]
u=53889
%--------------------------matrici--------------------------------
% conduzione AB
A_AB=[0          0      -2/(3*Ls) +1/(3*Ls) +1/(3*Ls) 0;
      0          0      +1/(3*Ls) -2/(3*Ls) +1/(3*Ls) 0;
      1/Cr       0       0         0         0         -1/Cr;
      0          1/Cr    0         0         0         1/Cr;
      -1/Cr     -1/Cr    0         0         0         0;
      0          0       1/Lr     -1/Lr      0         0];
B_AB=[+2/(3*Ls)    -1/(3*Ls)    -1/(3*Ls);
      -1/(3*Ls)    +2/(3*Ls)    -1/(3*Ls);
      0             0            0;
      0             0            0;
      0             0            0;
      0             0            0];
Q=[1 0 0 0 0;
   0 1 0 0 0;
   0 0 1 0 0;
   0 0 0 1 0;
   0 0 0 0 1;
   0 0 0 0 0];
P=Q';
c=[0 0 0 0 0 1];
% da PSIM
%y_0=[ia(15)   ia(30)   ia(45)
%     ib(15)   ib(30)   ib(45)
%     Var(15)  Var(30)  Var(45)
%     Vbr(15)  Vbr(30)  Vbr(45)
%     Vcr(15)  Vcr(30)  Vcr(45)];
y_0_AB=[-3.4266541e+002   -3.2149151e+002   -1.7191101e+003
         6.6739957e+002    6.4335587e+002    3.4387329e+003
         3.0430644e+005    3.0159814e+005    5.4722809e+004
        -2.2791423e+003    6.3412382e+001   -2.0224236e+000
        -3.0202732e+005   -3.0166155e+005   -5.4720786e+004];
e_AB= [2.5975105e+005    2.5975105e+005    4.6666420e+004
       1.1311334e+002    1.1311334e+002    5.6447680e+000
      -2.5986416e+005   -2.5986416e+005   -4.6672065e+004];
n_cycles=10;
Cab_abc_AB=[1 0; 0 1;-1 -1];
Cabc_ab_AB=[0 -1 -1; -1 0 -1];
V_0_AB=2/3*[cos(0+pi/6) cos(0-pi/2) cos(0-7*pi/6)
           -sin(0+pi/6) -sin(0-pi/2) -sin(0-7*pi/6)];
W_0_AB=3/2*V_0_AB';   % ho messo V_0_AB' x nascondere l'errore
```

```
NI_0_AB=[V_0_AB zeros(2,3); zeros(2,3) V_0_AB];
DOUBLE_NI_0_AB=[W_0_AB zeros(3,2); zeros(3,2) W_0_AB];
V_60_AB=2/3*[cos(pi/3+pi/6) cos(pi/3-pi/2) cos(pi/3-7*pi/6)
        -sin(pi/3+pi/6) -sin(pi/3-pi/2) -sin(pi/3-7*pi/6)];
W_60_AB=3/2*V_60_AB';
NI_60_AB=[V_60_AB zeros(2,3); zeros(2,3) V_60_AB];
%----------------------------Program-----------------------------------
close all
clc
SVC_dati_input_triangle_prova_XXX
A=A_AB;
B=B_AB;
[V,Ad] = eig(A);
PAQ=P*A*Q;
[C,PAQd] = eig(PAQ);
n=size(A);
m=size(PAQ);
u_d=[1 0]';
u_q=[0 1]';
for k=1:n_el
        for i=1:n
            exp_A_sigma(i,i)=exp(Ad(i,i)*(sigma(k)/w));
        end
        exp_A_sigma_1=V*exp_A_sigma*inv(V);
        for i=1:m
            exp_PAQ_pi_sigma(i,i)=exp(PAQd(i,i)*(pi/3-sigma(k))/(2*w));
        end
        exp_PAQ_pi_sigma_1=C*exp_PAQ_pi_sigma*inv(C);
        DH(:,:,k)=exp_PAQ_pi_sigma_1*P*exp_A_sigma_1*Q*exp_PAQ_pi_sigma_1;
        %DH(1:2,1:2,k)=DH(:,:,k);
        E(:,k)=eig(DH(:,:,k));
        %figure (1)
        %title ('Posizione degli autovalori di DH nel piano complesso al variare
di sigma');
        %plot (real(E(:,k)),imag(E(:,k)),'*');
        %hold on
  calcolo del primo integrale nell'intervallo [0, phi] con passo
% d'integrazione relativo di 1/10000 (cioè prendendo 10000 campioni)
    csi=linspace(0,(pi/3-sigma(k))/2,1e4);

    for kk=1:1e4
    Wa=[cos(csi(kk)+pi/6) -sin(csi(kk)+pi/6)
        cos(csi(kk)-pi/2) -sin(csi(kk)-pi/2)
        cos(csi(kk)-7*pi/6) -sin(csi(kk)-7*pi/6)];
        for i=1:m
            exp_PAQ_phi_csi(i,i)=exp(PAQd(i,i)*((pi/3-sigma(k))/2-csi(kk))/w);
        end
    exp_PAQ_phi_csi_1=C*exp_PAQ_phi_csi*inv(C);
    int_1_d(:,:,kk)=exp_PAQ_phi_csi_1*P*B*u*Wa*u_d;
    M_1_d(kk,1)= int_1_d(1,1,kk);
    M_1_d(kk,2)= int_1_d(2,1,kk);
    M_1_d(kk,3)= int_1_d(3,1,kk);
    M_1_d(kk,4)= int_1_d(4,1,kk);
    M_1_d(kk,5)= int_1_d(5,1,kk);
    int_1_q(:,:,kk)=exp_PAQ_phi_csi_1*P*B*u*Wa*u_q;
    M_1_q(kk,1)= int_1_q(1,1,kk);
    M_1_q(kk,2)= int_1_q(2,1,kk);
    M_1_q(kk,3)= int_1_q(3,1,kk);
    M_1_q(kk,4)= int_1_q(4,1,kk);
    M_1_q(kk,5)= int_1_q(5,1,kk);
    end
INT_1_d(1,1,k)=trapz(csi/w,M_1_d(:,1));
```

```matlab
INT_1_d(2,1,k)=trapz(csi/w,M_1_d(:,2));
INT_1_d(3,1,k)=trapz(csi/w,M_1_d(:,3));
INT_1_d(4,1,k)=trapz(csi/w,M_1_d(:,4));
INT_1_d(5,1,k)=trapz(csi/w,M_1_d(:,5));
INT_1_q(1,1,k)=trapz(csi/w,M_1_q(:,1));
INT_1_q(2,1,k)=trapz(csi/w,M_1_q(:,2));
INT_1_q(3,1,k)=trapz(csi/w,M_1_q(:,3));
INT_1_q(4,1,k)=trapz(csi/w,M_1_q(:,4));
INT_1_q(5,1,k)=trapz(csi/w,M_1_q(:,5));
    for i=1:m
        exp_PAQ_phi(i,i)=exp(PAQd(i,i)*((pi/3-sigma(k))/2)/w);
    end
exp_PAQ_phi_1=C*exp_PAQ_phi*inv(C);
y_phi(:,k)=exp_PAQ_phi_1*y_0_AB(:,k)+INT_1_d(:,1,k);
x_phi(:,k)=Q*y_phi(:,k);
x_phi_AB(:,k)=x_phi(:,k);
% calcolo dH/dphi
x_punto_phi(:,k)=A*x_phi(:,k)+B*e_AB(:,k);
x_punto_phi_AB(:,k)=x_punto_phi(:,k);
dH_dphi(:,k)=-exp_PAQ_pi_sigma_1*P*exp_A_sigma_1*c'*c*x_punto_phi(:,k);
%-------------------------------------------------------------------------
% calcolo del secondo integrale nell'intervallo [phi, tau]
csi=linspace((pi/3-sigma(k))/2,((pi/3+sigma(k))/2),1e4);
for kk=1:1e4
     Wa=[cos(csi(kk)+pi/6) -sin(csi(kk)+pi/6)
        cos(csi(kk)-pi/2) -sin(csi(kk)-pi/2)
        cos(csi(kk)-7*pi/6) -sin(csi(kk)-7*pi/6)];
        for i=1:n
            exp_A_tau_csi(i,i)=exp(Ad(i,i)*((pi/3+sigma(k))/2-csi(kk))/w);
        end
    exp_A_tau_csi_1=V*exp_A_tau_csi*inv(V);
    int_2_d(:,:,kk)=exp_A_tau_csi_1*B*u*Wa*u_d;
    int_2_q(:,:,kk)=exp_A_tau_csi_1*B*u*Wa*u_q;
    M_2_d(kk,1)= int_2_d(1,1,kk);
    M_2_d(kk,2)= int_2_d(2,1,kk);
    M_2_d(kk,3)= int_2_d(3,1,kk);
    M_2_d(kk,4)= int_2_d(4,1,kk);
    M_2_d(kk,5)= int_2_d(5,1,kk);
    M_2_d(kk,6)= int_2_d(6,1,kk);
   M_2_q(kk,1)= int_2_q(1,1,kk);
    M_2_q(kk,2)= int_2_q(2,1,kk);
    M_2_q(kk,3)= int_2_q(3,1,kk);
    M_2_q(kk,4)= int_2_q(4,1,kk);
    M_2_q(kk,5)= int_2_q(5,1,kk);
    M_2_q(kk,6)= int_2_q(6,1,kk);
end
INT_2_d(1,1,k)=trapz(csi/w,M_2_d(:,1));
INT_2_d(2,1,k)=trapz(csi/w,M_2_d(:,2));
INT_2_d(3,1,k)=trapz(csi/w,M_2_d(:,3));
INT_2_d(4,1,k)=trapz(csi/w,M_2_d(:,4));
INT_2_d(5,1,k)=trapz(csi/w,M_2_d(:,5));
INT_2_d(6,1,k)=trapz(csi/w,M_2_d(:,6));
INT_2_q(1,1,k)=trapz(csi/w,M_2_q(:,1));
INT_2_q(2,1,k)=trapz(csi/w,M_2_q(:,2));
INT_2_q(3,1,k)=trapz(csi/w,M_2_q(:,3));
INT_2_q(4,1,k)=trapz(csi/w,M_2_q(:,4));
INT_2_q(5,1,k)=trapz(csi/w,M_2_q(:,5));
INT_2_q(6,1,k)=trapz(csi/w,M_2_q(:,6));
    for i=1:n
        exp_A_tau_phi(i,i)=exp(Ad(i,i)*(sigma(k)/w));
    end
exp_A_tau_phi_1=V*exp_A_tau_phi*inv(V);
```

```matlab
x_tau(:,k)=exp_A_tau_phi_1*x_phi(:,k)+INT_2_d(:,1,k);
y_tau(:,k)=P*x_tau(:,k);
%-------------------------------------------------------------------------
% calcolo del terzo integrale nell'intervallo [tau, pi]
csi=linspace(((pi/3+sigma(k))/2),pi/3,1e4);
for kk=1:1e4
    Wa=[cos(csi(kk)+pi/6) -sin(csi(kk)+pi/6)
        cos(csi(kk)-pi/2) -sin(csi(kk)-pi/2)
        cos(csi(kk)-7*pi/6) -sin(csi(kk)-7*pi/6)];
        for i=1:m
            exp_PAQ_pi_csi(i,i)=exp(PAQd(i,i)*(pi/3-csi(kk))/w);
        end
    exp_PAQ_pi_csi_1=C*exp_PAQ_pi_csi*inv(C);
    int_3_d(:,:,kk)=exp_PAQ_pi_csi_1*P*B*u*Wa*u_d;
    int_3_q(:,:,kk)=exp_PAQ_pi_csi_1*P*B*u*Wa*u_q;
    M_3_d(kk,1)= int_3_d(1,1,kk);
    M_3_d(kk,2)= int_3_d(2,1,kk);
    M_3_d(kk,3)= int_3_d(3,1,kk);
    M_3_d(kk,4)= int_3_d(4,1,kk);
    M_3_d(kk,5)= int_3_d(5,1,kk);
    M_3_q(kk,1)= int_3_q(1,1,kk);
    M_3_q(kk,2)= int_3_q(2,1,kk);
    M_3_q(kk,3)= int_3_q(3,1,kk);
    M_3_q(kk,4)= int_3_q(4,1,kk);
    M_3_q(kk,5)= int_3_q(5,1,kk);
end
INT_3_d(1,1,k)=trapz(csi/w,M_3_d(:,1));
INT_3_d(2,1,k)=trapz(csi/w,M_3_d(:,2));
INT_3_d(3,1,k)=trapz(csi/w,M_3_d(:,3));
INT_3_d(4,1,k)=trapz(csi/w,M_3_d(:,4));
INT_3_d(5,1,k)=trapz(csi/w,M_3_d(:,5));
INT_3_q(1,1,k)=trapz(csi/w,M_3_q(:,1));
INT_3_q(2,1,k)=trapz(csi/w,M_3_q(:,2));
INT_3_q(3,1,k)=trapz(csi/w,M_3_q(:,3));
INT_3_q(4,1,k)=trapz(csi/w,M_3_q(:,4));
INT_3_q(5,1,k)=trapz(csi/w,M_3_q(:,5));
    for i=1:m
        exp_PAQ_pi_tau(i,i)=exp(PAQd(i,i)*((pi/3-sigma(k))/2)/w);
    end
exp_PAQ_pi_tau_1=C*exp_PAQ_pi_tau*inv(C);
y_pi(:,k)=exp_PAQ_pi_tau_1*y_tau(:,k)+INT_3_d(:,1,k);
h_phi_ud(:,k)=exp_PAQ_pi_tau_1*P*(exp_A_tau_phi_1*Q*INT_1_d(:,1,k)/u+INT_2_d(:,1
,k)/u)+INT_3_d(:,1,k)/u;
h_phi_uq(:,k)=exp_PAQ_pi_tau_1*P*(exp_A_tau_phi_1*Q*INT_1_q(:,1,k)/u+INT_2_q(:,1
,k)/u)+INT_3_q(:,1,k)/u;
% trasformo il sistema in 5 varibili di stato a 6 variabili di stato in
% modo da poter fare poi la trasformazione dq
DH_1_1(:,:,k)=DH(1:2,1:2,k);
DH_1_2(:,:,k)=DH(1:2,3:5,k);
DH_2_1(:,:,k)=DH(3:5,1:2,k);
DH_2_2(:,:,k)=DH(3:5,3:5,k);
DH_1_1_abc(:,:,k)=Cab_abc_AB*DH_1_1(:,:,k)*Cabc_ab_AB;
DH_1_2_abc(:,:,k)=Cab_abc_AB*DH_1_2(:,:,k);
DH_2_1_abc(:,:,k)=DH_2_1(:,:,k)*Cabc_ab_AB;
DH_2_2_abc(:,:,k)=DH_2_2(:,:,k);
dH_dphi_1_abc(:,k)=Cab_abc_AB*dH_dphi(1:2,k);
h_phi_d_1_abc(:,k)=Cab_abc_AB*h_phi_ud(1:2,k);
h_phi_q_1_abc(:,k)=Cab_abc_AB*h_phi_uq(1:2,k);
DH_abc(1:3,1:3,k)=DH_1_1_abc(:,:,k);
DH_abc(1:3,4:6,k)=DH_1_2_abc(:,:,k);
DH_abc(4:6,1:3,k)=DH_2_1_abc(:,:,k);
DH_abc(4:6,4:6,k)=DH_2_2_abc(:,:,k);
```

```matlab
dH_dphi_abc(1:3,k)=dH_dphi_1_abc(:,k);
dH_dphi_abc(4:6,k)=dH_dphi(3:5,k);
h_phi_d_abc(1:3,k)=h_phi_d_1_abc(:,k);
h_phi_d_abc(4:6,k)=h_phi_ud(3:5,k);
h_phi_q_abc(1:3,k)=h_phi_q_1_abc(:,k);
h_phi_q_abc(4:6,k)=h_phi_uq(3:5,k);
DELTA_phi_AB(:,k)=NI_60_AB*dH_dphi_abc(:,k);
dH_dphi_abc_AB(:,k)=dH_dphi_abc(:,k);
DELTA_U(:,:,k)=[h_phi_d_abc(:,k) h_phi_q_abc(:,k)];
DELTA_U_AB_ing_dq(:,:,k)=DELTA_U(:,:,k);
DELTA_U_AB(:,:,k)=DELTA_U(:,:,k)*V_60_AB;
DELTA_U_dq_AB(:,:,k)=NI_60_AB*DELTA_U_AB(:,:,k)*W_60_AB;
PHI_AB(:,:,k)=NI_60_AB*DH_abc(:,:,k)*DOUBLE_NI_0_AB;
Y_0=[0 0 0             % Is_d
     0 0 0             % Is_q
     0 0 0             % Vr_d
     0 0 0];           % Vr_q
for i=0:(n_cycles-2)
Y(:,:,k)=PHI_AB(:,:,k)*Y_0(:,k)+DELTA_phi_AB(:,k)*0/180/120+DELTA_U_dq_AB(:,1,k)
*5/100*53889;   % a seconda dell'asse in
% cui è data la perturbazione in ampiezza bisogna scegliere h_phi_ud o h_phi_uq.
    Is_tilde_d(i+1,k)=Y(1,k);
    Is_tilde_q(i+1,k)=Y(2,k);
    Vc_tilde_d(i+1,k)=Y(3,k);
    Vc_tilde_q(i+1,k)=Y(4,k);
    Y_0(:,k)=Y(:,:,k)
end
end
% PHI_45=real(PHI_AB(:,:,3));
% DELTA_U_45(:,:)=real(DELTA_U_dq_AB(:,:,3));
% DELTA_phi_45=real(DELTA_phi_AB(:,3));
figure (1)
plot (i_d_angle.time(1:70000), i_d_angle.signals.values(1:70000,:), '- ' );
title ('Perturbed Id ');
xlabel('time (s)');
ylabel('(A)');
figure (2)
plot (i_q_angle.time(1:70000), i_q_angle.signals.values(1:70000,:), '- ' );
title ('Perturbed Iq ');
xlabel('time (s)');
ylabel('(A)');
figure (3)
plot (e_d_angle.time(1:10000), e_d_angle.signals.values(1:10000,:), '- ' );
title ('Perturbed e_d ');
xlabel('time (s)');
ylabel('(V)');
figure (4)
plot (e_q_angle.time(1:70000), e_q_angle.signals.values(1:70000,:), '- ' );
title ('Perturbed e_q ');
xlabel('time (s)');
ylabel('(V)');
A_3f_dq=[0 w -1/Ls 0;-w 0 0 -1/Ls;1/Cr 0 0 w; 0 1/Cr -w 0];
B_3f_dq=[1/Ls  0
         0      1/Ls
         0      0
         0      0];
[A_3f_dq_v,A_3f_dq_diag] = eig(A_3f_dq);
%for i=1:4
%           exp_A_3f(i,i)=exp(A_3f_dq_diag(i,i)/120);
%        end
%        exp_A_3f_1=A_3f_dq_v*exp_A_3f*inv(A_3f_dq_v);
%        prova=inv(A_3f_dq_v)*exp_A_3f_1*A_3f_dq_v;
```

```matlab
% [exp_A_3f_1_v,exp_A_3f_1_d] = eig(exp_A_3f_1);
PHI_0=PHI_AB(:,:,1);
DELTA_U_0=DELTA_U_dq_AB(:,1,1);
PHId_0=inv(A_3f_dq_v)*PHI_0*A_3f_dq_v;
S_0=A_3f_dq_v;
% [S_0,PHId_0] = eig(PHI_0);
% S1=inv(S_0)
N=eye(4);
DIAG_0=eye(4);
A_3f_dq_diag = inv(S_0)*(A_3f_dq)*(S_0);
for i=1:size(PHId_0,1)
LOG_PHId_0(i,i)=log(abs(PHId_0(i,i)))+1i*angle(PHId_0(i,i));
% N(i,i)=real((A_3f_dq_diag(i,i)/300-(LOG_PHId_0(i,i)))/(1i*pi));
N(i,i)=real((A_3f_dq_diag(i,i)/300-(LOG_PHId_0(i,i)))/(1i*pi));
%N(i,i)=2*(-1)^(i+1);
%N=[2 0 0 0;0 -2 0 0; 0 0 4 0; 0 0 0 -4];
DIAG_0(i,i)=LOG_PHId_0(i,i)+1i*N(i,i)*pi;
end
A_CTM_0=300*A_3f_dq_v*(DIAG_0)*inv(A_3f_dq_v);
B_phi_CTM_0=inv(PHI_0-eye(4))*A_CTM_0*DELTA_phi_AB(:,1);
B_u_CTM_0=inv(PHI_0-eye(4))*A_CTM_0*DELTA_U_dq_AB(:,:,1);
%========================================================================
PHI_15=PHI_AB(:,:,2);
DELTA_U_15=DELTA_U_dq_AB(:,:,2);
DELTA_phi_15=DELTA_phi_AB(:,2);
[S_15,PHId_15] = eig(PHI_15);
LOG_PHId_15=eye(4);

    for i=1:size(PHId_15,1)
     LOG_PHId_15(i,i)=log(abs(PHId_15(i,i)))+1i*angle(PHId_15(i,i));
     DIAG_15(i,i)=LOG_PHId_15(i,i)+1i*pi*N(i,i);
    end
A_CTM_15=300*S_15*(DIAG_15)*inv(S_15);
B_phi_CTM_15=inv(PHI_15-eye(4))*A_CTM_15*DELTA_phi_15;
B_u_CTM_15=inv(PHI_15-eye(4))*A_CTM_15*DELTA_U_15;
%========================================================================
PHI_45=real(PHI_AB(:,:,3));
DELTA_U_45=real(DELTA_U_dq_AB(:,:,3));
DELTA_phi_45=real(DELTA_phi_AB(:,3));
[S_45,PHId_45] = eig(PHI_45);
LOG_PHId_45=eye(4);
N_45=[0 0 0 0; 0 0 0 0; 0 0 -2 0;0 0 0 +2];
    for i=1:size(PHId_45,1)
     LOG_PHId_45(i,i)=log(abs(PHId_45(i,i)))+1i*angle(PHId_45(i,i));
     DIAG_45(i,i)=LOG_PHId_45(i,i)+1i*pi*N_45(i,i);
    end
A_CTM_45=300*S_45*(DIAG_45)*inv(S_45);
B_phi_CTM_45=inv(PHI_45-eye(4))*A_CTM_45*DELTA_phi_45;
B_u_CTM_45=inv(PHI_45-eye(4))*A_CTM_45*DELTA_U_45;
B_CTM_45=[B_u_CTM_45, B_phi_CTM_45];
----------------INPUT DATI PSIM----------------------------------------
%clear all
% clc
nomefile1 = fopen( 'inputTCRMAT1_TR_d_sfasata.txt','r');
inputsPSIM = fscanf ( nomefile1 , '%g %g %g %g %g %g %g %g %g %g' , [10 inf] );
%Time    eds_pert-eds_rif    eqs_pert-eqs_rif    alphaTCR    idTCR_pert-idTCR_rif
iqTCR_pert-iqTCR_rif    ed_pert-ed_rif    eq_pert-eq_rif    id_pert-id_rif    iq_pert-
iq_rif
fclose(nomefile1);
inputsPSIM_v=inputsPSIM';
tstart1=inputsPSIM_v(1,1);
tstart=ceil(tstart1*(100*3))*1/(100*3)
```

```
inputsPSIM_v(:,1)=inputsPSIM_v(:,1)+(tstart-tstart1)-1/600;
tend=inputsPSIM_v(end,1)
```
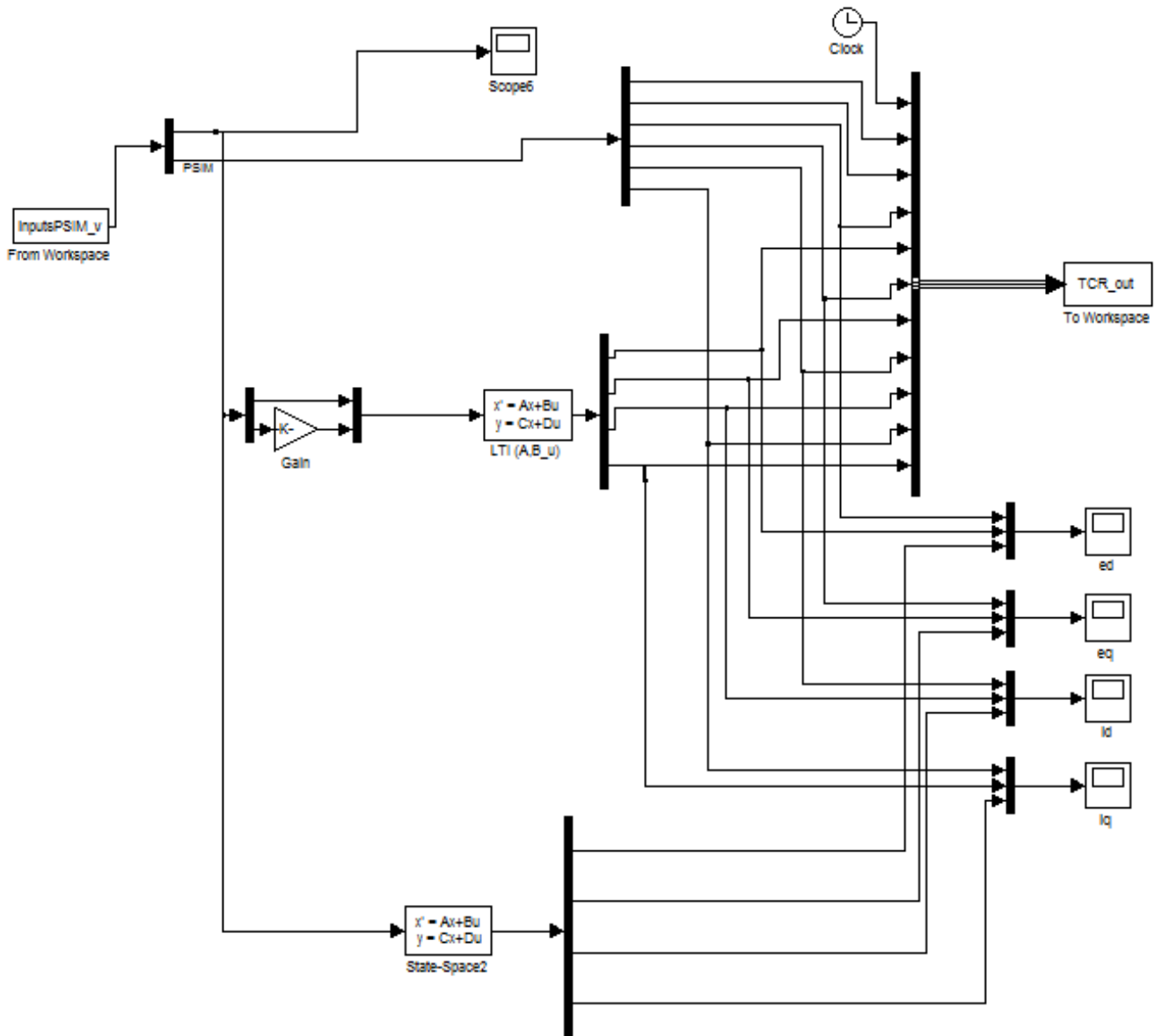

Figure III-5 Simulink scheme to compare PSIM, Continuous time model (derived from discrete-time approach) and Dynamic Model results

The list belows refers to frequency analysis (made by Fast Fourier Transform FFT) of the outputs given by Simulink (whose scheme is reported above) simulations presented in Section 4.3.1 and 4.3.2.

```
%----------------FFT-------------------------------------
%clear all
%clc
close all
fs = 1e6; % sample frequency
fref=300; %frequenza periodo
fper=10;
% Tend=0.1+1/fper;
% TCR_v(1:(Tend-0.1)*fs,:)=TCR_out((0.1*fs+1):(Tend*fs),:);
dim=length(TCR_out(:,1));
```

```matlab
time=TCR_out((dim-99999):dim,1);

m = length(time(:,1))           % Window length
%n = pow2(nextpow2(m));   % Transform length

ed_PSIM = fftshift(fft(e_d_angle.signals.values((dim-99999):dim,1),m));
% DFT
ed_CTM = fftshift(fft(e_d_angle.signals.values((dim-99999):dim,2),m));
% DFT
ed_DM = fftshift(fft(e_d_angle.signals.values((dim-99999):dim,3),m));
% DFT
ed=[ed_PSIM ed_CTM ed_DM];

eq_PSIM = fftshift(fft(e_q_angle.signals.values((dim-99999):dim,1),m));
% DFT
eq_CTM = fftshift(fft(e_q_angle.signals.values((dim-99999):dim,2),m));
% DFT
eq_DM = fftshift(fft(e_q_angle.signals.values((dim-99999):dim,3),m));
% DFT
eq=[eq_PSIM eq_CTM eq_DM];

id_PSIM = fftshift(fft(i_d_angle.signals.values((dim-99999):dim,1),m));
% DFT
id_CTM = fftshift(fft(i_d_angle.signals.values((dim-99999):dim,2),m));
% DFT
id_DM = fftshift(fft(i_d_angle.signals.values((dim-99999):dim,3),m));
% DFT
id=[id_PSIM id_CTM id_DM];

iq_PSIM = fftshift(fft(i_q_angle.signals.values((dim-99999):dim,1),m));
% DFT
iq_CTM = fftshift(fft(i_q_angle.signals.values((dim-99999):dim,2),m));
% DFT
iq_DM = fftshift(fft(i_q_angle.signals.values((dim-99999):dim,3),m));
% DFT
iq=[iq_PSIM iq_CTM iq_DM];

f0 = (-m/2:m/2-1)*(fs/m);  % 0-centered frequency range
power0_ed = abs(ed)*2/m;   % 0-centered power
power0_eq = abs(eq)*2/m;   % 0-centered power
power0_id = abs(id)*2/m;   % 0-centered power
power0_iq = abs(iq)*2/m;   % 0-centered power

figure(1)
plot(f0,power0_ed(:,1),f0,power0_ed(:,2),f0,power0_ed(:,3));
legend('ed-PSIM','ed-CTM','ed-DM')
xlabel('Frequency (Hz)')
ylabel('Power')
title('{\bf 0-Centered Periodogram}')
axis([0 300 0 inf])
grid on

figure(2)
plot(f0,power0_eq(:,1),f0,power0_eq(:,2),f0,power0_eq(:,3));
legend('eq-PSIM','eq-CTM','eq-DM')
xlabel('Frequency (Hz)')
ylabel('Power')
title('{\bf 0-Centered Periodogram}')
axis([0 300 0 inf])
grid on
```

```matlab
figure(3)
plot(f0,power0_id(:,1),f0,power0_id(:,2),f0,power0_id(:,3));
legend('id-PSIM','id-CTM','id-DM')
xlabel('Frequency (Hz)')
ylabel('Power')
title('{\bf 0-Centered Periodogram}')
axis([0 300 0 inf])
grid on

figure(4)
plot(f0,power0_iq(:,1),f0,power0_iq(:,2),f0,power0_iq(:,3));
legend('iq-PSIM','iq-CTM','iq-DM')
xlabel('Frequency (Hz)')
ylabel('Power')
title('{\bf 0-Centered Periodogram}')
axis([0 300 0 inf])
grid on

phase_ed = (angle(ed));
phase_eq = (angle(eq));
phase_id = (angle(id));
phase_iq = (angle(iq));%unwrap

figure(5)
plot(f0,phase_ed(:,1)*180/pi+90,f0,phase_ed(:,2)*180/pi+90,f0,phase_ed(:,3)*180/
pi+90);
xlabel('Frequency (Hz)')
ylabel('Phase (Degrees)')
legend('ed-PSIM','ed-CTM','ed-DM')
grid on
axis([0 100 -90 270])

figure(6)
plot(f0,phase_eq(:,1)*180/pi+90,f0,phase_eq(:,2)*180/pi+90,f0,phase_eq(:,3)*180/
pi+90);
xlabel('Frequency (Hz)')
ylabel('Phase (Degrees)')
legend('eq-PSIM','eq-CTM','eq-DM')
grid on
axis([0 100 -90 270])

figure(7)
plot(f0,phase_id(:,1)*180/pi+90,f0,phase_id(:,2)*180/pi+90,f0,phase_id(:,3)*180/
pi+90);
xlabel('Frequency (Hz)')
ylabel('Phase (Degrees)')
legend('id-PSIM','id-CTM','id-DM')
grid on
axis([0 100 -90 270])

figure(8)
plot(f0,phase_iq(:,1)*180/pi+90,f0,phase_iq(:,2)*180/pi+90,f0,phase_iq(:,3)*180/
pi+90);
xlabel('Frequency (Hz)')
ylabel('Phase (Degrees)')
legend('iq-PSIM','iq-CTM','iq-DM')
grid on
axis([0 100 -90 270])
```

41

```
nomefile2 = fopen( 'PSIM.txt','a');
fprintf(nomefile2 , '%f\t %e\t %e\t %e\t %e\t %e\t %e\t %e\t %e\n', fref,
power0_ed(fs/fper/2+1+abs(fref)/fper,1),
power0_eq(fs/fper/2+1+abs(fref)/fper,1),
phase_ed(fs/fper/2+1+abs(fref)/fper,1)*180/pi+90,
phase_eq(fs/fper/2+1+abs(fref)/fper,1)*180/pi+90,
power0_id(fs/fper/2+1+abs(fref)/fper,1),
power0_iq(fs/fper/2+1+abs(fref)/fper,1),
phase_id(fs/fper/2+1+abs(fref)/fper,1)*180/pi+90,
phase_iq(fs/fper/2+1+abs(fref)/fper,1)*180/pi+90);
fclose(nomefile2);


nomefile3 = fopen( 'CTM.txt','a');
fprintf(nomefile3 , '%f\t %e\t %e\t %e\t %e\t %e\t %e\t %e\t %e\n', fref,
power0_ed(fs/fper/2+1+abs(fref)/fper,2),
power0_eq(fs/fper/2+1+abs(fref)/fper,2),
phase_ed(fs/fper/2+1+abs(fref)/fper,2)*180/pi+90,
phase_eq(fs/fper/2+1+abs(fref)/fper,2)*180/pi+90,
power0_id(fs/fper/2+1+abs(fref)/fper,2),
power0_iq(fs/fper/2+1+abs(fref)/fper,2),
phase_id(fs/fper/2+1+abs(fref)/fper,2)*180/pi+90,
phase_iq(fs/fper/2+1+abs(fref)/fper,2)*180/pi+90);
fclose(nomefile3);


nomefile4 = fopen( 'DM.txt','a');
fprintf(nomefile4 ,  '%f\t %e\t %e\t %e\t %e\t %e\t %e\t %e\t %e\n', fref,
power0_ed(fs/fper/2+1+abs(fref)/fper,3),
power0_eq(fs/fper/2+1+abs(fref)/fper,3),
phase_ed(fs/fper/2+1+abs(fref)/fper,3)*180/pi+90,
phase_eq(fs/fper/2+1+abs(fref)/fper,3)*180/pi+90,
power0_id(fs/fper/2+1+abs(fref)/fper,3),
power0_iq(fs/fper/2+1+abs(fref)/fper,3),
phase_id(fs/fper/2+1+abs(fref)/fper,3)*180/pi+90,
phase_iq(fs/fper/2+1+abs(fref)/fper,3)*180/pi+90);
fclose(nomefile4);
```

III.4. *Three-phase delta-connected TCR with* $\sigma \epsilon$ $(60°, 120°)$

The list below refers to simulations presented in Section 4.2.2. PSIM scheme used is presented in [2], so here is omitted.

```
%--------------------------- dati input---------------------------------
w=2*pi*50; %[Hz]
T=2*pi/w;
t=linspace(0,1,1e06);
sigma=[75 90 105]*pi/180;
n_el=size(sigma,2);
Lr=112.174e-3; %[H]
Cr=183e-06; %[F]
Ls=8.278e-3; %[H]
u=53889;
%---------------------------matrici-------------------------------------
A_AB=[0        0        -2/(3*Ls)  +1/(3*Ls)  +1/(3*Ls)  0        0;
      0        0        +1/(3*Ls)  -2/(3*Ls)  +1/(3*Ls)  0        0;
      1/Cr     0        0          0          0          -1/Cr    +1/Cr;
      0        1/Cr     0          0          0          1/Cr     0;
      -1/Cr    -1/Cr    0          0          0          0        -1/Cr;
      0        0        1/Lr       -1/Lr      0          0        0
      0        0        -1/Lr      0          1/Lr       0        0];
B_AB=[+2/(3*Ls)     -1/(3*Ls)     -1/(3*Ls);
      -1/(3*Ls)     +2/(3*Ls)     -1/(3*Ls);
      0             0             0;
      0             0             0;
      0             0             0;
      0             0             0;
      0             0             0];
P=[1 0 0 0 0 0 0;
   0 1 0 0 0 0 0;
   0 0 1 0 0 0 0;
   0 0 0 1 0 0 0;
   0 0 0 0 1 0 0;
   0 0 0 0 0 1 0];
P_b=[1 0 0 0 0 0 0;
     0 1 0 0 0 0 0;
     0 0 1 0 0 0 0;
     0 0 0 1 0 0 0;
     0 0 0 0 1 0 0;
     0 0 0 0 0 0 1];
Q=P';
Q_b=P_b';
c=[0 0 0 0 0 0 1];
% da PSIM
%y_0=[ia(15)   ia(30)   ia(45)
%     ib(15)   ib(30)   ib(45)
%     Var(15)  Var(30)  Var(45)
%     Vbr(15)  Vbr(30)  Vbr(45)
%     Vcr(15)  Vcr(30)  Vcr(45)];
y_0_AB=[-2.6135903e+003  -3.7885283e+002   -3.0685792e+002
         2.6136557e+003   3.7885929e+002    6.1394050e+002
         3.0423635e+004   1.6352966e+005    3.0114713e+005
         3.0406449e+004   1.6341986e+005   -1.1746086e+001
        -6.0830084e+004  -3.2694952e+005   -3.0113538e+005
         6.4002602e+002   1.8240011e+002        -39.16];
e_AB= [2.6964045e+004  2.5975105e+005   2.5980133e+005
```

```
          2.6924950e+004   1.1311334e+002   1.2577472e+001
         -5.3888995e+004  -2.5986416e+005  -2.5981391e+005];
n_cycles=10;
Cab_abc_AB=[1 0; 0 1;-1 -1];
Cabc_ab_AB=[0 -1 -1; -1 0 -1];
V_0_AB=2/3*[cos(0+pi/3) cos(0-pi/3) cos(0-pi)
            -sin(0+pi/3) -sin(0-pi/3) -sin(0-pi)];
W_0_AB=3/2*V_0_AB';    % ho messo V_0_AB' x nascondere l'errore
NI_0_AB=[V_0_AB zeros(2,3) zeros(2,3);zeros(2,3) zeros(2,3) V_0_AB];
DOUBLE_NI_0_AB=[W_0_AB zeros(3,2) zeros(3,3); zeros(3,2) W_0_AB zeros(3,3);
zeros(3,2) zeros(3,2) W_0_AB ones(3,1)];
V_60_AB=2/3*[cos(pi/3+pi/3) cos(pi/3-pi/3) cos(pi/3-pi)
            -sin(pi/3+pi/3) -sin(pi/3-pi/3) -sin(pi/3-pi)];
W_60_AB=3/2*V_60_AB';
NI_60_AB=[V_60_AB zeros(2,3) zeros(2,3); zeros(2,3) V_60_AB  zeros(2,3);
zeros(2,3) zeros(2,3) V_60_AB; zeros(1,6) 1/3*ones(1,3)];
DOUBLE_NI_60_AB=[W_60_AB zeros(3,2) zeros(3,3); zeros(3,2) W_60_AB zeros(3,3);
zeros(3,2) zeros(3,2) W_60_AB ones(3,1)];

%--------------------------------program--------------------------------
--
close all
clc
SVC_dati_input_triangle_75_cambio_rif
A=A_AB;
B=B_AB;
[V,Ad] = eig(A);
PAQ=P*A*Q;
PAQb=P_b*A*Q_b;
[Cb,PAQdb] = eig(PAQb);
[C,PAQd] = eig(PAQ);
n=size(A);
m=size(PAQ);
u_d=[1 0]';
u_q=[0 1]';
 for k=1:1 %n_el
        for i=1:n
            exp_A_sigma(i,i)=exp(Ad(i,i)*((sigma(k)-pi/3)/w));
        end
        exp_A_sigma_1=V*exp_A_sigma*inv(V);
        for i=1:m
            exp_PAQb_pi_sigma(i,i)=exp(PAQdb(i,i)*(pi/3-sigma(k)/2)/(w));
            exp_PAQ_pi_sigma(i,i)=exp(PAQd(i,i)*(pi/3-sigma(k)/2)/(w));
        end
        exp_PAQb_pi_sigma_1=Cb*exp_PAQb_pi_sigma*inv(Cb);
        exp_PAQ_pi_sigma_1=C*exp_PAQ_pi_sigma*inv(C);
        DH(:,:,k)=exp_PAQb_pi_sigma_1*P_b*exp_A_sigma_1*Q*exp_PAQ_pi_sigma_1;
        %DH(1:2,1:2,k)=DH(:,:,k);
        E(:,k)=eig(DH(:,:,k));
        %figure (1)
        %title ('Posizione degli autovalori di DH nel piano complesso al variare
di sigma');
        %plot (real(E(:,k)),imag(E(:,k)),'*');
        %hold on
% calcolo del primo integrale nell'intervallo [0, phi] con passo
% d'integrazione relativo di 1/10000 (cioè prendendo 10000 campioni)
    csi=linspace(0,pi/3-sigma(k)/2,1e4);
    for kk=1:1e4
    Wa=[cos(csi(kk)+pi/3) -sin(csi(kk)+pi/3)
        cos(csi(kk)-pi/3) -sin(csi(kk)-pi/3)
        cos(csi(kk)-pi) -sin(csi(kk)-pi)];
        for i=1:m
```

44

```matlab
            exp_PAQ_phi_csi(i,i)=exp(PAQd(i,i)*(pi/3-sigma(k)/2-csi(kk))/w);
        end
    exp_PAQ_phi_csi_1=C*exp_PAQ_phi_csi*inv(C);
    int_1_d(:,:,kk)=exp_PAQ_phi_csi_1*P*B*u*Wa*u_d;
    M_1_d(kk,1)= int_1_d(1,1,kk);
    M_1_d(kk,2)= int_1_d(2,1,kk);
    M_1_d(kk,3)= int_1_d(3,1,kk);
    M_1_d(kk,4)= int_1_d(4,1,kk);
    M_1_d(kk,5)= int_1_d(5,1,kk);
    M_1_d(kk,6)= int_1_d(6,1,kk);
    int_1_q(:,:,kk)=exp_PAQ_phi_csi_1*P*B*u*Wa*u_q;
    M_1_q(kk,1)= int_1_q(1,1,kk);
    M_1_q(kk,2)= int_1_q(2,1,kk);
    M_1_q(kk,3)= int_1_q(3,1,kk);
    M_1_q(kk,4)= int_1_q(4,1,kk);
    M_1_q(kk,5)= int_1_q(5,1,kk);
    M_1_q(kk,6)= int_1_q(6,1,kk);
    end
INT_1_d(1,1,k)=trapz(csi/w,M_1_d(:,1));
INT_1_d(2,1,k)=trapz(csi/w,M_1_d(:,2));
INT_1_d(3,1,k)=trapz(csi/w,M_1_d(:,3));
INT_1_d(4,1,k)=trapz(csi/w,M_1_d(:,4));
INT_1_d(5,1,k)=trapz(csi/w,M_1_d(:,5));
INT_1_d(6,1,k)=trapz(csi/w,M_1_d(:,6));
INT_1_q(1,1,k)=trapz(csi/w,M_1_q(:,1));
INT_1_q(2,1,k)=trapz(csi/w,M_1_q(:,2));
INT_1_q(3,1,k)=trapz(csi/w,M_1_q(:,3));
INT_1_q(4,1,k)=trapz(csi/w,M_1_q(:,4));
INT_1_q(5,1,k)=trapz(csi/w,M_1_q(:,5));
INT_1_q(6,1,k)=trapz(csi/w,M_1_q(:,6));
    for i=1:m
        exp_PAQ_phi(i,i)=exp(PAQd(i,i)*(pi/3-sigma(k)/2)/w);
    end
exp_PAQ_phi_1=C*exp_PAQ_phi*inv(C);
y_phi(:,k)=exp_PAQ_phi_1*y_0_AB(:,k)+INT_1_d(:,1,k);
x_phi(:,k)=Q*y_phi(:,k);
x_phi_AB(:,k)=x_phi(:,k);
% calcolo dH/dphi
x_punto_phi(:,k)=A*x_phi(:,k)+B*e_AB(:,k);
x_punto_phi_AB(:,k)=x_punto_phi(:,k);
dH_dphi(:,k)=-exp_PAQb_pi_sigma_1*P_b*exp_A_sigma_1*c'*c*x_punto_phi(:,k);
%--------------------------------------------------------------------------
% calcolo del secondo integrale nell'intervallo [phi, tau]
csi=linspace(pi/3-sigma(k)/2,(sigma(k)/2),1e4);
for kk=1:1e4
    Wa=[cos(csi(kk)+pi/3) -sin(csi(kk)+pi/3)
        cos(csi(kk)-pi/3) -sin(csi(kk)-pi/3)
        cos(csi(kk)-pi) -sin(csi(kk)-pi)];
        for i=1:n
            exp_A_tau_csi(i,i)=exp(Ad(i,i)*(sigma(k)/2-csi(kk))/w);
        end
    exp_A_tau_csi_1=V*exp_A_tau_csi*inv(V);
    int_2_d(:,:,kk)=exp_A_tau_csi_1*B*u*Wa*u_d;
    int_2_q(:,:,kk)=exp_A_tau_csi_1*B*u*Wa*u_q;
    M_2_d(kk,1)= int_2_d(1,1,kk);
    M_2_d(kk,2)= int_2_d(2,1,kk);
    M_2_d(kk,3)= int_2_d(3,1,kk);
    M_2_d(kk,4)= int_2_d(4,1,kk);
    M_2_d(kk,5)= int_2_d(5,1,kk);
    M_2_d(kk,6)= int_2_d(6,1,kk);
    M_2_d(kk,7)= int_2_d(7,1,kk);
    M_2_q(kk,1)= int_2_q(1,1,kk);
```

```matlab
        M_2_q(kk,2)= int_2_q(2,1,kk);
        M_2_q(kk,3)= int_2_q(3,1,kk);
        M_2_q(kk,4)= int_2_q(4,1,kk);
        M_2_q(kk,5)= int_2_q(5,1,kk);
        M_2_q(kk,6)= int_2_q(6,1,kk);
        M_2_q(kk,7)= int_2_q(7,1,kk);
end
INT_2_d(1,1,k)=trapz(csi/w,M_2_d(:,1));
INT_2_d(2,1,k)=trapz(csi/w,M_2_d(:,2));
INT_2_d(3,1,k)=trapz(csi/w,M_2_d(:,3));
INT_2_d(4,1,k)=trapz(csi/w,M_2_d(:,4));
INT_2_d(5,1,k)=trapz(csi/w,M_2_d(:,5));
INT_2_d(6,1,k)=trapz(csi/w,M_2_d(:,6));
INT_2_d(7,1,k)=trapz(csi/w,M_2_d(:,7));
INT_2_q(1,1,k)=trapz(csi/w,M_2_q(:,1));
INT_2_q(2,1,k)=trapz(csi/w,M_2_q(:,2));
INT_2_q(3,1,k)=trapz(csi/w,M_2_q(:,3));
INT_2_q(4,1,k)=trapz(csi/w,M_2_q(:,4));
INT_2_q(5,1,k)=trapz(csi/w,M_2_q(:,5));
INT_2_q(6,1,k)=trapz(csi/w,M_2_q(:,6));
INT_2_q(7,1,k)=trapz(csi/w,M_2_q(:,7));
    for i=1:n
        exp_A_tau_phi(i,i)=exp(Ad(i,i)*((sigma(k)-pi/3)/w));
    end
exp_A_tau_phi_1=V*exp_A_tau_phi*inv(V);
x_tau(:,k)=exp_A_tau_phi_1*x_phi(:,k)+INT_2_d(:,1,k);
y_tau(:,k)=P_b*x_tau(:,k);
%-----------------------------------------------------------------------
% calcolo del terzo integrale nell'intervallo [tau, pi]
csi=linspace((sigma(k)/2),pi/3,1e4);
for kk=1:1e4
    Wa=[cos(csi(kk)+pi/3) -sin(csi(kk)+pi/3)
        cos(csi(kk)-pi/3) -sin(csi(kk)-pi/3)
        cos(csi(kk)-pi) -sin(csi(kk)-pi)];
        for i=1:m
            exp_PAQb_pi_csi(i,i)=exp(PAQdb(i,i)*(pi/3-csi(kk))/w);
        end
    exp_PAQb_pi_csi_1=Cb*exp_PAQb_pi_csi*inv(Cb);
    int_3_d(:,:,kk)=exp_PAQb_pi_csi_1*P_b*B*u*Wa*u_d;
    int_3_q(:,:,kk)=exp_PAQb_pi_csi_1*P_b*B*u*Wa*u_q;
    M_3_d(kk,1)= int_3_d(1,1,kk);
    M_3_d(kk,2)= int_3_d(2,1,kk);
    M_3_d(kk,3)= int_3_d(3,1,kk);
    M_3_d(kk,4)= int_3_d(4,1,kk);
    M_3_d(kk,5)= int_3_d(5,1,kk);
    M_3_d(kk,6)= int_3_d(6,1,kk);
    M_3_q(kk,1)= int_3_q(1,1,kk);
    M_3_q(kk,2)= int_3_q(2,1,kk);
    M_3_q(kk,3)= int_3_q(3,1,kk);
    M_3_q(kk,4)= int_3_q(4,1,kk);
    M_3_q(kk,5)= int_3_q(5,1,kk);
    M_3_q(kk,6)= int_3_q(6,1,kk);
end
INT_3_d(1,1,k)=trapz(csi/w,M_3_d(:,1));
INT_3_d(2,1,k)=trapz(csi/w,M_3_d(:,2));
INT_3_d(3,1,k)=trapz(csi/w,M_3_d(:,3));
INT_3_d(4,1,k)=trapz(csi/w,M_3_d(:,4));
INT_3_d(5,1,k)=trapz(csi/w,M_3_d(:,5));
INT_3_d(6,1,k)=trapz(csi/w,M_3_d(:,6));
INT_3_q(1,1,k)=trapz(csi/w,M_3_q(:,1));
INT_3_q(2,1,k)=trapz(csi/w,M_3_q(:,2));
INT_3_q(3,1,k)=trapz(csi/w,M_3_q(:,3));
```

```matlab
INT_3_q(4,1,k)=trapz(csi/w,M_3_q(:,4));
INT_3_q(5,1,k)=trapz(csi/w,M_3_q(:,5));
INT_3_q(6,1,k)=trapz(csi/w,M_3_q(:,6));
    for i=1:m
        exp_PAQb_pi_tau(i,i)=exp(PAQdb(i,i)*(pi/3-sigma(k)/2)/w);
    end
exp_PAQb_pi_tau_1=Cb*exp_PAQb_pi_tau*inv(Cb);
y_pi(:,k)=exp_PAQb_pi_tau_1*y_tau(:,k)+INT_3_d(:,1,k);

h_phi_ud(:,k)=exp_PAQb_pi_tau_1*P_b*(exp_A_tau_phi_1*Q*INT_1_d(:,1,k)/u+INT_2_d(
:,1,k)/u)+INT_3_d(:,1,k)/u;
h_phi_uq(:,k)=exp_PAQb_pi_tau_1*P_b*(exp_A_tau_phi_1*Q*INT_1_q(:,1,k)/u+INT_2_q(
:,1,k)/u)+INT_3_q(:,1,k)/u;
% trasformo il sistema in 5 varibili di stato a 6 variabili di stato in
% modo da poter fare poi la trasformazione dq
DH_1_1(:,:,k)=DH(1:2,1:2,k);
DH_1_2(:,:,k)=DH(1:2,3:5,k);
DH_1_3(1:2,1,k)=DH(1:2,6,k);
DH_2_1(:,:,k)=DH(3:5,1:2,k);
DH_2_2(1:3,1:3,k)=DH(3:5,3:5,k);
DH_2_3(1:3,1,k)=DH(3:5,6,k);
DH_3_1(1,1:2,k)=DH(6,1:2,k);
DH_3_2(1,1:3,k)=DH(6,3:5,k);
DH_3_3(1,1,k)=DH(6,6,k);
DH_1_1_abc(:,:,k)=Cab_abc_AB*DH_1_1(:,:,k)*Cabc_ab_AB;
DH_1_2_abc(:,:,k)=Cab_abc_AB*DH_1_2(:,:,k);
DH_1_3_abc(:,1,k)=Cab_abc_AB*DH_1_3(:,:,k);
DH_1_3_abc(:,2,k)=[0 0 0]';
DH_1_3_abc(:,3,k)=[0 0 0]';
DH_2_1_abc(:,:,k)=DH_2_1(:,:,k)*Cabc_ab_AB;
DH_2_2_abc(:,:,k)=DH_2_2(:,:,k);
DH_2_3_abc(:,1,k)=DH_2_3(:,:,k);
DH_2_3_abc(:,2,k)=[0 0 0]';
DH_2_3_abc(:,3,k)=[0 0 0]';
DH_3_1_abc(1,1:3,k)=DH_3_1(:,:,k)*Cabc_ab_AB;
for z=2:3
    for zz=1:3
    DH_3_1_abc(z,zz,k)=0;
    end
end
DH_3_2_abc(1,1:3,k)=DH_3_2(:,:,k);
for z=2:3
    for zz=1:3
    DH_3_2_abc(z,zz,k)=0;
    end
end
DH_3_3_abc(1,1,k)=DH_3_3(1,1,k);
DH_3_3_abc(1,2,k)=0;
DH_3_3_abc(1,3,k)=0;
for z=2:3
    for zz=1:3
    DH_3_3_abc(z,zz,k)=0;
    end
end
dH_dphi_1_abc(:,k)=Cab_abc_AB*dH_dphi(1:2,k);
h_phi_d_1_abc(:,k)=Cab_abc_AB*h_phi_ud(1:2,k);
h_phi_q_1_abc(:,k)=Cab_abc_AB*h_phi_uq(1:2,k);
DH_abc(1:3,1:3,k)=DH_1_1_abc(:,:,k);
DH_abc(1:3,4:6,k)=DH_1_2_abc(:,:,k);
DH_abc(1:3,7:9,k)=DH_1_3_abc(:,:,k);
DH_abc(4:6,1:3,k)=DH_2_1_abc(:,:,k);
DH_abc(4:6,4:6,k)=DH_2_2_abc(:,:,k);
```

```
DH_abc(4:6,7:9,k)=DH_2_3_abc(:,:,k);
DH_abc(7:9,1:3,k)=DH_3_1_abc(:,:,k);
DH_abc(7:9,4:6,k)=DH_3_2_abc(:,:,k);
DH_abc(7:9,7:9,k)=DH_3_3_abc(:,:,k);
DH_abc([7 9],:,k)=DH_abc([9 7],:,k);
dH_dphi_abc(1:3,k)=dH_dphi_1_abc(:,k);
dH_dphi_abc(4:6,k)=dH_dphi(3:5,k);
dH_dphi_abc(7,k)=0;
dH_dphi_abc(8,k)=0;
dH_dphi_abc(9,k)=dH_dphi(6,k);
h_phi_d_abc(1:3,k)=h_phi_d_1_abc(:,k);
h_phi_d_abc(4:6,k)=h_phi_ud(3:5,k);
h_phi_d_abc(7,k)=0;
h_phi_d_abc(8,k)=0;
h_phi_d_abc(9,k)=h_phi_ud(6,k);
h_phi_q_abc(1:3,k)=h_phi_q_1_abc(:,k);
h_phi_q_abc(4:6,k)=h_phi_uq(3:5,k);
h_phi_q_abc(7,k)=0;
h_phi_q_abc(8,k)=0;
h_phi_q_abc(9,k)=h_phi_uq(6,k);
DELTA_phi_AB(:,k)=NI_60_AB*dH_dphi_abc(:,k);
dH_dphi_abc_AB(:,k)=dH_dphi_abc(:,k);
DELTA_U(:,:,k)=[h_phi_d_abc(:,k) h_phi_q_abc(:,k)];
DELTA_U_AB_ing_dq(:,:,k)=DELTA_U(:,:,k);
DELTA_U_AB(:,:,k)=DELTA_U(:,:,k)*V_60_AB;
DELTA_U_dq_AB(:,:,k)=NI_60_AB*DELTA_U_AB(:,:,k)*W_60_AB;
PHI_AB(:,:,k)=NI_60_AB*DH_abc(:,:,k)*DOUBLE_NI_0_AB;
PHI_AB(:,7,k)=-PHI_AB(:,7,k);
Y_0=[0 0 0            % Is_d
     0 0 0            % Is_q
     0 0 0            % Vr_d
     0 0 0            % Vr_q
     0 0 0            % Id_TCR
     0 0 0            % Iq_TCR
     0 0 0];          % I0_TCR
for i=0:n_cycles-2
    Y(:,:,k)=PHI_AB(:,:,k)*Y_0(:,k)+DELTA_phi_AB(:,k)*1/180/100;
    Y_0(:,k)=Y(:,:,k)
end
end
PHI_75=real(PHI_AB(:,:,1));
DELTA_U_75(:,:)=real(DELTA_U_dq_AB(:,:,1));
DELTA_phi_75=real(DELTA_phi_AB(:,1));
figure (1)
plot (i_d_angle.time, i_d_angle.signals.values, '- ' );
title ('Perturbed Id ');
xlabel('time (s)');
ylabel('(A)');
figure (2)
plot (i_q_angle.time, i_q_angle.signals.values, '- ' );
title ('Perturbed Iq ');
xlabel('time (s)');
ylabel('(A)');
figure (3)
plot (e_d_angle.time, e_d_angle.signals.values, '- ' );
title ('Perturbed e_d ');
xlabel('time (s)');
ylabel('(V)');
figure (4)
plot (e_q_angle.time, e_q_angle.signals.values, '- ' );
title ('Perturbed e_q ');
xlabel('time (s)');
```

```matlab
ylabel('(V)');
figure (5)
plot (i_dTCR_angle.time, i_dTCR_angle.signals.values, '- ' );
title ('Perturbed ITCR_d ');
xlabel('time (s)');
ylabel('(A)');
figure (6)
plot (i_qTCR_angle.time, i_qTCR_angle.signals.values, '- ' );
title ('Perturbed ITCR_q ');
xlabel('time (s)');
ylabel('(A)');
figure (7)
plot (i_0TCR_angle.time, i_0TCR_angle.signals.values, '- ' );
title ('Perturbed ITCR_0 ');
xlabel('time (s)');
ylabel('(A)');
%------------------------INPUT DATI PSIM--------------------------------
%clear all
% clc
nomefile1 = fopen( 'inputTCRMAT1_TR_q_75.txt','r');
inputsPSIM = fscanf ( nomefile1 , '%g %g %g %g %g %g %g %g %g %g %g' , [11 inf]
);
%Time    eds_pert-eds_rif      eqs_pert-eqs_rif       alphaTCR
%idTCR_pert-idTCR_rif    iqTCR_pert-iqTCR_rif      ed_pert-ed_rif   eq_pert-eq_rif
id_pert-id_rif   iq_pert-iq_rif i0_pert-i0_rif
fclose(nomefile1);
inputsPSIM_v=inputsPSIM';
tstart1=inputsPSIM_v(1,1);
tstart=ceil(tstart1*(100*3))*1/(100*3)
inputsPSIM_v(:,1)=inputsPSIM_v(:,1)+(tstart-tstart1);


tend=inputsPSIM_v(end,1)
```
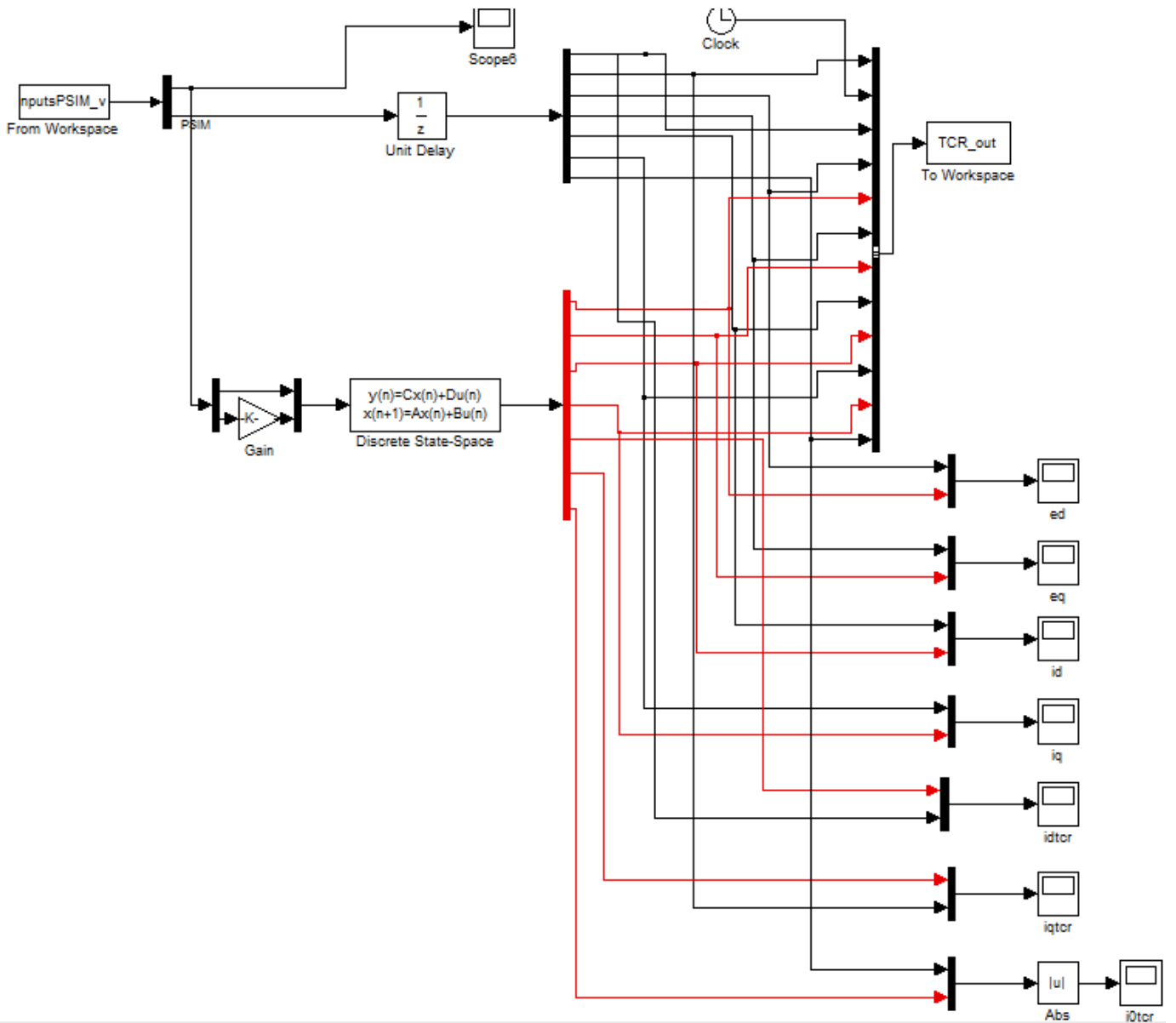
Figure III-6 Simulink scheme to compare PSIM and LTI discrete state-space model results